Dissolved gases and radioelements in groundwaters

Youngman, Michael J.

Award date:
1989

Awarding institution:
University of Bath

DISSOLVED GASES AND RADIOELEMENTS IN GROUNDWATERS

submitted by Michael J Youngman

for the degree of Ph.D.

of the University of Bath

1989

M. J. Youngman.

ProQuest LLC
789 East Eisenhower Parkway
P.O. Box 1346
Ann Arbor, MI 48106-1346

SUMMARY

Naturally occurring radioelements and dissolved inert gases have been used to determine groundwater age, conditions prevailing at recharge and the interactions between groundwater and the rock matrix.

Helium-4 increases with groundwater age, it is generated in the matrix by natural radioactive decay. Helium concentrations can yield semi-quantitative estimates of groundwater residence times. The diffusion of helium in an aquifer has been modelled using measured helium diffusion coefficients and stored helium contents of aquifer rocks.

The He-3/He-4 ratio of dissolved helium can be used to determine the source of helium in groundwater. Changes in helium isotopic ratio have the potential for studying groundwater movement.

Dissolved Ar-40/Ar-36 ratios have been found above the air-equilibration value. Enhanced ratios are most likely due to release of argon by chemical alteration of the aquifer matrix.

Inert gas measurements have been used to identify the groundwater-air equilibration temperature. This information has been correlated with other palaeoclimatic data.

Gases produced in the aquifer after groundwater-air equilibration have been shown to have an influence on possible degassing. The effect of degassing on apparent groundwater-air equilibration temperature has been

investigated. Measurements of nitrogen, methane and other dissolved gases have been made to identify collection pressures which are sufficient to prevent groundwater degassing.

Uranium concentrations in groundwaters have been shown to be controlled mainly by redox potential. U-234/U-238 ratios in excess of one are frequently encountered and are explained by selective leaching and direct alpha recoil of U-234.

Variation of rock Rn-222 content has been used as indicator of aquifer variability.

The concentration of Ra-226 in solution has been found to be primarily controlled by groundwater chemistry.

Residence times for short lived members of the U-238 series have been calculated using their recoil solution rate and the extent of the rock-water interface.

ACKNOWLEDGEMENT

Firstly, and most importantly, I would like to thank Dr. J.N. Andrews for his help and guidance throughout my nine years at Bath University.

For providing analytical facilities and data I would like to thank the following: Professor R.K. O'Nions and Professor E.R. Oxburgh for determination of helium isotopic ratios; Dr J.E. Goldbrunner for chemical analyses of Austrian water samples; Dr. W.G. Darling and other staff of B.G.S. Wallingford for assistance with isotopic ratio analysis.

For assistance with field sampling I thank Rohol-Aufsuchungs-Gesellschaft (R.A.G.) which holds the exploration rights in the Molasse basin. Also for assistance with sampling at Stripa I would like to thank H. Norlander and D. Lunstrum.

I gratefully acknowledge the assistance of the technical staff at the University of Bath for their help in building gas analysis equipment.

Finally, I would like to thank the Natural Environment Research Council who have supported this work throughout my time at Bath.

LIST OF FIGURES

CHAPTER 2

CHAPTER 3

CHAPTER 6

CHAPTER 7

CHAPTER 8

LIST OF TABLES

TABLE OF CONTENTS

CHAPTER 1

INTRODUCTION

1.1.1 The Nature of Radioactivity

Atoms consist of a small positive nucleus, containing nearly all of the mass surrounded by an electron cloud. The size of the nucleus is of the order of 10^{-12}cm, and the atomic diameter 10^{-8} cm.

The number of protons in a nucleus is given by the atomic number Z, and the number of nucleons by the mass number A. Nuclei which have the same atomic number but differing mass number are known as isotopes.

1.1.2 Nuclear Reactions

Nuclear reactions are the process by which a nucleus reacts with another nucleus, elementary particle or a photon to produce one or more nuclei; and possibly other particles.

The notation used to represent nuclear reactions is:

Target nucleus (projectile, product) residual nucleus

Nuclear reactions are always accompanied by the release or adsorption of energy. This energy is always much larger than that involved in chemical reactions, i.e. in the the reaction $^{14}N\ (\alpha,p)\ ^{17}O$, 1.91×10^{-13}J of energy are released which is equal to 1.19 MeV (one eV is the kinetic energy acquired by an electron when passing through a potential difference of 1V.

Alpha particles have energies of several MeV, β particles have energies from a fraction of an eV to

several MeV. Gamma rays have energies in the order of 1 MeV. Cosmic rays have much higher energies in the order of GeV.

1.1.3 Radioactive Decay

Spontaneous nuclear reactions are characterised by the type of emitted radiation. Radioactive events occur at random but in a large number of radioactive atoms a certain fraction will decay in a given time. This fraction is given by the decay constant λ, the fraction of atoms decaying in a unit time. Thus the number of radioactive decays therefore depends upon λ and the total number of nuclei present, N. The rate of change is given by:

$$\frac{dN}{dt} = - \lambda N$$

this integrates into the equation:

$$N = No\ e^{-\lambda t}$$

where No is the number of atoms present at t = 0.

Decay rates are normally expressed in terms of the half life $t_{\frac{1}{2}}$, where:

$$t_{\frac{1}{2}} = \frac{Ln\ 2}{\lambda}$$

This equation is the fundamental basis for nuclear age determinations.

The quantity of radioactive nuclide is usually expressed in terms of its activity, in the units of Bequerels where 1 Bq is equal to one disintegration per second. This unit replaces the much larger unit of the

Curie (Ci) which is equal to 3.7 x 10^{10} disintigrations per second.

1.1.4 Radioactive Decay Processes

1.1.4.1 Alpha decay

Almost all natural alpha emitters are found among the heavier elements in the 238-Uranium, 235-Uranium and 232-Thorium series. Emission of an alpha particle results in a mass reduction of four atomic mass units, and two charge units. The energy of alpha particles are always discrete and isotopes can be identified by the characteristic energy of their alpha particle.

The α particle is a helium atom stripped of electrons, when it collides with matter it slows and captures electrons to become a helium atom. In air α particles have a range of a few centimetres, in solids the range is only a few tens of microns.

When a radionuclide decays it releases energy in the form of kinetic energy of the α particle and also in the recoil energy of the product nucleus. Recoil energy can be calculated from the law of momentum conservation, which amounts to around 2% of the total energy released. This is however sufficient energy to produce chemical and other effects.

The energy of a recoil nucleus is given by:

$$E = \frac{P^2}{2M}$$

where E is the recoil energy and M is the mass of the recoil nucleus. For pure α decay P is given by:

$$P = \sqrt{2E_\alpha M_\alpha}$$

Therefore,

$$E = \frac{E_\alpha M_\alpha}{M}$$

This process of α recoil is an important one in the hydrogeochemistry of uranium, radium and radon. During the decay of ^{238}U the daughter ^{234}Th may be ejected into solution. In a similar way other nuclides may be ejected into solution following α decay. Table 1.1 shows the recoil energies of some important hydrochemical nuclear reactions.

1.1.4.2 Beta decay

In the process of beta decay the mass number remains unchanged. Natural beta decay is called negatron decay, in this process a neutron is converted into a proton plus an electron, thus increasing Z by one.

An example of negatron decay is given by:

$$^{234}_{90}Th \longrightarrow ^{234}_{91}Pa + \beta^-$$

Positron decay arises from the transformation of a proton to a neutron and is accompanied by a decrease in atomic number by one unit. Alternatively a nucleus may accomplish a decrease in Z with A remaining constant by

Table 1.1 The Recoil and alpha particle Energy of some Hydrochemically important Nuclear Reactions.

Nuclear Reaction		alpha energies	Recoil Mass	Recoil Energy (MeV)	% of energy as recoil
U-238	U-234	4.2 (100%)	234	0.072	1.7
Th-230	Ra-226	4.615 (24%)	226	0.082 (24%)	1.7
		4.682 (76%)		0.083 (76%)	
Ra-226	Rn-222	4.589 (5.7%)	222	0.083 (5.7%)	1.7
		4.777 (94.3%)		0.086 (94.3%)	

Figure 1.1

Decay scheme diagram for the branched decay of ^{40}K to ^{40}Ar

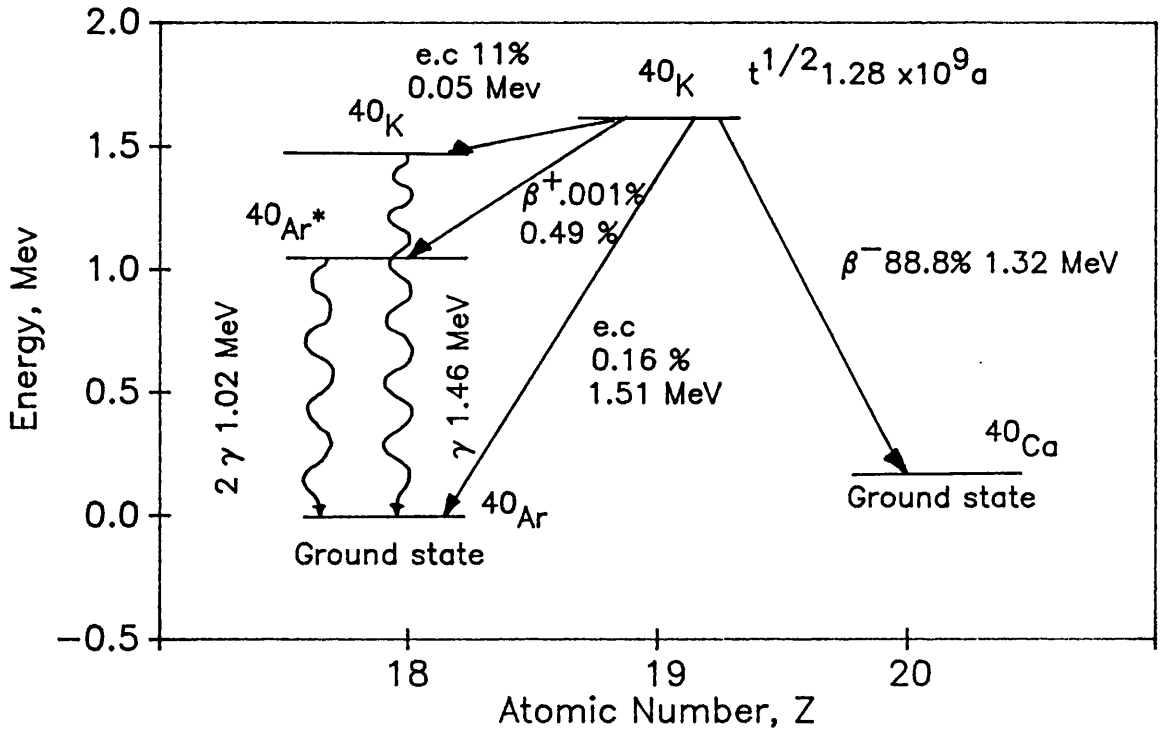

capturing an orbital electron. Usually a K electron as in (K capture) decay of potassium-40 to argon-40 (Figure 1.1). Beta particles are emitted with a continuous energy distribution.

1.1.4.3 Gamma decay

Decay by alpha or beta particle emission frequently leaves the product nucleus in an excited state. The most common way of losing excitation energy is by emission of electromagnetic radiation. The frequency of the emitted energy is determined by the energy transition involved. Gamma ray emission may be accompanied or replaced by emission of internal conversion electrons. Or the nucleus may be deactivated by formation of an electron-positron pair. All these changes are characterised by a change in energy without a change in Z and A.

1.1.5 Radioactive Series

Some radionuclides decay to daughters which are also radioactive, which may in turn also be radioactive. This is known as a radioactive series. Series decay is important in geochemistry as there are three naturally occuring decay series: uranium-238, uranium-235 and thorium-232. A series is said to be in radioactive equilibrium, when for each decaying parent ion, one of each daughter atoms also decays, on average. At equilibrium the number of each intermediate daughter will be

directly proportional to its half life.

Natural decay series are normally old enough for equilibrium to be established. However disequilibrium is often found because of chemical fractionation of parent ions from daughter ions. This fractionation is a result of the different chemical properties of parent and daughter ions. The nature and degree of disequilibrium may be used as an indicator of geochemical history. The natural decay series of uranium-238 (4n + 2) series, and the thorium-232 (4n) series can be found in appendix A and B respectively.

1.1.6 The determination of geological age using radioactive decay methods

The use of radioactive decay as a basis of time determination relies on three assumptions. These are as follows:

1. Parent element decays at a known and constant rate.
2. The system is closed with respect to the radioactive species involved in the decay process.
3. When the rock or water to be dated is formed it must be free of daughter isotopes, or alternatively contain the isotope in a known ratio with other isotopes so the original content may be determined.

Geological age may be estimated by measuring either the amount of radionuclide that has decayed (by measuring that which remains) or the amount of accumulated daughter

Table 1.2 Radioactive systems used in Geochronology

Parent/Daughter	Type of decay	Half life (yr)	Effective range (yr)	Crustal abundance parent/daughter	Typical materials dated
U-238/Pb-206	$8\alpha + 6\beta$	4.5×10^9	10^7-T_0	.993 g/g U .252 g/g Pb	Zircon, uraninite Pb bearing minerals
U-235/Pb-207	$7\alpha + 4\beta$	0.91×10^9	10^7-T_0	.0072 g/g U .215 g/g Pb	zircon, uraninite Pb bearing minerals
Th-232/Pb-208	$6\alpha + 4\beta$	1.39×10^{16}	10^7-T_0	1.00 g/g Th .520 g/g Pb	zircon, uraninite Pb bearing minerals
Rb-87/Sr-87	β	5.0×10^{10}	10^7-T_0	.278 g/g Rb .007 g/g Sr	biotite, muscovite microcline
K-40/Ar-40	e capture	1.3×10^9	5000-T_0	.0001 g/g K .996 g/g Ar	biotite, muscovite microcline
K-40/Ca-40	"	"	"		
K-40/Ar-39	"	"	"		
C-14/N-14	β	5730	0-7000	10^{-12} g/g C .996 g/g N	charcoal, wood, peat carbonate
Sm-147/Nd-143	α	1.06×10^{11}	10^6-T_0	.151 g/g Sm .122 g/g Nd	phosphate minerals alkalic igneous rocks
Lu-176/Hf-176	β	3.5×10^{10}	10^6-T_0	.026 g/g Lu .052 g/g Hf	zircon minerals
Re-187/Os-187	β	4.6×10^{10}	10^6-T_0	.629 g/g Re .016 g/g Os	metallic mineral deposits

T_0 = age of the Earth

atoms.

Considering the case where initial and final concentration of parents are determined, if the number of parent atoms present is Ps, and it decays according to its decay constant λ, then the amount remaining is a function of elapsed time. This is given by:

$$P_t = Ps\ e^{-\lambda t}$$

where Pt is the amount of P remaining after time t. This method is limited because Pt becomes increasingly small as t increases. The maximum range is 10 half lives of the parent by which time the activity is 0.1% of the original activity.

For the situation where measurement of the accumulation of daughters is made, the number of daughter atoms, D, present at time, t, is given by:

$$D = Po - Pt$$

where Po and Pt are the numbers of atoms of parent present at times o and t. If, however, there were Do atoms of daughter initially present then:

$$D^* = D\ total - Do$$

where D* is the number of radiogenic daughter atoms.

D* is also given by

$$D^* = Po - P$$

or $$D^* = P(e^{\lambda t} - 1)$$

where λ is the decay constant of the parent.

Solving for elapsed time gives the equation:

$$t = \frac{1}{\lambda} \text{ Ln } (D^*/_P + 1)$$

If t is small compared to $1/_\lambda$ then D* will be small compared with P, then this equation approximates to

$$t \simeq \frac{D^*}{P}$$

This method has been successfully used to date geological material A list of the more useful parent/daughters used are given in table 1.2.

The problems relating to these absolute age determinations result from a breakdown of the basic assumptions. These assumptions are as follows:

1. The geologic material has neither lost nor gained either parent or daughter atoms, so that the ratio $D^*/_P$ only changes as a result of radioactive decay.
2. It must be possible to assign a value to Do. This can usually be done reliably especially when D* is much greater than Do.
3. The value of λ must be known accurately.
4. The measurements of D and P must be accurate and representative of the material to be dated.

Disagreement of ages produced by more than one method is often useful in understanding the processes involved. Discrepancies are often encountered for gaseous decay products which may diffuse from the site of production. This is likely to be important for $^{40}K/^{40}Ar$ dating and

$^{238}U/^{206}Pb$ (where the decay scheme passes through ^{222}Rn gas).

Hydrothermal activity may redistribute elements, this is particularly important if either parent or daughter is much more mobile than the other. Another source of likely error is in assessing the amount of daughter isotope present in the system when it was formed. This is particularly important for Rb/Sr dating and where low levels of daughter atoms are produced.

1.2 The Geochemistry of Uranium and Thorium

The geochemical importance of U and Th arises from their radioactivity and widespread distribution in the lithosphere. U is also widely distributed in the hydrosphere because of its ability to form soluble complexes, unlike Th which is readily hydrolysed.

U-238 is the most abundant U isotope forming 99.27% of natural U. It has a half life of 4.5×10^9 years and forms the first member of a decay chain which ends in Pb-206. In this decay scheme shown in Appendix A are many geochemically important daughters such as U-234, Ra-226, and Rn-222. The other U isotopes are U-235 with an abundance of 0.72% and a half life of 7.1×10^8 years, and U-234 with an abundance of 0.06% and a half life of 2.4×10^5 years.

Thorium occurs naturally only as Th-232 which has a half life of 1.41×10^{10} years.

The geochemistry of Th and U is characterised by their crystallochemical relationships to several elements with similar ionic radii. Because of the similarity in size of their tetravalent ions U and Th tend to accompany one another in nature.

1.2.1 The Uranium and Thorium Content of Igneous Rocks

Thorium is strongly concentrated in acidic rock during magmatic differentiation resembling Zr, Y, and the lanthanide group. Concentration of thorium continues during the pegmatite stage because of its high valency and because Th^{4+} resembles Ca^{2+} in ionic radii (Table 1.3). There are only two independent thorium minerals which may crystallise, these are thorianite, $(Th,U)O_2$ and thorite, $Th[SiO_4]$. The latter is isomeric with zircon and thus thorium tends to be incorporated with zircon. Thorium is also concentrated in the rare earth minerals, monazite and xenotine and in Ce minerals because of its similar ionic radius.

Like thorium, uranium forms many oxygen compounds and does not form sulphides. Uranium is strongly concentrated in the upper lithosphere and relatively enriched to thorium in acidic igneous rocks. During magmatic differentiation U is often concentrated in granite and pegmatites in which it may form a number of independent minerals. U^{4+} like Th^{4+} resembles Ca^{2+} in ionic radius and becomes enriched in residual solutions. Table 1.4

Table 1.3

Ionic Radii of Selected Elements

Group	Ion	Radius, nm
II A	Ca^{2+}	0.099
II A	Ra^{2+}	0.140
III A	Y^{3+}	0.093
III A	Ta^{3+}	0.081
IV A	Zr^{4+}	0.080
Lanthanide	Ce^{3+}	0.111
Lanthanide	Ce^{4+}	0.101
Lanthanide	Gd^{3+}-Lu^{3+}	0.102-0.093
Actinide	Th^{4+}	0.095
Actinide	U^{4+}	0.089
IV B	Pb^{2+}	0.120
IV B	Pb^{4+}	0.084
V B	Bi^{3+}	0.120
V B	Bi^{5+}	0.074

Table 1.4

Average Uranium Thorium and Radium Contents of rocks

Rock Type	Radioelement Content U (ppm)	Th (ppm)	Ra ($\times 10^{-6}$ ppm)
Acid Igneous	9.1	20.5	3.01
Int. Igneous	6.2	16.4	2.57
Basic Igneous	3.2	5.6	1.28
Sandstones	4.2	6.0	1.5
Claystones	4.5	13.0	1.3
Limestones	4.7	0.5	0.5
Basalt 1	0.83	5.0	
Diabase 2	0.83	2.0	
Granite 2	3.96	13.45	
Basic Igneous 3	0.96	3.9	
Int. Igneous 3	2.61	9.97	

1 Evans and Goodman 1941
2 Senftle and Keevil 1947
3 Tomkeieff 1946

shows the uranium and thorium content of some average igneous rocks.

The ionic radii of U^{4+} and Th^{4+} are too great to allow the admission of significant U and Th into common igneous rock minerals. Crystallisation at high temperature produces predominantly UO_2 minerals which are of primary origin, (Tomkieff, 1946). Hydrothermal stages concentrate U in high temperature fractions in association with Sn veins. Hydrothermal sulphide and arsenide veins are also uraniferous. U also accompanies Zr and Th in zircon, thorium and rare earths in thorionite, monozite and tantalum in tantalates.

The most common U form is UO_2 in pitchblende and uranite, uranite is usually associated with pegmatites, pitchblende is associated with hydrothermal sulphides and arsenides. Alteration of uranite results in hydroxides, carbonates and silicates of uranium with complicated structure, and are frequently found in weathered uranium ore bodies.

1.2.2 Uranium and Thorium in Sedimentary Rocks

The uranium and thorium contents of sedimentary rocks are generally lower than the parent igneous rocks. Weathering releases uranium which is deposited syngenetically (sometimes epigenetically) in many sediment types. Zircon is highly resistant to mechanical alteration and accumulates in the heavy mineral fraction

of clastic sediments (Bell, 1954).

Most secondary U minerals are susceptible to alteration and leaching and are quickly reduced during transportation. However precipitation may occur in oxidizing environments to produce complex compounds. U in solution may be redeposited by precipitation, adsorption and isomorphous substitution for Ca^{2+}. Adsorption can occur on the hydroxylate gel precipitates of Fe, Al and Mn and also on clay compounds and organic substances. The presence of oxide and carbonate species in solution tends to preserve U in solution as complexes.

Thorium minerals are resistant and become concentrated in the heavy mineral resistate fraction of clastic rocks and placers. Th like U is highly insoluble, but unlike U does not form complexes which are soluble. Some Th is dissolved in weathering but this is quickly hydrolysed under oxidizing conditions, being deposited as hydrolyzate sediments, thus separating it from uranium.

1.3 The Geochemistry of Radium

Radium occurs as four isotopes namely 223, 224,226 and 228, their abundance is largely determined by their half lives. Although Ra-224, and Ra-228 are daughters of the abundant Th-232, the much longer half life of Ra-226 (1620 years) explains its much higher abundance. The age of the parent uranium-238 occurrence and the degree to which decay products are fractionated by geochemical

processes determines the extent to which Ra-226 is in equilibrium with U-238 (Andrews and Wood, 1972). These processes tend to occur on a timescale which is large compared with the time taken for equilibrium to be established.

The chemistry of Ra resembles Ba reflecting its position in group IIA (Table 1.5). The Ra content of average rocks is given in Table 1.4. The rocks with larger Ra contents fall into three categories (Stoker and Kruger, 1975). These are:

a) Rocks with an increased but uniform content due to adsorption, ion exchange or coprecipitation.

b) Hydrothermal zones with very high U and Ra content. The major transport processes are transport in solution in the presence of high carbon dioxide and deposition as carbon dioxide is lost, or deposition following redox reactions with iron.

c) Secondary concentration of radium in local formations associated with adsorptive formations in water conducting fissures.

During weathering radioactive equilibrium is disrupted and Ra may become separated from its precursors.

Quartz sandstones and limestones often have very low Ra contents < 0.1pCi/g (Beers and Goodman). Limestones generally have lower values than sandstones, except in argillaceous limestones where higher contents are found.

Like uranium, radium is found in high concentrations

Table 1.5

Chemical Properties of the Group II A Elements

		Be	Mg	Ca	Sr	Ba	Ra
Atomic No.		4	12	20	38	56	86
Config.		$2s^2$	$3s^2$	$4s^2$	$5s^2$	$6s^2$	$7s^2$
Ionization Energy (kJ/mol)	1st	900	736	590	548	502	1040
	2nd	1760	1450	1150	1060	966	381
Atomic Radii (nm)		0.089	0.136	0.174	0.191	0.198	0.220
Standard heat of formation of MSO_4 (kJ/mol)		-1197	-1278	-1433	-1444	-1465	-1480
Standard heat of formation of $M(OH)_2$ (kJ/mol)		-907	-925	-987	-3352	-3345	-3350

in oil field brines. Chloride rich waters readily dissolve radium by producing highly soluble $RaCl_4$ (Zartsev et al, 1959). Mazor (1962) found levels of 1000 pCi/l in oil field brines rich in chloride.

The hydrochemistry of radium is complex (Tanner, 1964), the contents are highly variable. Hot springs generally have high contents such as in the Bath thermal water where the content is 12.6 pCi/l compared to 0.19 pCi/l for the proximate carboniferous limestone groundwater (Andrews and Wood, 1974).

The lack of correlation between Ra-226 concentration in groundwater and Rn-222 indicates Ra is relatively immobile. Because the parent of Ra-226 is very immobile (Th-230), the concentration in the water is unlikely to be derived from Th-230 in solution but by Ra extracted from the sediments. Ra may be extracted if the pH is low enough to dissolve alkaline earth carbonates, or if chelating agents are available to remove alkaline earth cations which hold Ra. Above pH 7.5 radium solution is unlikely as carbonate solution is prevented and chelating agents are unlikely to be present. The importance of high chloride waters is magnified by its complement of positive ions which compete for adsorption sites with Ra-226.

Precipitation of Ra from solution is usually as $RaSO_4$. However the levels of Ra in solution are much less than indicated by the solubility product of $[Ra^{2+}][SO_4]^{2-}$. This is because radium is effectively removed by coprecipitation with $BaSO_4$, providing Ba and SO_4 concentrations

allow precipitation. Coprecipitation with $CaCO_3$ and $CaSO_4$ is also possible for Ra. Radium might also be removed from solution by coprecipitation with ferric hydroxide in high iron containing waters with high oxygen contents.

1.4 The Geochemistry of Radon

Radon has three isotopes Rn-219, 220 and 222. These have half lives of 3.92 seconds, 54.5 seconds and 3.825 days respectively. Details of the decay schemes to which each is connected is given in appendix A, B and C. Because of its longer half life Rn-222 is the most important isotope. The occurrence of Rn-222 is dependent upon the occurrence of radium in subsurface materials and the mechanism by which it is transferred.

Migration of Rn may be considered in three stages (Tanner, 1964).

a) Formation and recoil of Rn-222 from Ra-226.
b) Diffusion of the atom from the mineral interior.
c) Diffusion and transport of the atom through permeable rock and water.

Impervious minerals such as zircon are unlikely to lose much of their produced Rn, but minerals with more open structures will lose most. Radon can accumulate to high concentrations in natural gases (Faul et al, 1954). Because of radon's gaseous nature and thus ease of transport the behaviour in the atmosphere is an important aspect of its geochemistry. The average concentration in

the atmosphere is 10-30 x 10^{-14} Ci/l. The daughters of radon are positive ions which attach themselves to inert dusts in the atmosphere. If the parent gas exists with the dust for a few hours equilibrium will be achieved between Rn-222 and its daughters.

1.5 The Geochemistry of the Inert Gases

Inert gases are cosmically abundant but rare terrestially. This is because their inertness did not allow them to be captured and retained in their cosmic proportions (Hollander et al, 1953). Their present terrestial composition can be attributed to:

1) The quantities of primeval gas captured by the earth during its formation
2) That formed after the earth's formation by radioactive decay.
3) Loss of inert gas to outer space throughout the earth's history.
4) Fission production
5) Inert gas produced by cosmic radiation in the atmosphere and at shallow depths in the lithosphere.

Most of the inert gases in the atmosphere are of primordial origin with the exception of the He isotopes and Ar-40. Table 1.6 shows the air abundance of inert gases and the isotopic abundances.

Table 1.6

Isotopic Compositional data for Noble gases in air

		Isotopic ratios(h)	% Abundance
He	3(a)	1.399+/-13	.000140
	4	10	100
Ne	20(b)	100	90.50
	21	0.296+/-2	0.268
	22	10.20+/-8	9.23
Ar	36	.3378+/-6	.3364
	38	.0635+/-1	.0632
	40	100	99.60
Kr	78(def)	.6087+/-20	.3469
	80	3.9599+/-20	2.2571
	82	20.217+/-4	11.523
	83	20.136+/-21	11.477
	84	100	57.00
	86	30.524	17.398
Xe	124(de)	.3537+/-11	.0951
	126	.3300+/-17	.0887
	128	7.136+/-9	1.919
	129	98.32+/-12	26.44
	130	15.136+/-11	4.070
	131	78.90+/-11	21.22
	132	100	26.89
	134	38.79+/-6	10.43
	136	32.94+/-4	8.857

a Mamyrin et al 1970
b Eberhardt et al 1965
c Nier 1950
d Basford et al 1973
e Nier 1950
f Nief 1960
h Uncertainties refer to the last digits given

1.5.1 Physical properties of the inert gases

A summary of the physical properties of inert gases is given in Table 1.7. In the natural environment inert gases do not form chemical bonds, but are subject to the attractive forces produced by mutual electric dipole interaction (Van der Waals forces). These forces are weak limited to a few kJ/mole, because of the strong electronic repulsion. The size of the Van der Waals forces depends on the atomic radius and atomic number of the gas rather than the detailed electronic configuration. Podosek et al (1981) has measured the amount and enthalpy change when inert gases are absorbed on different surfaces, this data is shown in Table 1.8.

The diffusion of inert gases is important when considering their use as age indicators. The equation governing their diffusion in a medium is given by the Arrhenius equation:

$$D = Do \quad e^{-E/RT}$$

where D is the diffusion constant, Do is a constant, E the activation energy for diffusion, R the gas constant and T the temperature in Kelvins. Various authors have experimentally determined the parameters Do and E for diffusion of He and Ar in rocks and minerals. The data obtained is summarised in Table 1.9.

1.5.2 Helium geochemistry

The isotopes of helium are He-3 and He-4, they occur

Table 1.7

Physical Properties of the Inert Gases

	He	Ne	Ar	Kr	Xe	Rn
Gas Density 0°C and 1 atm g/l	.17850	.90002	1.7838	3.7493	5.8971	-
Boiling point °C	-269	-246	-186	-153	-108	-62
Triple point °C	none	-248	-189	-157	-112	-71
Critical temp. °C	-268	-229	-122	-64	17	105
Dielectric const. at 25°C and 1atm.	1.0000639	1.000229	1.0005085	1.000768	1.001238	-
First Ionization Energy, kJ/mol	2370	2080	1520	1350	1170	1040
Second Ionization Energy, kJ/mol	5250	3950	2660	2370	2050	1930
Van der Waals radius, nm	-	0.160	0.192	0.197	0.217	-

Table 1.8

Adsorbtion properties of Krypton and Xenon

After Podosek et al 1981

Sorbent	T°C	Henry's Constant cm^3 STP/g/atm		Heat of Adsorption kJ/mole-	
		Xe	Kr	Xe	Kr
Activated charcoal	0	5385	292	-31.4	-20.5
Shale	0	1.2	0.43	-22.2	-13.0
Basalt	0	0.7	0.28	-18.8	-13.8
Quartzite	0	5×10^{-5}	3×10^{-4}	-28.0	-17.2

Table 1.9

Data for Noble gas Diffusion in rocks and minerals

Ref	Sample	Gas	Temperature range °C	Energy of diffusion (kJ/mole)	D_o (cm^2/s)
d	orthoclase	Ar	500-800	180	0.00982
e	phlogopite	Ar	550-1080	242	0.75
f	volcanic glass	He	125-400	80	0.067
g	obsidian	He	200-300	34	0.00077

d Folland 1974
e Giletti and Tullis 1977
f Kurz and Jenkins 1981
g Jambon and Shelby 1980

in minerals, rocks and natural gases in variable proportions. Some helium is of primordial origin but the majority is produced by radioactive decay. He-3 is the daughter of H-3 and He-4 is produced when alpha particles are produced in natural decay series. A list of the varying He-3/He-4 ratios in natural rocks and gases is given in Table 1.10.

He-3 is produced in rocks by the following mechanisms (Hill, 1941) and (Morrison and Pine, 1955).

Li - 6 (n, α) H-3

Li - 7 (α, Be-8) H-3

H-2 (n, γ) H-3

followed in each case by beta decay of the tritium to helium-3. It is also produced in the atmosphere (Libby, 1946)

N-14 (n, C-12) H-3

N-14 (n, 3 α) H-3

again followed by beta decay.

Both processes in the atmosphere need neutrons which are amply supplied by cosmic rays, and the atmospheric He-3 content can be explained by these methods, despite the uncertainty in the rate of He-3 loss to space. The generation of He-3 below the surface also needs neutrons, cosmic ray neutrons are quickly absorbed by rocks. Only a small number of neutrons are produced by (α,n) reactions and by spontaneous uranium fission, so subsurface He-3 production is low.

He-4 is continuously being formed by the decay of uranium and thorium, and being lost to the atmosphere. The rate of production in the lithosphere exceeds the atmospheric loss, so that He-4 is being stored (Hurley, 1954). This introduces the possibility of using helium for age determinations. Holmes (1941) has shown acid rocks did not retain helium as well as basic rocks. Keevil (1942) showed that ferromagnesium minerals retained more helium than feldspars and quartz, and that acid felsitic and glassy rocks stored little helium. This was attributed to looseness of the crystal packing by Gerling (1939). Near regions of damage caused by concentrations of radioactivity He can easily escape to grain boundaries.

Helium migrating to the surface may become trapped in structures similar to those which form petroleum and natural gas reservoirs.

The release of helium is promoted by leaching with CH_4 and H_2 which can lead to natural gases which contain up to 10% of helium.

The He-3/He-4 ratio may vary by more than two orders of magnitude. Morrison and Pine (1955) calculated the average granitic ratio to be $1 \pm 0.5 \times 10^{-7}$. This ratio may be modified depending upon the actual radioelement content, neutron flux, and the rock chemistry; especially the Li content. Recently ratios have been measured as high as 10^{-5} (Lupton and Weiss, 1977) and (O'Nions and Oxburgh, 1983), which has been attributed to primordial helium outgassing from the mantle. Similar He-3 enrich-

Table 1.10

The Helium Content and Isotopic Ratio of some Natural gases and minerals

Sample		$^3He / ^4He \times 10^7$	He % of gas
Stamford Conneticut air		12.0	.004
Shiprock New Mexico	nat. gas	0.5	7.7
Otis Field Kansas	nat. gas	2.0	1.6
Panhandle field Texas	nat.gas	1.5 a	1.0
Alpine Basins			
Molasse	water	0.92 a	
Rhine graben	water	9.02 a,b	
Po basin	nat. gas	0.099 b	
Pannonian basin	nat. gas	10.72 a,b	
North sea rifts	nat. gas	0.71 a,b	
U.K. groundwaters			
Altnabreac		0.056-0.21	
Bunter sst		0.282-0.578	
Lincolnshire Limestone		0.409-0.592	
Llandridnod Wells		0.437	
Bath		0.268-0.395 b	
South Crofty granite		0.719	
Rosemanowes quarry granite		0.381	
Marchwood Triassic sandstone		0.113-0.197	
Radioactive minerals			
Hitlero Norway	Blomstrandite	0.2	
Bahal Brazil	Monazite	0.2	
G. Bear lake Canada	Pitchblende	0.3	
Joachimsthal Czechoslovakia	Uranite	0.3	
Non Radioactive minerals			cm^3/g
Keyston S. Dakota	Beryl	0.5	.011
West Rumney			
Cat lake Canada	Spodumene	24	.01
Guttenberg	Diabase	-	7.5×10^{-6}
Sudbury Ontario Canada	Granite	-	165×10^{-6}
	Gabbro	-	33×10^{-6}

a average of several sites
b data from Oxburgh, O'Nions and Hill 1986

ment has been found in Red Sea rift (Clark et al, 1969) and (Craig et al, 1975), in natural gases (Mamyrin et al, 1972) and (Mamyrin et al, 1969); and in pillow basalts (Lupton and Craig, 1975) and (Craig and Lupton, 1976).

The helium content of the atmosphere is a balance between crustal degassing and cosmic ray production balanced with escape from the upper atmosphere. The rate of production in the crust has been estimated as 1-3 x 10^6 atoms/cm^2/sec (Macdonald, 1963). The production rate of He-3 in the crust by cosmic ray interaction has been estimated at 0.5-5 atoms/cm^2/s. A certain proportion of the helium produced in the crust reaches the atmosphere, the flux from the crust is 1.13 x 10^{20} atoms/cm^2 for He-4 and 1.41 x 10^{13} atoms/cm^2 for He-3.

It is uncertain whether the atmosphere is in equilibrium with respect to He (Badhwar, 1969) it is likely to be acquiring He at the present time.

1.5.3 The Geochemistry of Argon

Argon has three isotopes of mass 36, 38 and 40. The terrestial abundance of Ar-40 has increased enormously because of production by decay of 40-K. The presence of both radiogenic Ar and non radiogenic Ar in minerals was first shown by Aldrich and Nier (1948). The production of Ar-40 from K is the basis of K/Ar age dating. The Ar-36/Ar-38 ratio is low in some minerals (Fleming and Thode, 1953) and has been attributed to Ar-38 production by

reactions involving Cl-35.

$$\text{Cl-35} \quad (\alpha, p) \quad \text{Ar-38}$$
$$\text{or Cl-35} \quad (\alpha, n) \quad \text{K-38}$$
$$\text{then K-38} \quad (\beta^{+}) \quad \text{Ar-38}$$

There are two views regarding the Ar content of the atmosphere. Damon and Kulp argue that most of the Ar was introduced from the mantle during the first billion years of earth's history. Shillibeer and Russell calculated earth's age from the atmospheric Ar-40 content and support the view that Ar has been continuously released.

1.5.4 The Geochemistry of Neon, Krypton and Xenon

The atmospheric abundances of Ne, Kr and Xe are given in Table 1.6.

Excess Ne-21 has been found in some radioactive minerals. Wetherill concluded this was due to the nuclear reaction.

$$\text{O-18} \ (\alpha, n) \ \text{Ne-21}$$

and is the source of nearly all atmospheric Ne-21. The neon cosmic abundance is much greater than in the atmosphere. Russel and Menzel concluded this is due to losing most of the primordial Ne before solidification of the earth.

Suess showed that the selective escape from the earth's gravitational field has led to a concentrating of Xe relative to Ne in the atmosphere. This work also

indicates that approximately 10^7 parts to one of rare gas originally present in the atmosphere have escaped.

Krypton and xenon have been found in some rocks to contain abundance ratios which are very different to the atmospheric ratios. This can be explained by production of heavy inert gases by natural fission and neutron fission.

1.5.5 The Radiogenic component of Inert Gas

He-4 and Ar-40 are the primary components of terrestial noble gases. Uranium produces He-4 at the rate of $1.19 \times 10^{-7} cm^3$ STP/gU/yr. The present He-4 production from Th is $2.28 \times 10^{-8} cm^3$ STP/gTh/yr. The Th/U ratio in most common rocks is sufficiently uniform that it is convenient to think of them as a single source of He-4. For a Th/U ratio of 3.3 the combined production is $1.94 \times 10^{-7} cm^3$ STP/gU/yr.

U-238 has a spontaneous fission branch which produces Xe-136 at the rate of $5.08 \times 10^{-16} cm^3$ STP/gU/yr. Other heavy isotopes of Xe and Kr are also produced. Inert gases can also be formed by (n, γ) reactions on halogens, but these can only be observed when non radiogenic gas abundanc es are unusually low, and either U and/or Th or a target element is particularly high. The radiogenic production of inert gases is shown in Table 1.11.

The radiogenic production of He-3 is of special interest and this will be discussed in detail later.

Table 1.11

Radiogenic component to inert gas concentrations

Nuclide	Principal source	Current Production	Air abundance
^{4}He	α decay	$1.94 \times 10^{-7} cm^3/gU/yr$	100 %
^{3}He	$^{6}Li(n,\alpha)^{3}H$	$^{3}He/^{4}He \sim 10^{-7}$	2 %
^{21}Ne	$^{18}O(\alpha,n)\ ^{21}Ne$	$^{21}Ne/^{4}He = 4 \times 10^{-8}$	< 4 %
^{136}Xe	^{238}U fission	$^{136}Xe/^{4}He = 2.3 \times 10^{-9}$	< 1 %
^{40}Ar	^{40}K decay	$3.89 \times 10^{-12} cm^3/gK/yr$	100 %
^{129}Xe	^{129}I decay	Nil	7 %
^{136}Xe	^{244}Pu decay	Nil	4 %
^{86}Kr	fission ?	?	1 %

Another special case is the production of large excesses of Ne-21 in U and Th rich minerals (Wetherill, 1954). Heyman et al (1976) calculated a Ne-21/He-4 ratio of 4.2 x 10^{-8}. Other Ne isotopes are produced but at much lower rates (Rison, 1980).

The production rate of Ar-40 from K-40 decay is 3.89 x $10^{-12}$$cm^3$ STP/gK/year. As K tends to be geochemically coherent with U typically with a ratio of K/U $\sim 10^4$ (Wasserburg, 1964). These radiogenic gases will be produced currently with a He-4/Ar-40 ratio of 5.5 Because of the shorter lifetime of K-40 the production ratio was lower in the past. Integrated over 4.55 x 10^9 years the production ratio is 2.1.

1.6 The Nature of Groundwater

Rock formations which contain significant quantities of unbound water are known as aquifers. The earth's surface layers are a vast natural reservoir in the hydrologic cycle, absorbing rainfall and storing it for long periods.

1.6.1 The Occurrence of Groundwater

Virtually all groundwater comprises precipitated atmospheric moisture which has percolated down into the soil. Meteoric water may reach the zone of saturation directly, whereby rain infiltrates the soil layers or water vapour condenses in the soil interstices, or

indirectly by seepage from lakes or rivers.

Only a small proportion of the saturated zone will be comprised of aquifer rocks which can store and transmit water. There are also impermeable beds which contain no interconnected openings or interstices and therefore can not transmit water or absorb it. There are also semi-permeable beds which although porous and capable of slowly absorbing water they can not transmit it in a significant quantity.

1.6.2 Porosity of Aquifer Rocks

The porosity is the degree to which a rock contains interstices. The intergranular spaces may be minute voids between clays and shales to large spaces such as fractures, joints and bedding planes. Meizner (1923) used the relationship of rock porosity to classify types of rock interstices. Figure 1.2 shows several types of rock interstices. Figure 1.3 gives the range of porosities for various deposits.

1.6.3 Groundwater Boundaries

Only in the saturated zone are aquifer interstices completely filled with water. Downward movement of groundwater is often limited by a lower zone where interstices are small and scarce. This boundary is frequently formed by a layer of dense rock, often clay or slate; or by the upper boundary of a parent rock when the aquifer is

Figure 1.2

Diagram showing types of rock interstices

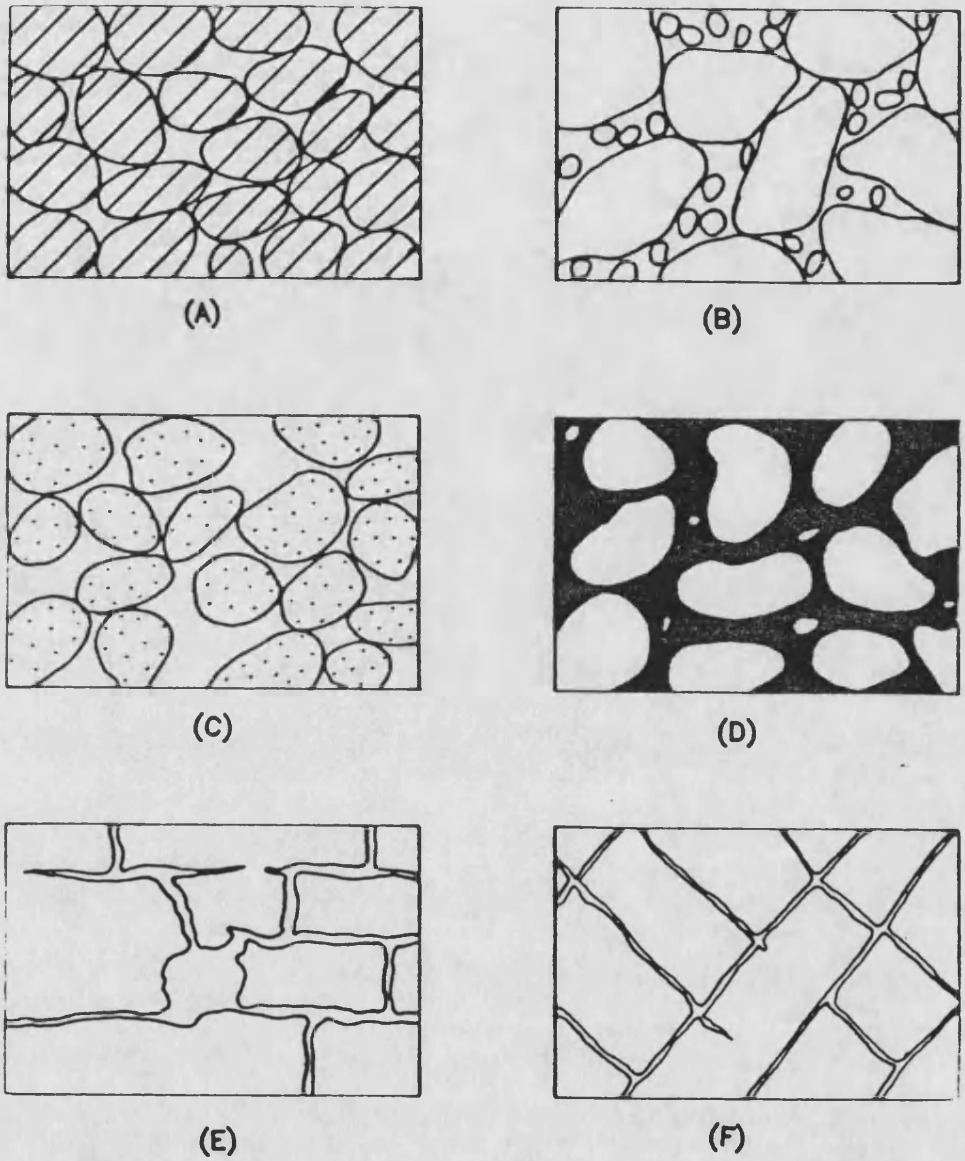

(A) between relatively impermeable well sorted particles

(B) between relatively impermeable unsorted particles

(C) between permeable particles

(D) between grains which are partially cemented

(E) formed by solution along joints and bedding planes in carbonate rocks

(F) formed by fractures in crystalline rocks

after Meizner (1923)

Figure 1.3

Porosity ranges for various deposits

after Todd (1959)

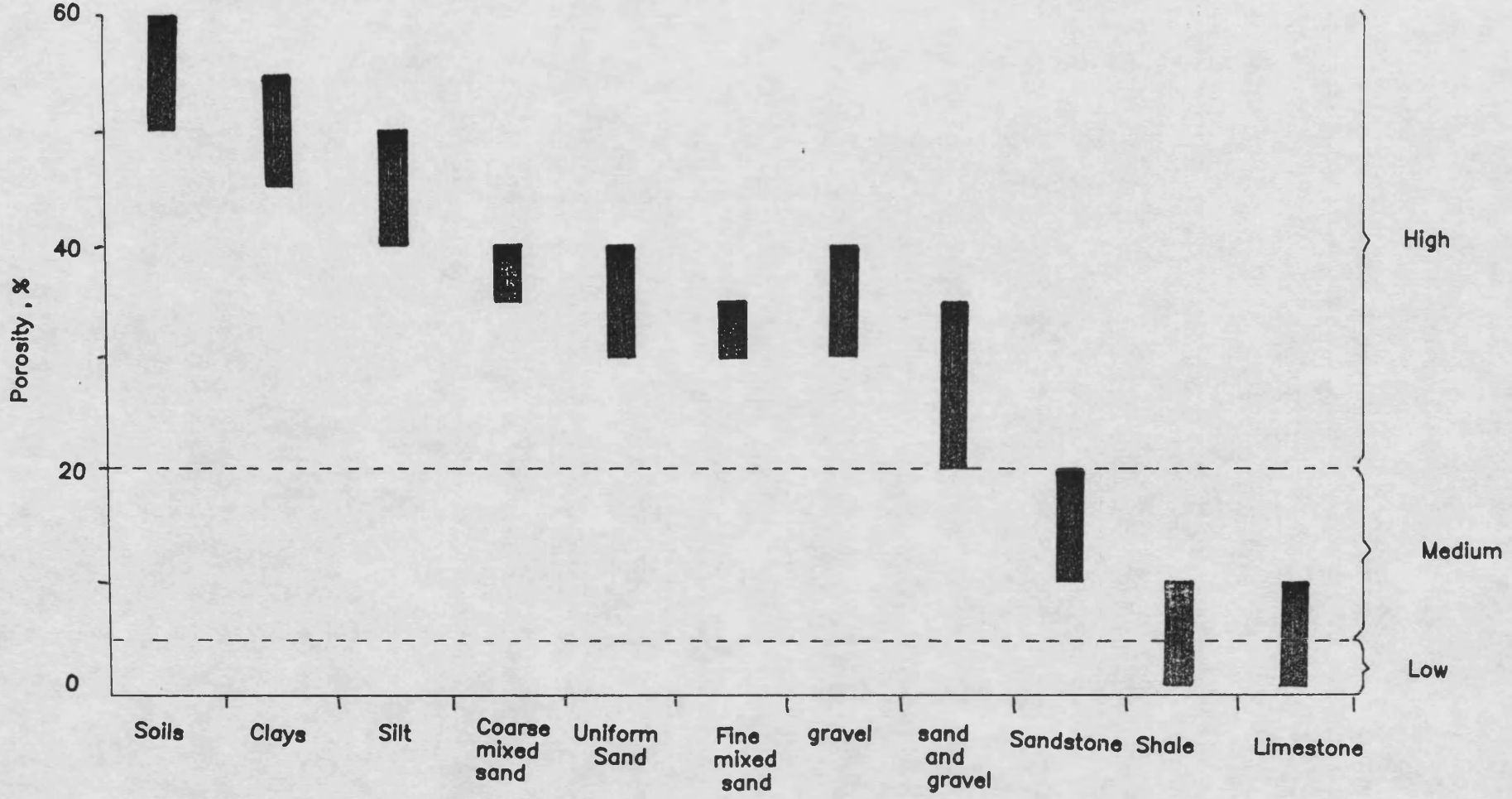

a surface deposit of weathered material. An alternative boundary may be formed by a gradual compression of strata with depth, as a result of the increasing weight of overlying rocks.

The upper boundary depends on whether the groundwater is confined or unconfined. In the case of an unconfined aquifer the boundary is known as the water table. This is the contact plane of groundwater and the capillary fringe (Tolman), this approximates to the level where porewater pressure is equal to atmospheric pressure. In the case of confined groundwater the upper boundary is formed by an overlying impermeable bed. All confined aquifers must have an unconfined zone through which recharge occurs. Impermeable beds rarely form an absolute barrier to groundwater movement, so there is normally some interchange and therefore a degree of hydraulic continuity.

The pressure of groundwater in the confined zone is given by the difference in hydrostatic levels between the water table and the confined level. The water level in a well or borehole in a confined aquifer will rise to the height of the hydrostatic head.

1.6.4 Groundwater Storage and Movement

Aquifers with small interstices may store groundwater for thousands of years. Movement in large interstices is very much faster and residence times may range from a few hours for Mendip conduit flow (Atkinson, 1977) to a few

years in the Bunter sandstone aquifer (Williams et al, 1972).

The amount of stored water depends on the porosity. Porosity is determined by the shape arrangement and degree of sorting of constituent materials (Fig. 1.3). Materials of high porosity do not necessarily form good aquifers as not all the water is mobile. The water mobility depends on the way interstices are inter-connected. Recharge by precipitation occurs by (Ward, 1975):

a) Infiltration at the ground surface
b) Seepage through the banks and bed of surface water bodies
c) Leakage from adjacent aquifers
d) Artificial recharge

The components of discharge are:

a) Evapotranspiration in the unconfined zone where the water table is near to ground level
b) Discharge through springs and into surface waters
c) Leakage into adjacent aquifers
d) Artificial extraction.

The driving force of groundwater movement is the hydraulic gradient. The rate and direction of flow are described quantitatively by Darcys' Law.

$$Q = Kp \; A \; \frac{\phi_1 - \phi_2}{\Delta S}$$

Figure 1.4
Diagram showing the Elevation head, Pressure head and Total potential for a point in a flow field

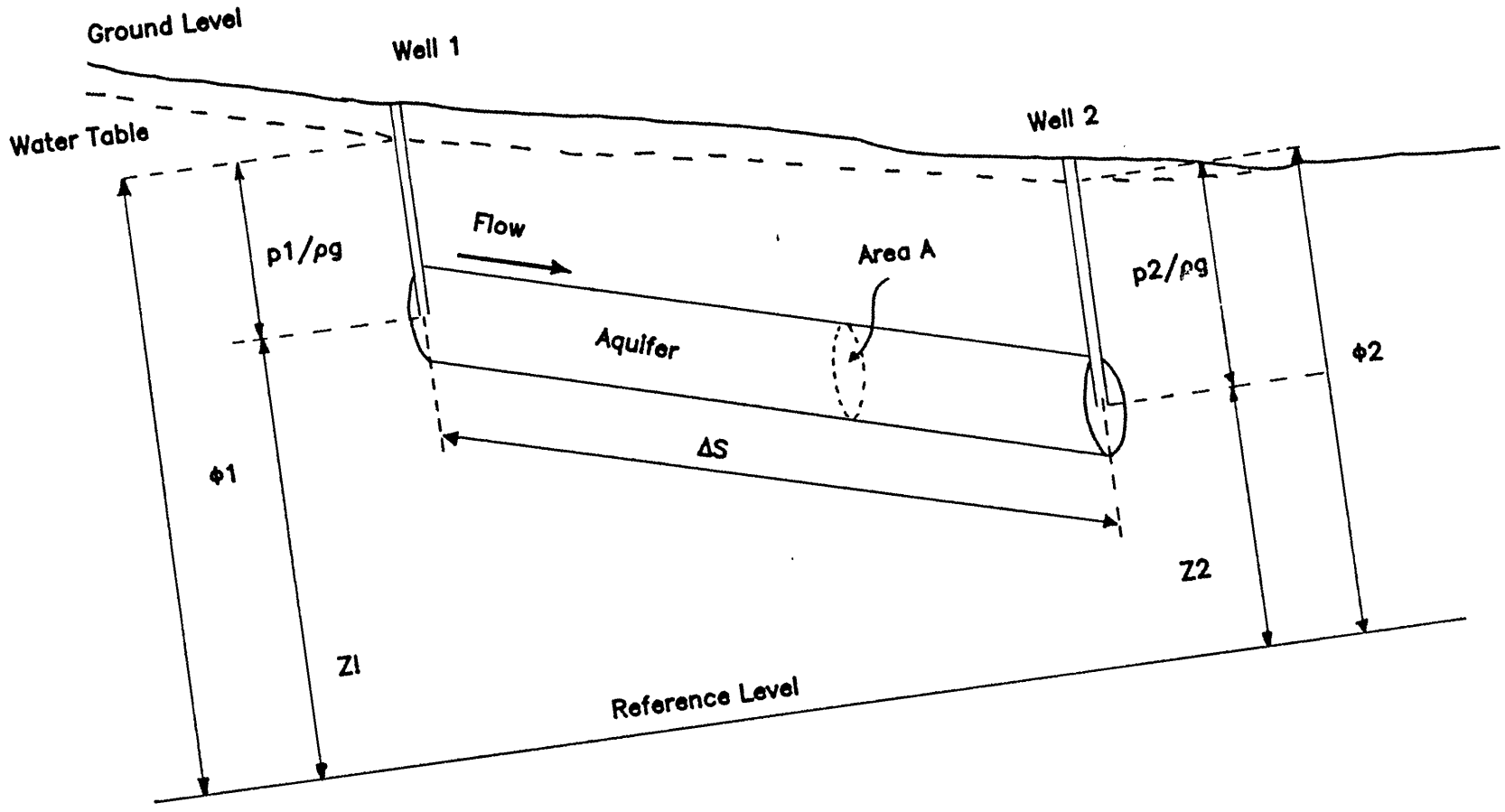

where Q is the volume flow velocity, m^3s^{-1}

Kp is the coefficient of permeability

A is the cross sectional area of aquifer, m^2

$\emptyset$ is the potential, m

ΔS is the length of flow, m

Kp has units ms^{-1} and is independent of the sample size and is therefore a constant for a particular material. Figure 1.4 shows the height to which water rises in wells 1 and 2 denoted by $\emptyset_1$ and $\emptyset_2$ respectively. The resistance to flow is large in the aquifer compared to the standpipes, and the water velocity is small due to this resistance. Therefore the pressure at the bottom of each pipe may be considered to be due to hydrostatic pressure alone.

Therefore

$$p_1 = (\emptyset_1 - Z_1)\ \rho\ g$$

$$p_2 = (\emptyset_2 - Z_2)\ \rho\ g$$

where ρ is the density of water and g the acceleration due to gravity. p_1 and p_2 are the pressure at the bottom of each pipe, therefore

$$\emptyset_1 = Z_1 + p1/\rho g$$

$$\emptyset_2 = Z_2 + p2/\rho g$$

It is not therefore merely pressure that makes water flow through an aquifer, but a combination of pressure and height above a certain horizontal layer. This combination

is called the groundwater head, Z is the elevation head and $p/\rho g$ the pressure head.

The quantity Q/A in the discharge per unit of cross sectional area is called the specific discharge v. If $\emptyset_2-\emptyset_1 = \Delta\emptyset$ then the Darcy equation becomes:

$$v = - Kp \frac{\Delta\emptyset}{\Delta S}$$

The specific discharge has been defined as the total discharge per unit area of the aquifer, and not as the discharge per unit volume of pore space; therefore specific discharge is not the actual velocity of water. If the porosity is n the area through which water can flow Vw is given by

$$Vw = \frac{Q}{nA} = \frac{V}{n}$$

The relationship between Kp and the material and fluid properties is given by:

$$Kp = k \frac{w}{\mu}$$

where w is the specific weight of the fluid

μ is the absolute viscosity

k is the intrinsic permeability and is a property of the aquifer material alone such that

$$k = Cd^2$$

where C is a constant involving shape and packing

d is the average pore size

Substituting into Darcy's equation gives:

$$v = \frac{-kw}{\mu} \frac{\Delta \emptyset}{\Delta S}$$

k is usually expressed in units of Darcys (Bear, 1972) where one Darcy is when a porous medium is said to have an intrinsic permeability [illegible] if a fluid of one centipose viscosity that completely fills the pore space will flow with a rate of $1cm^3/s$ $/cm^2$ of cross sectional area, under a pressure gradient of 1 atm/cm. One Darcy is numerically equal to 0.987×10^{-12} m^2.

Inserting values of w and μ for water at 20°C gives one Darcy = 10^{-5}Kp.

Table 1.12 shows the range of permeabilities of rock forming materials and table 1.13 the range of permeabilities of rocks forming aquifers.

The flow velocity through interstices will be much higher than that calculated through Darcys law, because the actual flow path is much greater than the apparent flow path. Another complicating factor is hydraulic conductivity is often markedly anisotropic particularly in fracture systems.

Darcys law suffices to describe only steady flow conditions, so that for most field applications the law must be combined with the law of mass conservation.

Table 1.12

The Permeability of rock forming materials

	Kp (ms^{-1})	K (Darcys)
Impervious clays	10^{-9}	$< 10^{-4}$
Sandy clay	10^{-9}–10^{-8}	10^{-4}–10^{-3}
Peat	10^{-9}–10^{-7}	10^{-4}–10^{-2}
Silt	10^{-8}–10^{-7}	10^{-3}–10^{-2}
Very fine sand	10^{-6}–10^{-5}	10^{-1}– 1
Fine sand	10^{-5}–10^{-4}	1 – 10
Coarse sand	10^{-4}–10^{-3}	10 – 10^{2}
Sand and Gravel	10^{-3}–10^{-2}	10^{2} – 10^{3}
Gravel	$>10^{-2}$	$>10^{3}$

Table 1.13

The Permeability of rocks

	Kp (ms^{-1})	K (Darcys)
Unfractured metamorphic and igneous rocks	10^{-10}–10^{-14}	10^{-5}–10^{-9}
Sandstone	10^{-6}– 1	10^{-1}–10^{-5}
Limestone and Dolomite	10^{-5}–10^{-9}	1 – 10^{-4}
Fractured metamorphic and igneous rocks	10^{-4}–10^{-8}	10 – 10^{-3}
Permeable basalt	10^{-2}–10^{-7}	10^{3}–10^{-2}
Karst Limestone	10^{-2}–10^{-6}	10^{3}–10^{-1}

1.7 Groundwater Quality

The quality of groundwater is usually described in terms of its suitability of the water for its intended use. The most important of these standards are those established for drinking water. The parameters which are considered are the bacteriological content, the physical characteristics of temperature, turbidity, colour, odour and the chemical content (Ward, 1969). The chemical content is often represented on a Piper diagram, which are convenient graphic presentation of a large number of analyses. These are useful in describing differences in major ion chemistry (Piper, 1944) (see Figure 1.5).

Toth (1970) lists the factors which affect the chemical composition of groundwater:

a) Types of soluble mineral present.
b) Amount of soluble mineral present
c) Solubility of minerals
d) Prevalent rock temperature
e) Extent of the rock/water interface
f) The orginal composition of dissolved material
g) The original water temperature
h) Fluid pressure
i) The flow velocity

The most important physical parameter is temperature. Temperature shows a small seasonal and diurnal change in the case of shallow waters and virtual constancy in case of waters below 30 metres. At depths of 10-20 metres the

Figure 1.5

Classification diagram for waters in terms of major cation and anion percentages (Piper diagram)

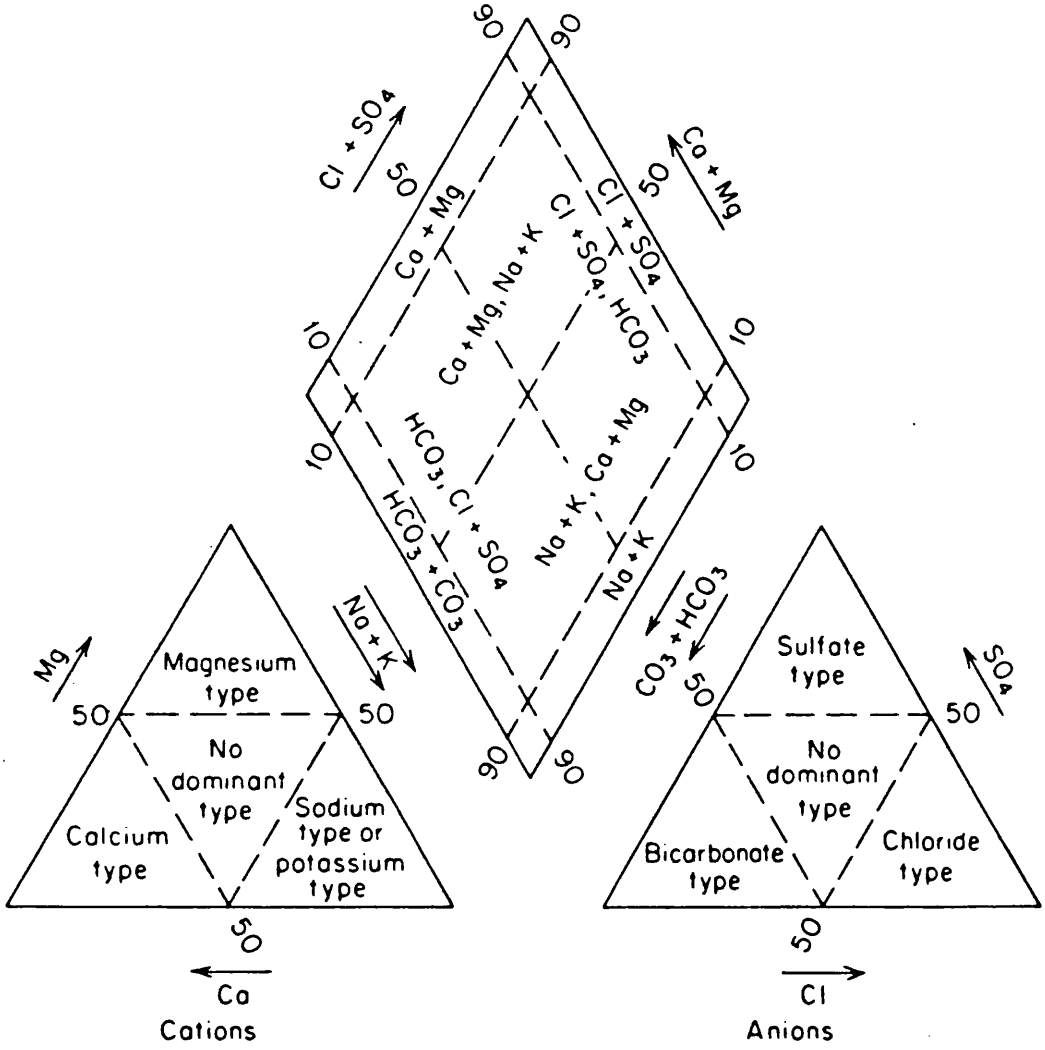

groundwater temperature will normally exceed the mean annual air temperature by 1-2 degrees centigrade (Todd). At greater depths, heated by the geothermal gradient, groundwater temperature increases by 3°C/100m (Garnish, 1976).

1.7.1 Chemical Evolution of Groundwater

As groundwater moves along its flow paths in the saturated zone, increases of total dissolved solids and most of the major ions normally occur. Cherbotarev (1955) concluded that groundwater tends to evolve chemically towards the composition of seawater. He observed that the evolution is normally accompanied by the following regional changes in dominant anion species:

$$HCO_3^- \rightarrow HCO_3^- + SO_4^{2-} \rightarrow SO_4^{2-} + HCO_3^- \rightarrow SO_4^{2-} + Cl^- \rightarrow Cl^- + SO_4^{2-} \rightarrow Cl^-$$

For large sedimentary basins the Chebotarev sequence can be described in terms of three main zones, which correlate in a general way with depth (Domenico, 1972).

1) The upper zone - characterised by active groundwater flushing through relatively well-leached rocks. Water in this zone has HCO_3^- as the dominant anion and is low in total dissolved solids.
2) The intermediate zone - with less active groundwater circulation and higher total dissolved solids. Sulphate is the dominant anion.
3) The lower zone - with slow groundwater flow. Highly soluble minerals are commonly present in this zone

because very little groundwater flushing has occurred. High chloride and high total dissolved solids are characteristic.

These three zones cannot be correlated specifically with distance or time. In some sedimentary basins groundwater in the upper zone may be years or tens of years old, whereas in other basins ages of hundreds or thousands of years are common. Waters of the lower zone may be thousands of millions of years old.

The anion evolution sequence can be explained in terms of mineral availability and mineral solubility. The bicarbonate is derived from soil zone carbon dioxide, and from the dissolution of calcite and gypsum. There are several soluble minerals that release sulphate or chloride upon dissolution. The most common of the sulphate minerals are gypsum $CaSO_4.2H_2O$ and anhydrite $CaSO_4$. Gypsum and anhydrite are considerably more soluble than calcite and dolomite but much less soluble than the chloride minerals such as halite (NaCl) and sylvite (KCl). The reason most groundwater travels a considerable distance before sulphate becomes a dominant anion is that gypsum or anhydrite are rarely present in more than trace amounts. Given enough time, dissolution and flushing will cause the readily soluble minerals to be completely removed from the active flow zone. Subsurface systems rarely advance to this stage because of the rejuvenating effects of continental uplift and sedimentation.

In deep flow systems groundwaters evolve to a chloride rich brine. This occurs if the groundwater comes into contact with highly soluble chloride minerals such as halite or sylvite, which in deep sedimentary basins can occur as salt strata originally deposited during the evaporation of closed or restricted marine basins, millions of years ago. Solubilities of these minerals are orders of magnitude higher than those of calcite, anhydrite etc. If groundwater that has not travelled far comes into contact with halite then water will evolve directly to one with dominant chloride.

Large variations in the major cations commonly occur in groundwater flow systems. Since cation exchange commonly causes alterations or reversions in cation sequences, generalisation of cation evolution sequences would be of little use. Table 1.14 gives the solubilities of some common minerals in water at 25°C.

1.7.2 Interpreting Water Chemistry

Chemical analyses only show the gross makeup of a natural water sample, (i.e. the total amount of Ca, Mg in solution), rather than the concentration of individual free ions. Furthermore such analyses do not immediately reveal the thermodynamic state (or saturation level) of a water sample with respect to various common minerals such as calcite, gypsum, and dolomite. This information is important in determining if the solution is capable of

Table 1.14

Dissociation reactions, Equilibrium constants and solubilities of some minerals that dissolve congruently in water at 25°C

Mineral	Dissociation Reaction	Equilibrium constant	Solubility at pH 7 (mg/l)
Gibbsite	$Al_2O_3.2H_2O + H_2O = 2Al^{3+} + 6OH^-$	10^{-34}	.001
Quartz	$SiO_2 + 2H_2O = Si(OH)_4$	$10^{-3.7}$	12
Amorp. Silica	$SiO_2 + 2H_2O = Si(OH)_4$	$10^{-2.7}$	120
Fluorite	$CaF_2 = Ca^{2+} + 2\,F^-$	$10^{-9.8}$	160
Dolomite	$CaMg(CO_3)_2 = Ca^{2+} + Mg^{2+} + 2CO_3^{2-}$	10^{-17}	90* 480+
Calcite	$CaCO_3 = Ca^{2+} + CO_3^{2-}$	$10^{-8.4}$	100* 500+
Gypsum	$CaSO_4.2H_2O = Ca^{2+} + SO_4^{2-} + 2H_2O$	$10^{-4.5}$	2100
Sylvite	$KCl = K^+ + Cl^-$	$10^{+0.9}$	264000
Halite	$NaCl = Na^+ + Cl^-$	$10^{+1.6}$	360000

* pp CO_2 10^{-3} bar + pp CO_2 10^{-1} bar

further dissolution or precipitation of a given mineral, which allows conjecture about the past and present evolution of the water.

Some useful information can be gained by an examination of changes in total species, cation or anion ratio and other directly measured variables, but these say little about the thermodynamic state of the water. To resolve this problem computer programs have been written to interpret chemical data such as WATEQ ((Wigley (1977) and Truesdell and Jones (1974)). These programs break the sample into constituent parts. Most chemical species are present in solution in a number of forms including free ions and ion pairs which are loosely combined with other species. In addition the thermodynamic behaviour of a species in solution is determined by its activity rather than its concentration. WATEQ determines the detailed composition of the solution, the concentration and activity of all species in solution. Once the detailed composition is known it is possible to determine in a fundamental and precise way the level of saturation of the solution with respect to any mineral. The saturation level then determines whether the solution has the thermodynamic potential for further dissolution or for precipitation of that mineral. The charge balance error of dissolved species is also calculated which is useful in detecting gross errors in the chemical analyses.

1.8 Isotope Techniques in Hydrology

Groundwater dating is an important consideration in developing a water supply. In such a development it is important to determine the place and amount of recharge, and the rate of groundwater movement. It is therefore important to obtain a reliable mean age. A mixed water cannot however be reliably dated unless the proportions of each end member can be determined and dated independently (Evans et al, 1978).

Dating is also important when considering the use of aquifer rocks as a storage medium for radioactive waste.

The basic principle underlying the application of isotopes to the problem of groundwater tracing, is the use of the variation of the isotope input to determine the time and place of recharge. Other isotopes may be used to determine residence times as a fixed input decays during transport. The stable isotopes of water H-2, H-1, O-16 and O-18 are examples of the first use of isotopes. Radioactive isotopes which are of value in groundwater dating are listed in Table 1.15.

1.8.1 Stable Isotope Tracing

Information concerning groundwater recharge conditions can be obtained from studying the stable isotopes of hydrogen and oxygen which are contained in the water molecule. Oxygen is the most abundant element in the earth's crust, it has three stable isotopes whose

Table 1.15

Radionuclides of Atmospheric origin of potential use in groundwater dating

Nuclide	Half life (years)	Initial concentration in rainfall (dpm/l)
^{85}Kr	10.7	$< 10^{-8}$ dpm prior 1950
^{3}H	12.26	3.6 prior 1954
^{39}Ar	270	4×10^{-5}
^{32}Si	330	1×10^{-3}
^{14}C	5730	2×10^{-1}
^{81}Kr	210000	0.7×10^{-8}
^{36}Cl	301000	$1 \times 10^{-5} - 2 \times 10^{-4}$

abundances are O-16 99.756%, O-17 0.039%, and O-18 0.205%. Hydrogen has two stable isotopes whose abundances are H-1 99.985% and H-2 0.015%.

Differences in the isotopic composition of water reflect mass fractionation effects caused by evaporation and subsequent cloud condensation (Dansgaard, 1964). Providing no water-rock interaction takes place and there is no substantial mixing with other water sources the isotopic composition will be retained indefinitely.

Isotopic compositions of oxygen and hydrogen are reported in terms of differences in O-18/O-16 and H-2/H-1 ratios relative to a standard SMOW (standard mean ocean water). The deviation in isotopic composition from SMOW is expressed in terms of the delta value, i.e.

$$\delta^{18}O = \frac{(^{18}O/^{16}O)SPL - (^{18}O/^{16}O)SMOW}{(^{18}O/^{16}O)SMOW} \times 1000$$

$$\delta^{2}H = \frac{(^{2}H/^{1}H)SPL - (^{2}H/^{1}H)SMOW}{^{2}H/^{1}H)SMOW} \times 1000$$

The delta values are multiplied by 1000 to express the data in permil. Positive values of $\delta^{18}O$ and $\delta^{2}H$ indicate enrichment in O-18 and H-2 compared to SMOW, whilst negative values imply depletion in these isotopes.

Dansgaard (1964) has been largely responsible for deducing how hydrological and climatological information can be derived by plotting $\delta^{18}O$ against $\delta^{2}H$. The process of evaporation and condensation of oceanic water produces precipitation compositions which on a worldwide basis

gives the general relationship:

$$\delta^2H = 8\,\delta^{18}O + 10$$

Figure 1.6 shows the relationship graphically. Increments of an air mass undergoing equilibrium condensation would plot along a line towards progressively lighter compositions. This line would be characterised by a slope of 8 if the process can be described by Rayleigh fractionation. The equation for worldwide precipitation does have a slope of 8 but it is displaced by +10 permil in δ^2H relative to SMOW. If equilibrium condensation and evaporation were the only processes acting then the line would intersect the origin (SMOW) since all meteoric water is initially derived from the oceans. This deviation can be explained by a non equilibrium (kinetic) evaporation process. In regions where kinetic evaporation is dominant the local rainfall may plot with a slope <8 due to differing evaporation rates producing corresponding shifts in the composition of the first rains. In a similar way regions of excessive rainfall may give a slope >8. The local climate will therefore be indicated by the slope of the precipitation data, such data is plotted with the worldwide precipitation line for reference, and reflects the balance between equilibrium and non equilibrium processes.

Air masses which produce high latitude precipitation originate in the tropics, where extensive evaporation occurs. Here the kinetic evaporation produces rainfall

Figure 1.6

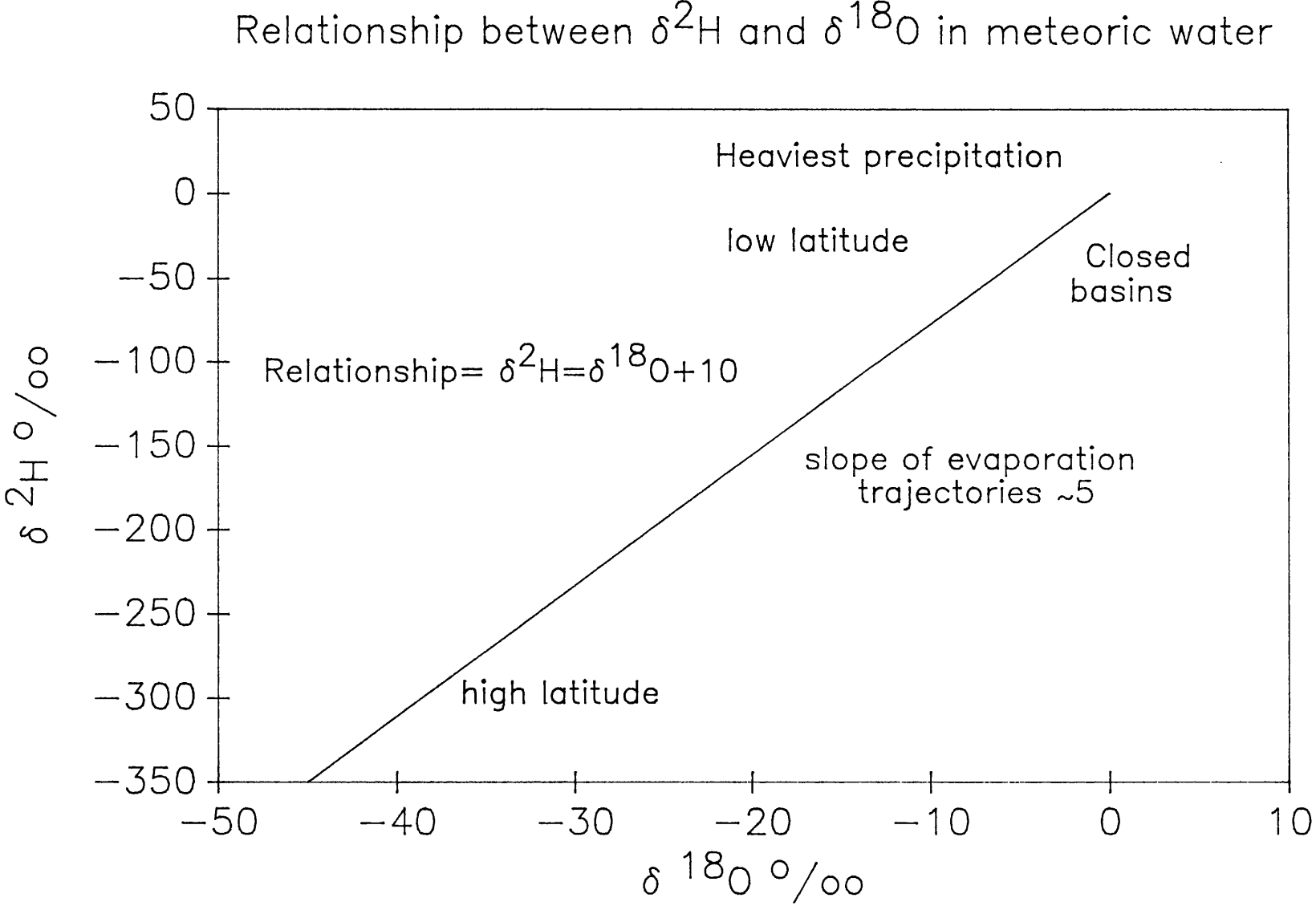
Relationship between δ^2H and $\delta^{18}O$ in meteoric water
Heaviest precipitation
low latitude
Closed basins
Relationship= $\delta^2H=\delta^{18}O+10$
slope of evaporation trajectories ~5
high latitude
50
0
−50
−100
−150
−200
−250
−300
−350
−50
−40
−30
−20
−10
0
10
δ^2H °/oo
$\delta^{18}O$ °/oo

enriched in O-16 and H-1. Subsequent condensation as the air mass tracks polewards produces rainfall progressively enriched in O-18 and H-2, thus producing a latitudinal effect in isotopic rainfall composition. This will also produce a continental effect as precipitation will become isotopically heavier as air masses pass over a continent. (Payne and Halevy, 1968).

Fractionation is affected by temperature at the time of condensation, the lower the temperature gives a greater depletion in heavy isotopes. This produces a variation of stable isotope composition with latitude (because of the relationship between Mean Annual Air temperature and latitude). In fact a relationship exists between $\delta^{18}O$ and average annual air temperature t:

$$\delta^{18}O = 0.69t - 13.6$$

where t is in °C.

Stable water isotopes have been used to identify the seasonal variation in rainfall (Payne and Halevy, 1968). Lake waters show the effect of open water evaporation in changing the slope of the $\delta^{18}O/\delta^{2}H$ graph. Waters subject to high temperature underground are identified through O-18 exchange (Craig, 1966).

Since there has been essentially no latitudinal variation in the position of Britain over the timescale of the Pleistocene, any variations in $\delta^{18}O$ and $\delta^{2}H$ in groundwaters will reflect climatological changes.

1.9 Dating Groundwater

Theoretical ages for groundwaters can be estimated in several ways: (1) The travel time can be estimated using Darcys law; (2) The decay of radionuclides which have entered the water from contact with the atmosphere; (3) The accumulation of products of radioactive reactions; (4) The degree of disequilibrium between radionuclides and their daughter products; (5) The time dependent changes in the molecular structure of molecular compounds dissolved in water; (6) The presence of man-made materials in groundwaters; (7) The correlation of known chronology of past climates with palaeoclimatic indicators; (8) The presence or absence of ions which can be related to past geologic events that have been previously dated.

Owing to the uncertainties in each method as many methods as possible should be used in each field situation. Because of hydrodynamic dispersion and molecular diffusion which always occurs a single precise age for a given groundwater does not exist. If dispersion, diffusion and cross mixing are minimal then ages are possible for waters less than 30,000 years old, and rough approximations for waters up to 1 million years old.

1.9.1 Dating with Radionuclides of atmospheric origin

Large numbers of radionuclides are produced continuously in the upper atmosphere by interactions

between gases and cosmic radiation (Lal and Peters, 1962) and (Oeschger H, 1978). Some of these are also produced in soil and surface water by deeply penetrating cosmic radiation.

During the past 35-40 years H-3, K-85 and C-14 have been masked by man made input. In the case of Kr-85 the original pre-1954 levels are masked by an enormous input. Natural H-3 levels are much larger and are still detectable in groundwaters older than 60 years. C-14 concentrations in groundwaters older than 35 years can easily be detected. Other radionuclides are not produced artificially in great quantities. The use of atmospherically derived radionuclides to date groundwater has been discussed by Davis (1979), Gaspar and Onescu (1972) and Freeze and Cherry (1979).

The fundamental assumption for all these dating methods is that the cosmic radiation flux has been constant with time and hence the atmospheric production rate is constant.

1.9.2 Tritium

Prior to 1954 H-3 was produced in small quantities by cosmic rays interacting with the upper atmosphere, by reactions such as:

N-14 (n, C-12) H-3

N-14 (n, 3 α) H-3

H-2 (n, γ) H-3

At this time rainwater H-3 levels were 10 Tritium units (1 T.U. = one H-3 atom per 10^{18} atoms of stable H). Testing of fusion devices since 1954 has injected large amounts of H-3. Because the half life is small (12.3 years) it is useful in dating recent recharge using the large concentration since 1952.

H-3 content of the atmosphere (and hence recharged water) varies with latitude, increasing towards the poles. It also varies with season, reaching a peak in summer and is 10 times more concentrated in the northern hemisphere than the southern. If H-3 were evenly distributed in space and time it would be ideal for dating young groundwater because it forms part of the water molecule. Unfortunately an accurate historical reconstruction of H-3 in recharge water is a difficult task (Carlston et al, 1960 and Libby, 1961). The complexity of the tritium content of the atmosphere is indicated by Figure 1.7.

The isotope hydrology section of the I.A.E.A. recommends following 3 divisions of tritium ages:

(1) Water with < 3 T.U. indicates groundwater age in excess of 20 years

(2) 3-20 T.U. indicates presence of H-3 from first fusion devices testing period 1953-1961

(3) Tritium in excess of 20 T.U. indicates water originating since 1961.

However these criterion require frequent modification because of the short half life involved, and are applicable only for mid-latitudes in the northern hemisphere.

Figure 1.7

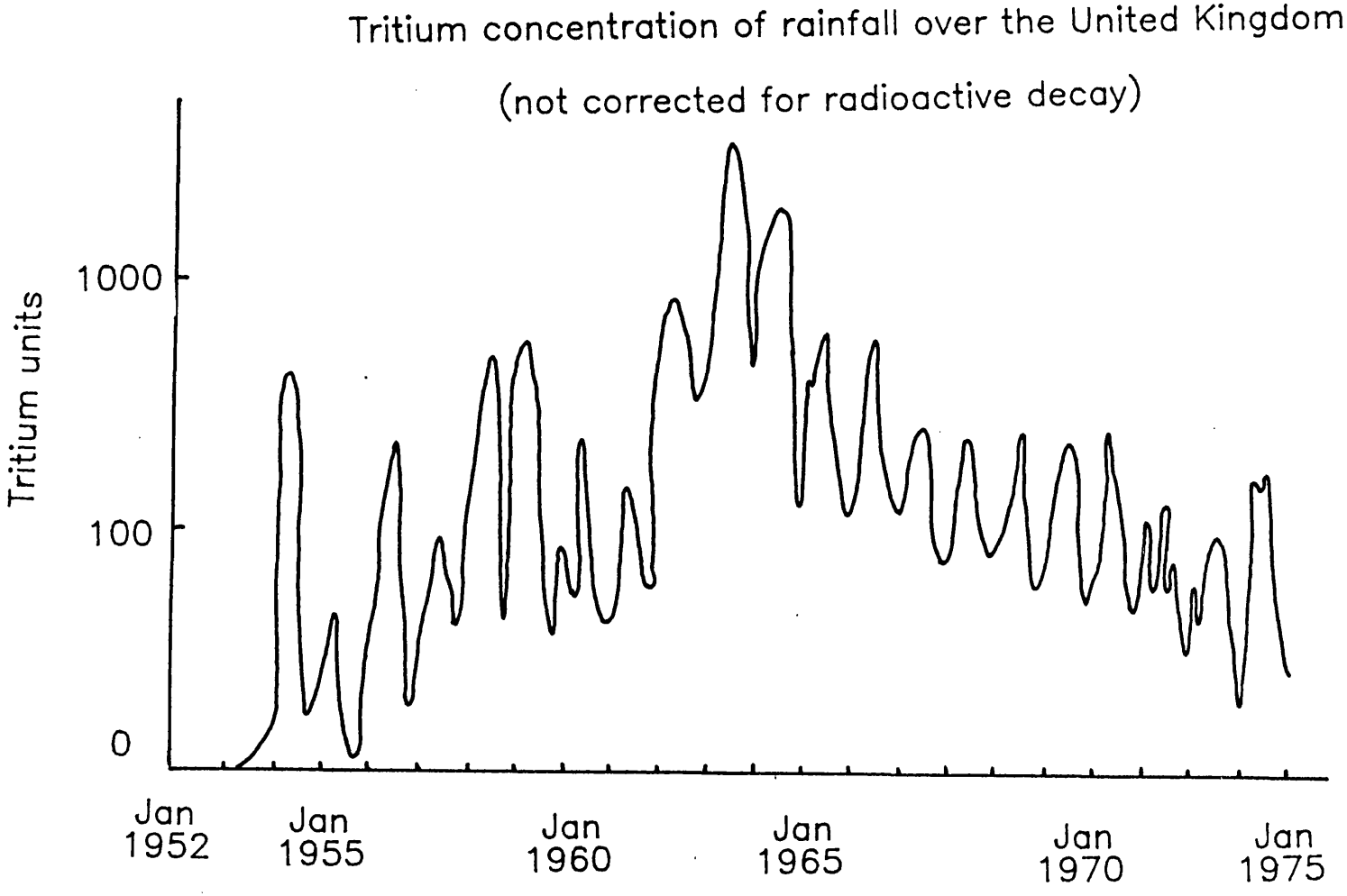
Tritium concentration of rainfall over the United Kingdom
(not corrected for radioactive decay)
Tritium units
1000
100
0
Jan 1952
Jan 1955
Jan 1960
Jan 1965
Jan 1970
Jan 1975

Tritium has been used for recharge studies in Australia (Allison and Hughes, 1975) and in arid sand dunes (Dincer et al, 1974).

Because H-3 decays to He-3 the original groundwater H-3 can be measured by determining the excess He-3 present (Torgerson et al, 1979). However H-3 has been shown to be produced in the subsurface by neutron fission of U-238, and by capture of thermal neutrons by Li-6. These processes normally only produce 0.5 T.U. but high Li and U concentrations can produce 1.5 T.U.

1.9.3. Carbon-14

Carbon-14 is produced in the atmosphere by interaction of N-14 with a neutron:

$$N\text{-}14\ (n,p)\ C\text{-}14$$

This C-14 is produced at a constant rate, and is quickly oxidised to CO_2 and can then enter the carbon cycle. Natural pre-thermonuclear weapons testing equilibrium content of C-14 is 1.2×10^{-12} g/g of carbon, which gives an activity of 16 d.p.m./g of carbon. C-14 decays by beta emission with a half life of 5683 years. With current high sensitivity counting techniques this gives a maximum useful age of 50,000 years (Ingrid and Karlen, 1963).

Many attempts have been made to date groundwater using C-14 (Fritz et al, 1979; Bath et al, 1978; Pearson and White, 1967). However there are numerous

difficulties. Firstly carbonate geochemistry, carbonate minerals are commonly in a state of near equilibrium with groundwater, and only slight changes in water temperature or chemistry will promote either dissolution or precipitation of carbonate ions. Thus the proportion of modern carbon in the groundwater can be changed and isotopic fractionation can occur. Secondly bicarbonate from ancient coal can predominate in a young groundwater. Thirdly C-14 can be produced in the subsurface limiting the extent of effective dating. Craig (1983) has listed the possible errors in C-14 dating and their importance. Nydal (1967) has found the average residence times for mixing of C-14 with various reservoirs to be in range two months to five years depending on the reservoir (stratosphere, troposphere).

Mixing of the troposphere with oceans averages 4.5 years. Evidence has been found for variation of the C-14 production rate with sunspot activity (Aegerter et al, 1967). As a result it has been necessary to calibrate the radiocarbon time scale.

Analytical results of C-14 determinations are commonly expressed as % of C-14 relative to modern pre-thermonuclear C-14. The apparent age is given by the equation:

$$t = 8267 \ \mathrm{Ln} \ {}^{Ao}/_{At}$$

where 8267 is the half life of C-14 in years

At is the activity of sample C-14 counts/min/gC

Ao is the activity of standard C-14 counts/min/gC.

If all carbon dissolved at recharge is CO_2 and of biogenic origin and no dilution with dead carbon occurs t is the age of water since recharge. Normally the situation is complicated by processes occurring within the aquifer such as dilution by non-radiogenic carbon and mixing of different aged waters. Various procedures have been reported for the correction by dilution of non radiogenic carbon. One method is based on the assessment of simple dilution of biogenic carbon by rock carbon from measured C-13/C-12 ratio of dissolved carbonates (Ingerson and Pearson, 1964). Evans et al (1978) identified two stages of C-14 dilution, firstly congruent solution which is dissolution of bedrock principally by:

$$CaCO_3 + CO_2 + H_2O \rightleftharpoons Ca^{2+} + 2HCO_3^-$$

Followed by incongruent solution and reprecipitation of carbonate minerals:

$$CaCO_3(s) + H_2O \rightleftharpoons CaCO_3\ (aq)$$

The problem remains that with incongruent solution C-14 is lost by precipitation and also fractionated from C-13 and C-12. Evans et al (1978) have made corrections for this fractionation.

Wigley (1976) used an alternative correction who considers the effect of incongruent solution on the fractionation of carbon isotopes and then combines this with the radioactive decay expression. A third method of

correction is given by Reardon and Fritz (1978) where C-14 ages are corrected by computer modelling of C-13 and C-14 with WATEQF (Plummer et al, 1970).

Other methods of correcting for dead carbon have been developed by Mook (1972) and Fontes and Garnier (1976).

1.9.4 Chlorine-36

Chlorine-36 was first suggested for use in dating groundwater because of its ideal half life. This covers the range from 50,000 to 1,000,000 years which is beyond the range of C-14. In addition chlorine in groundwater is neither derived from or reacts with the matrix. Thus the geochemical interpretations are not as formidable as with C-14.

At first conventional radioactive counting techniques were used but later a Van der Graaf generator coupled with a mass spectrometer has been utilized.

The variation in Cl-36/Cl x 10^{15} atoms are a function of latitude, age and proximity to the coast. The age of chloride in oceans is probably in excess of 10^8 years.

The effect of this dead marine chloride near the coast is clearly observed.

When Cl-36 enters the subsurface decay occurs and concentration of Cl-36 should decrease downdip. In one aquifer studied Cl-36 increased downdip, probably by upwelling of dead chloride from lower aquifers (Pearson and White, 1967). Lowering of sea levels reduces the

amount of dead chloride entering groundwaters and concentration of Cl-36 by higher evapotranspiration in arid climates could affect the measured ratios.

Complications which are also applicable to other radionuclides are: (1) isotope fractionation due to membrane effects of groundwater passing through silt and clay beds; (2) Cross formational flow of groundwaters in aquifers; (3) Possible diffusion of dead chloride from fluid inclusions; (4) Subsurface production of Cl-36 by neutron flux (Bentley); Subsurface production has been found to be significant after two half lives decay of recharge chloride. This limits the effective oldest dating to 1 million years.

1.9.5 Silicon-32

Silicon-32 has a half life intermediate between H-3 and C-14 and is thus important for dating between 50-1,000 years.

Most Si-32 dates are younger than comparable C-14 dates which can be explained by mixing of waters in shallow aquifers.

Si-32 has many problems, firstly the amount of Si-32 in fallout from nuclear tests has not been determined and also the amount of sub-surface production. The geochemistry of silicon is also complex and largely unknown which means at the present time it is an unreliable way of determining absolute age.

1.9.6 Krypton-81

Krypton-81 has a long half life beyond C-14. Its inert gas geochemistry greatly simplifies the interpretation of ages. The production of significant Kr-81 is confined to natural nuclear reactions in the atmosphere and in shallow horizons induced by cosmic radiation. Thus the subsurface production and artificial nuclear reactions should not complicate the interpretation. Unfortunately the low concentrations of Kr-81 requires processing of one million litres of water which can be source of contamination from the atmosphere.

1.9.7 Krypton-85

Almost all Kr-85 is produced from artificial nuclear fission. It has approximately the same half life as H-3, but has the advantage over H-3 that levels have been steadily increasing. This allows a more accurate estimation of the input to an aquifer. However because levels are low determinations require a minimum of 120-360 litres (Rozanski and Florkowski, 1978) of water.

1.9.8 Argon-39

The half life of Ar-39 applies it to dating of groundwaters from 50-2,000 years, between H-3 and C-14. The resulting dates are much younger than C-14. These discrepancies may be due to the large natural abundance of potassium, which makes the reaction.

K-39 (n, p) Ar-39

quite important. Under certain conditions subsurface production could exceed atmospheric input.

1.10 Uranium Series Disequilibrium in Groundwaters

In closed systems given sufficient time the members of a radioactive decay series will achieve secular equilibrium when the rate of production equals the removal rate by decay. The use of variations in U-234/U-238 activity ratio of dissolved uranium for groundwater dating is complicated by the fact that uranium does not form a closed system (Kronfield et al, 1975; Osmond et al, 1974; and Andrews and Kay, 1978).

The properties of U-234/U-238 disequilibrium which make it potentially useful are:

a) The isotope activity ratio variation is extreme, varying by a factor of 20.

b) The determination of abundances is straightforward using the α activity

c) The isotope U-234 is a daughter of U-238 and both the rate of disequilibrium development and decay are governed by the half life of U-234 (250,000 years).

Secular equilibrium between U-234 and U-238 in a rock matrix will be established according to the decay law -

$$^{234}At = {}^{238}\lambda \quad {}^{238}No \quad (1 - e^{-234\lambda t})$$

where ^{234}At is the activity of U-234 and No is the

original number of U-238 atoms present. Growth to equilibrium will be complete in 1.25 million years, during which time the decrease in U-238 will be insignificant. The mechanism by which disequilibrium in groundwaters is achieved are:

1) U-234 is preferentially leached from a lattice because it is in lattice damaged sites.
2) U-234 is more likely to form soluble uranyl complexes because it is in a higher oxidation state following electron stripping after decay of U-238.
3) Recoil itself produces disequilibrium as Th-234 atoms are ejected into solution or into grain boundaries where diffusion can easily occur (Kigoshi, 1976).

Dissolved Th-234 from alpha recoil will reach a maximum activity after 100 days of rock/water contact. The activity of U-234 will reach equilibrium with Th-234 after 1.25 million years, providing alpha recoil proceeds at a constant rate. Only Th-234 atoms formed by U-238 activity within the Th-234 recoil range can escape from the mineral. Only 23.5% of those generated in the alpha recoil thickness will escape from the mineral (Andrews and Wood).

The isotopic ratio for dissolved uranium is given by:

$$\frac{\text{U-234}}{\text{U-238}} = \frac{\text{U-234 from recoil + U-234 from etch}}{\text{U-238 from etch}}$$

The possibility of calculating activity ratios exists if the recoil range of Th-234 and etch rates can be

estimated.

The relative contributions of alpha recoil and chemical etch dictate the path along which U-234/U-238 activity ratio and groundwater uranium content will evolve. In an idealised situation the following changes may occur.

1) In upper regions of the aquifer the waters are oxidizing and tend to conserve uranium. U-234 enhancement will occur by preferential leaching from recoil sites.
2) In the second region the waters are more reducing and uranium is precipitated on surfaces. Alpha recoil solution from this uranium can produce considerable disequilibrium.
3) In lower regions uranium concentration in solution is very low because of precipitation. This region corresponds to a loss of U-234 by decay and a shift towards equilibrium. This is the only region which lends itself to the measurement of ages using uranium activity ratios (Osmond and Cowart, 1976; Andrews and Kay, 1978).

1.11 Radon in Groundwaters

The short half life of Rn-222 allows it to be in approximate equilibrium with Ra-226 in the surface of nearby rocks. The concentration in groundwater is less than that generated by Ra-226 as some is trapped in the

rock matrix (Andrews and Wood). There are four possible mechanisms by which Rn is released into the water phase.

a) Recoil of Rn atoms, following decay of Ra, directly into the water phase
b) Diffusion of Rn from the crystal lattice
c) Recoil into crystal imperfections followed by rapid diffusion
d) Release into porous secondary phases, i.e. cementing material followed by rapid diffusion.

The contribution of direct alpha recoil solution can be measured from the recoil range of Rn-222 in the matrix and the rock particle diameter. The diameter of most rock particles is very much greater than the recoil range of Rn-222 (.036 microns in glass of composition $Na_2OCaO6SiO_2$ (Heckter, 1934)). If radium is evenly distributed, the recoil escape percentage is given by 4.9/d where d is the particle diameter in microns. Therefore even for a small particle size of 100μm the recoil escape percentage is 0.049%, so this mechanism is negligible in most rocks.

If the mechanism of Rn release is principally diffusion in the lattice the rate of release is inversely proportional to the particle diameter. However it has been found to be inversely proportional to the square root of diameter for particles of carboniferous limestone, indicating the mechanism is primary recoil, or diffusion into crystal imperfections, followed by rapid diffusion to

the surface.

Radon released at the rock surface will be carried into the surrounding air or water by diffusion or solution transport. The concentration gradient normal to the rock surface caused by diffusion alone will be given by

$$Nx = No \quad e^{-x/L}$$

where Nx is number of atoms at distance x from surface

No is number of atoms at the surface

L is diffusion length = D/λ

D is diffusion coeffient of Rn-222

λ is decay constant of Rn-222

The concentration gradient normal to the rock surface caused by solution transport is given by

$$Nx = No \quad e^{-\lambda x/v}$$

where v is the velocity of water movement normal to the surface. The relative contributions to diffusion and solution transport are compared in Figure 1.8. Evidently solution transport is much more effective than diffusion.

The equilibrium Rn-222 content of a groundwater is related to the uranium content of the matrix ([U]r, μg/g) the bulk density (p, g/cm^3) and the rocks fractional porosity (Ø) by the equation.

$$[Rn] = \frac{F \times 0.7336 \times p \times [U]r \times 10^3}{\emptyset \quad 2.2 \times 10^6}$$

where [Rn] is the equilibrium radon content in μCi/kg, and

Figure 1.8

Relative radon concentration in water adjacent to rock surface due to radon movement by diffusion and by transport for various transport velocities (cm/s)

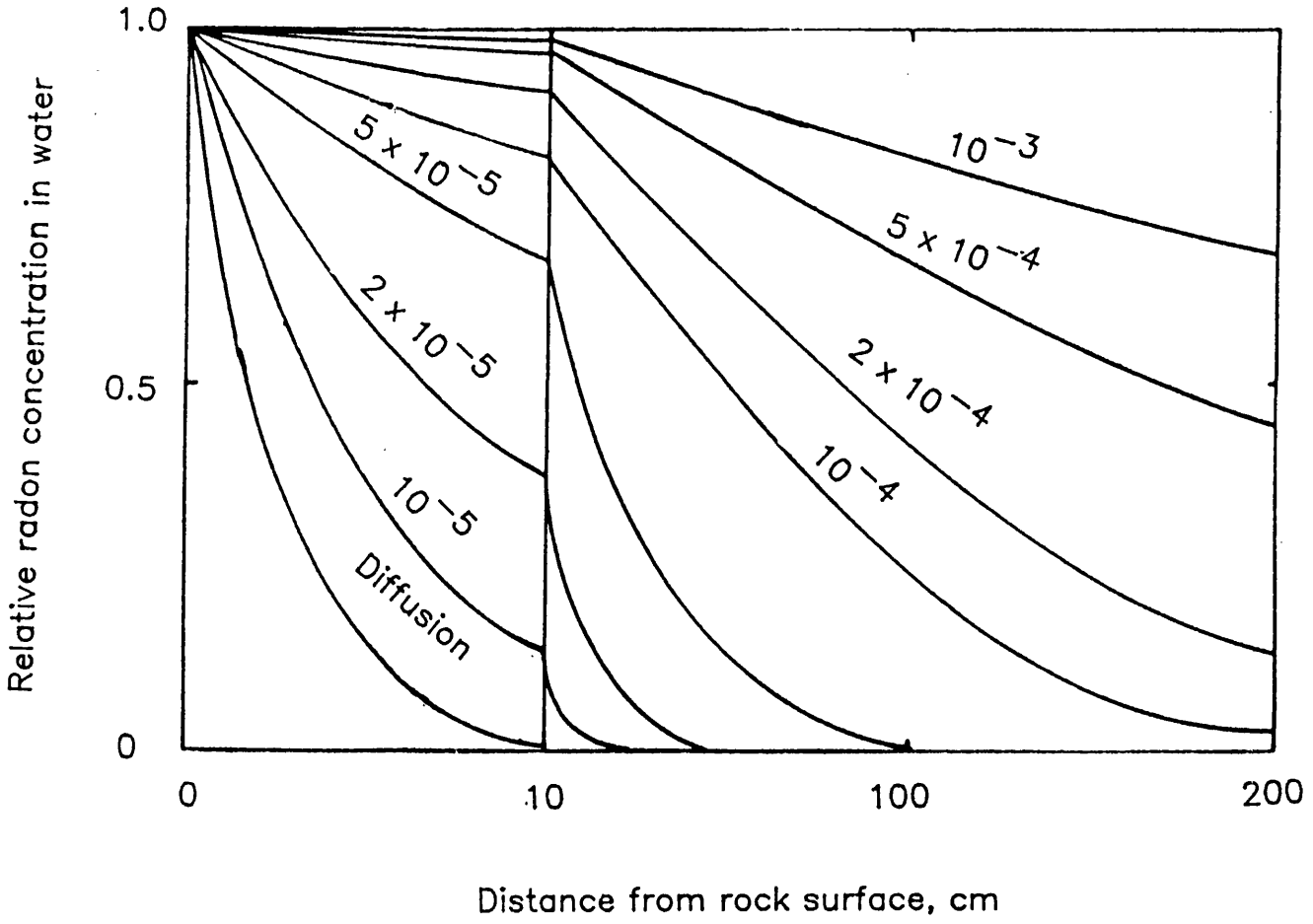

F is the fractional release efficiency of Rn-222. The value of F has been experimentally determined to be in the range 0.01-0.05.

Rn-222 has been used for locating geothermal reservoirs (Stoker and Kruger, 1975). High concentrations of radon have also been observed in groundwaters associated with oil and gas reservoirs (Mazor, 1962), in thermal springs (Chirkov, 1971) and in proximity of volcanic activity and faults (Rogers, 1956).

1.12 Radium in groundwaters

Equilibrium between U-238 and Ra-226 in a uranium bearing mineral will be established according to the equation

$$At = Ae\ (1 - e^{-\lambda t})$$

where At is activity of Ra-226 at time t

Ae is the equilibrium activity of Ra-226

λ is the Ra-226 decay constant.

Providing there is no geochemical separation of U-238 from Ra-226 equilibrium will be established in 8,000 years. Solution of radium is possible by a number of processes:

1) chemical solution by rock-etch process
2) decay of Th-230 in solution
3) alpha recoil solution of Ra-226 on decay of Th-230
   (a) which was deposited from solution onto the rock surface

(b) which was formed by U-234 decay in the rock surface.

The chemical solution of Ra-226 increases in importance as the salinity of the groundwater increases providing that sufficient Ba or Ca ions are present in solution. The residence time of Ra-226 in solution depends upon the congruent-incongruent solution of Ba and Ca as well as upon its half life (1620 years). The Ra content of recent groundwaters in karstic aquifers would therefore be expected to be proportional to their bicarbonate content. The formation of Ra-226 due to decay of Th-230 in solution is negligible since Th-230 is never present in solution to any significant extent.

Chemical solution of Ra-226 and U-238 from a mineral in radioactive equilibrium, will not result in a solution in equilibrium. The chemical conditions which favour Ra-226 release are very different to those that favour U release. Radium solution is favoured by high chlorinity, and is precipitated in carbonate waters as the highly insoluble carbonate. Uranium dissolves mainly in the form of complex uranyl ions in oxidizing waters and is deposited under reducing conditions.

Groundwater ages may be calculated from the equation

$$[Ra]_t = [Rn]_e \ (1 - e^{-226\lambda t})$$

where $[Rn]_e$ is the equilibrium radon content of the groundwater and $[Ra]_t$ is its Ra-226 content. The Ra-226 activity should then equal the Rn-222 activity after 8000

years. However the incongruent solution of calcium carbonate leads to precipitation of radium and prevents it ever attaining its equilibrium value in solution. Nevertheless high Ra-226 contents are indicators of groundwater maturation.

1.13 Inert Gases in Groundwater

The chemical inertness of the noble gases makes them ideal for deriving palaeoclimatic information from groundwaters. In principle their concentrations will reflect the conditions during initial water input into the aquifer, even though thousands of years may separate the time of recharge from the time of abstraction.

The initial inert gas concentrations are governed by the gas solubility laws. By applying the temperature/solubility curves to the observed concentrations the original surface temperature at the time of recharge may be determined. Identifying the likely gas concentrations at recharge may allow the presence of radiogenic inert gas to be determined.

The pattern of atmospheric noble gases provides information on recharge temperatures, the mode of recharge flow in the aerated zone (porous media or conduit flow dominated), sources of salinity (evaporation/dissolution), presence of oil in the fluid system, and degree of mixing with shallow water during recharge.

Mantle derived methane and carbon dioxide identifi-

cation is marked by the absence of atmospheric noble gases.

1.13.1 Modes of Recharge

Slow recharge through a homogenous porous medium or rapid recharge through a conduit dominated medium are the two types of flow in the unsaturated zone. Slow recharge allows the groundwater to attain the local ground temperature before it enters the saturated zone. Thus groundwaters reflect the local average annual temperature (Andrews and Lee, 1979). Conduit recharge is rapid and the recharged water reflects the annual temperature of the rainy season (Herzberg and Mazor, 1979).

1.13.2 Additions of Excess Air

Additions of excess air are recognisable by the specific patterns in the inert gas contents. High neon contents are a good indicator of excess air. The removal of excess air to leave inert gas contents due to equilibration at recharge is demonstrated later. The correction for Kr and Xe is minimal so the temperatures calculated by these gases may be the most reliable. Table 1.16 shows the effect of air contamination on the inert gas contents of air saturated water recharged at 15°C. Even 0.001cm^3 of air per cm^3 of air saturated water increases helium and neon contents by 10%.

Table 1.16 The Effect of air contamination on inert gas contents of air saturated water

		He	Ne	Ar	Kr	Xe
a.	Volume of gas in $1cm^3$ fresh water equilibrated with air at 15^oC (cm^3 STP)	4.6×10^{-8}	1.95×10^{-7}	3.5×10^{-4}	7.60×10^{-8}	10.5×10^{-9}
b.	Volume of gas in $0.01cm^3$ air (cm^3 STP)	5.0×10^{-8}	1.82×10^{-7}	0.9×10^{-4}	1.14×10^{-8}	0.9×10^{-9}
c.	Volume of gas in $0.001cm^3$ air (cm^3 STP)	0.5×10^{-8}	0.18×10^{-7}	0.1×10^{-4}	0.11×10^{-8}	0.1×10^{-9}
d.	Volume of gas in a 1% volume air contamination i.e. a + b (cm^3 STP)	9.6×10^{-8}	3.77×10^{-7}	4.4×10^{-4}	8.74×10^{-8}	11.4×10^{-9}
e.	Volume of gas in a 0.1% volume air contamination i.e. a + c (cm^3 STP)	5.1×10^{-8}	2.13×10^{-7}	3.6×10^{-4}	7.71×10^{-8}	10.6×10^{-9}
f.	Volume % contamination of each gas in e	10%	9%	3%	1.5%	1%

1.13.3 Gas Solubility Laws

Early work on the solubility of the inert noble gases was made by Morrison and Johnstone (1954) for pure water and by Konig (1963) for seawater. Since then more accurate experimental data has led to a refinement of the solubility data. Complementary to this, advances in statistical treatments and the use of computational techniques have been developed which model the behaviour of gas solubility in liquids. The 'Scaled-Particle Theory' has in particular shown some success in describing the distinct behaviour observed at room temperature for simple aqueous solutions as opposed to those in non polar solvents (Shoor and Gubbins, 1968). The predictions of this theory are based essentially upon the values of the molecular size parameters for both solute and solvent, the solvent density and its temperature dependence.

There are a number of conventions used to report naturally occurring gas concentrations in solution. Here it is defined as the number of cm^3 of gas at S.T.P. dissolved in cm^3 of water. The dissolved gas concentration, c, is proportional to the partial pressure of the gas above the solution, p (atm) by:

$$c = p.k.$$

where k is the Henrys law constant expressed in $cm^3/cm^3 H_2O/atm$.

In order to remove the effect of pressure and hence make comparisons between solubilities, the solubilities

are commonly reported under 1 atm. pressure for the gas in question. This value is known as the Bunsen coefficient.

1.13.3.1 The Inert Gases, Nitrogen and Oxygen

The most recent and comprehensive work for the solubility of the noble gases in pure water is the data given by Benson and Krause (1976). They fitted their data to the functional form:

$$\text{Ln } \frac{1}{K} = T_2 \, (T_1/T-1) + A_2 \, (T_1/T-1)^2$$

where T is the absolute temperature,

A_2 is a dimensionless constant = 36.855

T_1 and T_2 are constants specific to each gas.

Values for the constants are given in table 1.17. The Benson and Krause equation enables values of the Henrys law constant, K, to be determined in units of solute mole fraction per atmosphere. This is related to the Bunsen coefficient by:

$$\beta = \frac{1244.142.p}{K}$$

where p is the partial pressure. Inserting any chosen partial pressure value in, p, will give the corresponding solubility. The atmospheric partial pressures assumed for atmospherically equilibrated inert gas are listed in Table 1.17. The variation of the Bunsen coefficient with temperature for each of the gases is illustrated in Figure 1.9. The solubility of each gas depends strongly on

Table 1.17 Gas Solubility Parameters
(from Benson and Krause,1976)

Gas	T_1	T_2
He	131.42	41.824
Ne	142.5	41.667
Ar	168.87	40.404
Kr	179.21	39.781
Xe	188.78	39.273
N_2	162.02	41.712
O_2	168.85	40.622

Partial Pressures of Atmospheric Gases in Air

Gas	P (atm)
He	5.239×10^{-6}
Ne	1.818×10^{-5}
Ar	9.34×10^{-3}
Kr	1.139×10^{-6}
Xe	8.6×10^{-8}
N_2	0.7803
O_2	0.2099

Figure 1.9

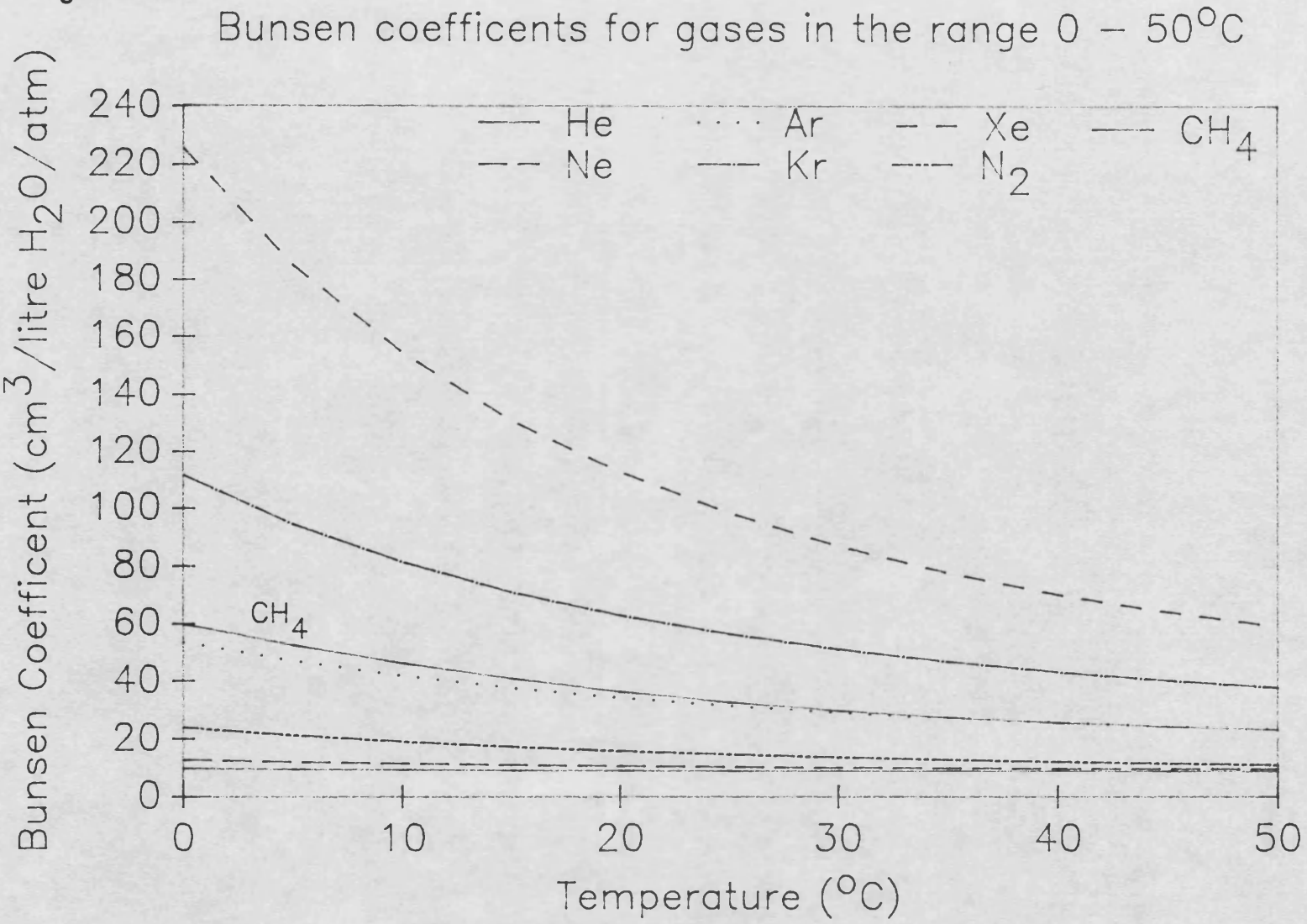
Bunsen coefficents for gases in the range 0 – 50°C
Bunsen Coefficent (cm³/litre H₂O/atm)
240
220
200
180
160
140
120
100
80
60
40
20
0
He
Ne
Ar
Kr
Xe
N₂
CH₄
CH₄
0
10
20
30
40
50
Temperature (°C)

Table 1.18 Bunsen Coefficents in the temperature range 0 - 50 °C

(cm^3/litre/atm)

T(°C)	He	Ne	Ar	Kr	Xe	N_2
0	9.53	12.62	53.5	111.4	225.5	23.65
5	9.27	11.93	46.9	94.2	184.8	20.96
10	9.07	11.36	41.66	81.16	154.1	18.80
15	8.92	10.9	37.5	70.9	130.6	17.1
20	8.82	10.53	34.1	62.7	112.4	15.6
25	8.76	10.24	31.3	56.2	98.1	14.5
30	8.74	10.00	29.01	50.9	86.7	13.5
35	8.75	9.83	27.13	46.6	77.5	12.7
40	8.80	9.70	25.58	43.0	70.0	12.0
45	8.87	9.62	24.28	40.0	63.9	11.47
50	8.96	9.57	23.20	37.6	58.9	11.00

temperature, and both the solubilities and the slope of the solubility/temperature graph increases with molecular weight of the gas. Table 1.18 lists the bunsen coefficients for gases in the temperature range 0-50°C.

1.13.3.2 Carbon Dioxide and Methane

The solubilities of carbon dioxide and methane are not included in recharge temperature estimation. This is because of their low atmospheric content and the high input of these gases after recharge. Stumm and Morgan (1970) and the International Critical Tables respectively list Henrys law constants for CO_2 and CH_4 (Table 1.19).The temperature solubility dependence of the Bunsen Coefficients was then fitted to the polynomial cubic equation of the form

$$\beta(cm^3/cm^3/atm) = AZ^3 + BZ^2 + CZ + D$$

where $Z = T(K)/100$.

The constants A, B, C and D for each of these gases are listed in Table 1.20. The solubilities of these gases are important when considering the total partial pressure of gas in equilibrium with a groundwater. This can then be used in assessing the likelihood of groundwater outgassing. This topic will be discussed in detail later.

1.13.4 The Effect of Salinity on Solubility

The gas solubilities in seawater or any saline aqueous solutions are effected by 'salting out', that is

Table 1.19

Henry's law Constants for Carbon Dioxide and Methane in pure water, (cc/l/atm)

T (C)	Carbon dioxide	Methane
0	1738	59.7
10	1202	45.9
20	871	36.1
30	661	29.5
40	513	25.4
50	428	23.0
60	372	19.9
70	325	18.7
80	298	18.2

Table 1.20

Parameters for calculation of Carbon Dioxide and Methane Bunsen Coefficents in pure water

Gas	A	B	C	D
CO_2	-6.5444	63.611	-207.2720	226.3128
CH_4	-0.1229	1.2416	-4.1919	4.7509

Figure 1.10

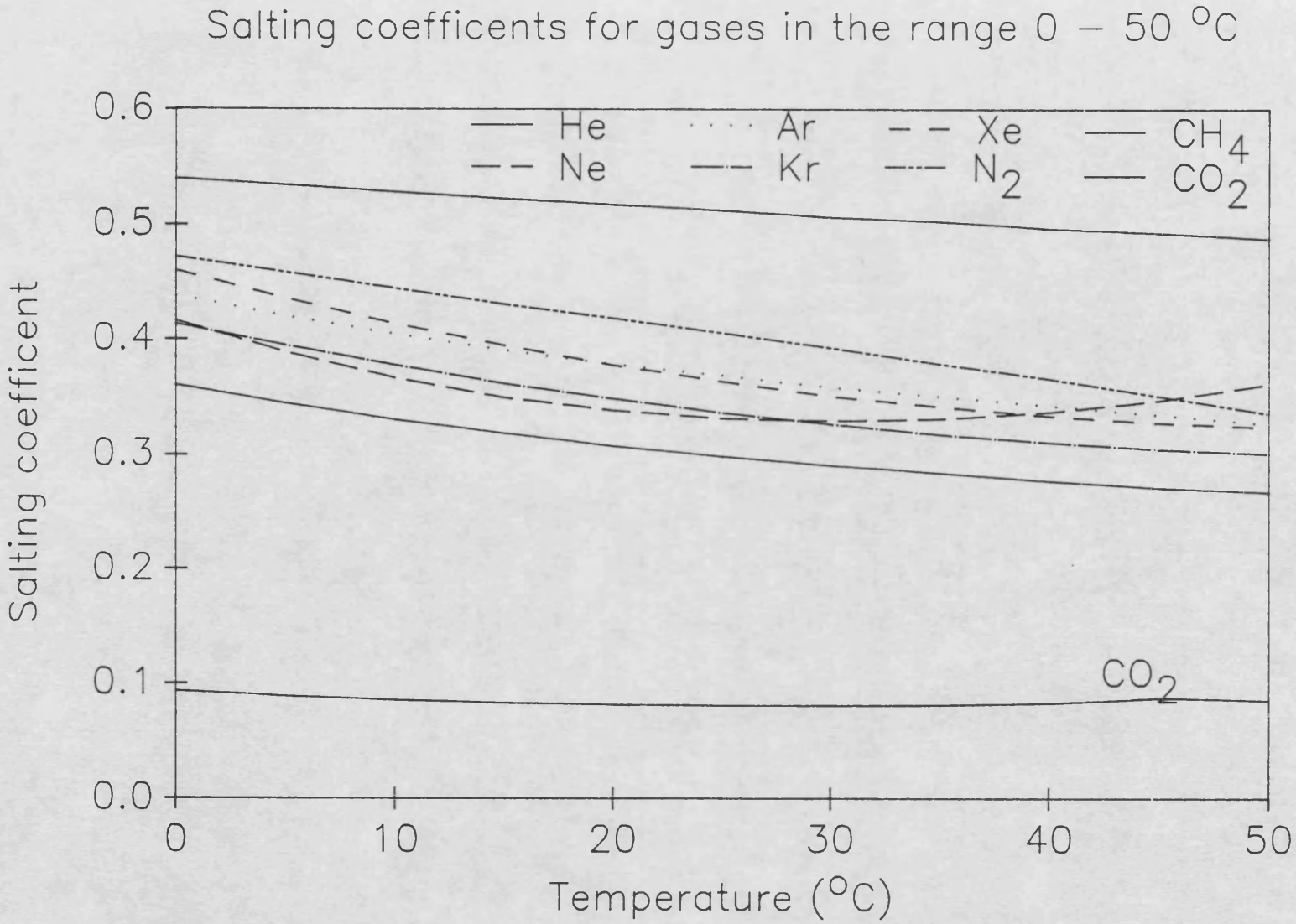
Salting coefficents for gases in the range 0 – 50 °C
Salting coefficent
0.6
0.5
0.4
0.3
0.2
0.1
0.0
He
Ne
Ar
Kr
Xe
N2
CH4
CO2
CO2
0
10
20
30
40
50
Temperature (°C)

the more saline the solution the less soluble the gases.

Providing air equilibration at recharge is with fresh water the initial gas concentrations are not effected by any addition of salts into the groundwater after recharge. If recharge occurs through a saline water body such as a sea then the original gas contents will be considerably lowered by salting out. Saline recharge will then be identifiable in the measured gas concentrations. The effect of 'salting out' is also important when assessing the possibility of outgassing of groundwaters prior to collection.

The salting-out effect can be modelled by the Setchenow equation, which states that at constant temperature the logarithm of the solubility coefficient is a linear function of salt-concentration, i.e.

$$\text{Ln} \quad (Bo_{/B}) \quad = \quad M.Ks$$

where Bo is the freshwater Bunsen coefficient at the temperature of interest, and M the alkali-halide molarity. The salting coefficient, Ks, can be either positive or negative, according to whether the non-electrolyte in solution is being salted in or salted-out. Ks varies with temperature but is independent of the molarity.

To find the salting coefficients for a range of temperatures, the solubility of each gas for a salinity of seawater was used with the freshwater solubilities to obtain values of Ks. Freshwater solubilities were obtained from Benson and Krause (1976) and seawater

salinities from Weiss (1970), (N_2,O_2, Ar); Weiss (1971), (He, Ne); Smith and Kennedy (1982), (Kr, Xe); Broecker (1974), (CO_2); and Shoor and Gubbins (1968), (CH_4). Repeating this procedure for a range of temperatures enables the Ks - temperature dependence to be listed.

Calculation of the saline water solubility requires determination of the alkali-halide molarity, M. In seawater the salinity (S) is related to the chlorinity (Cl) by:

$$S = 1.806.\ Cl \quad \text{(Brownlow, 1979).}$$

The molecular weight of the seawater solutes is therefore 1.806 multiplied by the atomic weight of chlorine (35.5) = 64.113. The molarity of a saline fluid is therefore:

$$M = \frac{S\ (ppm)}{64.113}$$

This approach is only applicable to waters of seawater composition. A true value of M will only be found using an analysis of the total ions in solution.

Each of the measured Ks/temperature lists were then fitted to a polynomial cubic equation, using the temperature variable:

$$Z = T(K)/100$$

to give the equation:

$$Ks = AZ^3 + BZ^2 + CZ + D$$

Table 1.21

Comparison of Atmosperically equilibrated gas concentrations in pure water and seawater

(cm^3/cm^3 H_2O)

Salinity = 0 mg/l

T(°C)	Ne ($\times 10^{-7}$)	Ar ($\times 10^{-4}$)	Kr ($\times 10^{-8}$)	Xe ($\times 10^{-8}$)	N_2 ($\times 10^{-2}$)
0	2.295	4.997	12.659	1.939	1.845
10	2.065	3.891	9.244	1.325	1.467
20	1.914	3.182	7.146	.967	1.220
30	1.819	2.710	5.796	.746	1.053
40	1.764	2.389	4.896	.602	.938

Salinity = 35.5 mg/l

T(°C)	Ne ($\times 10^{-7}$)	Ar ($\times 10^{-4}$)	Kr ($\times 10^{-8}$)	Xe ($\times 10^{-8}$)	N_2 ($\times 10^{-2}$)
0	1.823	3.921	10.070	1.503	1.421
10	1.686	3.111	7.503	1.054	1.147
20	1.588	2.580	5.893	0.785	0.968
30	1.516	2.222	4.839	0.614	0.848
40	1.464	1.977	4.123	0.501	0.767

Table 1.22

Salting Coefficents for modification of Bunsen Coefficents in the temperature range 0 - 50 °C

T(oC)	He	Ne	Ar	Kr	Xe	N_2	CH_4	CO_2
0	.360	.416	.438	.413	.46	.472	.540	.093
5	.344	.388	.42	.394	.435	.458	.534	.088
10	.330	.366	.404	.377	.413	.444	.528	.085
15	.318	.349	.390	.361	.394	.438	.522	.082
20	.307	.338	.378	.348	.377	.418	.517	.081
25	.298	.331	.368	.336	.363	.405	.512	.080
30	.290	.329	.358	.326	.350	.392	.506	.08
35	.283	.331	.35	.317	.341	.378	.502	.081
40	.276	.337	.342	.310	.333	.365	.496	.083
45	.270	.347	.334	.304	.327	.350	.492	.085
50	.266	.361	.326	.300	.323	.335	.487	.087

Table 1.23

Parameters for determination of salting coefficents

Gas	A	B	C	D
He	-0.2304	2.2951	-7.7154	9.0060
Ne	-0.3022	3.6278	-13.6641	16.8309
Ar	-0.4050	3.8471	-12.3389	13.6921
Kr	-0.1124	1.3282	-5.1432	6.8403
Xe	-0.1611	1.9007	-7.3019	9.5072
N_2	-0.2427	2.1504	-6.6100	7.4294
O_2	-0.3616	3.3454	-10.5501	11.6687
CH_4	-0.0210	0.2089	-0.7894	1.5653
CO_2	-0.0964	1.0183	-3.5065	4.0378

The parameters A, B, C, D used in calculating Ks are listed in Table 1.23. Figure 1.10 illustrates the temperature dependence of Ks for each gas. Table 1.21 lists the solubilities of some gases at salinities appropriate to fresh water and sea water. The original data for solubilities covers the range 0 to 40°C in temperature and up to seawater salinity. These data have been extrapolated to higher temperatures in some cases. A full list of salting coefficients is given in Table 1.22.

1.14 The Use of Helium in Hydrology

Helium is continually produced in the crust by decay of uranium and thorium in rocks. The wide geochemical distribution of uranium and thorium in rocks gives rise to a wide dispersal of helium in the crust. Depending on the structure at its site of production helium is either retained or diffuses away. The degree to which helium is retained at its site of production is important when considering both the determination of geological age and using helium as a groundwater tracer.

The possibility of using helium as a geological dating tool was first proposed by Rutherford (1906). Early attempts at dating minerals were unsuccessful because of helium leakage (Strutt, 1908). Further work found that some minerals retained more helium than others (Keevil, 1942 and Gerline, 1939).

Successful dating of minerals using helium has used

the few minerals which retain helium well. Schaeffer (1966) used He in aragonite to date fossil carbonates, and Damon and Green (1963) found dates comparable to K/Ar dates when minerals were carefully selected.

Once helium has diffused from the crystal lattice it may then diffuse rapidly and become dissolved in groundwater. If the helium generation rate is known then the minimum residence time of water in contact with rock can be determined.

High helium concentrations have been found associated with a number of geologic features. Clarke and Kugler (1973) suggested using the fact that radiation damage in high uranium containing minerals would lead to very high helium contents. Bulashevich and Bashorin (1971) have correlated high helium contents with structural faults. Nikonov (1969) found high helium contents in brines associated with hydrocarbon deposits. Roberts et al (1975) used helium contents for locating geothermal reservoirs.

1.14.1 He-4 Dating of Groundwater

The decay of one atom of U-238 to the stable Pb-206 releases 8 atoms of He-4, decay of one atom of Th-232 releases 6 atoms of He-4, and U-235 releases 7 atoms of He-4. Helium diffusing out of minerals should move into groundwater which fills the pores in rocks. Dating groundwater by means of the accumulation of radiogenic

helium was first suggested by Davis in 1966. The He-4 production per gram of rock per year when U and Th concentrations are expressed in parts per million is given by

$$[\text{He-4}]_r = 1.19 \times 10^{-13}[\text{U}] + 2.88 \times 10^{-14}[\text{Th}] \quad \text{cm}^3/\text{g rock/year}$$

The He-4 content of a groundwater after t years for an aquifer of porosity Ø is given by:

$$[\text{He}]_t = p\text{Ø}^{-1}t\,(1.19 \times 10^{-13}[\text{U}] + 2.88 \times 10^{-14}[\text{Th}])$$

where $[\text{He}]_t$ is in $\text{cm}^3\text{STP/cm}^3$ H_2O.

This equation assumes all the helium produced is dissolved in the groundwater.

Radiogenic He-4 has several advantages as a groundwater dating tool:

1) Helium is chemically inert. This lack of chemical interaction makes the behaviour of helium much easier to predict than that of other radionuclides useful for dating. In particular it avoids the precipitation-dissolution problems of C-14 and the ion filtration complications of Cl-36.
2) Helium exhibits minimal physical adsorbtion, due to its neutrality, small mass and small degree of polarizability. This results in negligible retardation during flow through aquifers.
3) In a medium with conductive fractures separated by less conductive aquifer matrix most tracers will be transported more slowly than the bulk water flow

rate. This retardation is due to retention in the less permeable material (matrix diffusion). Because helium is produced within the aquifer matrix, and diffuses outward toward more hydraulically conductive areas, it will not be affected by matrix diffusion retardation.

4) Methods which rely on decay of an atmospherically produced nuclide have an age limit where the nuclide has decayed below detection, or has become equal to a concentration produced by aquifer nuclear processes. Helium however will continue to accumulate providing the water is isolated.

For helium dating a fairly detailed knowledge of the various aquifer parameters is required. These are density, porosity and radioelement content. Rn-222 activities may be used to estimate the He-4 production rate from the aquifer providing the escape fraction of Rn-222 is known and the Th/U ratio. As radon is drawn from a larger volume than a normal core sample this gives a more representative estimation of U content.

Table 1.24 lists the helium production rate for some average rock matrices. The production rate varies by a factor of 10 for most aquifers, although in extreme situations of low radioelement content the rate of helium production may be up to 3 orders of magnitude lower.

Table 1.24 Production rate and isotopic ratio for radiogenic helium in various rock matrices

Rock Type	U content ug/g	Th content ug/g	Li content ug/g	He-4 production rate, cm^3/a	$^3He/^4He$ $x10^{-8}$
ultramafic	0.002	0.0045	0.5	3.69×10^{-16}	0.114
basalt	0.75	3.5	16.0	1.91×10^{-13}	1.30
granite	3.5	18.0	40.0	9.38×10^{-13}	2.23
sandstone	0.45	1.7	15.0	1.03×10^{-13}	0.58
limestone	2.2	1.7	5.0	3.12×10^{-13}	0.23
shale	3.2	11.0	60.0	7.00×10^{-13}	1.99

1.14.2 Helium Isotopes

He-3 is characterised by an extremely low nuclear binding energy and is unlikely to have resulted from radioactive decay. It is however emitted by fission of heavy nuclei (Fluss et al, 1972). The number of atoms of He-3 produced can be calculated (Andrews, 1984) and compared with the U-238 generation rate of He-4. This produces a He-3/He-4 ratio of 8×10^{-12}, thus fission produced negligible He-3.

Alpha particles from decay of uranium and thorium react with nuclei of light elements to produce a neutron flux by (α,n) reactions. As this neutron flux reaches epithermal energies the reaction with the nucleus of lithium produces He-3.

$$\text{Li-6} + \text{n} \longrightarrow \alpha + \text{H-3}$$

$$\text{H-3} \longrightarrow \text{He-3} + \beta$$

The fraction of neutrons produced in a rock matrix which interact with Li-6 must be calculated using the neutron cross sections and abundances of elements in the matrix (Andrews, 1984). Fiege et al (1968) identified the important (α,n) reactions responsible for the neutron flux. Table 1.24 shows the He-3/He-4 ratio produced in various model rocks using this approach, and the He-4 generation rates by decay of U-238 and Th-232 series elements. The elemental abundances for these rocks is taken from Parker (1967). The ratio of radiogenic He is independent of uranium content but depends strongly on the

lithium content. The Table 1.24 shows that his method produces He-3/He-4 ratios in the order of 10^{-8}, in agreement with those calculated by Gerling et al (1971).

Other possible sources of He-3 are

$$\text{Li-7} + \alpha \longrightarrow \text{B-8} + \text{H-3}$$

Kunz and Schntlemeister (1965) calculated this produces a He-3/He-4 ratio of 10^{-10} and is therefore not a significant source of He-3. The same authors also investigated the reaction:

$$\text{Li-7} + \gamma \longrightarrow \text{He-4} + \text{H-3}$$

this reaction produces helium with a ratio of 10^{-13}.

The reactions between lithium nuclei and thermal neutrons produce almost all the terrestial He-3. The conclusion of Morrison and Pine (1955) about the radiogenic origin of helium isotopes in ancient granitic rocks of the continental crust is confirmed. However, the measured He-3/He-4 ratios in young erupted rocks of possible mantle origin exceed these calculated values by 3 orders of magnitude.

1.14.3 Mantle Helium

The He-3/He-4 ratios in Icelandic fluids exceed radiogenic values by 3 orders of magnitude, to give a Mid-Atlantic ridge value of 3.3×10^{-5}. Craig and Lupton (1976) found value 2.1×10^{-5} from fumarole gas on Hawaii. Fluids from regions of high tectonic and magmatic activity

and high heat flow show high isotopic values of 1-3 x 10^{-5} (O'Nions and Oxburgh, 1983). Thus it appears mantle helium is enriched in the light isotope. Oceanic basalts have a value of 10^{-5} (Lupton and Craig, 1975) which is in full agreement with the idea of a He-3 excess in the deep interior of the earth. Other instances of excess He-3 have been reported by Clark et al (1969), Craig et al (1975) and Jenkins et al (1980).

1.14.4 The Use of He Isotopic Ratios in Dating of Groundwaters

The helium-3/helium-4 ratio of a groundwater is determined by the proportions of atmospheric and radiogenic helium present. The helium ratio may be used in two ways to deduce information on groundwater movement. These are: (1) Estimates of the mixing proportions of young and old waters (which contain radiogenic helium). (2) Estimates of the groundwater residence times in a confined aquifer in which radiogenic helium accumulates.

In groundwater mixing the helium ratio is given by:

$$RM = \frac{VaRa + VrRr}{Va + Vr}$$

where RM is the helium $^3/_4$ ratio

Va and Vr are the volumes of atmospheric and radiogenic He

Ra and Rr are the ratios for atmospheric and radiogenic helium.

If the isotopic ratio of the radiogenic component can be estimated using the rock matrix lithium content, and the value of atmospheric He $^3/_4$ ratio is 1.41×10^{-6} then the proportion of radiogenic helium can be estimated. This assumes there is no contribution from mantle helium. Figure 1.11 shows how the helium ratio changes for various radiogenic helium mixing with atmospheric helium.

Groundwater flowing downdip through aquifers flushes stored He from the rock. If the aquifer has a uniform radioelement and lithium content then the helium ratio can be used to calculate the groundwater age, t, using the equation:

$$Rt = \frac{\emptyset \, HA \, RA + p \, P_3 t}{\emptyset \, HA \, (1-RA) + p \, P_4 t} \qquad \text{(Andrews, 1984)}$$

where HA is the helium content at recharge

$\emptyset$ is the porosity

p is the bulk density

RA is the ratio of atmospheric helium

P_3 and P_4 are the production rates of helium 3 and 4

For groundwaters where the atmospheric input is small this reduces to

$$Rt = \frac{P_3}{P_4}$$

Figure 1.12 shows the change in ratio with age for a sandstone of lithium content of 60 ppm and a porosity of 0.1. It should be noted that influx of crustal helium

Figure 1.11

The $^3He/^4He$ ratio for mixtures of radiogenic helium with atmospheric helium

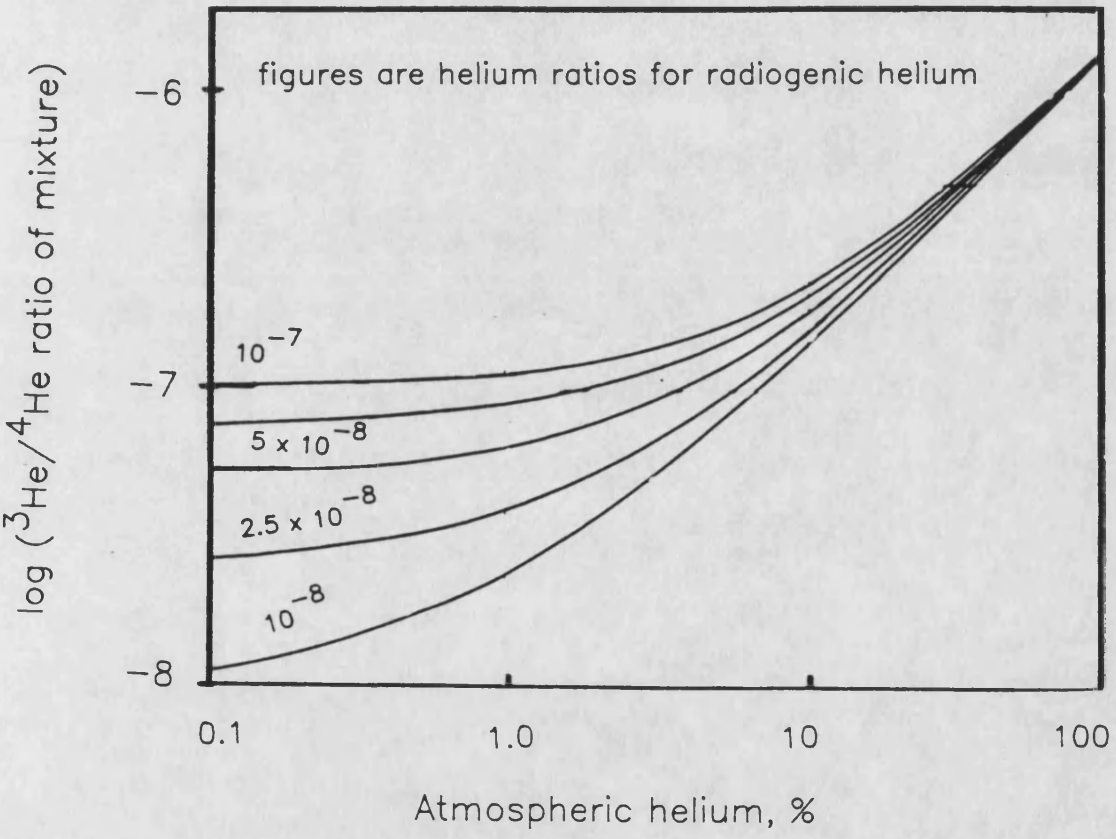

Figure 1.12

The change in $^3He/^4He$ ratio of dissolved helium as a consequence of radiogenic helium production for an average sandstone aquifer

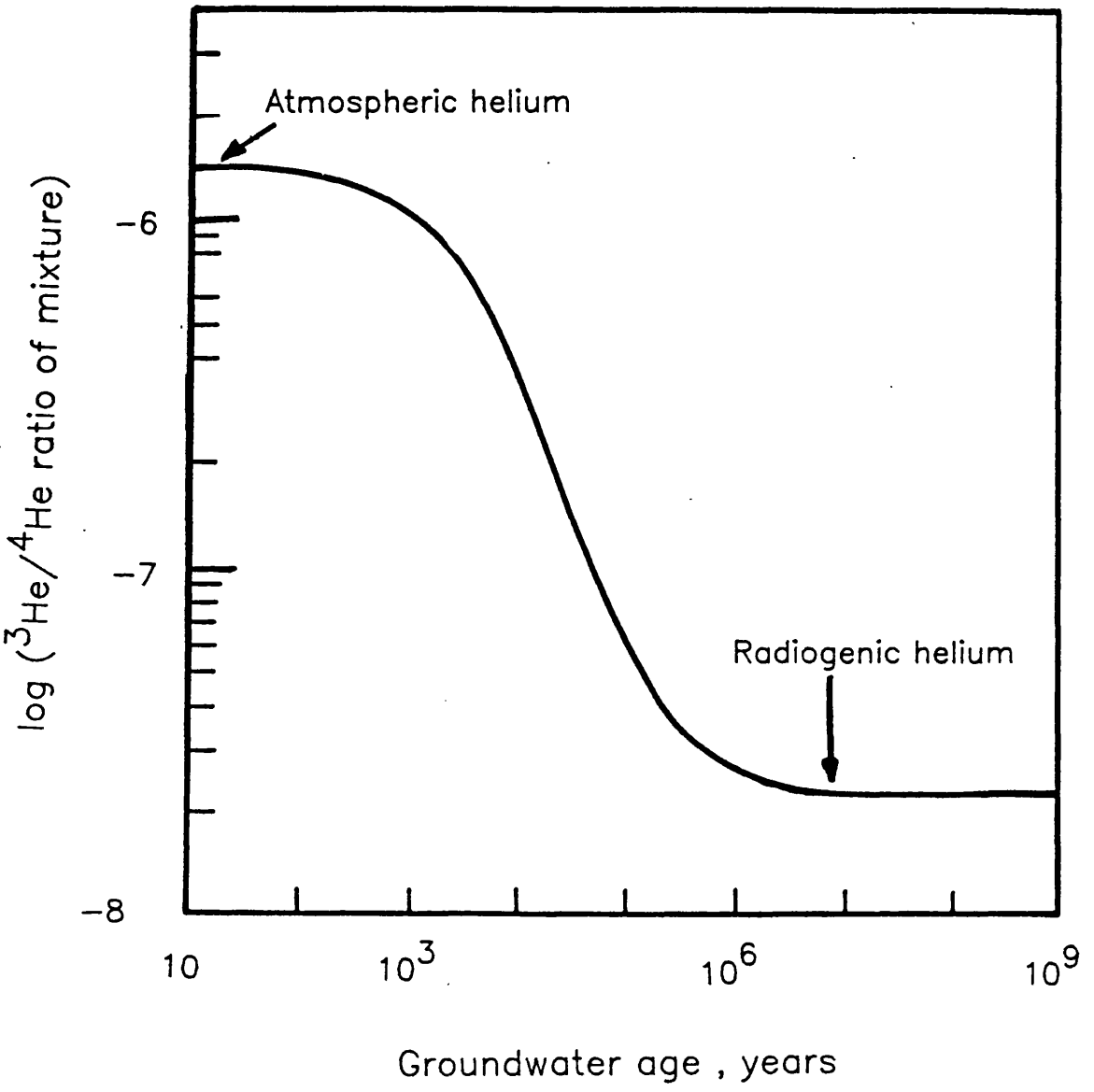

with the same isotopic ratio as the formation helium will produce an apparent older age. Also any input of mantle helium will have a very large effect on the helium ratio and severely limit the usefulness of this technique for dating. Thus this means of dating can only be applied when there is very limited influx of helium from outside of the aquifer, either crustal or mantle.

1.14.5 Diffusion of Helium in Aquifers

The low concentration of helium in the atmosphere permits a diffusive loss of aquifer helium and a concentration gradient dc/dz is established (where dc is the change in concentration of helium and dz the change in depth). Considering the crust as a thick layer of rock with a uniform radioelement content and a diffusion coefficient D the appropriate diffusion equation for change in helium concentration with time is:

$$\frac{dc}{dt} = G + D\frac{d^2c}{dz^2}$$

where $\frac{dc}{dt}$ is the rate of increase in helium atoms in a unit volume

G is the rate of generation of helium atoms by radioactive decay

$D\frac{d^2c}{dz^2}$ is the number of helium atoms entering the volume by diffusion from adjacent volumes in a z direction.

The conditions for this equation are:

1) At deposition of the aquifer the helium content is zero

2) The helium concentration at the aquifer/atmosphere interface is zero

3) When the depth is large there is no diffusion gradient for helium.

A simplified version of this diffusion equation is:

$$c\,(z,t) = G\,t\left[1-\exp\left(-\frac{2}{\pi^{0.5}}\cdot\frac{z}{(Dt)^{0.5}}\right)\right]$$

This gives the helium concentration at any depth and time to within 5% of the exact solution.

The helium concentration gradient near the surface, which has been generating helium for t years can be found by differentiating this equation, which when z = 0 yields:

$$\left(\frac{dc}{dz}\right)_o = 2\,G\left(\frac{t}{\pi D}\right)^{0.5}$$

and the helium flux at the surface is then:

$$D\left(\frac{dc}{dz}\right)_o = 2\,G\left(\frac{Dt}{\pi}\right)^{0.5}$$

The quantity $2\,(Dt/\pi)^{0.5}$ is the effective generation depth, as the surface flux is all generated within a layer of this depth. At depths greater than the effective generation depth the helium content is determined only by age and radioelement content.

The age and radioelement content of continental basement is such that they will contain 10 to 100 times

Figure 1.13

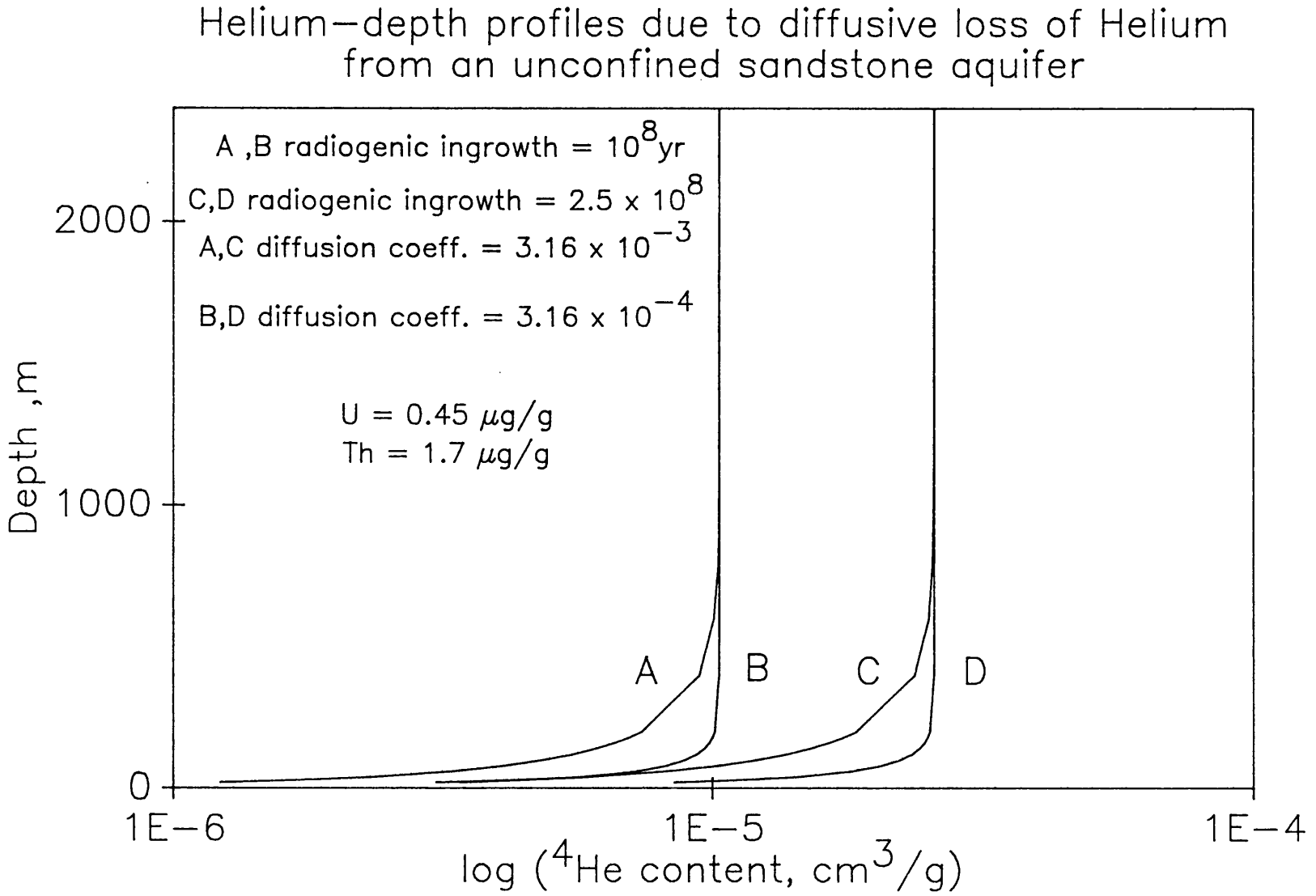
Helium–depth profiles due to diffusive loss of Helium
from an unconfined sandstone aquifer
A ,B radiogenic ingrowth = 10^8 yr
C,D radiogenic ingrowth = 2.5 x 10^8
A,C diffusion coeff. = 3.16 x 10^-3
B,D diffusion coeff. = 3.16 x 10^-4
U = 0.45 μg/g
Th = 1.7 μg/g
Depth ,m
2000
1000
0
A
B
C
D
1E–6
1E–5
1E–4
log (4He content, cm3/g)

Figure 1.14

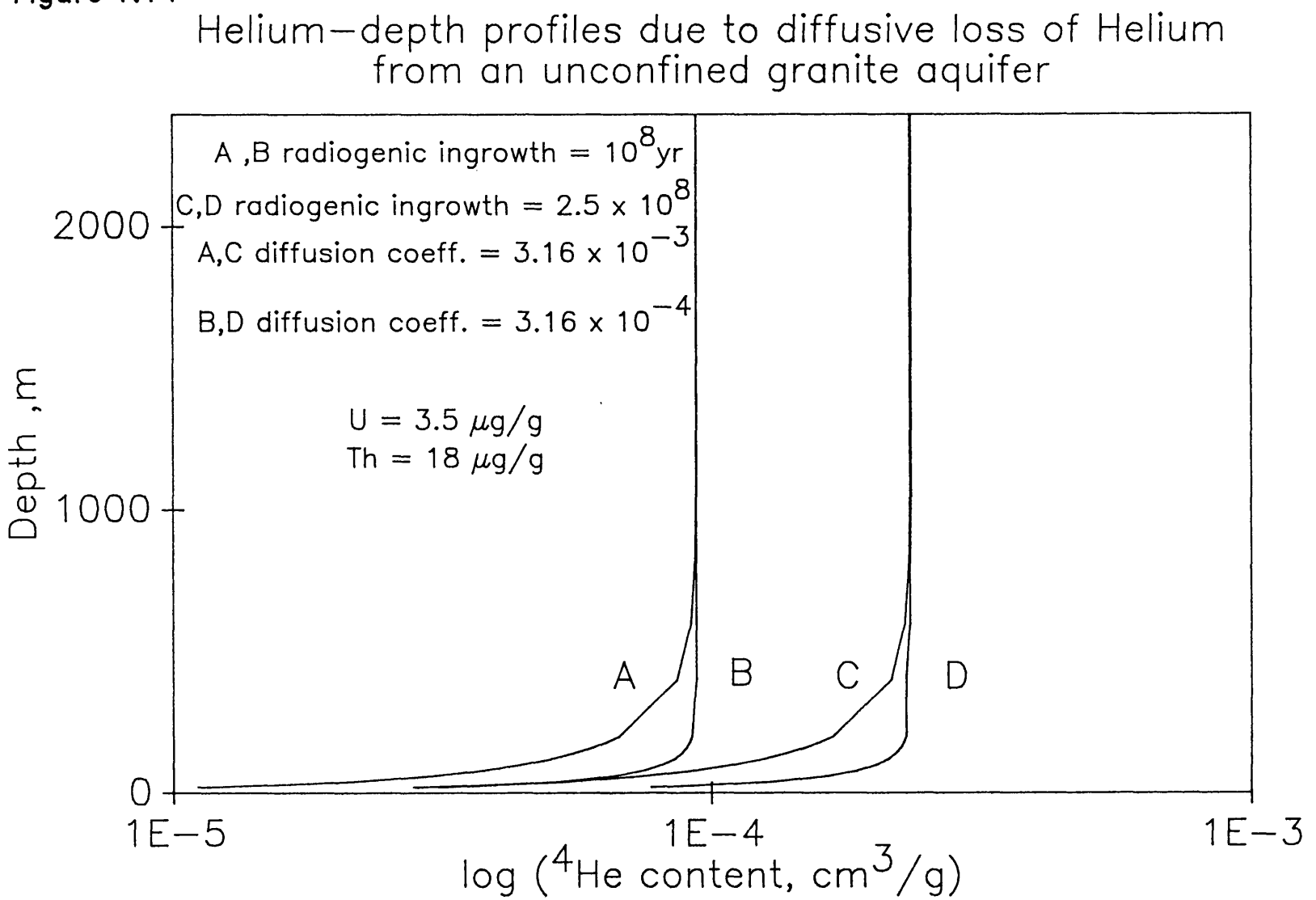
Helium–depth profiles due to diffusive loss of Helium
from an unconfined granite aquifer
A ,B radiogenic ingrowth = 10^8 yr
C,D radiogenic ingrowth = 2.5 x 10^8
A,C diffusion coeff. = 3.16 x 10^-3
B,D diffusion coeff. = 3.16 x 10^-4
U = 3.5 μg/g
Th = 18 μg/g
Depth ,m
2000
1000
0
A
B
C
D
1E–5
1E–4
1E–3
log (4He content, cm3/g)

the helium of most sediments. This means that diffusion of deep crustal helium into crustal sediments is a likely occurrence.

Helium profiles with depth have been generated. Figure 1.13 shows the situation for a sandstone aquifer. This assumes there is no diffusion into the layer from below. This figure illustrates the effect of changing the time over which radioelement decay has occurred and the diffusion coefficient of helium. The diffusion coeffficients chosen are intermediate between that for water and matrix diffusion. Even with the higher diffusion coefficient helium is effectively stored below 500 metres. Figure 1.14 shows a similar profile for a granite matrix with its corresponding higher radioelement content.

1.15 The Use of Radiogenic Argon in Hydrology

One of the assumptions necessary for K/Ar dating is that there is no diffusion of Ar from the site of production. For many minerals however the loss is significant and can be used as the basis of a qualitative dating method. Because of the quantity of Ar-40 dissolved at recharge is high the detection of additional radiogenic Ar-40 is made difficult.

1.15.1 Subsurface Production of Ar-40

The decay of K-40 produces stable Ca-40 and Ar-40. Although only 10.7% of the decay products of K-40 will be Ar-40 this is the primary source of new argon, because of the abundance of K-40. Using a half life of 1.28×10^9 years gives a production rate of 1.084×10^8 atoms of Ar-40 per gram of total potassium, which occupies a volume of 4.0×10^{-15} litres at STP. The change in Ar-40/Ar-36 ratio of a groundwater which accumulates radiogenic Ar is given by:

$$R = \frac{Vair(40) + Vrad(40)}{Vair(36)}$$

where Vair(40) and Vair(36) are the volumes of argon dissolved in the water at recharge and Vrad is the volume of radiogenic argon. The effect of adding radiogenic argon for water recharged at 10°C with no excess air is shown in Table 1.25. This table illustrates the importance of potassium content and porosity on the Ar-40/Ar-36 ratio. In each case the water must be 10,000 years old before any change in ratio is detected. For lower K contents and higher porosities this figure will be 100,000 years or older. These figures assume that all the radiogenic argon is released. Actually probably less than 10% is released so that changes in ratio by steady state release would not be observed for 1 million years. However enhanced ratios have been observed in groundwaters which are likely to be less than 100,000 years. This suggests that Ar-40 release into some groundwaters is not

Table 1.25

Subsurface production of Ar-40 and its effect on recharge Ar-40/Ar-36 ratios

Porosity %	1	1	10
Potassium content, %	10	5	5
Ar-40 production rate cm^3/cm^3 H_2O/year	1.04×10^{-10}	5.19×10^{-11}	5.19×10^{-12}
Water age (years)	Ar-36 / Ar-40 ratio		
10^4	296.3	295.9	295.5
10^5	303.4	299.5	295.9
10^6	376.0	334.9	299.4
5×10^6	690.4	492.6	315.2
10^7	1085	689.6	334.9

a steady state process and that very old Ar-40 is released by weathering processes. Mazor (1977) and Mazor and Fournier (1973) have used enhanced Ar-40/Ar-36 ratios to qualitatively date groundwater.

1.15.2 Subsurface Production of Ar-36

The Ar-40/Ar-36 method of groundwater dating discussed previously assumes that there is no subsurface production of Ar-36. Nevertheless Ar-36 is derived in the subsurface from the decay of Cl-36 which has a half life of 3×10^5 years. In a granitic rock the neutron flux would be large enough to produce 1.4×10^3 atoms of Cl-36 per gram of chlorine present. In an equilibrium situation 1.4×10^3 atoms of Ar-36 will be produced which occupies $5.2 \times 10^{-20} cm^3$ at STP.

In a fractured granite with a brine filling the pores with a 1% porosity then roughly 10^3 atoms of Cl-36 will be produced in a kilogram of rock per year. This is very much too small to affect the Ar-40/Ar-36 ratio. However in a uranium and thorium rich granite the production rate might easily be 10,000 times higher than in an ordinary rock. In this case the Ar-36 production might approach $^1/295.5$ of the Ar-40 production. This would make the identification of radiogenic argon very difficult as there would be no change in the observed Ar-40/Ar-36 ratio.

1.16 The Geochemistry of Nitrogen

Almost all nitrogen not contained in the earth's interior is in the form of N_2 molecules. Molecular nitrogen does not readily undergo transformations or form other nitrogen species, firstly because of its low reactivity and secondly because reactions which involve nitrogen are extremely slow. The process which makes the nitrogen of the atmosphere into combined nitrogen is fixation, involving the enzyme nitrogenase. Biological activity is solely responsible for nitrogen fixation, and the conversion of this amino-nitrogen to nitrate. This fixation of nitrogen is balanced by organisms which convert organic nitrates to gaseous nitrogen in the process of denitrification. The industrial fixation of nitrogen now equals the natural fixation in terrestial ecosystems (Delwiche, 1970). Most denitryfying bacteria are facultatively anaerobic this means that under oxidizing conditions they respire by reduction of oxygen. Once oxygen availability diminishes the bacteria respires by using nitrate. A bacterial denitryfying population is most likely limited to the availability of organic carbon and nitrogen.

Nitrogen gas in groundwaters has three possible sources. The most important in young groundwaters is that dissolved during equilibration of water with the atmosphere. The concentration is governed by solubility laws and the nitrogen partial pressure. The quantity of

nitrogen may be increased soon after recharge by denitrification. This will depend on the availability of nitrate, and denitryfying bacteria and also on the nutrient supply to the bacteria. Another source of nitrogen is thermodegradation of nitrogen containing hydrocarbons. This can be an important source and may add nitrogen in the quantities dissolved at recharge.

The microbiological nitrogen cycle is shown in Figure 1.14.

1.16.1 The Use of Nitrogen/Argon Ratios in Hydrology

The concentration of argon stays constant in groundwaters after recharge, except for possibly small quantities of radiogenic argon. The N_2/Ar ratio therefore provides an index of elevated nitrogen concentrations. As argon is the most abundant inert gas this particular ratio is experimentally the easiest to measure.

Measurements of N_2/Ar ratios have been applied to marine environments (Benson and Parker, 1961) and soil atmospheres (Focht, 1978). N_2/Ar values in soils are variable, however values have been found above the atmospheric value of 83.54 which can only be due to denitrification. These soil atmosphere studies are important as such atmospheres subsequently dissolve into groundwaters.

A component of nitrogen formed by denitrification has been recognised by Vogel et al (1981) in a study of the

Figure 1.15

The microbiological Nitrogen cycle

Numbers in brackets refer to the oxidation state of nitrogen

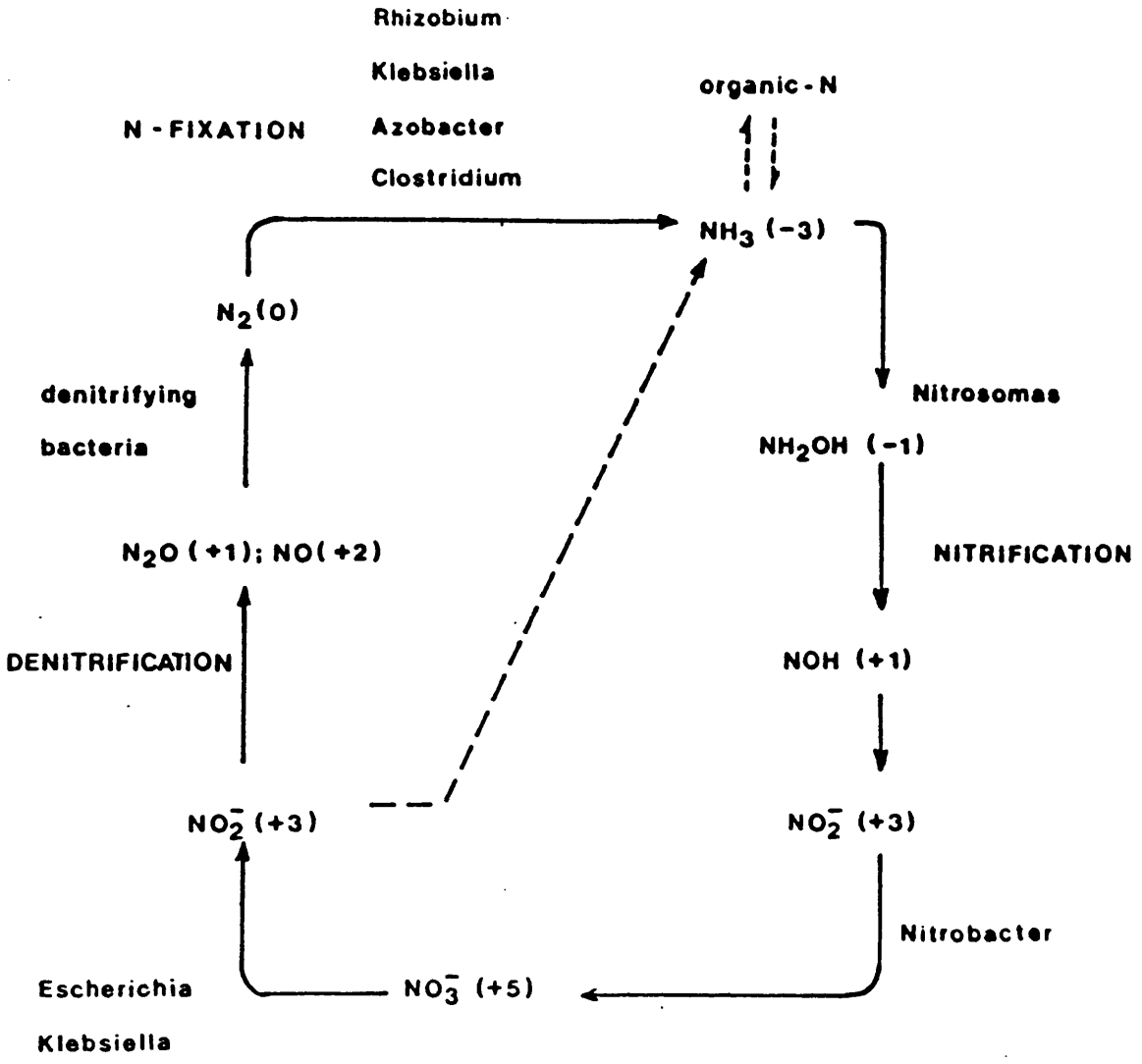

Auob sandstone of the Western Kalahari Desert. Here N_2/Ar ratio have been measured up to 73, which represents significant extra nitrogen over the recharge value of around 38 for air equilibrated water.

1.17 Methane in Groundwater

Methane does not form any significant proportion of air and therefore very little is present in groundwaters at recharge. However it is possible for large concentrations of methane to exist in groundwater. There are two sources for this methane: (1) Bacterial fermentation and (2) thermodegradation of organic matter.

Bacterial fermentation follows the reaction:

$$C \text{ organic} + 2H_2O \longrightarrow CO_2 + CH_4$$

This occurs only under very low values of pE when oxygen, nitrate and sulphate have all been reduced. Methanes produced in this way have delta C-13 values of around -60. Water which produce methane by fermentation will have low values of CH_4/N_2 ratio since nitrogen will be formed by similar processes.

Methane produced by thermodegration of organic matter will have isotopically much heavier delta C-13 value of -25. Waters containing methane produced by thermodegradation will have higher CH_4/N_2 ratios as very little nitrogen is produced by these processes. Thermodegradation is also likely to produce higher gaseous hydrocarbons such as ethane, while fermentation will produce nearly

exclusively methane.

The amount of methane present in groundwaters is important to quantify for two reasons. Firstly from a safety viewpoint as methane forms explosive mixtures with air. Secondly high methane contents can induce outgassing in groundwaters before collection for dissolved gas analysis. The importance of methane in outgassing processes will be discussed in detail.

CHAPTER 2

EXPERIMENTAL METHODS

2.1 ^{222}Rn Determination

The most reliable method for the determination of Rn-222 and its parent ^{226}Ra, in air and water is by recovery of the ^{222}Rn gas. In the case of water samples ^{222}Rn is outgassed using dry air. The gas stream is then dried and then trapped on an adsorbent for transfer into a scintillation flask for alpha counting.

2.1.1 Sample Collection

Samples for ^{222}Rn analysis are collected in $300cm^3$ stainless steel vessels with a metal valve at each end. Prior to collection the vessels are flushed with water to remove all the air present. If outgassing of the water is likely then water samples may be collected under pressure as for inert gas copper tube samples.

Air samples are taken by simply opening an evacuated scintillation flask at the sampling site. Large flasks of approximately $250cm^3$ volume are used for this purpose.

2.1.2 Recovery of ^{222}Rn from Water Samples

^{222}Rn is recovered by passing dry air through the cylinder. The air stream is then dried firstly with calcium chloride and then concentrated sulphuric acid. The dry gas is then passed over a trap containing activated charcoal at -80°C to absorb the ^{222}Rn. The effluent from the trap is then recirculated through the water. In this way Rn cannot be lost from the closed

system. Generally a minimum of 10 sample volumes of gas are passed through the sample at a rate not exceeding 1 litre per minute. This ensures Rn is quantitatively removed from the water. The drying line for Rn is shown in Figure 2.1.

The recovered Rn is transferred from the charcoal trap to a flask coated in ZnS(Ag) scintillator. The counting efficiencies of the scintillation flasks are determined using standard radium solutions which have been stored to ensure equilibrium with ^{222}Rn.

The charcoal trap still maintained at -80°C is connected to a vacuum system (Figure 2.2) and pumped to 5×10^{-2} mbar. The trap is then isolated from the vacuum and the trap heated to 200°C in a furnace. After 10-15 minutes, when complete desorbtion of the Rn has occurred, air is slowly admitted through the vacuum system to flush Rn into the scintillation flask.

2.1.3 ^{222}Rn Counting by Alpha Scintillation

The α-particle counting rate was determined after a delay of 3 hours to allow ingrowth of ^{214}Po in the decay series.

$$^{222}Rn \xrightarrow{\alpha} {}^{218}Po \xrightarrow{\alpha} {}^{214}Pb \xrightarrow{\beta} {}^{214}Bi \xrightarrow{\beta} {}^{214}Po$$

Details of this decay scheme can be found in appendix A.

The scintillation flask is placed on the photocathode window of a 3 inch diameter photomultiplier. The particle emission from ^{222}Rn and its daughters was

Figure 2.1
Apparatus for ^{222}Rn outgassing and recovery on activated charcoal

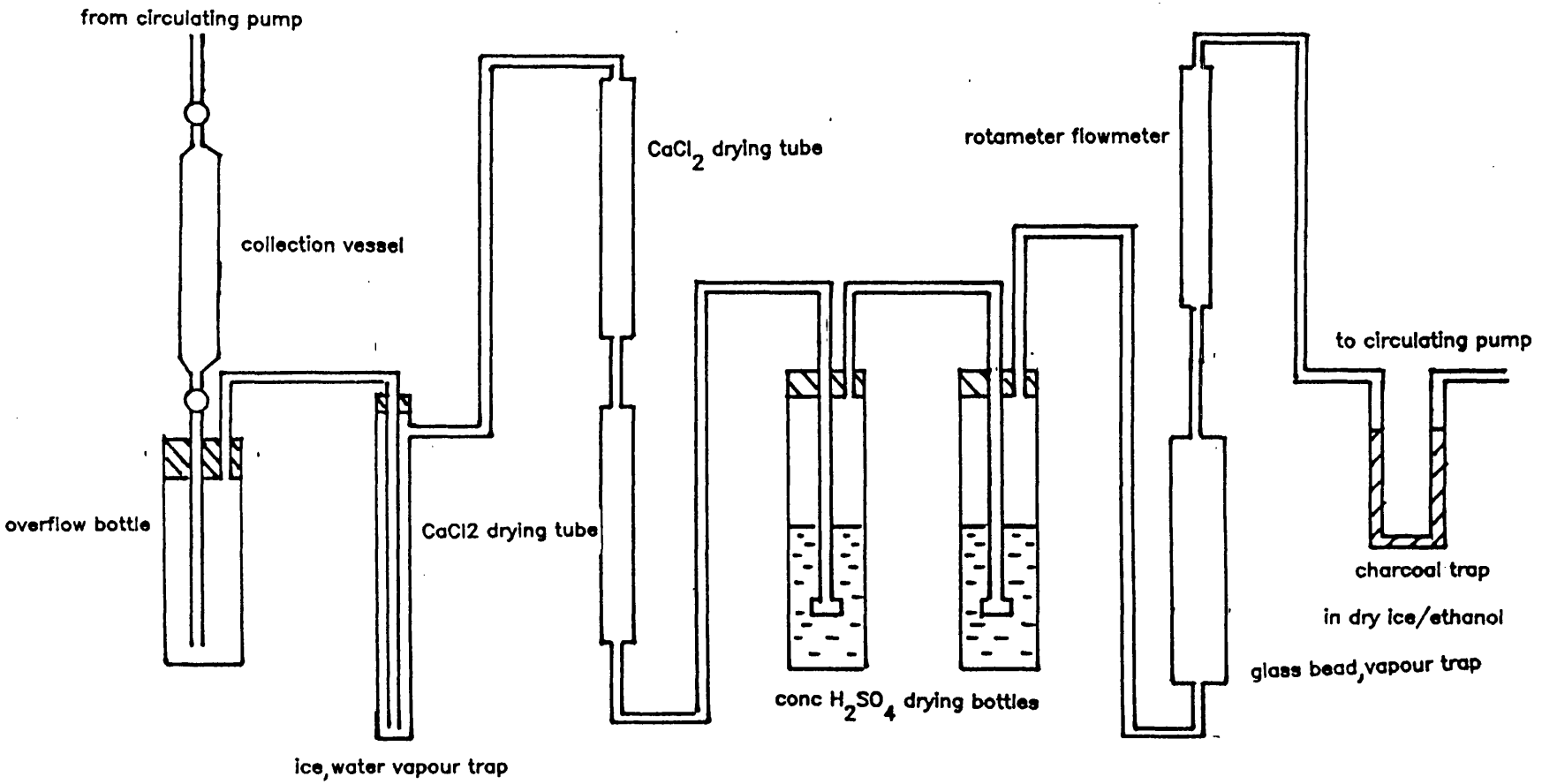

Figure 2.2

Apparatus for loading ^{222}Rn into a Scintillation Flask

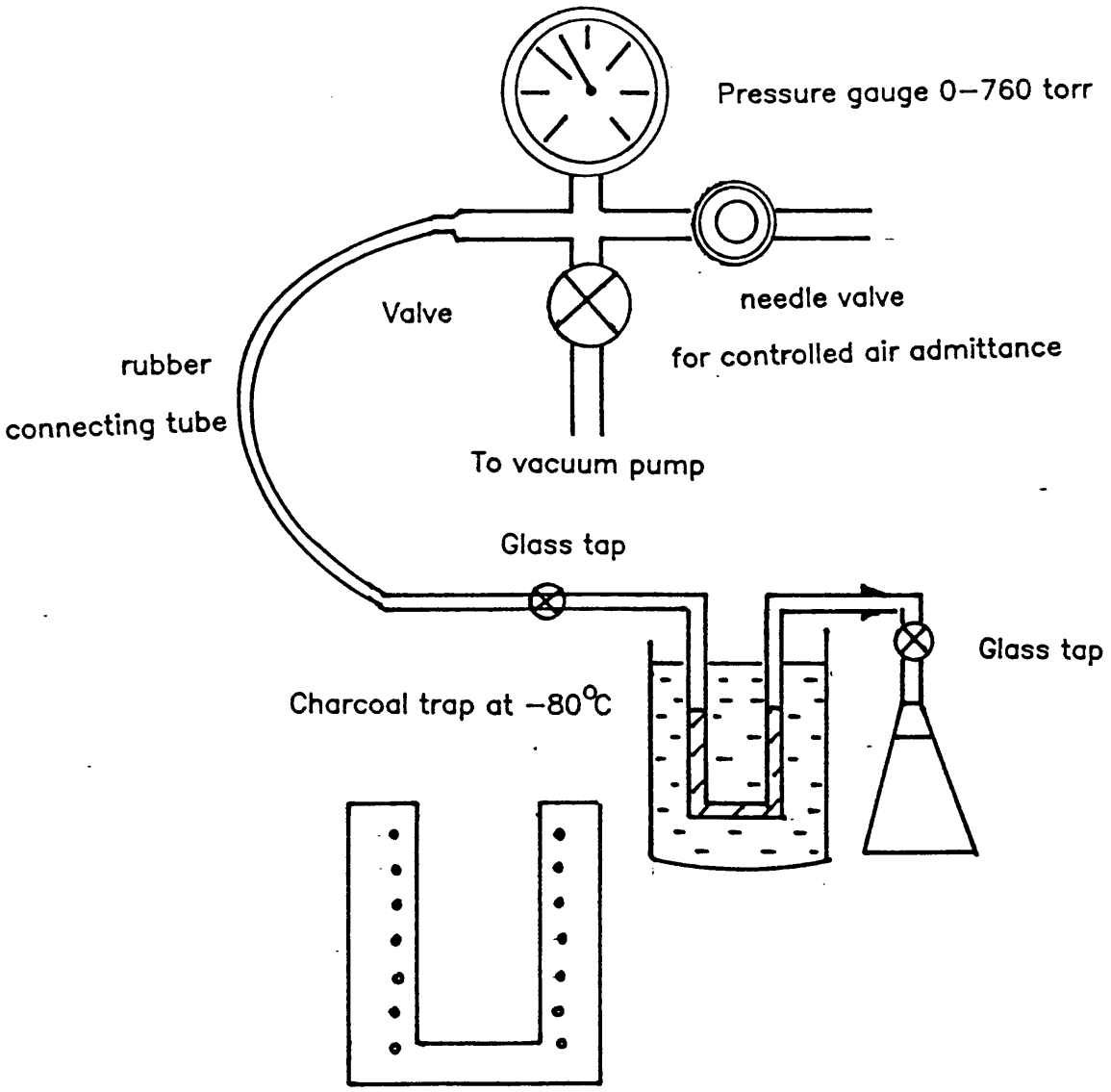

recorded with a pulse amplifier/scaler system. Figure 2.3 gives details of the counting geometry.

The counting efficiency of a scintillation flask is around 4 counts per minute per pCi of ^{222}Rn. The flask backgrounds are less than 0.5 counts per minute. This background slowly increases with use due to accumulation of ^{210}Pb. For this reason backgrounds are periodically determined, especially when high activities have been measured.

2.2 ^{226}Ra Determination

^{226}Ra was determined by estimating the equilibrium ^{222}Rn activity.

2.2.1 Sample Collection

Samples are collected in 5 litre plastic containers. Immediately after collection samples are acidified to pH2 with 6M hydrochloric acid. Samples are filtered using a 0.45 micron filter before analysis. In the laboratory samples are transferred to 5 litre glass bottles which are impermeable to radon. Since the ^{222}Rn contents of groundwaters are much greater than the ^{226}Ra contents, the excess ^{222}Rn was removed by degassing before radium determination. The removal of excess radon must be 99.9% efficient to avoid errors in the radium determination, this was achieved by outgassing with 20 times the water volume with bottled nitrogen. The samples were then

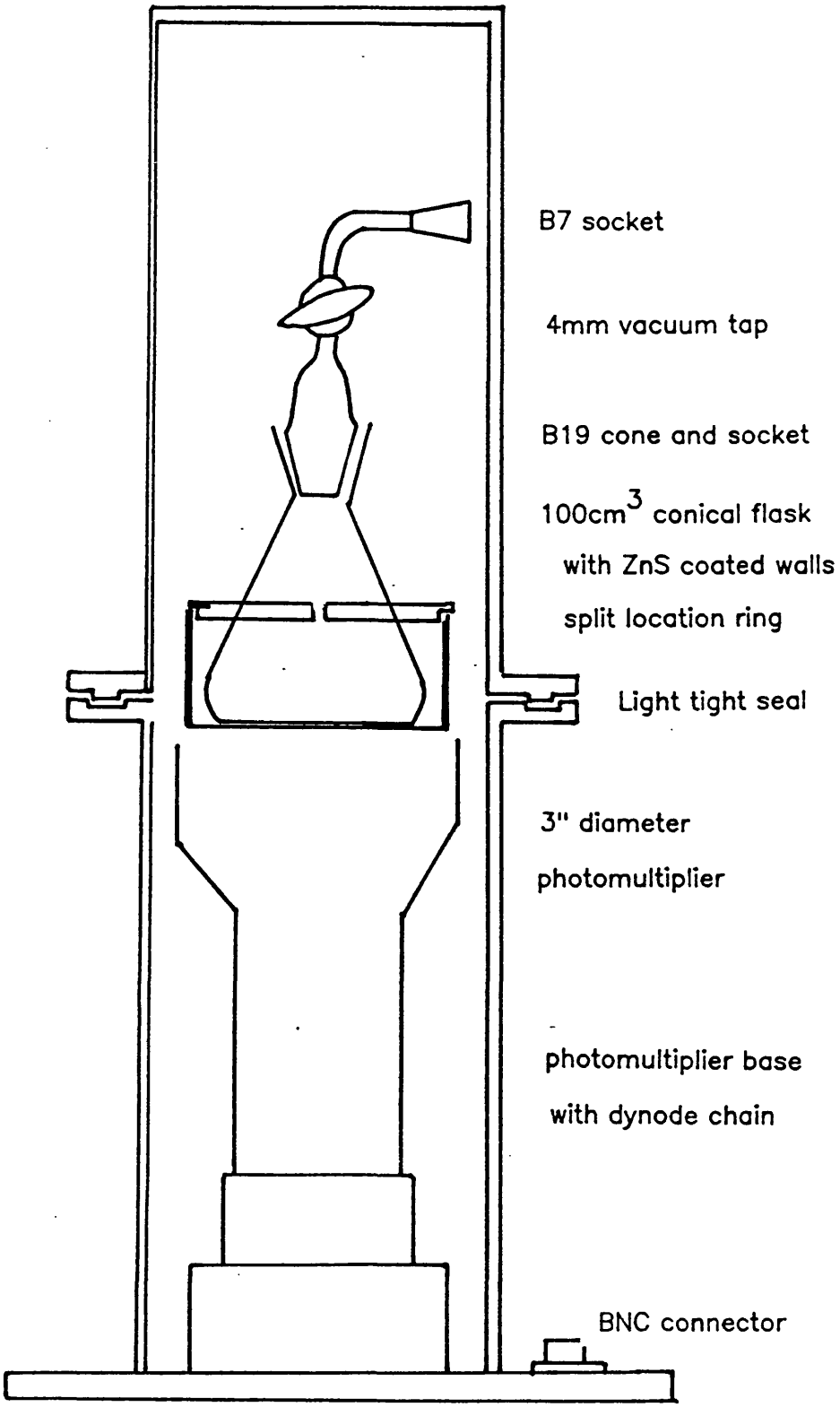

Figure 2.3

Scintillation flask and photomultiplier assembly for α-counting of ^{222}Rn and its daughters

sealed and allowed to stand for 20 days to permit ingrowth of ^{222}Rn.

2.2.2 ^{226} Ra Counting

After storage and ingrowth of ^{222}Rn, the radon is extracted and measured as for the determination of ^{222}Rn as described previously.

2.3 Determination of ^{222}Rn by Gamma Spectrometry

Occasionally samples with very high ^{222}Rn activities are encountered. Alpha scintillation counting is not necessary and would rapidly increase the backgrounds of these scintillation flasks. An alternative method is to count the charcoal traps which have the ^{222}Rn absorbed on them. After the ^{222}Rn absorbtion is complete the trap ends are sealed and then removed from the dry ice bath. This is then placed on a 6 x 4 inch NaI gamma spectrometer. The NaI gamma counter is fully described in the sections dealing with radiolement contents of rocks. The ^{214}Pb and ^{214}Bi peaks are then counted after the 3 hours ingrowth time.

Calibration of the system is achieved by outgassing a standard containing 0.37μg ^{226}Ra which has attained euqilibrium onto a charcoal trap.

The method should only be used when ^{222}Rn activities are greater than 1 μCi/kg. This is only likely to be found in granitic aquifers with high uranium contents.

2.4 Errors in the Determination of Rn-222 and Ra-226

One important error for Rn amd Ra determination by alpha counting is the counting error. This can be minimized by using large sample volumes. A litre sample containing 100 pCi/litre of Rn-222 would require a counting time of 40 minutes to reduce the statistical counting error to 2%. The counting time for a similar Rn content to achieve 1% error will be 400 minutes. For Rn-222 the usual 300cm^3 samples may be counted in 200 minutes for an average Rn content of 100-500 pCi/litre to achieve acceptable counting errors.

The much lower Ra-226 contents of 1 pCi/litre require much larger samples or longer count times. A 5 litre sample would need at least 1000 minutes counting time.

Errors due to standard preparation are likely to be very small as all dilutions are carried out by weighing. The primary standard has an overall uncertainty of 5%, which is passed onto the flask calibration.

Since the de-emanation technique for radon and radium involves the quantitative transfer of Rn-222 errors due to the transfer of radon from solution to scintillation flask will be small. At least 95% of the Rn is transferred providing minimum outgassing times are adhered to.

The overall precision for Rn and Ra analysis is +/- 5%. The precision for duplicate determinations will be +/- 2%. However due to losses at collection Rn deter-

minations will frequently have much larger errors up to +/- 20%.

2.5 Inert Gases in Groundwaters

2.5.1 Collection of Samples for Inert Gas Analysis

Samples for noble gas analysis were collected in 5cm^3 annealed copper tubes, isolated between pinch off clamps, which effected a vacuum tight cold weld of the copper tube. Details of the copper tube collecting technique are given in Figure 2.4 and a pinch off clamp is detailed in Figure 2.5. For noble gas analyses it is important that the sampling methods adopted should prevent gas losses and thus preserve dissolved gases in the same amount as they are present in the formation. The amount of gases which are present in solution at formation pressures generally exceed the amounts of gases present in solution due to the process of air equilibration during recharge (Chapter 6). The causes of such excess gas solution are briefly: (1) solution of excess air entrained at recharge; (2) solution of radiogenic gases (He and Ar), and (3) solution of biogenic and/or thermogenic gases such as CO_2, CH_4 and N_2. To avoid degassing the flow is restricted to increase the applied pressure. After pressurisation a restricted flow must be continued for sufficient time to remove the column of water in which degassing may have occurred. Figure 2.6 shows the well head apparatus used to collect inert gas

Figure 2.4 Copper tube ready for collection of a water sample (shown in an aluminium holder before sealing)

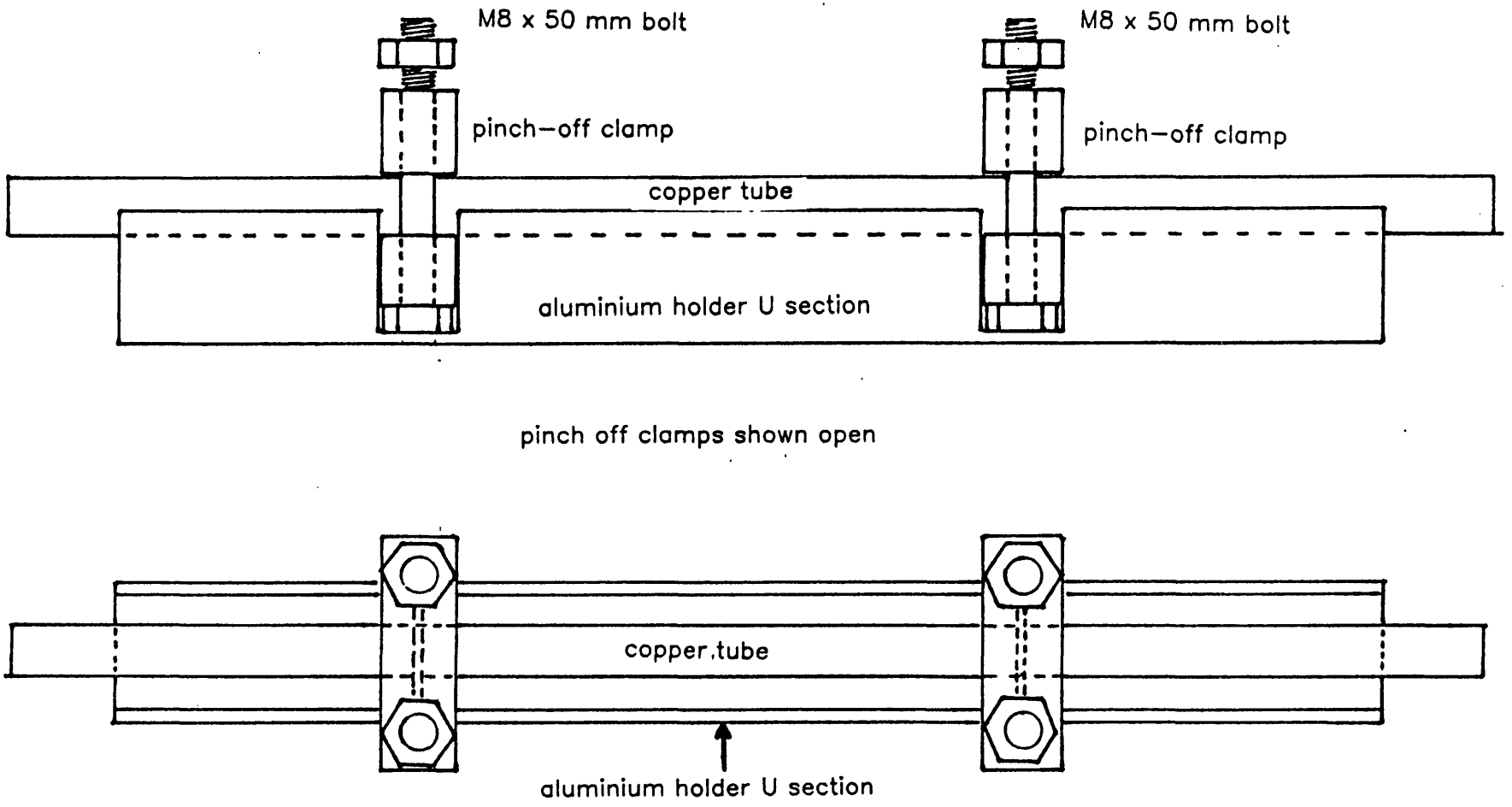

Figure 2.5

Front, Side and Top of a pinch–off Clamp

Clamp shown actual size

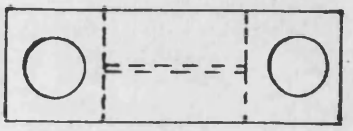

pinch off clamps shown closed

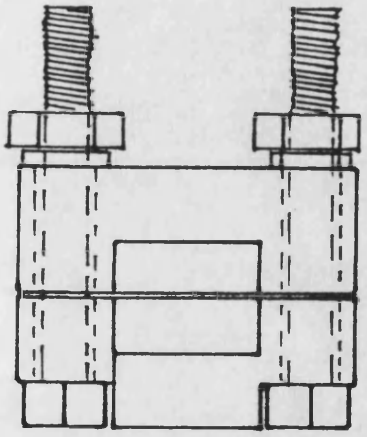

M8 x 50 mm bolt

Figure 2.6

Apparatus for collecting water samples under pressure

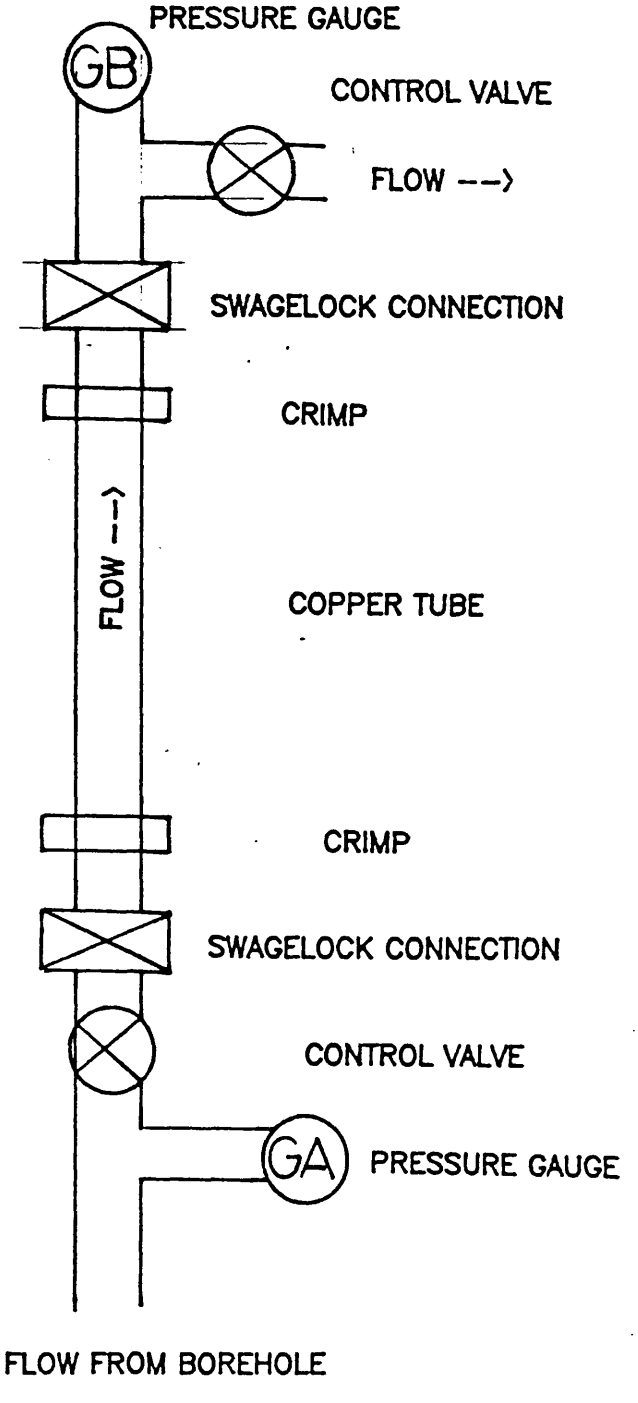

samples. Valve A was placed directly on the well head and adjusted to give a restricted flow. After allowing the well to flush at the higher pressure, the copper tube pressure gauge GB and valve B were attached and valve B was adjusted to obtain flow through the tube at a pressure of around 10 bars. The sample was then isolated by compressing the copper tube between the pinch-off clamps.

A copper tube collected in this way contains approximately 5.5cm^3 of water which typically will contain 0.1cm^3 of dissolved gas

2.5.2 Inert Gas Analysis Experimental Technique

For analysis the copper tube was attached to a vacuum line (Figure 2.7 and 2.8) with a O-ring seal. The system was then evacuated to a pressure of less than 10^{-5} mbar. A metered volume of isotopically enriched tracers for the inert gases was then admitted, and then the water sample was admitted by removing one of the pinch-off clamps. Detail of the inlet system is shown in Figure 2.8. The water was vapourised by warming the copper tube. Approximately half the water is vapourised by warming for 5 minutes. Water vapour is removed on a cold trap cooled with a dry ice/ethanol mixture. Nitrogen and other active gases were then absorbed on a zirconium/aluminium alloy at 400°C. This process takes from a few seconds to approximately one hour depending on the composition of

Figure 2.7 Stainless Steel Inert Gas Extraction Line

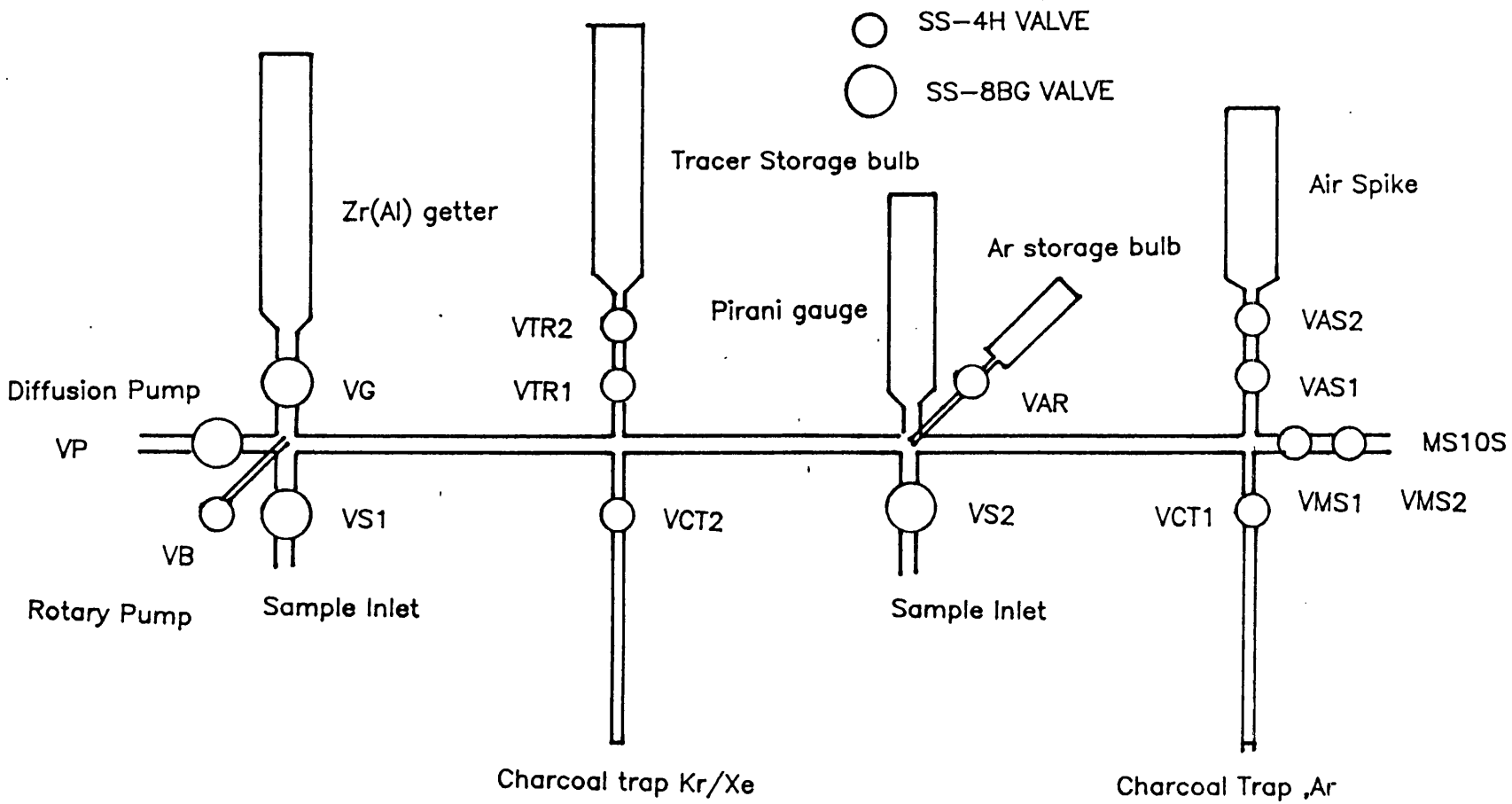

Figure 2.8

Detail of Water Sample Inlet

Inlet Shown full size

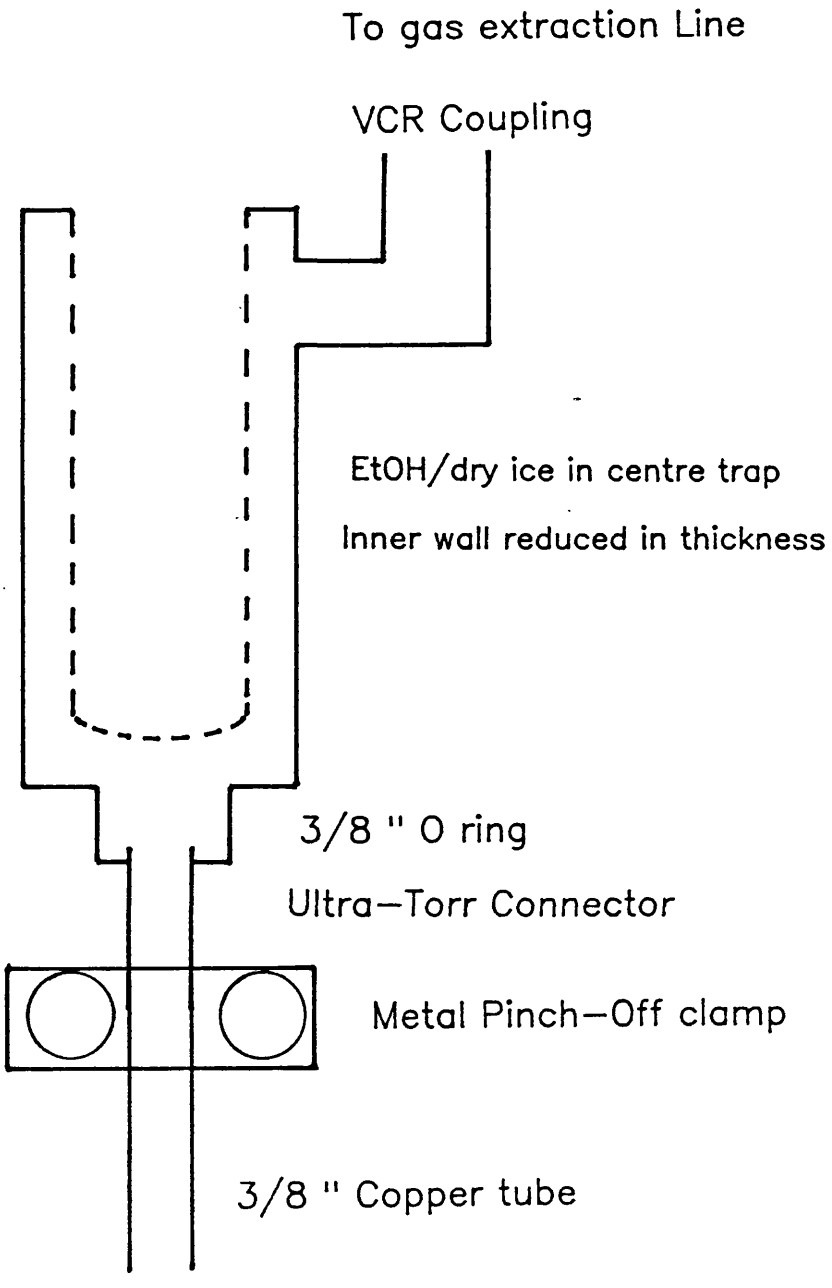

the active gases. A small sample is retained in a bulb for Ar isotopic analysis. The heavy inert gases Kr and Xe are then removed by absorbtion on charcoal cooled to -78°C. Argon is then absorbed on a similar trap cooled in liquid nitrogen at -196°C. The isotopic ratio of the helium and neon was then determined by metering the gas into a 5cm radius, 180° magnetic sector mass spectrometer (Kratos MS10S), (Appendix G) Kr and Xe are similarly analyzed after desorbing from the charcoal trap. Finally Ar is expanded from the storage bulb and the 36 and 40 ion current peaks determined. A more detailed procedure for inert gas analysis is shown in appendix E. Appendix F shows the relationships of tracer and atmospheric inert gases mass spectrums.

2.5.3 Calculation of Inert Gas Volumes

The volume of noble gases of natural isotopic composition is most readily measured by isotope dilution analysis. This requires mixing of the sample gas with a known volume of isotopically enriched tracer gas. Measurement of the tracer gas isotopic ratios, and the mixtures inert gas ratios, combined with the tracer volumes allows calculation of the sample inert gas contents. The advantage of this technique is that it enables accurate measurements to be made on very small samples, since only ratios are measured and not absolute values. An additional advantage is that measurements are

not dependent on the sensitivity of the mass spectrometer which varies from one gas to another.

An example of analysis by isotope dilution is given below. The parameters for a mixture of naturally occurring atmospheric Ar and tracer Ar may be symbolised as follows.

$Vat(Ar)$ = volume of atmospheric Ar at STP

$Vt(Ar)$ = volume of tracer Ar at STP

^{oo}Xat = mole fraction of isotope ^{oo}Ar in atmospheric Ar

^{oo}Xt = mole fraction of isotope ^{oo}Ar in tracer Ar

For the tracer and sample mixture, then:

$$R = \frac{^{36}Ar}{^{40}Ar} = \frac{^{36}Xat \,.\, Vat(Ar) + {}^{36}Xt \,.\, Vt(Ar)}{^{40}Xat \,.\, Vat(Ar) + {}^{40}Xt \,.\, Vt(Ar)}$$

If $Vt(Ar)$ and the isotopic composition of the tracer and atmospheric Ar are known, $Vat(Ar)$ may be calculated once the ratio, R, is determined experimentally. Rearrangement for $Vat(Ar)$ gives:

$$Vat(Ar) = Vt(Ar) \,.\, \frac{[^{36}Xt - {}^{40}Xt.R]}{[^{40}Xat.R - {}^{36}Xat]}$$

The BASIC computer program GASAN is used to calculate the sample contents. A listing of this program is given in Appendix H.

2.5.4 Calibration of Tracer Ratios and Volumes

Naturally occuring gas samples predominantly contain ^{4}He, ^{20}Ne, ^{40}Ar, ^{84}Kr and ^{129}Xe (Table 1.6). The tracer must therefore contain low concentrations of these isotopes and higher contents of atmospherically less abundant isotopes. In this case the isotopes ^{3}He, ^{22}Ne, ^{36}Ar, ^{78}Kr and ^{136}Xe have been chosen. In all cases the tracer peaks are far enough from the atmospheric peaks to avoid any interferences (Appendix F). Ampoules of these tracer gases were obtained and the gases mixed in appropriate proportions to give a single tracer gas. The isotopic ratios and concentrations in a single aliquot for the tracer gas are given in Table 2.1. The concentrations of the tracer are manipulated to produce ratios of atmospheric gas to tracer gas as near to unity as possible. Ratios close to unity are the easiest to measure and are likely to be the most precise.

In order to determine the precise tracer spike volumes at STP in the tracer, calibration of the tracer against a known quantity of air is necessary. This air is accurately metered in using the arrangement shown in Figure 2.9. The volumes of this system were accurately determined by filling and subsequent weighing with mercury.

Since the mole fractions of the isotopes for each gas in both the air spike and the tracer are known, and the volumes of inert gas in the air spike can be calculated,

Table 2.1

Mole fractions of light and heavy isotopes and concentrations of inert gas in an aliquot of tracer

Inert gas	Mass	Mole fraction in tracer
He	3	0.9992
	4	0.0008
Ne	20	0.0009
	22	0.9987
Ar	36	0.9958
	40	0.0035
Kr	78	0.9937
	84	0.0001
Xe	129	0.0001
	136	0.8051

Inert gas	concentration in tracer cm^3
He	2.190×10^{-5}
Ne	1.107×10^{-5}
Ar	1.694×10^{-3}
Kr	2.024×10^{-6}
Xe	2.251×10^{-7}

Figure 2.9

Air Spike for Tracer Calibrations

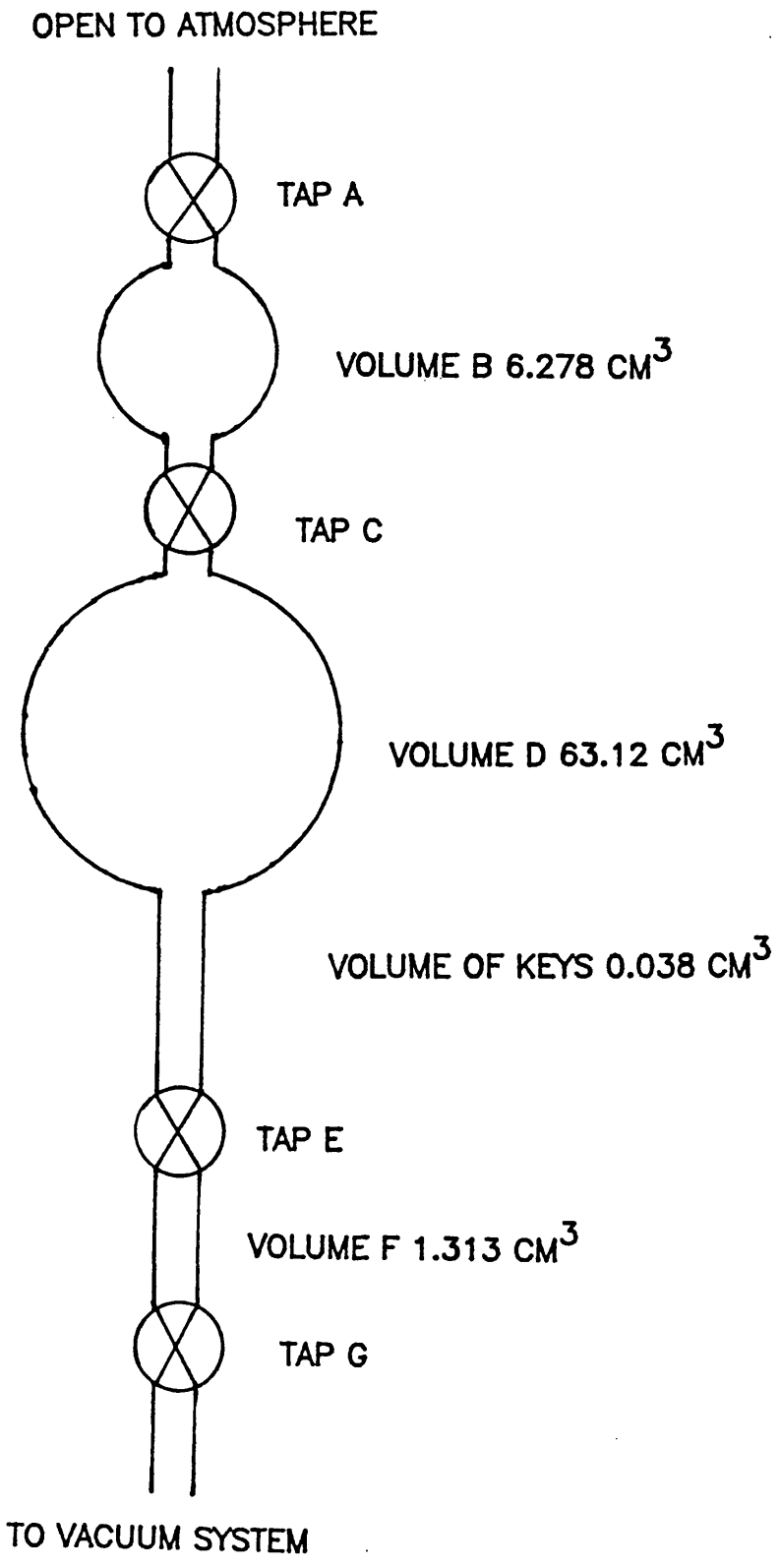

then Vt for each tracer gas can be found. This is done by measuring the isotopic ratios for each inert gas in the mixture of tracer and air, e.g.

$$Vt(Ar) = Vat(Ar) \cdot \frac{[^{40}Xat.R - {}^{36}Xat]}{[^{36}Xt - {}^{40}Xt.R]}$$

using the previously defined notation. In practice the values for the tracer concentrations are calculated using several different air spikes to obtain an average value. The program AIRCAL is used to calculate values of Vt.

The isotopic ratios in the tracer are measured on a sample of tracer to which no air has been added. This tracer is then treated like a water sample with separation of the inert gases. The isotopic ratios, which are heavily weighted toward the tracer isotope, can then be measured as previously described.

2.5.5. Correction for Successive Aliquot Extraction from the Tracer

Each tracer aliquot taken from the storage bulb will decrease the concentrations in each subsequent aliquot. A correction must therefore be applied to allow for the reduction in pressure of the tracer reservoir. If V is the volume of the storage bulb, and v the volume of the tracer aliquot and Vto is the volume of tracer gas at the time of air calibration. Vt the volume of tracer gas at a particular n'th aliquot extraction is given by:

$$Vt = Vto \cdot \frac{vV^{n-1}}{(V+v)^n}$$

In practice the reduction in tracer volume for each aliquot is very small, since V is very much larger than v. After 50 aliquots the reduction in tracer concentration will be around 5% of the initial values. Tracer calibrations using air are carried out after every 30 to 40 tracer aliquots. This ensures small errors in v and V do not produce significant errors in the tracer volumes.

The use of a stainless steel vessel for storing the tracer gas produces no measurable exchange of atmospheric gas with the tracer. Previously a glass (MONAX) storage bulb has been used, which produces a rapid loss of ^3He from the tracer.

2.5.6 Errors associated with inert gas analysis

The factors which may limit the precision of inert gas determinations are as follows:

1) Sample collection. The water samples collected must be re presentative of the in-situ water.
2) Sample storage. During storage there must be no equilibration of the water samples with air.
3) Sample weight. The sample must be accurately weighed before and after water extraction, to find the mass of water.
4) Mixing of the tracer gas with the water dissolved gas must be complete before any separation of inert gases takes place.

5) Precision of ion current measurements. The precision of the electrometer detector and its amplifying circuits will affect the reproducibility of ion current measurement. It is also important to accurately tune to the peak before commencing ion current measurement.
6) The gas extraction line may allow inert gas to diffuse in or out. This will become important if gas remains in the line for long periods.
7) Accuracy of the tracer calibration. Errors in tracer gas concentration determination will be carried forward onto the dissolved gas analysis.
8) Interfering ions. The presence of ions adding to the inert gas peaks may be important in some cases.

All these factors may produce errors in inert gas concentration determination. To assess their importance experiments were designed to test each in turn.

Sample collection may produce large errors if outgassing occurs prior to collection. Sampling must avoid these errors so sufficient pressure must be applied during sampling to prevent degassing. This problem will be discussed in detail later. Experiments have shown that there is no detectable leakage of helium from the copper tube samples or the gas extraction line. Since helium is the most diffusive of the inert gases it is concluded that diffusion is not a significant source of error.

The sample weight is determined on a three figure balance. As this balance has a tendency to 'drift' with time a standard weight is measured at each sample weighing so that masses of the tube before and after analysis can be directly compared. With this approach the error of weighing is +/- 0.002g which represents a 0.05% error.

It has been found that mixing of dissolved gas and tracer takes a minimum of 10 minutes. If mixing is allowed to occur for this period the errors due to incomplete mixing will be small.

The precision of measuring ion currents has been determined experimentally to give a 0.2% error of any determined isotopic ratio.

Interference of ions with inert gas has been found only to occur for neon. The occurrence of doubly charged Ar-40 produces a peak at m/e 20. Because argon concentrations are high compared with neon, it is necessary to measure neon ion currents at an electron accelerating voltage of 40V. In this way the importance of doubly charged argon is effectively reduced to within the error of measuring the neon ion current ratio.

The precision of tracer calibrations has been found to be the largest source of error. This varies from 0.3% for neon and helium to 4.9% for xenon. The large error for xenon is largely due to measuring an unfavourable ion current ratio. Other errors in tracer calibrations with air are produced from measurement of temperature and

pressure.

The overall error for an inert gas analysis based on 10 analysis of a single water source is very similar to that for replicate tracer calibrations. This suggests there are no extra errors produced during sample collection.

The accuracy of inert gas measurement should allow duplicate samples to agree to within a few percent of one another. The four temperature estimates in a single sample should have an error of less than +/- 1 degree centigrade. These small errors allow inert gas concentrations to be useful palaeoclimatic temperature indicators.

2.5.7 Estimation of Recharge Temperatures Using Inert Gases

The concentration of the dissolved noble gases are originally controlled by equilibration with the atmosphere at the time of aquifer recharge. Each analysed sample should then produce recharge temperatures for each inert gas. If there has been no modification of the inert gas contents since recharge these temperatures will be identical for each inert gas. However addition of radiogenic ^{4}He amd the insensitivity of helium concentration with temperature precludes its use as a recharge temperature indicator. Addition of radiogenic ^{40}Ar might also produce incorrect recharge temperatures. However in this case the presence of radiogenic ^{40}Ar may be detected

by the measurement of $^{40}Ar/^{36}Ar$ ratios in a sample which has no tracer added. The measured $^{40}Ar/^{36}Ar$ ratio may then be used to correct argon contents for a radiogenic component.

Concentrations of Ne, Ar, Kr and Xe can then be used to produce air equilibration temperatures. However during passage through the unsaturated zone groundwaters will incorporate bubbles of air.

These bubbles will eventually go into solution due to the increase in hydrostatic pressure as the water migrates downwards. This 'excess' air must therefore be removed from the inert gas contents in order to find the concentrations which give a unique recharge temperature.

Although groundwaters contain variable quantities of 'excess' air it is still possible to estimate the recharge temperature by an iterative method. The computer program RECHARGE is used for this purpose (Appendix I).

The program RECHARGE firstly calculates the noble gas solubilities in atmospherically equilibrated water for a temperature range of -10° to 60°C, using the method given by Benson and Krause (1976). For each of the four noble gases, Ne, Ar, Kr and Xe the program compares the sample concentrations with the solubility data to determine a set of potential recharge temperatures. Increments of air are then subtracted from the noble gas concentrations, the increment corresponds to $0.0625 \times 10^{-8} cm^3$ of neon. The other gases are subtracted in the proportions

governed by the composition of air. Each time an increment is subtracted a new set of temperatures is calculated by comparison with the solubility/temperature matrix. Quantities of air are subtracted until the temperature for neon exceeds a preselected limit. The program then selects the temperature set, corresponding to removal of a certain air volume, with the closest agreement. The average of this temperature set is taken as the recharge temperature (temperature at which air/water equilibration took place). An example of a RECHARGE program output is given in Figure 2.12.

Since the estimation of recharge temperature involves the subtraction of a fixed quantity of dissolved air, the amount of excess air can be determined. A measure of this excess air is given by dividing the measured Ne concentration by the calculated Ne concentration at recharge. This value is known as the (neon) contamination index. A value of 1 indicates no excess air, whilst increasing values indicate large volumes of excess air.

The emphasis on the use of neon for air contamination is for several reasons. Firstly neon is comparatively insensitive to changes in recharge temperature, but very sensitive to excess air. Secondly, there are only two likely sources of neon, air equilibration and excess air; it is most unlikely for radiogenic neon to be present in groundwaters.

The precision of inert gas analysis is treated in detail in 2.5.6 However in terms of recharge tempera-

tures the agreement between the 4 estimates of recharge temperature is +/- 1°C for a sample recharged at 10°C. Duplicate samples from the same source will also be expected to agree within +/- 1°C, for a similar recharge temperature.

2.6 Gas Ratio Analysis

2.6.1 Sample Preparation

Samples for gas ratio analysis are collected in the same way as inert gas samples, in copper tubes sealed by pinch-off clamps. Collection under pressure may also be necessary if large quantities of CH_4 or N_2 are present. From a single 5.5cm^3 sample the ratios CO_2/Ar, CH_4/Ar, N_2/Ar, H_2/Ar and the isotopic ratio $^{40}Ar/^{36}Ar$ are measured. Measurements may also be made on other types of sample. These may be gas samples collected in the field as a result of degassing processes (section 6) or from water samples which have been completely degassed in the laboratory.

For a copper tube type sample a gas extraction line is used which is similar to that described in Figure 2.7. The line is previously evacuated to better than 10^{-5} mbar. Warming of the stainless steel may be necessary to ensure adequate degassing of the internal surfaces. This is particularly important for N_2 analysis.

The copper tube is attached to the gas extraction

line with an O ring seal to a water vapour trap as shown in Figure 2.8. After evacuation the pumps are closed off and the upper crimp removed. The sample is then warmed for 10 minutes to ensure complete degassing. Water vapour is removed on the cold surface created by filling the inlet system with dry ice/ethanol.

Sub-samples of the gas are trapped in 250cm^3 stainless steel bottles attached to the line. These bottles have two metal valves separating them from the line which allows small quantities of gas to be metered into the vacuum line and then into the mass spectrometer. This arrangement has two main advantages. These are:

1) Replicate measurements of the same gas ratios are easily accomplished which produces a better statistical assessment of the errors involved.
2) The gas partial pressures from 5cm^3 of gas are very much too high to be analysed by mass spectrometry. Reduction of the pressure is made by expanding small aliquots of gas into the main line.

A set procedure is necessary for measuring gas ratios to remove the possibility of interferences between ions in the mass spectrometer. Ion source parameters are as for inert gas analysis.

Splitting patterns for all analyzed gases are given in Appendix J.

2.6.2 Procedure for Gas Ratio Analysis

After samples of dissolved gas have been trapped in 250cm^3 stainless steel bottles the remaining gas is pumped away. The ratios are then measured in the order CO_2/Ar, N_2/Ar, CH_4/Ar, H_2/Ar and finally $^{40}Ar/^{36}Ar$.

2.6.2.1 CO_2/Ar ratio determination

One aliquot of gas is expanded from the stainless steel bottle into the main part of the gas line. One aliquot of this gas is immediately metered into the mass spectrometer. The ion current of the mass/charge (m/e) 44 peak is immediately noted. If this peak is off scale then one aliquot from the stainless steel bottle is expanded into a second bottle and the procedure repeated. By using different sized stainless steel bottles the m/e 44 peak can be made to be close to full scale deflection on the highest scale range. The m/e 44 peak must be measured immediately on admitting sample to the MS10 as the ion current falls off steeply with time. This is due to absorbtion of CO_2 onto the ion cage walls. To effect immediate ion peak height measurement it is necessary to pre-tune to the highest point with an aliquot of gas, pump this away, and admit a further aliquot. When m/e 44 peak has been measured the m/e 40 peak for Ar can be determined. Since Ar is an inert gas it is not absorbed by the metal surfaces of the mass spectrometer. About 10 estimates of the 44/40 ion current ratio are made to

produce a statistical error.

Since a peak at m/e 44 is only possible for CO_2 there are no possible interferences. Thus the CO_2/Ar ratio can be calculated from the ion current ratio and the relative sensitivities of the MS10S for CO_2 and Ar. Background levels for CO_2 and Ar are very low in the gas line and mass spectrometer.

2.6.2.2 N_2/Ar Ratio Determination

If there is significant CO_2 in the sample then this must be removed before analysis of any other gases. This is done by using a cold finger immersed in liquid nitrogen. This very quickly absorbs CO_2 whilst having no noticeable effect on N_2, CH_4, H_2 or Ar.

To determine the N_2/Ar ratio an aliquot of gas is expanded into the line as for CO_2/Ar analysis. One aliquot of this is admitted to the mass spectrometer. N_2 levels are generally not as variable as CO_2 contents of groundwater as they are usually governed by air equilibration processes. For this reason one aliquot will usually produce an ion current for m/e 28 on the maximum range. The m/e 28 ion current also falls with time inside the mass spectrometer. However unlike CO_2 the fall is slow and linear with time. Thus if two measurements of m/e 28 are made separated by around 30 seconds, the ion current when the gas was first admitted can be found by simple extrapolation. If I_1 and I_2 are the

first and second ion current readings at times T_1 and T_2 Io the current at To is found by:

$$Io = I_1 + T_1 \times \frac{I_1 - I_2}{T_2 - T_1}$$

Because the m/e 28 ion current falls linearly then $28/_{40}$ ratios are much easier to determine accurately than CO_2/Ar ratios.

The main peak for nitrogen is at m/e 28, but there is also a subsidary peak at m/e = 14 due to the formation of $(^{14}N^{14}N)^{2+}$ ions. The m/e $28/_{14}$ ratio has been determined on pure nitrogen (BOC 99.998% N_2) to be constant at 13.93. This is shown in the cracking pattern of N_2 in Appendix J. This is useful because if the gas contains any residual CO_2, CO^+ ions will form which will contribute to the m/e 28 peak. The $^{14}/40$ ratio can be used as a check for the N_2/Ar ratio. However if significant CH_4 is present there will be a contribution to m/e 14 from CH_4. Since methane is difficult to separate from N_2 the $^{28}/40$ ratio is generally the more reliable.

The m/e 28/40 ratio is measured about 5 times on different aliquots to give an average value. For m/e 28/40 the precision of these repeat values will be +/- 1% or better.

2.6.2.3 CH_4/Ar Ratio Determination

CH_4/Ar ratio analysis is carried out in a similar way to N_2/Ar. Again CO_2 is removed from the gas mixture as

the m/e 16 peak from CO_2 will interfere with the main CH_4 peak (Appendix J). It is possible to use the subsidiary peak at m/e 15 (CH_3^+) which has no interfering ions. The ratio of m/e 15/16 has been experimentally determined on pure CH_4. This ratio is shown to be constant at 0.855 +/- .005.

For CH_4/Ar analysis an aliquot of gas is admitted to the line from a stainless steel bottle. One aliquot is admitted to the MS10S. The ion currents at m/e 12, 13, 14, 15, and 16 are measured and times noted for these measurements. The m/e 40 peak is then determined, and the m/e 12-16 peaks are remeasured. This allows correction for losses inside the spectrometer after sample admittance in a similar way to N_2/Ar ratio analysis. Measurement of the m/e 14 peak gives a second estimate of the N_2/Ar ratio. The m/e 14 peak must first be corrected for CH_4, if significant methane is present. Secondly the m/e 28/14 factor for pure nitrogen is applied to give a m/e $28/_{40}$ ratio. The necessary corrections are shown in Table 2.3.

Measurement of the m/e 12, 13, 15 peaks in addition to m/e 16 are important. The ratio of these subsidiary peaks to m/e 16 will indicate if they are due to CH_4 alone or if another gas is present. For example a very small m/e 15 peak in relation to m/e 16 could indicate the presence of carbon monoxide. However in all samples analysed the ratios are very close to those expected for pure CH_4.

Table 2.2

Ion Source parameters for the MS 10 S

Used in inert gas analysis and
gas ratio analysis.

alpha slit	0.25 mm
preamplifier	10^{11} ohm input resistor
sensitivity	4.35×10^{-5} A/mbar (argon)
Magnet	1.8 Kg
Trap Current	50 uA
Electron Accelerating Volts	+ 70 V
Electron Accelerating Volts	+ 40 V (neon)
Ion repeller voltage	+ 1 V

The m/e 16/40 ratio measurement was repeated on separate gas aliquots. The precision of these repeat measurements is generally +/- 5%.

2.6.2.4 H_2/Ar ratios

The approach to measuring H_2/Ar ratios is dependent on the presence of CH_4 in the sample. If a large amount of CH_4 is present this will produce a significant m/e 2 contribution. In some situations where a sample contains very high ^4He levels it is possible to measure the H_2/He ratio. This has the advantage that CH_4 can be removed from the gas mixture on a charcoal trap cooled in liquid nitrogen. In this situation there will be no contribution to m/e 2 from CH_4. Except in the case of very evolved waters this approach is not possible and the m/e 2 contribution from CH_4 must be estimated from the measured CH_4 cracking pattern (Appendix J) and the CH_4/Ar ratio.

For m/e 2 determination the mass spectrometer must be pretuned to the mass setting giving the maximum response to m/e 2. This is because H_2 is very quickly absorbed by the ion cage, in a way which is not linear with time.

Another contribution to m/e 2 is from the mass spectrometer background. There is a significant m/e 2 background which is not removed even after prolonged baking of the spectrometer. Because of this high background H_2/Ar ratios must always be measured with the m/e

2 on the maximum range. This will effectively reduce the proportion of background hydrogen.

The H_2/Ar ratio measurement is repeated on several separate aliquots of gas to obtain an average value. The errors involved in H_2 analysis are large. This is due not only to the large number of corrections needed, but also to the very rapid fall in m/e 2 ion current on admitting to the MS10S. The precision of H_2/Ar analysis is unlikely to be better than +/- 20% on repeat measurements of the same gas. It should also be noted that hydrogen levels may be underestimated because of the finite response time of the ion current measuring circuits. While the mass spectrometer is reacting to the m/e 2 signal, a proportion of the hydrogen will already have been removed. Since the fall in m/e 2 ion current is non linear it is impossible to correct for this reduction. In the course of this study hydrogen has only been found in a very small number of samples. All of these have been ancient waters from granitic aquifers.

2.6.2.5 $^{40}Ar/^{36}Ar$ ratio

The measurement of $^{40}Ar/^{36}Ar$ ion current ratios differs from the other ratio measurements in several ways. Firstly a much larger quantity of gas is needed as the ^{40}Ar ion current must be high on the maximum scale. Since a ratio of about 300 to 1 is being measured this will produce a measurable ^{36}Ar ion current. Secondly

because argon is a noble gas the remaining gases can be removed by gettering on a zirconium/aluminium alloy at 450°C. This removes any possibility of interfering ions.

For measurement of the ion current the stainless steel bottle is opened to the main gas line. The entire contents are then gettered and one or two aliquots admitted to the mass spectrometer. The remaining gas is left for subsequent Ar ratio analysis. After each measurement of ^{36}Ar the ^{40}Ar ion current is measured. The gas is then pumped from the spectrometer. Before a further aliquot of gas is admitted the ion current is allowed to return to zero. The large reservoir of argon in the gas line reduces the effect of any argon desorbed by the stainless steel walls of the gas line.

Ar isotopic measurements are repeated on new aliquots of gas. Repeat measurements show very good agreement to within +/- 0.5%

2.6.3 Calibration Factors for Gas Ratio Analysis

The sensitivity of the MS10S varies with the source parameters, and on the collector slit width. For this reason the source parameters and slit width are held constant for all gas ratio analysis. The parameters used are shown in Table 2.2. The sensitivity is measured as the number of positive ions produced by a given increase in sample pressure. Thus sensitivity is measured in amperes of ion current per mbar of pressure. In this

study the absolute determination of sensitivities is unimportant. This is because all gases are expressed relative to argon, which is measured independently by isotope dilution techniques. Thus all that is needed to calculate actual volumes of N_2,CH_4 etc is the relative sensitivity in relation to Ar.

To make sensitivity measurements mixtures of gas of known composition are needed. These were produced by using glass systems comprising of two bulbs and 3 taps. The size of the bulbs are varied so that if each bulb is filled with a separate pure gas, when they are mixed, different gas ratios are produced. One of the 3 combinations used is shown in Figure 2.10, along with the system of filling separate glass tubes with the mixture. The three mixtures which were produced had gas to argon ratios of 29.60, 43.72 and 61.87. In each case mixtures were made by filling the bulbs with pure gas by means of a glass tube inserted through the tap. After adequate flushing the gas flow is reduced and the tube slowly withdrawn. The tap is closed immediately after withdrawing the tube. After filling both bulbs the central tap was opened to allow mixing. This mixture is then used to fill several $1cm^3$ glass tubes (Figure 2.10) which are analysed for their ion current ratios by mass spectrometry. The splitting patterns for pure gas were measured by admitting pure gas to the mass spectrometer in the same way. The measured splitting patterns are given in Appendix J.

Figure 2.10

Apparatus for preparing gas mixtures for gas ratio analysis calibration

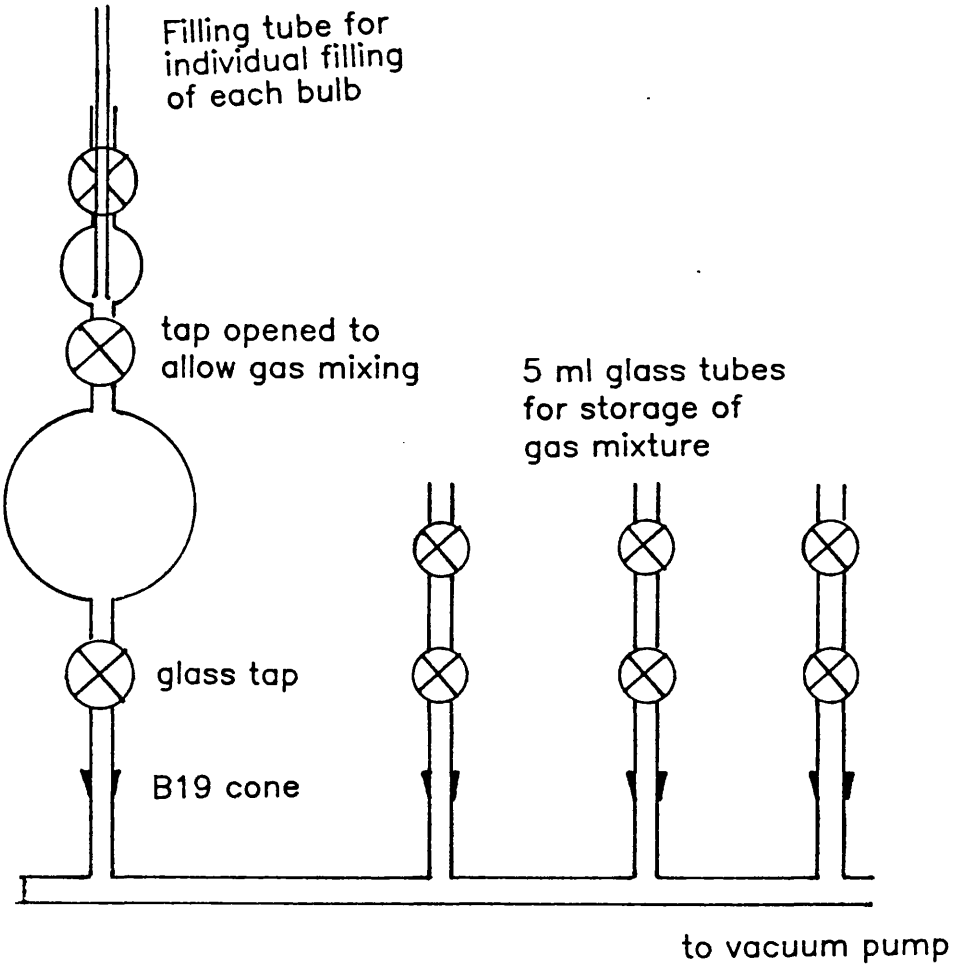

2.6.3.1 N_2/Ar Calibration

The N_2/Ar calibration factor has been determined on a large number of samples with differing ratios. These are the three prepared bulbs as discussed earlier, air saturated water at 10°C and air itself. In all cases a number of estimates of the gas ratio was made and the precision for these was 2% or better in all cases. The calibration factors for each mixture are shown in Table 2.3. It can be seen that there is a small change in calibration factor for different gas ratios. For low N_2/Ar values the calibration factor approaches 1. Thus it is important to use the calibration factor for the particular measured N_2/Ar ion current ratio. N_2/Ar ratios for air saturated water are in the range 36 to 40 which would need a correction factor of 1.23 to be applied. If in an extreme case the calibration factor for air was used, this would produce a 2% error in N_2/Ar ratio analysis.

In this case the correction factor is defined as:

$$\text{calibration factor} = \frac{N_2/Ar \text{ std}}{m/e \ 28/40 \text{ std}}$$

Calibration factors for other gas ratios are calculated in the same way. A list of calibration factors is shown in Table 2.3

N_2/Ar correction factors have been shown to vary around the value given on a day to day basis. For this reason daily N_2/Ar calibrations are made. This is

Table 2.3

Relative sensitivities of gases in the Kratos MS 10S for the source parameters in table 2.2

Gas	m/e	Ratio measured	Calibration factor experimental: Ar=1	MS 10 manual Ar=1
H_2	2	-	0.818	0.816
CH_4	16	-	1.061	1.094
N_2	28	83.54	1.250	1.167
		61.87	1.240	1.167
		43.72	1.214	1.167
		37.9	1.227	1.167
		29.6	1.161	1.167
CO_2		-	1.324	1.324
Ar	36	295.5	1.030	-

normally done on air as this is the most convenient mixture. Calibrations with air must then be related to the particular N_2/Ar ratios being measured.

2.6.3.2 CO_2/Ar Calibration

The CO_2/Ar correction factor was calculated in a similar way to N_2/Ar correction factors. Mixtures of CO_2/Ar ratio of 30, 44 and 62 were made and analysed for m/e 44/40 values. In this case there was found no correlation of correction factor with CO_2/Ar volume ratio. This is probably due to the larger errors involved in CO_2/Ar analysis. The calculated calibration factors are shown in Table 2.3.

2.6.3.3 CH_4/Ar Calibration

The CH_4/Ar correction factor was determined as for the N_2/Ar correction factor. However, as the CH_4 content of the atmosphere is very low, air and air saturated water are of no use as standards. The calibration factor was determined on the three standard mixtures of CH_4 and argon. The resulting calibration factor is shown in Table 2.3. No change in correction factor was observed for changing CH_4/Ar ratio. As for CO_2 it is likely that the uncertainty of measuring CH_4/Ar ratios is too great for any such effect to be noticeable.

2.6.3.4 H_2/Ar Calibration

The H_2/Ar correction factor was again determined using bottled hydrogen/argon mixtures. Hydrogen/argon ion current correction factors are unusual in that the sensitivity of hydrogen in the MS10S is higher than that of argon. This produces calibration factors less than one.

The precision of analysis for a particular hydrogen/argon mixture is approximately 5%. This is very much better than the precision for a groundwater hydrogen/argon analysis. This suggests the additional correction factors for a mixture of gases and argon are adversely affecting the analytical precision.

2.6.3.5. $^{40}Ar/^{36}Ar$ calibration

The only convenient calibration source for argon ratios is air. The value of $^{40}Ar/^{36}Ar$ of 295.5 is the most likely value to be found in groundwater samples which have no radiogenic Ar input.

The experimentally determined argon isotopic ratio for air is 286.9 +/- 1.5. However this ratio has been shown to fluctuate from day to day and thus daily air calibrations are necessary. The measured values range from 260 to 290 which is an error of 12%. The error for a particular air sample calibrated during one day is fortunately much smaller.

It is not known if the calibration factor for argon

isotopic ratio varies with the measured value. To determine this would need mixtures of argon with $^{40}Ar/^{36}Ar$ ratios in the range 300 to 350.

2.7 Oxygen and Hydrogen Isotopic Analysis

2.7.1 Principles

Oxygen and hydrogen isotope measurements on a VG Micromass 602E mass spectrometer. H_2 was prepared by reduction of water over zinc shot at 450°C. The hydrogen gas is then analyzed in the spectrometer, its stable isotope composition is given by:

$$\delta\,^{2}H°/_{oo} = \left[\frac{(^{3}H_2/^{2}H_2)\ spl - (^{3}H_2/^{2}H_2)\ STD}{(^{3}H_2/^{2}H_2)\ STD} \right] \times 1000$$

For oxygen isotopes the sample water is equilibrated with CO_2 and the CO_2 is the medium used to determine $\delta^{18}O$, i.e.

$$\delta^{18}O°/_{oo} = \left[\frac{(^{46}CO_2/^{44}CO_2)\ SPL - (^{46}CO_2/^{44}CO_2)\ STD}{(^{46}CO_2/^{44}CO_2)\ STD} \right] \times 1000$$

Results are expressed against Standard Mean Ocean Water (SMOW), as described fully in Darling et al, 1982.

2.7.2 Mass Spectrometric Analysis of Oxygen and Hydrogen Isotopes

2.7.2.1 Hydrogen

The reduction of water to H_2 takes place in the sample flask, which is then directly attached to the mass spectrometer inlet. 0.25g of Zn is sufficient to reduce 10 µl of water. The liquid is then frozen by immersion in liquid nitrogen and the air evacuated from the flask. After one hour at 450°C the water is reduced.

2.7.2.2 Oxygen

The preparation of oxygen is more complicated and can be split into two stages.

a) **CO_2 equilibration procedure**

10 µl of 50% HNO_3 are added to the equilibration flask followed by 5 mls of water. HNO_3 aids the equilibration process. The water is then frozen and air pumped away. The flasks are then flooded with CO_2 to a pressure of 300 mbar. Equilibration is then allowed to proceed by warming the flasks for 24 hours at 25°C.

b) **CO_2 collection procedure**

The equilibration flasks are opened to a vacuum line and the water removed on a 'U' tube at -80°C. The CO_2 is then trapped in a collection vessel in liquid nitrogen. The trapped CO_2 is then ready for mass spectrometric analysis.

The same source parameters are used as for nitrogen

isotope analysis. A number of corrections are necessary to the raw delta values produced. For δ^2H a correction must be made for the formation of $(H_3)^+$ ions because of its superimposition on the $(^2H^1H)^+$ peak. For $\delta^{18}O$ a correction is first made for the isotopic equilibration between gaseous CO_2 and water vapour. The fractionation factor is 1.0412 at 25°C. This correction is made quantitative by knowing the molar volume ratio of $H_2O:CO_2$ in the flask. A second correction is made to $\delta^{18}O$ to account for the presence of $(^{46}CO_2)^+$ and $(^{44}CO_2)^+$ ions which do not contain ^{18}O or ^{16}O. This second correction is very small.

The precision of each analysis is better than +/- 0.03°/$_{oo}$ for both δ^2H and $\delta^{18}O$. Reproducibility for $\delta^{18}O$ is +/- 0.1°/$_{oo}$ for $\delta^{18}O$ and +/- 1°/$_{oo}$ for δ^2H.

2.8 Nitrogen Isotope Analysis

2.8.1. Principle

All nitrogen isotopes were analysed on a V.G. Micromass 602E mass spectrometer. This machine is a double inlet/double collector instrument primarily designed for determination of oxygen and hydrogen isotopic ratios.

The mass spectrometric analysis of nitrogen isotopes involves admitting molecular dinitrogen, N_2. The isotopic ratio is determined by measuring the m/e 29 and m/e 28 ion currents.

This ratio is compared with a reference gas and the isotopic composition of the sample expressed as the difference from the reference. The delta notation is used to express results, where:

$$\delta^{15}N^{o}/_{oo} = \left[\frac{m/e\ (29/28)\ SPL - m/e\ (29/28)\ STD}{m/e\ (29/28)\ STD} - 1\right] x\ 1000$$

The advantage of this notation is that differences from a universal standard can be precisely determined. Sample delta values are by convention expressed as changes against atmospheric nitrogen, with intermediate working standards such as bottled nitrogen often being used.

In order to prevent interference on the m/e 28 and m/e 29 peaks from CO^+, some gas purification is necessary to remove O_2 and CO_2. For dissolved gas samples the gas is first deoxygenated by reaction with reduced copper at 700°C and then dried in a liquid nitrogen trap. The purified N_2 gas is then absorbed onto activated silica gel in sample flasks prior to mass spectrometric analysis. Uptake of N_2 gas onto activated silica gel is quantitative and no isotope fractionation can occur (Mariotti, 1983). The gel becomes active to gas absorption when cooled in liquid nitrogen, and completely desorbs at room temperature.

2.8.2 Mass Spectrometric Analysis of Nitrogen

The double inlet system of the V.G. Micromass 602E comprises two gas reservoirs, one filled with the sample gas and the other with reference gas. The double collector comprises a major and minor collector which allows the simultaneous measurement of two ion currents.

The gas pressure is independently adjustable in the two reservoirs to produce the same ion currents, for sample and standard, at the major collector. The two reservoirs are connected to the ion source through a viscous leak. This allows increments of gas from each reservoir to be alternately leaked to the ion source. The magnetic field of the spectrometer deflects the lighter $(^{14}N^{14}N)^+$ of mass 28 more than ions of the heavier $(^{15}N^{15}N)^+$, allowing separation of the two masses.

The minor collector slit is focused on the $(^{29}N_2)^+$ ion beam. The major beam was run at 2.5×10^{-9} A on both reference and sample sides. The source parameters are:

Accelerating voltage	:	4210 eV
Trap current	:	200 μA
Ion Repeller voltage	:	+ 7.1 V
Electron volts	:	94 V
Half plate voltage	:	1010 V
Half plate ΔV	:	max
Response	:	0.3 secs

The precision of each analysed sample is calculated

from ten instrumental measurements on one sample. All samples have a precision better than $2\sigma = 0.03°/_{oo}$.

2.9 Helium in Rock Cores

The total helium content and the diffusion coefficients of helium were determined on small cores taken from the centre of freshly cut surfaces of large diameter cores.

2.9.1 Total Helium Determination

Small cores of 1.1cm diameter and 0.5cm in length were weighed and sealed in a stainless steel tube. This tube is attached to a vacuum line with a 1 inch diameter Swagelock connector. The line used is shown in Figure 2.11. The sample was then pretreated by warming at 50°C for 12 hours under vacuum to remove surface adsorbed helium. The system is then isolated from the pumps and an aliquot of helium-3 gas is added as a tracer. The sample was then heated for a period greater than 8 hours at 800°C. At the end of this time a charcoal trap is opened which is cooled in liquid nitrogen. This removes most gases except helium and neon. Final purification is done by opening to the line a zirconium-aluminium getter at 400°C. The helium-3/helium-4 ratio was then measured to determine the volume of helium-4 evolved, as in Section 2.5.2.

It has been determined experimentally that at least

Figure 2.11

Stainless steel Rock Helium Extraction System

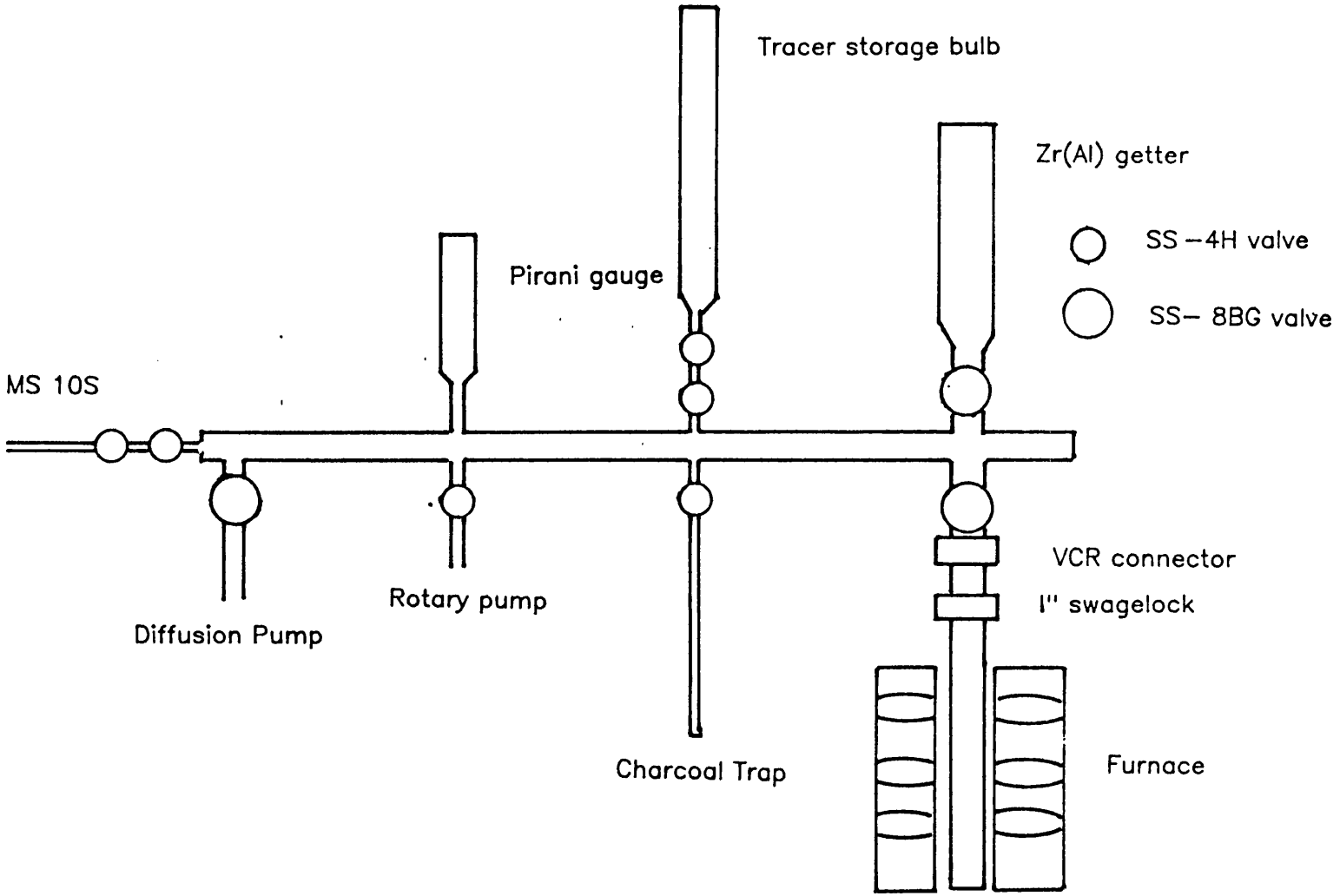

99% of helium released at 800°C is liberated within 8 hours of heating. After treatment at 800°C the cores are structurally very much changed. Even granite cores can be easily hand crushed in a pestle and mortar into a fine powder. This damage to crystal lattices facilitates helium release and is probably related to the alpha to beta quartz transformation. However helium trapped in minerals unaffected at 800°C may not release all their stored helium within 8 hours. This could lead to low helium values in some cases. However comparison of results for samples from the Palo Duro basin of Texas (Zaikowski and Hubbard, 1986) show no difference from results obtained by heating to 1400°C.

2.9.2 Determination of Diffusion Coefficients for Helium in Rock Matrices

For measurements of helium diffusion coefficients larger volumed 1.4cm diameter cores were used. These were cut and polished to remove surface irregularities. The cores are first heated at 50°C whilst pumping to remove surface adsorbed helium. An aliquot of helium-3 tracer was then added and the sample heated at a fixed temperature for around 24 hours. The helium was purified before ratio analysis as in the precious section. This experiment was repeated at temperatures of 100, 150, 200, 250, 300 degrees centigrade. The diffusion coefficients can be used to make Arrhenius style plots and determine values for the activation energy of diffusion. In these

experiments data was rejected if more than 30% of the stored helium is removed in any experiment. In this situation the depleted helium content will adversely affect the measured coefficient.

The measured diffusion coefficients were used to determine helium loss between coring and measurement. For a core with a helium diffusion constant of 1×10^{-11} m^2/a at 10°C it will take thousands of years to lose 5% of its stored helium by diffusion. However some rocks have much higher diffusion constants around 3×10^{-5} m^2/a which may lose 5% of stored helium in a few years. Thus only cores taken from the centre of large diameter (>10cm) cores should be used for this type of analysis.

Figure 2.12

RECHARGE TEMPERATURE CALCULATION

SAMPLE name : SIGHARTING 2
number : 1a
Ar-40/Ar-36 ratio : 295.5 Upper temperature limit : 20

Altitude of recharge zone, metres asl : 0
Mean annual air temperature at recharge zone : 273.18
Pressure in bars at recharge altitude : 1
Water vap. press., mm, unsat zone : 9.352997
Salinity parts per thousand (g/litre) : 0

He	Ne	Ar	Kr	Xe	CI	T	S.D.
12.75	2.06	3.94	9.27	1.26			

Full result set

12.73	2.05	3.94	9.27	1.26			
	9.4	9.0	9.6	11.5	1.00	9.88	1.11
12.71	2.05	3.93	9.26	1.26			
	9.7	9.1	9.6	11.5	1.01	9.98	1.05
12.70	2.04	3.93	9.26	1.26			
	10.0	9.1	9.6	11.5	1.01	10.05	1.03
12.68	2.04	3.93	9.25	1.26			
	10.3	9.1	9.6	11.5	1.01	10.13	1.04
12.66	2.03	3.92	9.25	1.26			
	10.6	9.2	9.6	11.5	1.02	10.23	1.03
12.64	2.02	3.92	9.25	1.26			
	10.9	9.2	9.6	11.5	1.02	10.30	1.08
12.62	2.02	3.92	9.24	1.26			
	11.3	9.2	9.6	11.5	1.02	10.40	1.17
12.61	2.01	3.91	9.24	1.26			
	11.6	9.3	9.7	11.5	1.02	10.53	1.20
12.59	2.00	3.91	9.23	1.26			
	11.9	9.3	9.7	11.5	1.03	10.60	1.29
12.57	2.00	3.91	9.23	1.26			
	12.3	9.3	9.7	11.5	1.03	10.70	1.43
12.55	1.99	3.90	9.23	1.26			
	12.6	9.4	9.7	11.5	1.03	10.80	1.52

CHAPTER 3

MOLASSE BASIN SHALLOW GROUNDWATERS

3.1 Geological and Hydrogeological Setting

The Upper Molasse basin is part of the large Alpine-Carpathian fore deep. On the surface, the geological boundary in the south is made up of the Flysch-zone; in the north, the crystalline rocks of the Bohemian Massif border the basin (Fig. 3.1). These dip toward the south and form the basement for the overlying sediment series (Fig. 3.2). With the exception of sporadic carboniferous deposits, Jurassic and Cretaceous sediments form the pre-tertiary floor. The Malm (Jurassic) limestone and dolomites can attain thicknesses up to 500m and due to karstification they are the most important deep aquifers in the Molasse basin. Malm waters have been used for balneological purposes since 1968. More recently waters at Geinberg have been used for geothermal heating systems. Hydraulic studies in the Bavarian part of the Molasse basin have shown that waters in the deep Malm are discharged into the Danube (Lemcke, 1976; Andres and Frisch, 1981).

The upper Cretaceous deposits are generally fine clastic sediments and have no significance as aquifers with the exception of a regionally limited Upper Campanian sandstone facies (Obernberg thermal). The Mesozoic sediments are dissected by NNW-SSE trending faults, with considerable throws. The block mosaic so formed was flattened before the Upper Eocene, when marine transgression occurred and sedimentation began. Three

Figure 3.1 The Geology of the Molasse basin of Upper Austria (showing sample sites)

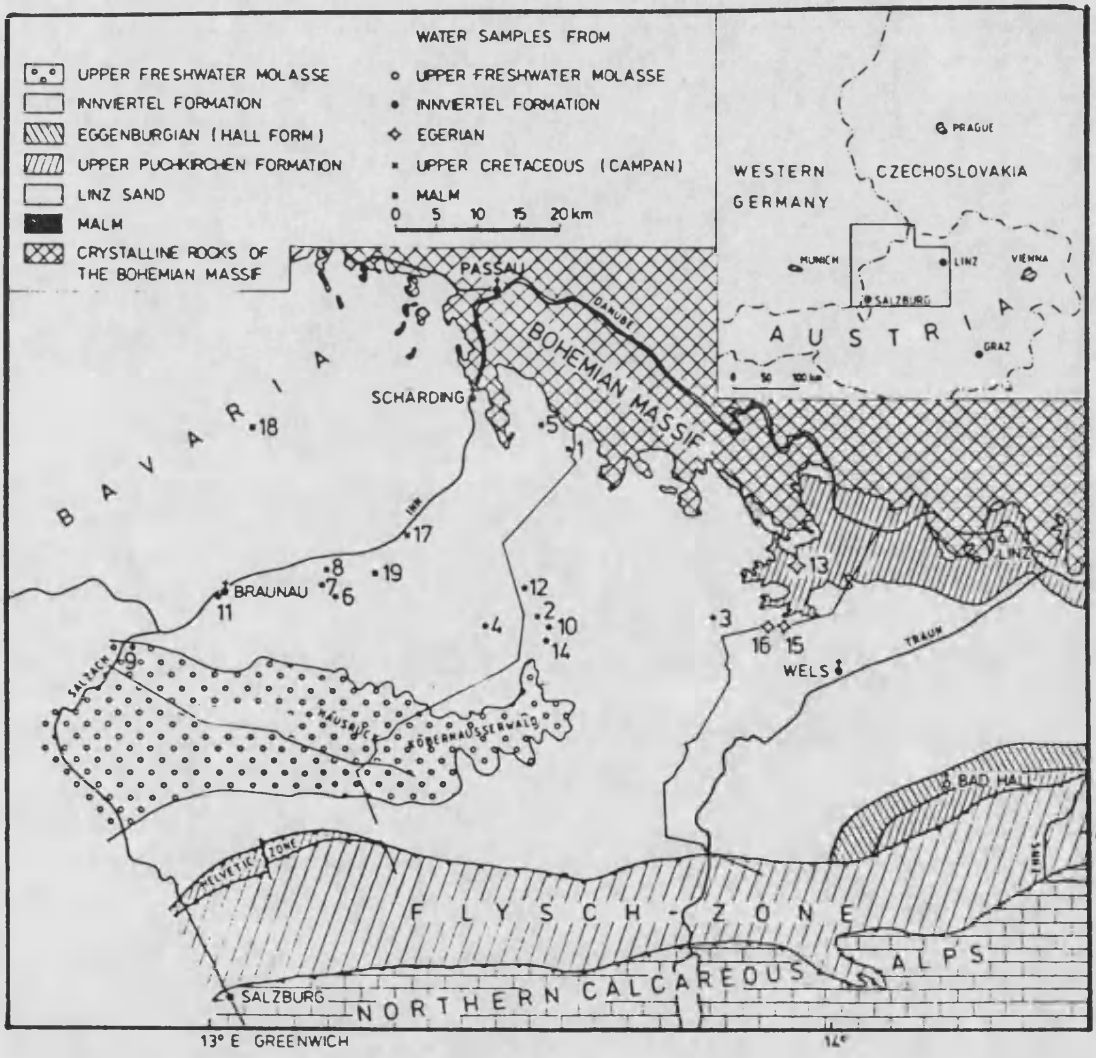

Figure 3.2 North – South section through the Molasse basin

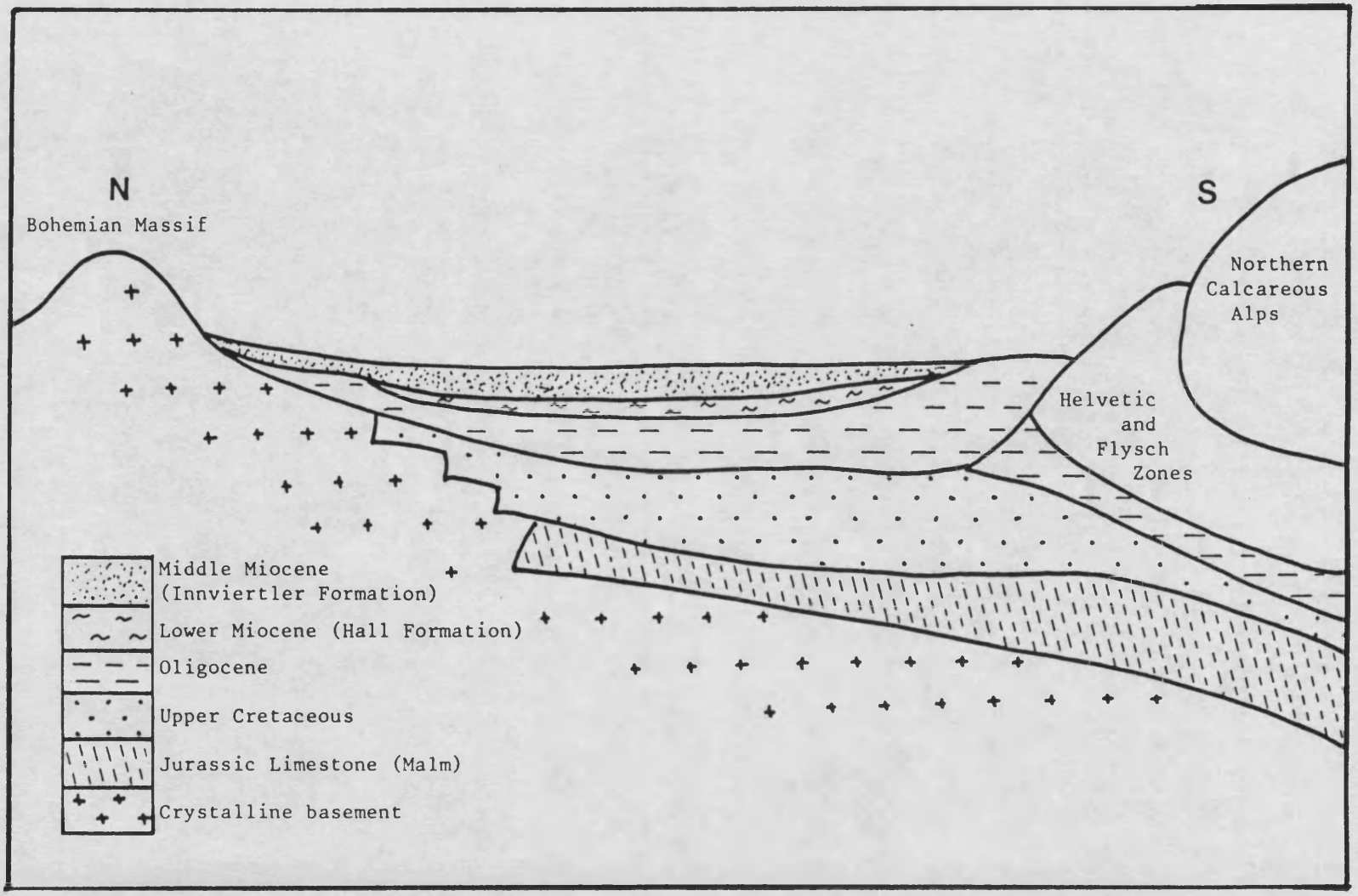

Figure 3.3 Geological strata in the Molasse basin

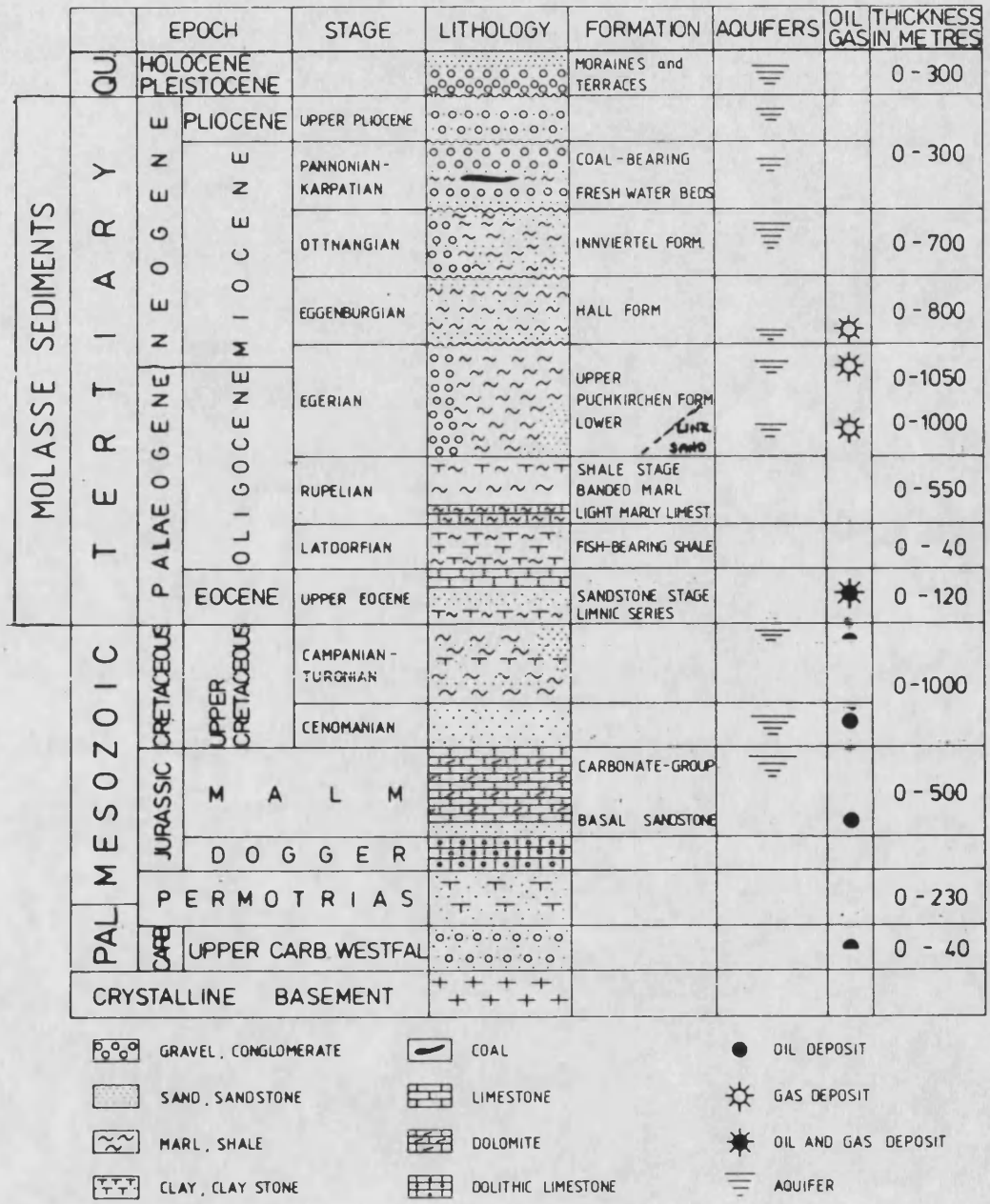

different sedimentation phases can be distinguished (Janoshek, 1964). The first phase was due to erosion of the Bohemian Massif and covers the period from Upper Eocene to the lowest Rupelian. The sandstones of this period are significant petroliferous beds, but there are no productive aquifers. The Latfordian "fish bearing shale" is viewed as a source rock for the Upper Eocene, Cenomanian and Upper Jurassic oil deposits.

Most of the Molasse sequences were deposited in the second phase (late Rupelian to Ottnangian) of sedimentation. The simultaneous subsidence of the basin led to a deposition of up to 3000m of finely clastic sequences. In the southern parts of the basin there are intercalations of pelagic clay and coarse sediments from the adjacent Alpine erosion; these facies form the Puchkirchen formation (Malzar, 1981). On the northern edge of the basin, at this time, a facies of quartz sand (Linz sand) was deposited. It forms a very important fresh water aquifer.

At the beginning of the Miocene the cessation of tectonic movement in the Alps led to a change in the sedimentation conditions. Pelitic deposits were dominant and productive aquifers are not therefore present in early Miocene deposits. During the Ottnangian (Innviertel Formation), shallow marine conditions predominated. The Innviertel sand horizons (Atzbach, Mehrnbach and Truebach sands) which occur in the central area of the basin are of major importance as aquifers. The aquifers are confined

by overlying silty-clay sediments. The catchment areas are the elevated region of the Kobernausser Wald and the Hausruck where coarse sediments of the Upper Freshwater Molasse occur. Hydraulic analyses show that the flow velocity is less than 1m/a.

The third Molasse cycle contains the mainly coarse-granular sediments of the Upper Freshwater Molasse. These bear unconfined, shallow lying groundwaters.

3.2 Hydrochemical Investigations

Water samples were taken from 19 wells in the Innviertel formation and deeper formations. Table 3.1 gives the source details. Table 3.2 shows the results of laboratory analyses together with field measurements of pH, Eh, dissolved oxygen and conductivity. All of the wells in the Innviertel flowed under artesian pressure. The deeper wells were either artesian or pumped by down well centrifugal lift pumps (Geinberg and Birnbach).

The waters of the Innviertel can be divided into three groups on the basis of their chemical composition (Table 3.2). Samples 1-3 (group 1) are oxidising waters of the Ca-bicarbonate type and have pCO_2 values greater than 0.01. Hydraulic observations and measured ^3H contents indicate they belong to very localised systems with short residence times. Samples 4-8 (group 2) belong to a regional flow system and have longer residence times. The variations in pCO_2, alkalinity, pH and Eh are due

Table 3.1 Details of groundwater sampling sites in the Molasse basin

No.	Location	Depth of well, m,	Depth of casing, m,	Artesian pressure m, H_2O	Yield litres/s	Date of sampling
Innviertel, Group 1						
1	Sigharting 2	30	30	1.5	0.5	28-7-82
2	Ried 3	20	12	1.8	0.4	27-7-83
3	St. Georgen	30	6	3.8	0.5	26-7-82
Innviertel, Group 2						
4	Mehrnbach 15	85	75	4.0	0.2	23-7-82
5	Rainbach 2	75	50	10.0	12.0	28-7-82
6	Altheim 6	142	-	2.5	0.1	23-7-82
7	Weng 3	209	-	2.9	0.1	22-7-82
8	Mining 7	150	4	8.0	0.8	22-7-82
Innviertel, Group 3						
9	Aufhausen	345	-	7.0	3.5	23-7-82
10	Ried 7	330	-	6.0	0.2	24-7-82
11	Braunau 1	138	4	1.8	1.0	21-7-82
12	Aurolzmünster	370	100	1.0	0.1	27-7-83
13	St. Marienkirchen*	105	30	27.0	1.2	26-7-82
14	Ried 18/D 1	452	452	10.0	-	26-7-83
Oligocene						
15	Schallerbach 1	460	430	23	40.0	2-8-82
16	Schallerbach 2**	670	552	4.0	ca. 28.0	27-7-82
Cretaceous (Campanian)						
17	Obernberg	1080	-	0.5	-	30-7-82
Jurassic (Malm)						
18	Birnbach 3	1618	1363	12(?)	55.0	29-7-82
19	Geinberg	2180	2166	18	ca. 3.5	30-7-82

* Aquifer Linz sand
** Aquifer Oligocene & Malm

Table 3.2 Chemical analyses of groundwaters from the Molasse basin

No.	Location	T °C	^3H TU	pH	Eh mV	O_2 µg/ℓ	Cond.$^{-1}$ µs.cm (25°C)	Na	K	Ca	Mg	NH_4	HCO_3	SO_4	Cl	log P_{CO_2}
								mg/ℓ								
Innviertel, Group 1																
1	Sigharting 1	10.2	72.	7.14	+ 220	14.0	530	3.8	0.96	93.0	19.1	-	360	19	3.0	- 1.66
2	Ried 3	10.1	26.	7.38	+ 96	0.2	596	6.8	1.40	98.0	24.6	<0.01	401	25	5.0	- 1.86
3	St. Georgen	11.3	9.	7.31	+ 72	0	617	6.1	2.1	75.0	34.9	-	390	32	2.0	- 1.80
Innviertel, Group 2																
4	Mehrnbach 15	12.0	≤ 2.4	7.81	+ 82	0.2	330	7.0	1.40	37.0	18.8	0.28	214	10	<1.0	- 2.62
5	Rainbach 2	11.4	≤ 0.6	7.76	- 15	0	370	4.0	0.82	55.0	14.0	-	220	14	<1.0	- 2.50
6	Altheim 6	13.2	≤ 0.4	7.98	+ 36	0	289	15.0	2.6	26.0	14.5	0.48	189	6	<1.0	- 2.79
7	Weng 3	15.2	≤ 0.4	8.14	+ 9	1.0	265	24.0	1.4	20.0	9.7	0.72	171	6	<1.0	- 3.02
8	Mining 7	12.3	≤ 1.1	8.15	- 6	2.0	245	20.0	1.2	20.0	9.3	0.64	162	9	<1.0	- 3.07
Innviertel, Group 3																
9	Aufhausen	13.4	≤ 1.8	7.95	+ 41	0	491	78.0	0.90	25.0	11.1	0.68	327	0	4.0	- 2.67
10	Ried 7	14.4	≤ 0.4	8.65	+ 12	0	406	86.0	2.2	5.4	2.2	4.8	272	2	<1.0	- 3.29
11	Braunau 1	12.6	≤ 0.4	8.57	- 12	1.0	543	126.0	0.79	4.0	2.2	0.72	348	0	4.0	- 3.15
12	Aurolzmünster	12.4	-	8.83	- 30	0.1	798	192.0	2.0	4.0	1.4	4.5	522	1	15.0	- 3.19
13	St. Marienkirchen	17.3	-	8.39	- 59	0	430	102.0	1.7	4.7	1.2	-	287	3	2.0	- 2.97
14	Ried 18/D 1	13.8	≤ 2.6	8.89	- 104	0.1	431	102.0	1.9	3.0	0.95	4.8	299	0	1.5	- 3.48
Oligocene																
15	Schallerbach 1	37.1	-	8.49	- 155	0.2	654	138.0	1.4	4.7	0.79	3.4	323	7	45.0	- 2.94
16	Schallerbach 2	34.4	-	8.78	- 129	0.7	1295	305.0	1.7	3.8	0.40	3.5	464	12	190.0	- 3.13
Cretaceous (Campanian)																
17	Obernberg	25.4	≤ 0.4	8.06	- 54	0	3975	854.0	1.7	10.0	0.97	3.6	525	5	1080.0	- 2.20
Jurassic (Malm)																
18	Birnbach 3	66.4	-	7.67	- 109	0	1776	428.0	5.7	5.7	1.5	-	736	17	241.0	- 1.54
19	Geinberg	70.2	-	7.15	- 131	0	1404	281.0	10.0	10.0	1.3	2.1	524	11	162.0	- 1.11

either to different infiltration conditions and or differences in the extent of hydrochemical evolution. The dominance of Ca^{2+} and HCO_3^- in groups 1 and 2 demonstrates the dissolution of calcite is the important geochemical process. Samples 9-14 (group 3) represent more highly evolved groundwaters of the Na- bicarbonate type. The Eh decreases to values more negative than -100mV whilst the pH increases relative to group 2. The pronounced decrease in Ca and Mg and increase in Na content relative to group 2 indicates that in the course of hydrochemical evolution, cation exchange processes have occurred with an exchanger mineral, E.

$$(Ca,Mg)\ (HCO_3)_2 + Na_2E = (Ca,Mg)E + 2NaHCO_3$$

With the removal of Ca and Mg ions from the liquid phase the solution becomes undersaturated with respect to calcite and dolomite, so that both minerals go into solution in the aquifer. The dissolved Ca^{2+} and Mg^{2+} are then immediately subject to exchange with the clay mineral. The solution of calcite and dolomite is reflected by a pronounced increase in alkalinity and pH accompanied by a decrease in Ca^{2+} and Mg^{2+}.

The low chloride contents found in all waters of the Innviertel Formation show that these marine sediments have been well flushed by meteoric water.

The waters from deeper aquifers are clearly distinguished from the Innviertel waters by their chemical composition and particularly by their high chloride

content. They are considered to be mixtures between meteoric input and connate interstitial fluids.

3.3 Dissolved U and its $^{234}U/^{238}U$ Activity Ratio

The U-contents of groundwaters from the Innviertel formation are generally less than 0.05µg/kg (Table 3.3). In the Ried-Braunau area the highest activity ratios are around Mining, Weng and Altheim, beyond which there is an activity ratio decrease toward Braunau and Aufhausen. An Eh-pH diagram shows that the samples are well within the UO_2 (Figure 3.4) stability field, consistent with their low U contents. Alpha recoil processes could explain the increase in activity ratio towards Weng, if there has been significant U deposition. The subsequent activity ratio decrease towards Braunau and Aufhausen could then be due to ^{234}U decay.

3.4 ^{222}Rn contents

The ^{222}Rn contents (Table 3.3) of groundwaters from the Innviertel formation are normally distributed (Figure 3.5) and average 220 pCi/Kg. The standard deviation 27% for the ^{222}Rn content is similar to that of the U content. The groundwater at St. Marienkirchen has not been included in this average since its high ^{222}Rn content shows it is dissimilar to the rest of the aquifer. This view is supported by the uranium chemistry and ^{4}He content of the site. Hydraulic observations suggest that St.

Table 3.3 Dissolved radioelement contents of groundwaters from the Molasse basin

No.	Location	^{222}Rn pCi/kg.	^{226}Ra pCi/kg	U-content µg/kg	$^{234}U/^{238}U$ activity ratio
Innviertel, Group 1					
1	Sigharting 2	502 ± 2.1 414 ± 1.8	0.20 ± 0.006	2.814 ± 0.098	1.14 ± 0.05
2	Ried 3	244 ± 1.5 236 ± 3.1	0.33 ± 0.008 0.33 ± 0.007	0.004 ± 0.001	1.27 ± 0.36
3	St. Georgen	250 ± 1.5 280 ± 1.8	0.35 ± 0.008 0.36 ± 0.009	0.080 ± 0.011	1.68 ± 0.29
Innviertel, Group 2					
4	Mehrnbach 15	142 ± 1.3 168 ± 1.5	0.13 ± 0.005 0.12 ± 0.004	0.005 ± 0.002	4.75 ± 2.07
5	Rainbach 2	139 ± 4.2 153 ± 4.6	0.19 ± 0.006 0.12 ± 0.006	0.063 ± 0.010	1.18 ± 0.26
6	Altheim 6	243 ± 5.3 249 ± 5.9	0.40 ± 0.008 0.42 ± 0.10	0.007 ± 0.002	3.45 ± 1.02
7	Weng 3	256 ± 3.7 232 ± 3.2	0.19 ± 0.006 0.23 ± 0.007	0.009 ± 0.002	4.24 ± 1.27
8	Mining 7	218 ± 1.4 251 ± 1.7	0.17 ± 0.005 0.20 ± 0.006	0.005 ± 0.001	4.11 ± 1.10
Innviertel, Group 3					
9	Aufhausen	156 ± 2.3 176 ± 2.4	0.14 ± 0.004 0.15 ± 0.005	0.047 ± 0.008	3.32 ± 0.62
10	Ried 7	458 ± 2.0 338 ± 1.6	0.23 ± 0.007 0.29 ± 0.008	0.003 ± 0.001	2.86 ± 1.44
11	Braunau 1	214 ± 3.8 233 ± 4.5	0.67 ± 0.01 0.63 ± 0.01	0.006 ± 0.006	1.8 ± 0.83
12	Aurolmünster	319 ± 6.0 256 ± 1.3	0.39 ± 0.008 0.39 ± 0.008	0.001 ± 0.005	1.08 ± 0.06

Table 3.3 Dissolved radioelement contents of groundwaters from the Molasse basin

No.	Location	^{222}Rn pCi/kg.	^{226}Ra pCi/kg	U-content µg/kg	$^{234}U/^{238}U$ activity ratio
13	St. Marienkirchen	746 ± 7.7 903 ± 7.7	0.47 ± 0.009 0.61 ± 0.01	0.037 ± 0.007	6.86 ± 1.43
14	Ried 18/D 1	3 ± 0.2 2 ± 0.2	0.08 ± 0.004 0.11 ± 0.005	0.069 ± 0.002	2.35 ± 0.10
Oligocene					
15	Schallerbach 1	602 ± 2.0 546 ± 1.7	1.43 ± 0.009 1.44 ± 0.01	0.193 ± 0.008	1.04 ± 0.06
16	Schallerbach 2	417 ± 6.3 351 ± 6.0	0.26 ± 0.007 0.29 ± 0.01	0.317 ± 0.013	1.04 ± 0.14
Cretaceous (Campanian)					
17	Obernberg	313 ± 6.6 311 ± 7.2	0.20 ± 0.006 0.29 ± 0.06	0.032 ± 0.009	1.74 ± 0.62
Jurassic (Malm)					
18	Birnbach 3	291 ± 4.1 265 ± 3.4	1.84 ± 0.02 1.64 ± 0.02	0.016 ± 0.003	1.62 ± 0.36
19	Geinberg	267 ± 4.0 289 ± 2.1	2.17 ± 0.021 2.09 ± 0.023		

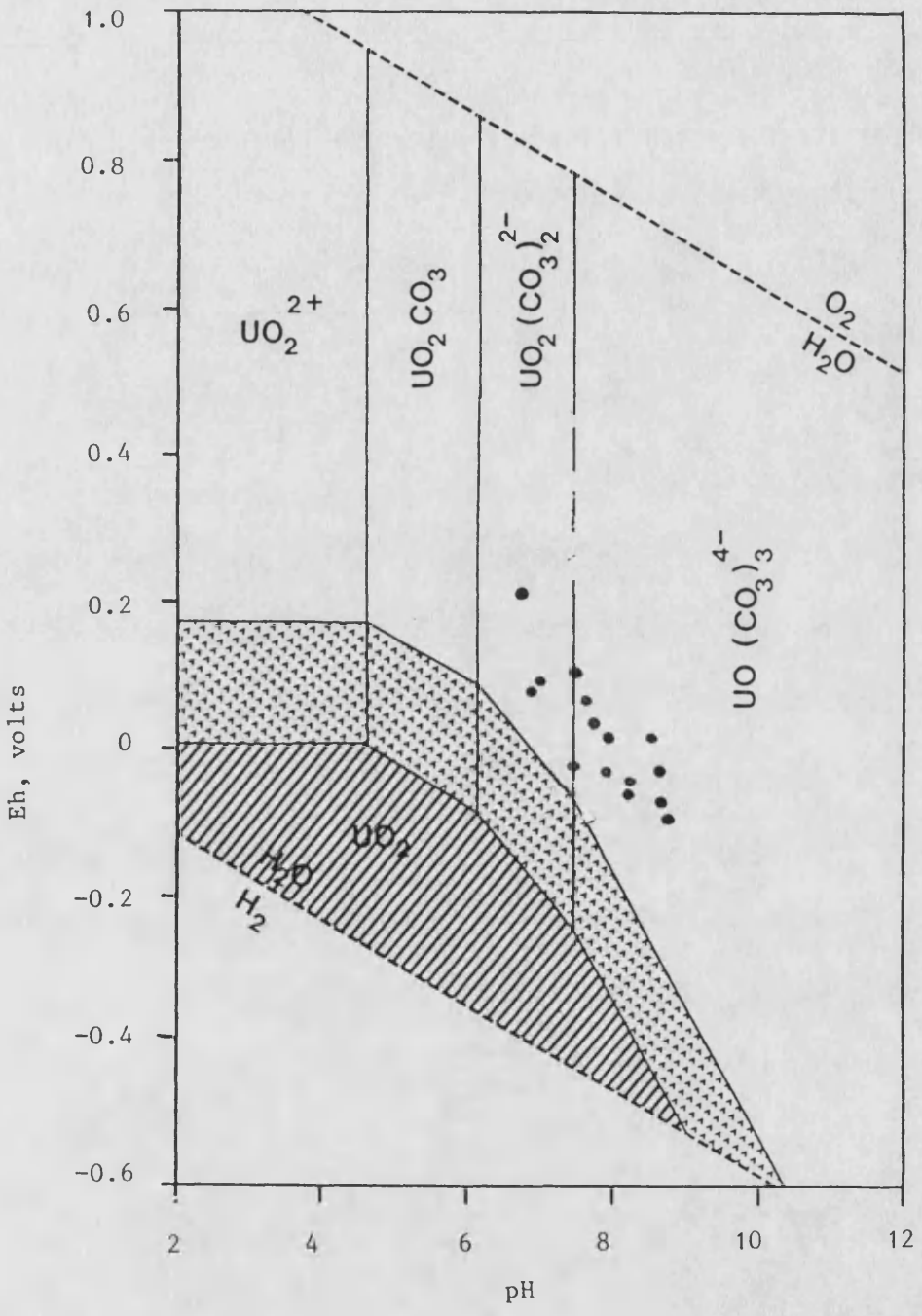

Figure 3.4 The stability of uranyl species in solution as a function of pH and Eh.

Marienkirchen is a mixture between deeper groundwaters which ascend in this region and shallow water.

Substitution of the average ^{222}Rn content into the equation

$$[Rn] = \frac{F.\ 0.7336.p.[U]_r.10^3}{\emptyset\ .\ 2.22}$$

where p is the bulk density, $\emptyset$ the fractional porosity, $[U]_r$ is the U content of the rock matrix, and [Rn] is in pCi/Kg, yields an overall Rn release efficiency, F, of 0.04. This is similar to the value reported for the Bunter sandstone aquifer in England (Andrews and Lee, 1979) in which the flow is predominantly interstitial. Since the ^{222}Rn content is primarily determined by the aquifer U content as well as the extent of the rock-water interface, the ^{222}Rn distribution for the groundwaters indicates that the extent of variability in the aquifer in these respects is ±27%.

3.5 ^{226}Ra contents

The ^{226}Ra contents of the Innviertel groundwaters are lognormally distributed (Figure 3.6) with a mean of 0.26 pCi/Kg. The presence of ^{230}Th at the rock/water interface should lead to α-recoil ejection of ^{226}Ra into solution. The ^{226}Ra activity would require about 8000 years (5 half lives of ^{226}Ra) to establish equilibrium with its production rate. Since the activity due to ^{226}Ra in

Figure 3.5

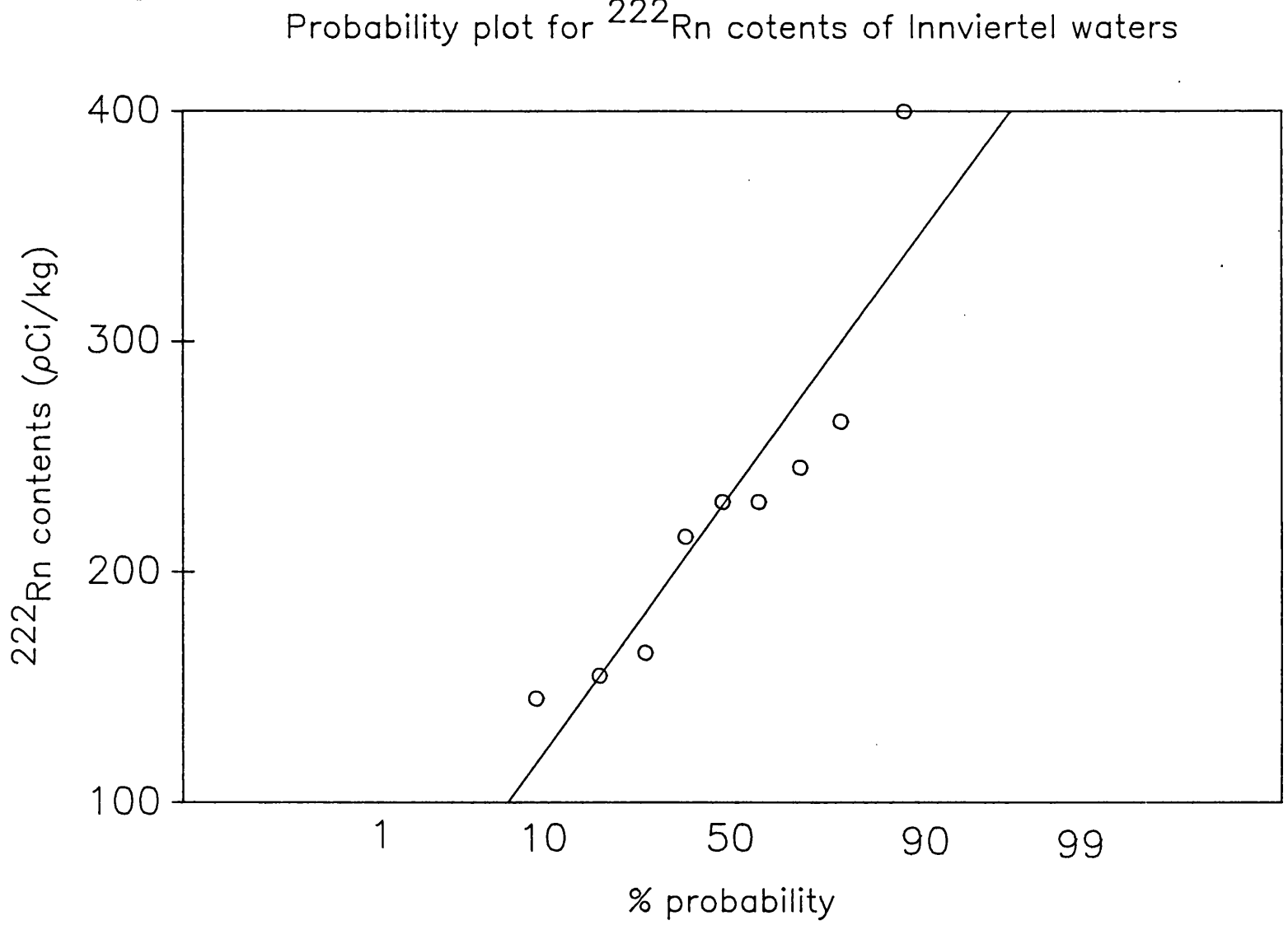
Probability plot for ^{222}Rn cotents of Innviertel waters
400
300
200
100
^{222}Rn contents (ρCi/kg)
1
10
50
90
99
% probability

Figure 3.6 Probability plot for ^{226}Ra contents of Innviertel waters

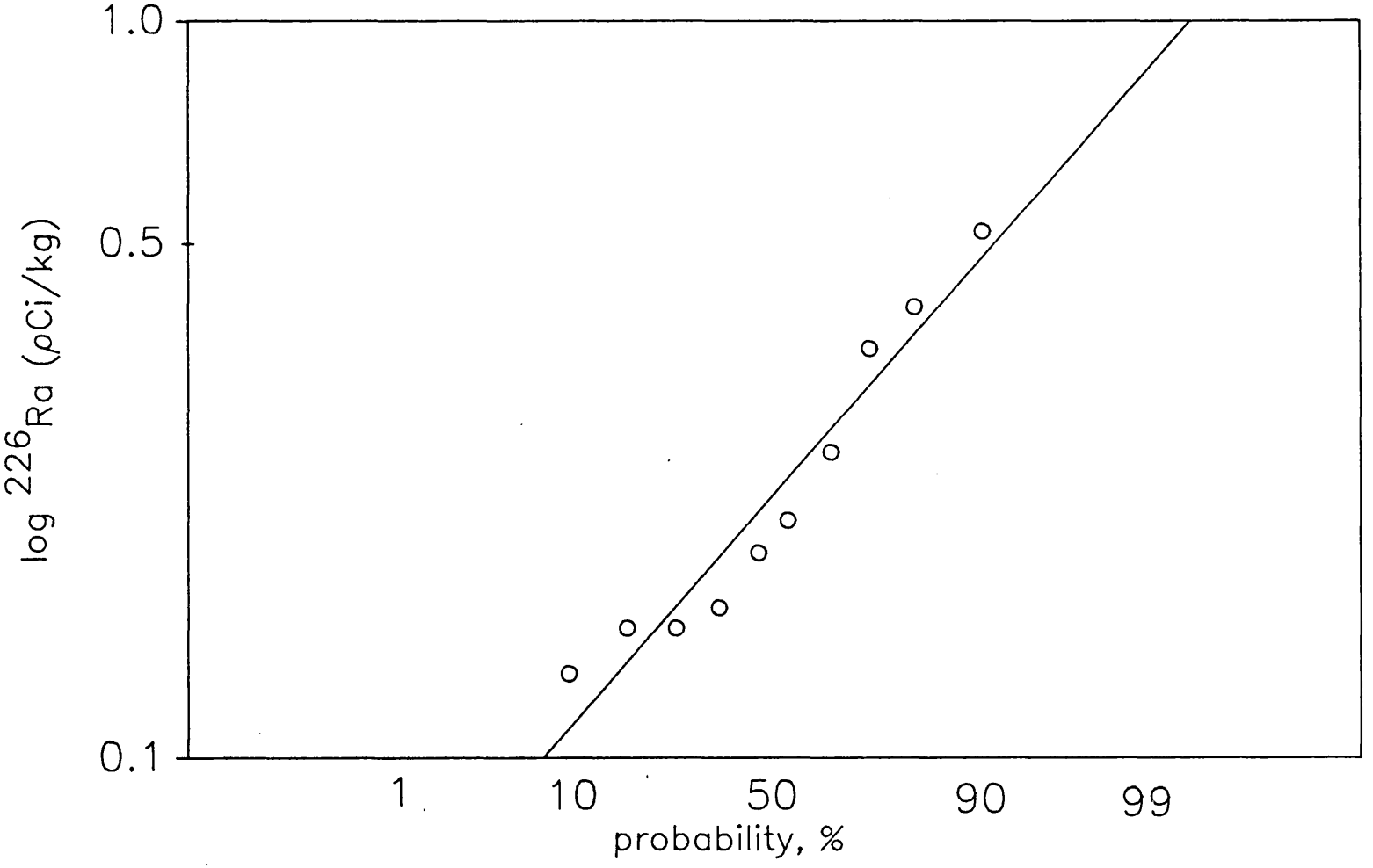

solution is very much less than that of ^{222}Rn, although these groundwaters are old enough to have lost all ^{14}C, it is clear that the residence time of ^{226}Ra atoms in solution must be short compared with their half-life. The Ca^{2+} ions in solution either cannot be effective as carriers for ^{226}Ra, or ^{226}Ra is lost from solution as incongruent exchange of Ca^{2+} occurs between solution and the carbonate phase of the rock. In the latter case the ^{226}Ra content of the groundwater would be controlled by the CO_3^{2-}/HCO_3^- equilibria. These equilibria are temperature dependent and it is interesting to note that the thermal waters have generally higher ^{226}Ra contents than those of the Innviertel formation, the highest ^{226}Ra contents are present in the highest temperature waters.

Figure 3.8 shows the relationship between ^{226}Ra content and collection temperature indicating the warmer waters have higher radium contents, showing a temperature dependence of radium solubility.

3.6 Radiogenic Helium

All of the inert gases are dissolved in the unsaturated zone where equilibration between the groundwater and the atmosphere occurs at the prevailing recharge temperature. The inert gas analyses are reported in Table 3.4. The groundwaters from the eastern part of the Innviertel have ^4He contents which are only slightly in excess of the atmospheric equilibration value, (apart

Figure 3.8 ^{226}Ra content against collection temperature for Molasse waters

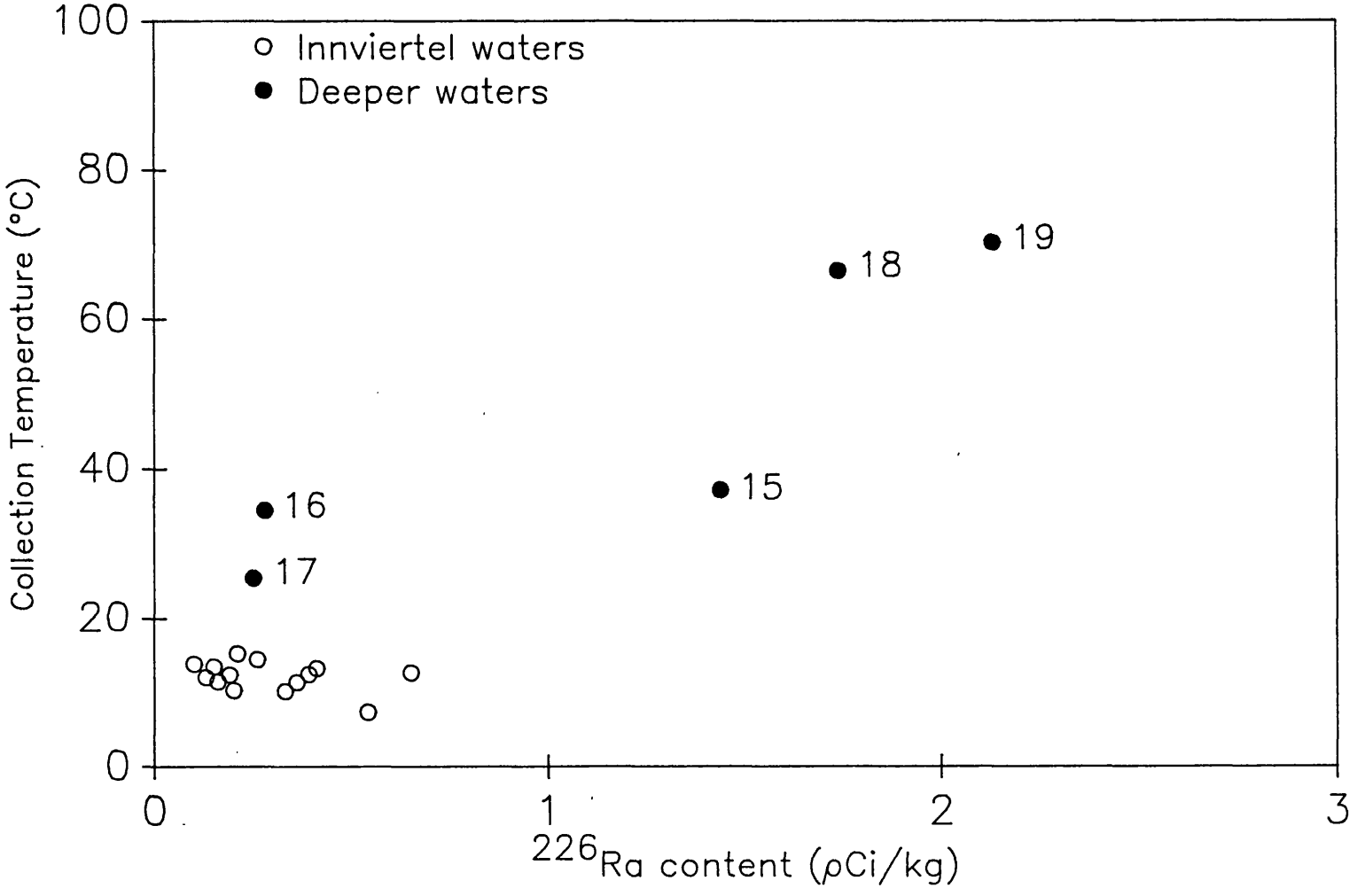

Table 3.4 N_2/Ar ratios, inert gas contents (cm^3 STP/$cm^3 H_2O$), and derived recharge temperatures

No.	Location	N_2/Ar ratio		$^4He.10^8$	$Ne.10^7$	$Ar.10^4$	$Kr.10^8$	$Xe.10^8$	C.I.	Average R.T.
Innviertel, Group 1										
1A	Sigharting 2	43.75	a	13.26	2.23	4.03	9.37	1.27		
			b	12.75	2.06	3.94	9.27	1.26	1.09	10.3
			c	-	10.1	9.5	10.0	11.5		
1B	Sigharting 2	43.39	a	17.99	2.35	4.07	9.20	1.32		
			b	17.3	2.06	3.92	9.01	1.31	1.15	10.4
			c	-	10.5	9.7	11.0	10.4		
2A	Ried 3		a	16.27	2.46	4.12	9.97	1.39		
			b	15.18	2.08	3.92	9.73	1.37	1.18	9.1
			c	-	9.2	9.7	8.3	9.1		
2B	Ried 3		a	12.37	2.42	3.99	9.91	1.37		
			b	11.36	3.07	3.81	9.70	1.35	1.17	9.6
			c	-	9.5	11.0	8.4	9.5		
3A	St. Georgen	41.25	a	10.55	2.92	4.56	10.56	1.47		
			b	8.22	2.11	4.15	10.05	1.43	1.38	7.5
			c	-	7.6	7.3	7.2	7.9		
3B	St. Georgen	41.22	a	17.99	2.96	4.61	10.17	1.47		
			b	15.54	2.11	4.17	9.63	1.43	1.40	7.8
			c	-	7.9	7.0	8.6	7.9		
Innviertel, Group 2										
4A	Mehrnbach 15	41.92	a	15.24	2.67	4.24	9.57	1.32		
			b	13.49	2.06	3.92	9.19	1.29	1.29	10.3
			c	-	10.2	9.7	10.3	10.9		
4B	Mehrnbach 15	40.39	a	13.74	2.89	4.08	9.55	1.36		
			b	11.32	2.04	3.65	9.02	1.32	1.41	11.3
			c	-	11.2	13.0	10.9	10.1		

Table 3.4

5A	Rainbach 2	41.06	a	15.89	2.32	4.09	9.57	1.32		
			b	15.16	2.07	3.96	9.41	1.31	1.12	9.7
			c	-	9.9	9.3	9.4	10.4		
5B	Rainbach 2	41.15	a	14.98	2.28	4.12	9.49	1.35		
			b	14.37	2.07	4.02	9.36	1.34	1.10	9.4
			c	-	9.7	8.7	9.6	9.7		
6A	Altheim 6	44.48	a	23.14	2.49	4.43	10.85	1.56		
			b	22.15	2.14	4.25	10.63	1.55	1.16	5.9
			c	-	6.1	6.2	5.4	5.8		
6B	Altheim 6	42.92	a	26.81	2.67	4.46	10.22	1.53		
			b	25.24	2.12	4.18	9.87	1.50	1.26	7.1
			c	-	7.0	7.0	7.8	6.6		
7A	Weng 3	37.64	a	52.38	3.56	5.01	11.45	1.63		
			b	48.35	2.16	4.29	10.57	1.56	1.65	5.6
			c	-	5.6	5.9	5.5	5.5		
7B	Weng 3	40.20	a	49.55	3.15	4.86	11.24	1.58		
			b	46.70	2.16	4.35	10.62	1.54	1.46	5.6
			c	-	5.6	5.3	5.4	6.0		
8A	Mining 7	35.82	a	38.22	3.06	4.72	10.98	1.57		
			b	35.57	2.14	4.25	10.40	1.52	1.43	6.2
			c	-	6.1	6.3	6.1	6.2		
8B	Mining 7	36.71	a	38.20	2.99	4.76	11.11	1.60		
			b	35.78	2.16	4.33	10.59	1.56	1.39	5.5
			c	-	5.6	5.5	5.5	5.6		
Innviertel, Group 3										
9A	Aufhausen	49.86	a	110.78	2.82	4.64	10.81	1.50		
			b	108.81	2.14	4.29	10.38	1.46	1.32	6.4
			c	-	6.4	5.9	6.1	7.2		
9B	Aufhausen	49.83	a	122.19	2.85	4.66	10.69	1.49		
			b	120.11	2.13	4.29	10.24	1.45	1.34	6.7
			c	-	6.7	5.9	6.6	7.5		
10A	Ried 7	38.99	a	44.18	3.18	4.68	10.96	1.58		
			b	41.17	2.14	4.14	10.31	1.53	1.49	6.5
			c	-	6.4	7.3	6.4	6.0		

Table 3.4

No.	Location	N_2/Ar ratio		$^4He.10^8$	$Ne.10^7$	$Ar.10^4$	$Kr.10^8$	$Xe.10^8$	C.I.	Average R.T.
10B	Ried 7	41.17	a	43.91	3.06	4.98	11.11	1.55		
			b	41.28	2.15	4.51	10.54	1.51	1.42	5.5
			c	-	5.9	3.9	5.6	6.5		
11A	Braunau 1	35.50	a	180.99	3.95	5.52	12.26	1.64		
			b	175.90	2.19	4.26	11.15	1.56	1.81	4.2
			c	-	4.2	3.0	3.8	5.6		
11B	Braunau 1	37.35	a	147.51	3.22	5.03	11.56	1.59		
			b	144.49	2.17	4.49	10.90	1.54	1.48	4.9
			c	-	4.8	4.1	4.6	5.9		
12A	Aurolmünster		a	346.51	3.59	4.96	10.95	1.65		
			b	342.51	2.14	4.21	10.04	1.58	1.68	6.4
			c	-	6.4	6.6	7.2	5.2		
12B	Aurolmünster		a	329.95	3.83	4.80	11.11	1.45		
			b	324.93	2.09	3.90	10.02	1.37	1.83	8.7
			c	-	8.6	9.9	7.3	9.1		
13A	St. Marienkirchen	38.34	a	214.14	3.01	4.80	11.12	1.55		
			b	211.64	2.14	4.36	10.58	1.51	1.40	5.8
			c	-	6.1	5.3	5.5	6.4		
13B	St. Marienkirchen	38.79	a	152.02	2.91	4.92	11.13	1.61		
			b	149.87	2.17	4.54	10.66	1.57	1.34	4.8
			c	-	5.0	3.7	5.3	5.3		
14A	Ried 18/D 1		a	63.54	2.89	4.62	11.04	1.46		
			b	61.34	2.13	4.22	10.56	1.43	1.36	6.7
			c	-	6.7	6.5	5.6	8.0		
14B	Ried 18/D 1		a	90.60	3.30	4.89	11.69	1.63		
			b	87.35	2.17	4.31	10.98	1.57	1.52	5.1
			c	-	5.0	5.7	4.3	5.3		
Oligocene										
15A	Schallerbach 1	38.81	a	625.89	2.90	4.74	11.01	1.53		
			b	623.70	2.14	4.35	10.53	1.49	1.35	5.9
			c	-	6.1	5.3	5.7	6.7		
15B	Schallerbach 1	39.05	a	508.21	2.89	4.43	11.04	1.58		
			b	506.03	2.14	4.05	10.56	1.55	1.35	6.4
			c	-	6.1	8.3	5.6	5.7		

Table 3.4

16A	Schallerbach 2		a	1908.76	2.89	4.95	13.15	1.52		
			b	1906.78	2.21	4.59	12.72	1.49	1.31	3.3
			c	-	3.4	3.2	-0.1	6.8		
16B	Schallerbach 2		a	1464.33	2.95	4.53	11.39	1.61		
			b	1464.01	2.15	4.11	10.89	1.57	1.37	5.9
			c	-	5.9	7.6	4.6	5.4		
Cretaceous (Campanian)										
17A	Obernberg	35.36	a	820.99	0.34	1.07	3.39	0.59	-	-
17B	Obernberg		a	616.31	0.55	1.09	3.29	0.62	-	-
Jurassic (Malm)										
18A	Birnbach 3	40.41	a	2130.37	1.16	2.46	6.55	0.98	-	-
18B	Birnbach 3		a	1171.02	1.13	2.34	6.25	0.97	-	-
19	Geinberg	48.01	a	5914.58	4.30	6.19	13.54	1.76		
			b	5908.67	2.24	5.14	12.25	1.67	1.92	1.4
			c	-	1.9	-0.9	1.0	3.8		

a. Original analysis. b. Analysis corrected for excess air. c. Recharge Temp., °C. C.I. Contamination Index.

from St. Marienkirchen). In the western Innviertel there is an increased ^4He content. There are also some very high contents for the deeper, thermal aquifers. These high ^4He contents must be due either to the production of ^4He by decay of U and Th in the aquifer or diffusion of ^4He from deeper strata or weathering release of stored helium in the aquifer matrix.

The highest ^4He contents in the Innviertel are present at Braunau and Aufhausen, these groundwaters are chemically the most evolved and on a hydrological basis should have the longest residence times. The thermal waters all have ^4He contents which are considerably higher than any of the Innviertel groundwaters.

The ^4He accumulation rate in the pore fluids of the Innviertel may be calculated on the assumption that all the He formed by U and Th decay in the aquifer is dissolved in the pore fluids. Using the uranium and thorium contents in Table 3.6 and a porosity of 0.15, such calculations show that the ^4He accumulation rate is $7.5 \times 10^{-12} cm^3$ STP/cm^3 H_2O per year. If this were the only He source the generation of the observed He contents would require much longer groundwater ages than those suggested by hydrological methods. The total stored helium in the Innviertel rocks would be $4.4 \times 10^{-6} cm^3/g$ providing there has been no loss before contact with the water. If a weathering rate of 3×10^{-11}g rock cm^{-3} H_2O yr^{-1} is used (Torgeson and Clarke, 1985) then the accumulation rate of helium due to weathering is

Table 3.5 $^3He/^4He$ isotopic ratios of dissolved helium

No.	Location	$^3He/^4He$* x 10^{-8}	^4He content x 10^{-8} $cm^3/g\ H_2O$	Estimated residence time, years†
Innviertel, Group 1				
1	Sigharting	279.57 ± 2.77	18	1340
2	Ried 3			
3	St. Georgen	137.02 ± 1.38	18	1340
Innviertel, Group 2				
4	Mehrnbach	103.38 ± 1.25	15	840
5	Rainbach	84.29 ± 1.11	16	1010
6	Altheim	37.64 ± 0.55	29	3190
7	Weng 3	24.36 ± 0.42	52	7060
8	Mining 7	28.65 ± 0.55	38	4700
Innviertel, Group 3				
9	Aufhausen	10.35 ± 0.22	111	17000
10	Ried 7	20.34 ± 0.42	61	8570
11	Braunau 1	9.23 ± 0.21	181	28730
12	Aurolmünster			
13	St. Marienkirchen	7.53 ± 0.22	214	34270
14	Ried 18/D 1			
Oligocene				
15	Schallerbach 1	5.23 ± 0.17	626	103500
16	Schallerbach 2	4.43 ± 0.17	1909	319000
Cretaceous (Campanian)				
17	Obernberg	7.70 ± 0.24	821	136000
Jurassic (Malm)				
18	Birnbach	5.65 ± 0.17	2130	356000
19	Geinberg	6.28 ± 0.19	5915	992000
	Atmospheric helium	138.4		

Table 3.6 U, Th, K contents of Molasse sediments and the granitic basement (γ-spectrometric measurements)

Sample name	Depth m	Formation	U-content $\mu g\ g^{-1}$	Th-content $\mu g\ g^{-1}$	Th/U	K-content %
		Pliocene				
	outcrop	gravels	0.57 ± 0.12	0.95 ± 0.71	1.67	0.43 ± 0.02
		Miocene				
Haag am Hausruck	outcrop	Upper Freshwater Molasse	1.63 ± 0.13	4.95 ± 0.72	3.04	0.87 ± 0.02
Braunau b/h	40-45	Braunauer Schlier	1.75 ± 0.12	10.62 ± 0.67	6.07	1.68 ± 0.02
Braunau b/h	80	Braunauer Schlier	1.72 ± 0.12	8.88 ± 0.67	5.16	1.70 ± 0.02
Braunau b/h	100-105	Braunauer Schlier	2.23 ± 0.12	11.02 ± 0.67	4.94	1.74 ± 0.02
Fraunstein b/h	11.2		1.27 ± 0.12	6.43 ± 0.66	5.06	1.55 ± 0.02
Mehrnbach	outcrop	Mehrnbacher Sand	1.97 ± 0.12	10.44 ± 0.12	5.30	1.49 ± 0.02
Mehrnbach	outcrop	Mehrnbacher Sand	1.21 ± 0.12	7.47 ± 0.66	6.17	1.47 ± 0.02
Ried	outcrop	Rieder Schichten	1.34 ± 0.12	9.55 ± 0.67	7.13	1.54 ± 0.02
Vöcklabruck	outcrop	Vöckla Schichten	1.06 ± 0.11	4.79 ± 0.65	4.52	0.12 ± 0.01*
		Jurassic				
Reichersberg b/h	1500	Malm Limestone	0.97 ± 0.11	0.83 ± 0.11	0.86	0.13 ± 0.01
		Archaen				
Schärding	outcrop	Schärding granite	7.33 ± 0.17	40.20 ± 0.83	5.48	4.75 ± 0.03

3.4×10^{-15} cm^3 STP/cm^3 H_2O per year. It is clear that weathering release and in situ production of helium are much too low to account for the observed ^4He contents of these waters. This implies that diffusion of He from deeper strata is a more significant helium source. Figure 3.9 illustrates the relationship between recharge temperature and ^4He content. This shows that waters recharged under cooler climatic conditions are from deeper horizons in the Molasse sediments and have greater contents of dissolved helium.

3.7 $^3He/^4He$ Ratio

The $^3He/^4He$ isotopic ratios of the dissolved helium was determined with a Micromass MM3000 mass spectrometer at the Department of Earth Sciences, University of Cambridge. The results are shown in Table 3.5. The $^3He/^4He$ ratio is plotted against the total dissolved He content in Figure 3.7. ^3He is produced in a rock matrix by the reaction

$$Li\ (n,\alpha)\ ^3H \xrightarrow{\beta} {}^3He$$

^4He is produced by alpha decay of radioelements. The $^3He/^4He$ production ratio is dependent mainly on the Li content of the formation (Andrews, 1984) whilst the ^4He production rate is determined by the radioelement content of the rock. Isotope production ratios and ^4He production rates for the various formations of the Molasse zone are in Table 3.5. Mixing lines are shown on Figure 3.7 for

Figure 3.9

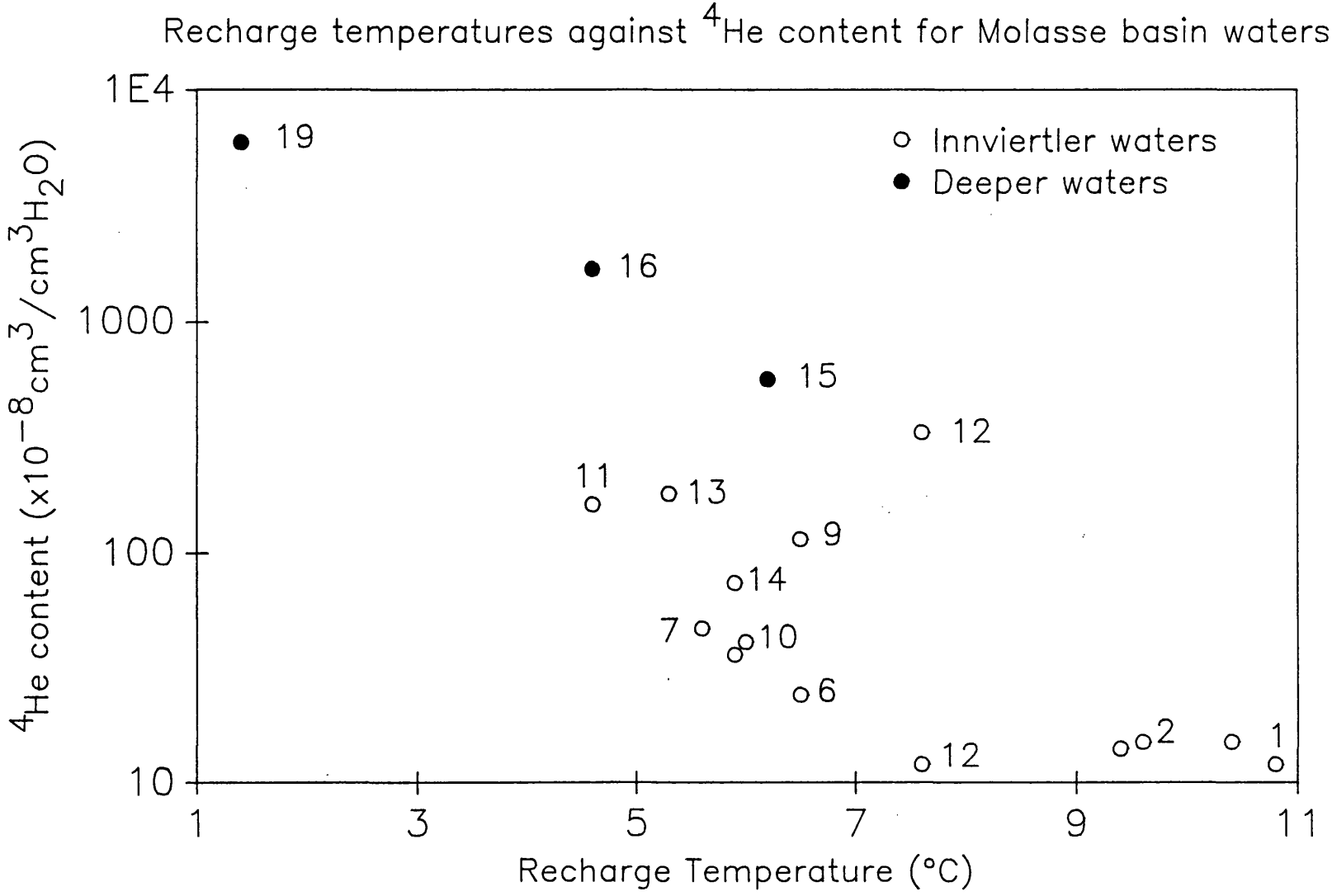
Recharge temperatures against ^{4}He content for Molasse basin waters
^{4}He content (x10^{-8}cm^3/cm^{3}H$_2$O)
1E4
1000
100
10
1
3
5
7
9
11
Recharge Temperature (°C)
Innviertler waters
Deeper waters
19
16
15
12
11
13
9
14
7
10
6
12
2
1

Figure 3.7 $^3He/^4He$ ratio as a function of He content for Molasse waters

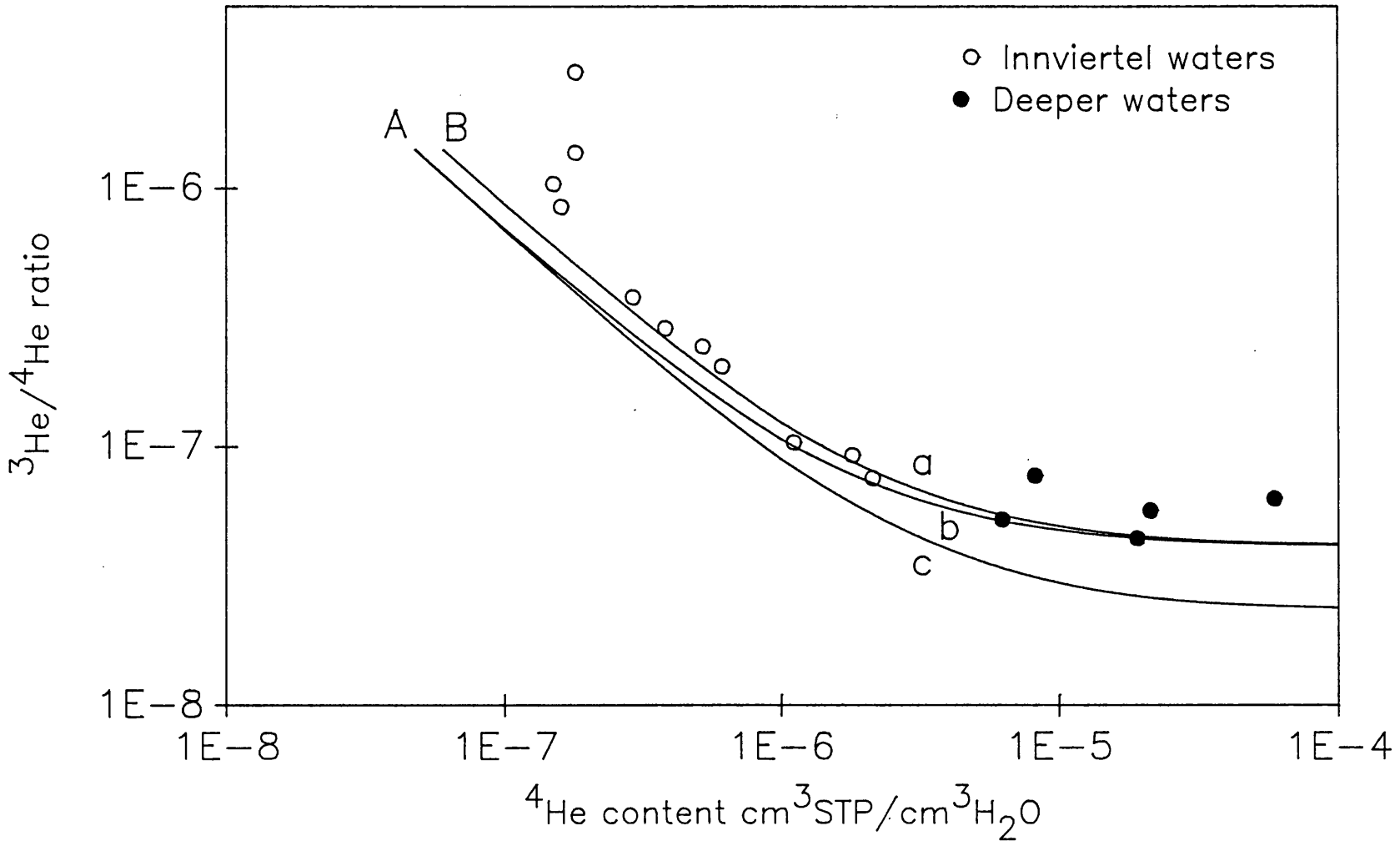

admixture of radiogenic helium from the Innviertel and granitic basement with atmospheric helium. The highest calculated $^3He/^4He$ ratio for radiogenic helium is found for the Sherding granite which outcrops close to the Bohemian Massif. This ratio is taken as representative of the granitic basement. Its $^3He/^4He$ ratio is 4×10^{-8} compared with 1.8×10^{-8} for geochemistry appropriate for the Innviertel sediments.

The dilution line for mixing of radiogenic helium from the basement with atmospheric helium in air saturated water is shown as line 'b' Figure 3.7. The dilution line for mixing of basement helium with air saturated water containing excess air is shown as line 'a'. The line 'c' represents mixing of Innviertel helium with atmospheric helium in air saturated water. From Figure 3.7 it can be seen that the helium ratios in these waters are too high to be produced by mixing of atmospheric helium with Innviertel radiogenic helium. One possible reason for this is the decay of thermonuclear ^3H in some of these waters, however, nearly all of these waters contain negligible ^3H. This would however account for the ratios for group 1 Innviertel waters which have $^3He/^4He$ ratios greater than the atmospheric ratio.

The more evolved Innviertel waters can be seen to fit on line 'a' their helium contents are therefore explained as being due to mixing of atmospheric helium dissolved in the water, which also contains excess air, with radiogenic helium from the granitic basement. The presence of excess

air is demonstrated in correcting the inert gas concentrations to obtain recharge temperatures. This model does not take into account the possibility of diffusion of mantle helium. This is considered unlikely to occur for the geological setting of this aquifer (Oxburgh et al, 1986).

3.8 Dating of Groundwaters using Helium Flux

For a uniform sedimentary layer which loses helium from its upper surface, the helium flux, F, is given by the equation

$$F = 2G\,(Dt/\pi)^{0.5}$$

where G is the ^4He generation rate, D its diffusion constant in sediments of age t years. Considering a basement age of 800Ma for the Scharding granite and a diffusion constant of $10^{-4}m^2a^{-1}$. The rate of lateral movement of the groundwater is likely to be very much greater than this diffusive movement (Andrews and Lee, 1979) so that water will collect the migrating helium as it moves through the aquifer.

For a helium flux of F cm^3/m^2 across the base of the aquifer which has a fractional porosity Ø and thickness h (metres) and velocity V (ma^{-1}) the total helium collected in the groundwater after moving a distance x metres is given by:

$$[He] = \frac{x.F}{V\emptyset h}$$

Cancelling the distance x with the velocity leaves the residence time tr (in years) for the groundwater

$$[He] = \frac{tr.F}{\emptyset h}$$

The groundwater residence times calculated using this method are shown in Table 3.5. Ages range from 640-6000 years for the more evolved Innviertel groundwaters.

3.9 Groundwater Recharge Temperatures

Waters with ages calculated to be less than 6000 years all have recharge temperatures, calculated using inert gas data, comparable to Holocene climatic conditions. Groundwaters older than 8000 years have recharge temperatures indicating a cooler climate during their recharge. There is a large uncertainty on groundwater ages because of the possible variation in radioelement content of the flux and uncertainty in the value of the diffusion coefficient. However it is probable that groundwater at Mining 7, Weng 3 and Ried 7 are post glacial recharge. The waters at Altheim, Mehrnbach, St. Georgen, Sigharting and Rainbach all have recharge temperatures and ages consistent with recharge in the late Holocene. The groundwaters at Braunau 1 and Aufhausen are much older with lower recharge temperatures than at present and were probably recharged in the interstadial prior to the last glaciation (Andrews and Lee, 1979).

3.10 Isotopic Composition

The isotopic composition of these groundwaters all lie close to the world meteoric line (Figure 3.10)

$$\delta^{2}H = 8\delta^{18}O + 10°/_{oo}$$

The recharge temperatures derived from inert gas contents of the groundwaters are plotted against $\delta^{18}O$ in Figure 3.11. Figure 3.11 also shows the Dansgaard (1964) relationship between mean annual air temperature and $\delta^{18}O$. The Dansgaard line is represented by the equation:

$$\delta^{18}O = 0.695t - 13.6°/_{oo}$$

This equation is based on high latitude data. Evans et al (1978) have shown for maritime western Europe the following relationship applies:

$$\delta^{18}O = 0.18t - 8.53°/_{oo}$$

If recharge temperatures are calculated using the relation of Evans or Dansgaard the resulting temperatures are very much too high. This may be explained by the continental effect in which heavy isotopes are preferentially precipitated on the western side of Europe. Thus the precipitation in Upper Austria is very light isotopically when compared with rainfall in western Europe. The relationship between $\delta^{18}O$ and recharge temperature for the Innviertel waters is:

$$\delta^{18}O = 0.506t - 14.9°/_{oo}$$

Figure 3.10 δ^2H against $\delta^{18}O$ for Innviertel groundwaters

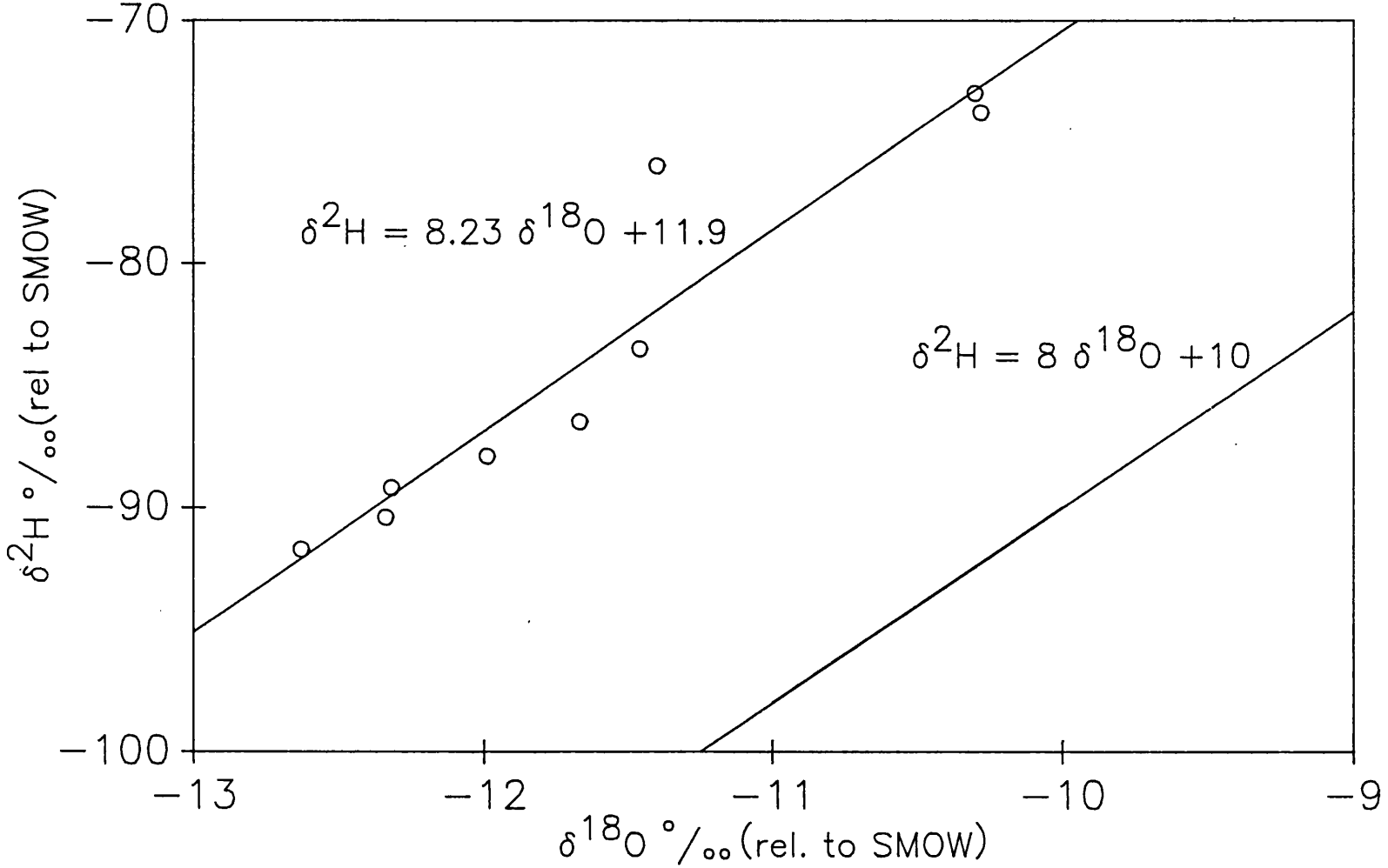

Figure 3.11 Recharge temperature against $\delta^{18}O$ for Innviertel waters

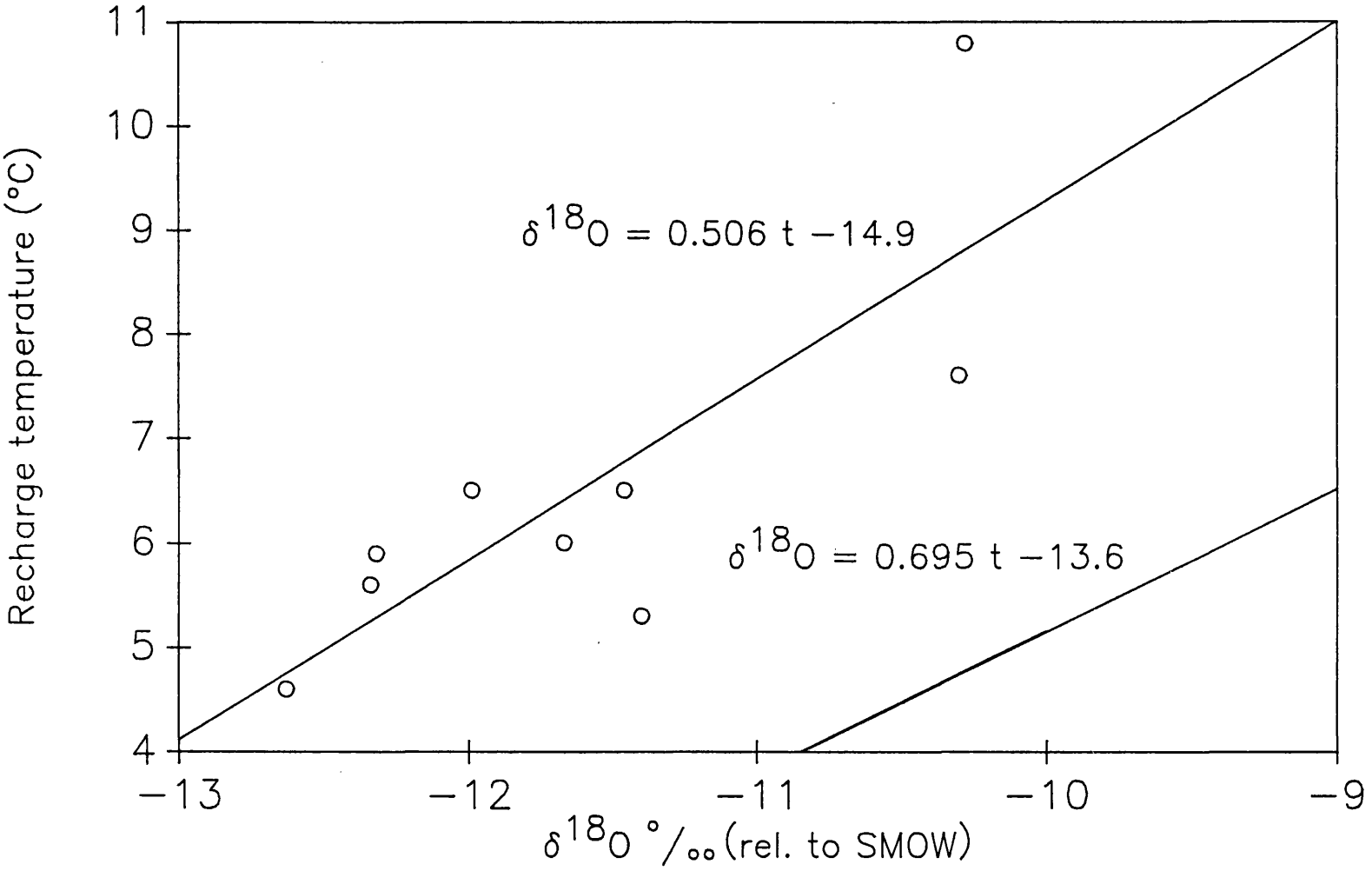

3.11 Nitrogen/Argon Ratio of Dissolved Gases

The N_2/Ar ratio for dissolved gas in air equilibrated water at 0-20°C is between 36.9 and 38.3. If excess air is added to this air equilibrated water value in the quantity found in the inert gas analysis the N_2/Ar values are increased to 41.5-42.8. The Innviertel groundwaters of groups 2 and 3 have N_2/Ar ratios between 36 and 40 (Table 3.4) which is in good agreement with ratios expected at these recharge temperatures. Exeptionally high N_2/Ar ratios were determined at Aufhausen and Geinberg; these may be due to the presence of exsolved gas (Chapter 6).

Figure 3.12 shows the measured nitrogen and argon values for the Molasse waters. Extrapolation along a line with a slope of 83.54 (equivalent to air N_2/Ar ratio) produces intersection with the air equilibrated water line. The point of intersection corresponds to air/water equilibration at between 5 and 15°C. The indicated recharge temperature groupings are similar to that derived from inert gas measurements.

Figure 3.12 Nitrogen content against argon content for Molasse waters
(slopes = 83.54 representing removal of excess air)

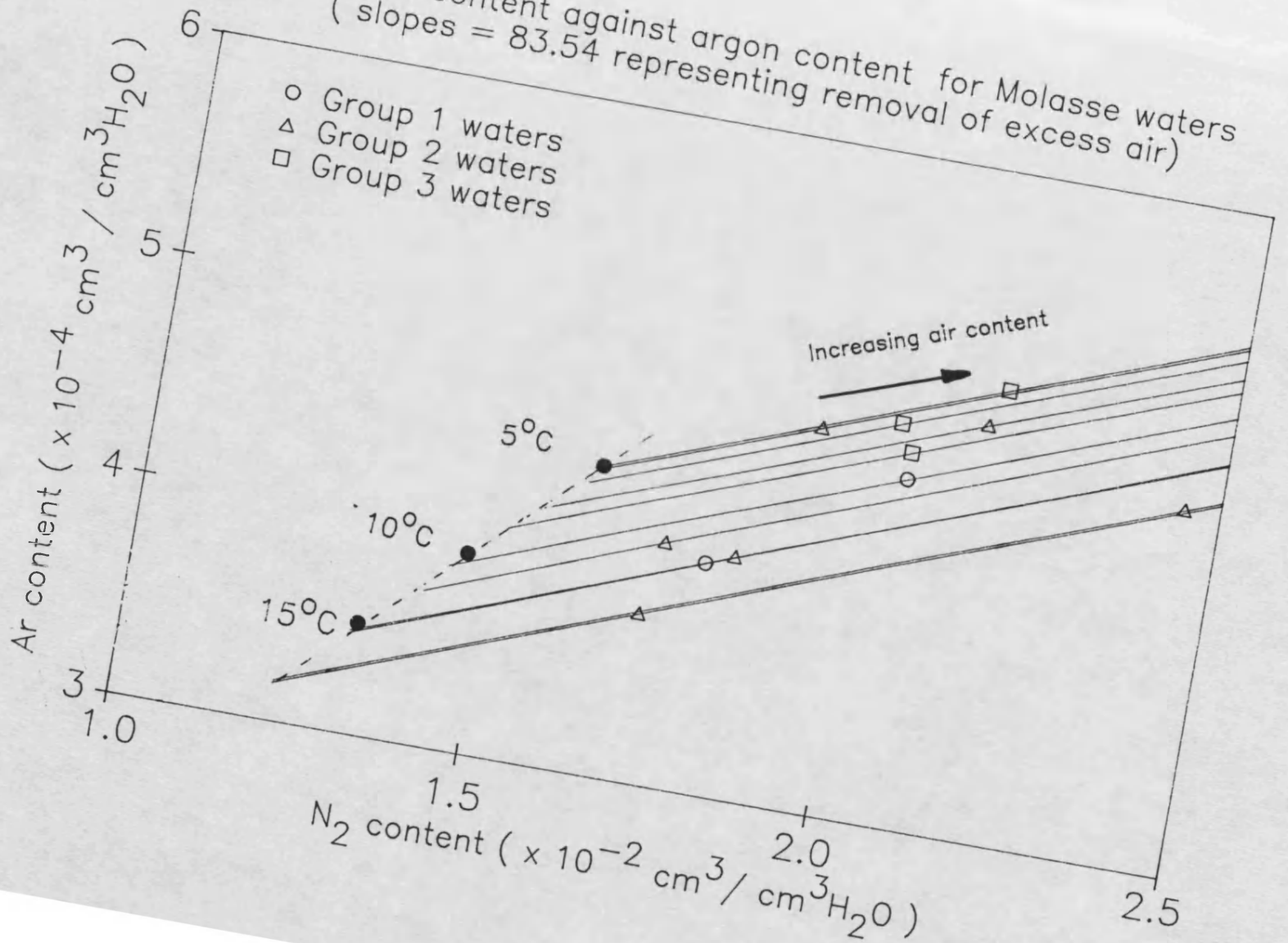

CHAPTER 4

UPPER AUSTRIA FORMATION WATERS

4.1 Geological Setting

The geological setting of these formation waters is described in Section 3.1. The sediment in this region covers a stratigraphic period from the carboniferous to the Pliocene (see Figure 3.2). Autochthonous Jurassic and Cretaceous sediments form most of the pre-Tertiary floor in which the carbonate rocks of the malm can attain thicknesses up to 500m. The Malm carbonates were karstified during the Lower Cretaceous, are highly permeable and form the most important deep aquifers bearing thermal waters. The Malm contains oil deposits. The Upper Cretaceous sandstones (Cenomanian) are also important as oil horizons and as thermal aquifers, especially where hydraulic contact between them and the Malm exists. Large faults with throws of several hundred metres intersect the horizons of the basin floor which complicates the circulation of deep groundwaters.

The Tertiary basin sediments have been described in Section 3.1. The Upper Eocene is the main oil horizon but does not contain much thermal water. Gas occurs in the Upper and Lower Puchkirchen formations (Miocene/Oligocene) where the reservoir facies is restricted to a narrow zone subparallel to the Flysch zone. The gas-bearing sequences consist of conglomerates and sandstones alternating with shales (Malzer, 1981). Permeability in the Miocene (Hall formation) is restricted to sand and silt deposits near the base of the formation. These contain gas deposits

which have been shown to be of bacterial origin (Schoell, 1977).

4.2 Geochemistry and Hydrochemistry

Water samples for radioelement analysis were collected only from wells with no hydrocarbon contamination because of the problems of analysis and phase separation. For isotopic analyses the water phase was extracted with tetrachloromethane to remove all hydrocarbon traces. Details of samples and field measurements are given in Table 4.1. The chemical analyses of the various waters are listed in Table 4.2 The total mineralisation of the waters range from 1000 mg/l to more than 26,000 mg/l. The low mineralisation of waters from some gas wells (Puchkirchen Ost 1 and Atzbach 1) are likely to be caused by evaporation/condensation effects. All other gas wells appear to contain high salinity formation water droplets. The waters from the Hall and Puchkirchen formations are the most highly mineralised and are of the NaCl type. They occur in isolated sandstone and conglomerate horizons which are also important gas reservoirs. Stable isotope measurements indicate these waters are formation waters which have not been flushed by meteoric water. Even for shallow aquifers in the Puchkirchen the influence of meteoric water is very small.

Groundwaters from the Hall and Puchkirchen formations are more tightly constrained on a Piper diagram than are

Table 4.1 **Field data and physical parameters for formation waters**

No.	Name	Formation	Well type	% H_2O	Well depth m	Pump depth m	Sample press. bar	Temp. °C	pH	Eh mV	Diss. oxy. ppm	Conduc. $\mu s\ cm^{-1}$ at 25°C
4021	Engenfeld 1	Upper Eocene	o	96	1054.2-1066.2	1054.2+	3-3.5	34.3	7.7	-20	0.1	3350
4022	Gundersdorf Hl	Upper Puchkirchen	w	100	1014.3-1028.5	1014.3+	2	41.4	7.44	-30	0.1	31846
4023	Oberaustall 6	Cenoman	o	71	1986.0-1970.0	≥1968	14	45-50	-	-	-	-
4024	Maierdorf Hl	Upper Puchkirchen	w	100	970.0-1061.5	≥ 970	10	42.7	7.39	-16	0.1	30470
4025	Steinhaus 1	Upper Eocene	o	86	1620.5-1626.0	≥1620.5	12	45.5	-	-	-	-
4026	Desselbrunn 2	Upper Puchkirchen	g	<0.1	152.0-1532.2	-	20	16.9	7.36	-34	0.1	24017
4027	Atzbach 5	Upper Puchkirchen	g	-	-	-	23	24.6	6.80	+76	0.1	1637
4028	Atzbach 1	Upper Puchkirchen	g	-	-	-	23	20.0	7.29	+ 2	0.2	22853
4029	Friedburg 2	Upper Puchkirchen	g	0.1	1839.9-1852.5	-	24	31.6	7.45	+ 8	0.1	21901
4030	Munderfing 1	Hall	g	0.03	1339.9-1344.5	-	24	21.8	7.50	-29	0.1	24863
4031	Kemating 5	Upper Puchkirchen	o	84	-	-	9-13	-	-	-	-	-

Table 4.1 (cont)

No.	Name	Formation	Well type	% H_2O	Well depth m	Pump depth m	Sample press. bar	Temp. °C	pH	Eh mV	Diss. oxy. ppm	Conduc. us cm^{-1} at 25°C
4032	Maria Schmolln	Upper Eocene	o	80	-	-	4	≈10	-	-	-	-
4033	Puchkirchen 20	Upper Puchkirchen	o	74	-	-	8	≈10	-	-	-	-
4034	Ried 18 (Hohenzell)	Innviertler Robulus Schlier	w	100	-	-	20	13.6	8.89	-100	0.1	344
4035	Trattnach 4	Cenoman	o	84	1598.9-1609.2	-	≈10	44.3	-	-	-	-
4036	Haindorf 1	Upper Jurrasic	o	45	1502.5-1504	≥1502.4	5-8	19.4	-	-	-	-
4037	Aurolzmunster 2	Innviertler Robulus Schlier	w	100	120.0-370	≈40	1	12.4	8.83	-46	0.2	555
4038	Ried 3	Innviertler Rieder Schichten	w	100	0-15	-	1	10.1	7.38	+96	0.2	384
4039	Bad Hall Tassilo Quelle	Upper Puchkirchen	w	100	-	15	1-2	12.1	7.56	+197	0.1	23064
4040	Bad Hall Paracelsus Quelle	Upper Puchkirchen	w	100	120-273	122	1-2	15.6	8.06	- 54	0.1	28989

Table 4.1 (cont)

No.	Name	Formation	Well type	% H_2O	Well depth m	Pump depth m	Sample press. bar	Temp. °C	pH	Eh mV	Diss. oxy. ppm	Conduc. us cm^{-1} at 25°C
4041	Steinerkirchen	Hall	g		935.2-937.4				7.4	+ 99		26600
4042	Puchkirchen 27	Upper Puchkirchen	g		1701.5-1705.5				7.36	+ 62		16800
4043	Hocheck	Lower Puchkirchen	g		2258.5-2260.5				7.66	-		16100
4044	Pfaffstätt 3	Lower Puchkirchen	g		2145.8-2149.0				6.95	+115		18400
4045	Schwanenstadt 17	Upper Puchkirchen	g		1634.0-1642.4				7.28	+ 90		15900
4046	Puchkirchen 24	Upper Puchkirchen	g		1122.8-1126.5				7.34	+ 58		17600
4047	Puchkirchen Ost 1	Hall	g		1057.0-1073.5				7.37	- 23		377
4048	Hörgersteig 1	Cenoman	o	12	2526.4-2532.3				-	-		-
4049	Eggerding 1	Rupelian	o	70	619.3-624.3				-	-		-
4050	Kemating NIA	Upper Eocene	o	60	1931.8-1938.0				-	-		-
4051	Kohleck 2	Upper Eocene	o	63	2240.0-2265.5				-	-		-

Table 4.1 (cont)

No.	Name	Formation	Well type	% H_2O	Well depth m	Pump depth m	Sample press. bar	Temp. °C	pH	Eh mV	Diss. oxy. ppm	Conduc. us cm^{-1} at 25°C
4052	Kohleck 6	Upper Eocene	o	60	2433.5-2444.0				-	-		-
4053	Trattnach 11	Cenoman	o	28	1583.2-1585.5				-	-		-
4054	Eberstalzell H1	Upper Puchkirchen	w	100	1028.5-1114.3				7.45	- 31		25900
4055	Eberstalzell H2	Upper Puchkirchen	w	100	1045.0-1054.8				7.62	- 45		25800
4056	Eberstalzell H5	Upper Puchkirchen	w	100	1032.0-1095.0				7.73	- 65		25200
4057	Schwanenstadt 4	Hall	w	100	936.7-952.5				8.08	-135		26200
4058	Voitsdorf 11	Upper Eocene	o	94	2087.5-2127.5				-	-		-
4059	Voitsdorf 15	Cenoman	o	98	2035.0-2064.0				-	-		-
4060	Voitsdorf 30	Cenoman	o	>90	2010.5-2018.5				-	-		-
4061	Voitsdorf 2	Cenoman	o	96	2122.3-2143.5				-	-		-
4062	Voitsdorf 10	Upper Eocene	o	96	2082.2-2097.5				-	-		-
4063	Voitsdorf 13	Cenoman	o	76	2105.4-2133.8							

Table 4.2 **Chemistry of waters from the Molasse Basin**

No.	Date	Location	Depth,m	Well type	Na	K	Ca	Mg	Fe	NH_4	HCO_3	SO_4	Cl	SiO_2
Hall Formation														
4030	22-7	Munderfing 1	1339.9-1344.5	g	5850	40.2	227	90.7	22700*	55.8	305	1	10160	15.2
4041	21-8	Steinerkirchen 1	935.2- 937.4	g	9290.0	46.6	554.6	242.6	1.87	87.3	204.4	-	16090	14.97
4047	23-8	Puchkirchen Ost 1	1057.0-1073.5	g	13.2	4.54	4.65	0.2	3.00	35.5	131.8	3.33	26	0.5
4057	29-8	Schwanenstadt 4	936.7- 952.5	w	8630.0	50.7	464.0	230.2	3.05	106.1	201.4	5.64	15000	13.18
Upper Puchkirchen														
4022	18-7	Gundersdorf H1	1014.3-1028.5	w	8380	40.9	406	177.5	690	74.1	220	0	14390	15.8
4024	19-7	Maierdorf H1	970.0-1061.5	w	8300	38.6	384	170.0	30	67.2	189	0	14340	15.2
4026	20-7	Desselbrunn 2	152.0-1532.2	g	5920	75.0	140	42.2	70400*	34.2	684	58	9810	19.5
4027	21-7	Atzbach 5		g	293	1.2	1.1	0.42	1750	28.6	143	1	450	<0.5
4028	21-7	Atzbach 1		g	5500	39.1	54	20.3	540	30.6	684	91	8870	28.2
4029	21-7	Friedburg 2	1839.9-1952.5	g	5530	33.6	104	32.8	290	29.2	470	69	8590	27.5
4031	25-7	Kemating 5		o	5870	67.7	252	53.8	100	22.2	1415	73	9210	45.9
4033	27-7	Puchkirchen 20		o	2160	62.2	150	20.2	970	11.1	1019	678	2720	60.1
4039	28-7	Bad Hall Tassilo Q		w	5500	21.7	144	99.8	40	38.3	281	0	9440	7.3
4040	28-7	Bad Hall Para. Q	120.0- 273.0	w	7740	31.6	254	159.0	80	49.3	256	<1	13000	7.5
4042	21-8	Puchkirchen 27	1701.5-1705.5	g	5570.0	38.23	117.0	28.9	2.66	35.0	524.8	96.9	8668	29.95
4045	23-8	Schwanenstadt 17	1634.0-1642.4	g	5734.0	41.20	111.4	32.1	0.81	27.1	518.7	110.2	9115	31.23
4046	23-8	Puchkirchen 24	1122.8-1126.5	g	6628.0	37.11	234.6	96.7	2.73	56.9	320.4	<2	11065	19.17
4054	28-8	Eberstalzell H1	1028.5-1114.3	w	8800.0	42.47	415.4	159.8	0.10	69.4	213.0	-	14730	17.71
4055	28-8	Eberstalzell H2	1045.0-1054.8	w	8380.0	41.20	336.0	130.4	1.02	60.5	222.7	-	13670	17.88
4056	28-8	Eberstalzell H5	1032.0-1095.0	w	8050.0	40.89	307.6	116.1	0.22	61.7	234.9	-	13270	17.63
Lower Puchkirchen														
4043	22-8	Hocheck 2	2258.5-2260.5	g	5105.0	37.53	55.44	19.9	0.13	27.2	1644.5	35.13	7090	39.79
4044	22-8	Pfaffstadt 3	2145.8-2149.0	g	6324.0	38.05	95.35	29.2	3.03	37.3	2172.0	-	8506	37.39
Rupelian														
4049	27-8	Eggerding 1	619.3- 624.3	o	812.0	5.78	7.08	2.1	-	1.5	997.7	2.77	678	-
Upper Eocene														
4021	19-7	Engenfeld 1	1054.2-1066.2	o	1130	11.1	16.1	3.1	50	4.4	421	5.0	1570	24.6
4025	20-7	Steinhaus 1	1620.5-1626.0	o	3360	26.8	68.0	19.6	29	13.4	1404	110.0	4680	34.5
4032	25-7	Maria Schmolln		o	1410	32.6	31.0	7.2	100	5.7	1086	14.0	1600	55.9

Table 4.2 (cont)

No.	Date	Location	Depth,m	Well type	Na	K	Ca	Mg	Fe	NH_4	HCO_3	SO_4	Cl	SiO_2
Upper Eocene														
4050	27-8	Kemating N1A	1931.8-1938.0	o	5617.0	117.8	388.4	80.2	-	224.0	1471.8	130.1	9309	-
4051	27-8	Kohleck 2	2240.0-2265.5	o	6548.0	186.8	209.4	41 1	-	94.6	954.4	55.0	10578	-
4052	27-8	Kohleck 6	2433.5-2444.0	o	6456.0	51.5	86.6	36.9	-	12.0	807.9	4.24	9798	-
4058	30-8	Voitsdorf 11	2087.5-2127.5	o	3920.0	67.52	220.2	27.7	-	9.2	729.2	54.6	6494	-
4062	30-8	Voitsdorf 10	2082.2-2097.5	o	2184.0	23.04	126.1	21.64	-	8.22	510.1	41.9	3467	-
Cenoman														
4023	19-7	Oberaustall 6	1986.0-1970.0	o	3720.0	50.1	264.0	24.7	70	8.5	398.0	367.0	6280	45.4
4035	26-7	Trattnach 4	1598.9-1609.2	o	620.0	10.5	6.1	1.2	20	2.7	1062.0	37.0	338	44.4
4048	24-8	Horgersteig 1	2526.4-2532.3	o										
4053	27-8	Trattnach 11	1583.2-1585.6	o	760.0	18.46	9.94	1.7	-	42.6	1022.1	149.2	585	-
4059	30-8	Voitsdorf 15	2035.0-2064.0	o	4075.0	67.1	375.0	23.9	-	9.37	344.8	102.4	6750	-
4060	30-8	Voitsdorf 30	2010.5-2018.5	o	4045.0	64.6	307.3	26.0	-	9.65	418.6	90.5	6650	-
4061	30-8	Voitsdorf 2	2122.3-2143.5	o	5000.0	72.26	622.8	37.6	-	8.73	361.9	376.7	8692	-
4063	31-8	Voitsdorf 13	2105.4-2133.8	o	4873.0	81.06	165.5	37.96	-	79.5	872.6	158.8	8012	-
Inviertler Robulus Schlier														
4034	26-7	Ried 18 (Hohensell)		w	102.0	1.9	3.0	0.95	80	4.8	299.0	0	1.5	25.1
4037	27-7	Aurolzmunster 2	120.0- 370.0	w	192.0	2.0	4.0	1.4	70	4.5	522.0	1	15	40.6
Innviertler Rieder Schichten														
4038	27-7	Ried 3	0.0- 15.0	w	6.8	1.4	98.0	24.6	220	-	401.0	25.0	5	31.2
Upper Jurrasic														
4036	26-7	Haindorf 1	1502.5-1504.0	o	970.0	12.8	9.0	2.4	390	3.9	934.0	120.0	885	42.9
Unclassified														
4064		Sattledt	Separator Tank											

Well type: g = gas; o = oil; w = water All results are in mg/l.
* Total Iron (acidified sample)

those from deeper in the basin (Figure 4.3). These waters are situated in the area appropriate for ocean waters, implying they are immobile connate formation waters with little or no replacement by meteoric water. However, detailed examination of their chemistry reveals their cationic ratios have been modified by cation exchange processes. Redox changes during diagenesis have reduced sulphate to sulphide and caused the deposition of the original uranium content of seawater.

Waters of the Upper Eocene and Upper Cretaceous are distributed along the Cl^-/HCO_3^- axis of the Piper diagram. This suggests dilution has occurred with meteoric water, which is also tending to reduce the mineralization of these waters. This dilution of waters beneath the saline waters of the Puchkirchen and Hall shows there is no vertical hydraulic continuity between these formations.

The Malm waters have the lowest mineralization of the deep aquifers in the Molasse as shown in Figure 4.3 The Malm waters are dominated by $Na\text{-}HCO_3^-/Cl^-$ ions. Locally Malm water is in hydraulic contact with adjacent horizons, for example the Upper Eocene well at Maria Schmolln and in the Trattnach field (Cenomanian).

Figure 4.1 shows the location map for samples collected from Upper Austria. Figure 4.2 shows geological cross sections through the Molasse basin, the locations of the cross section are shown on Figure 4.1.

Figure 4.1 Location map for Formation water samples from Molasse basin

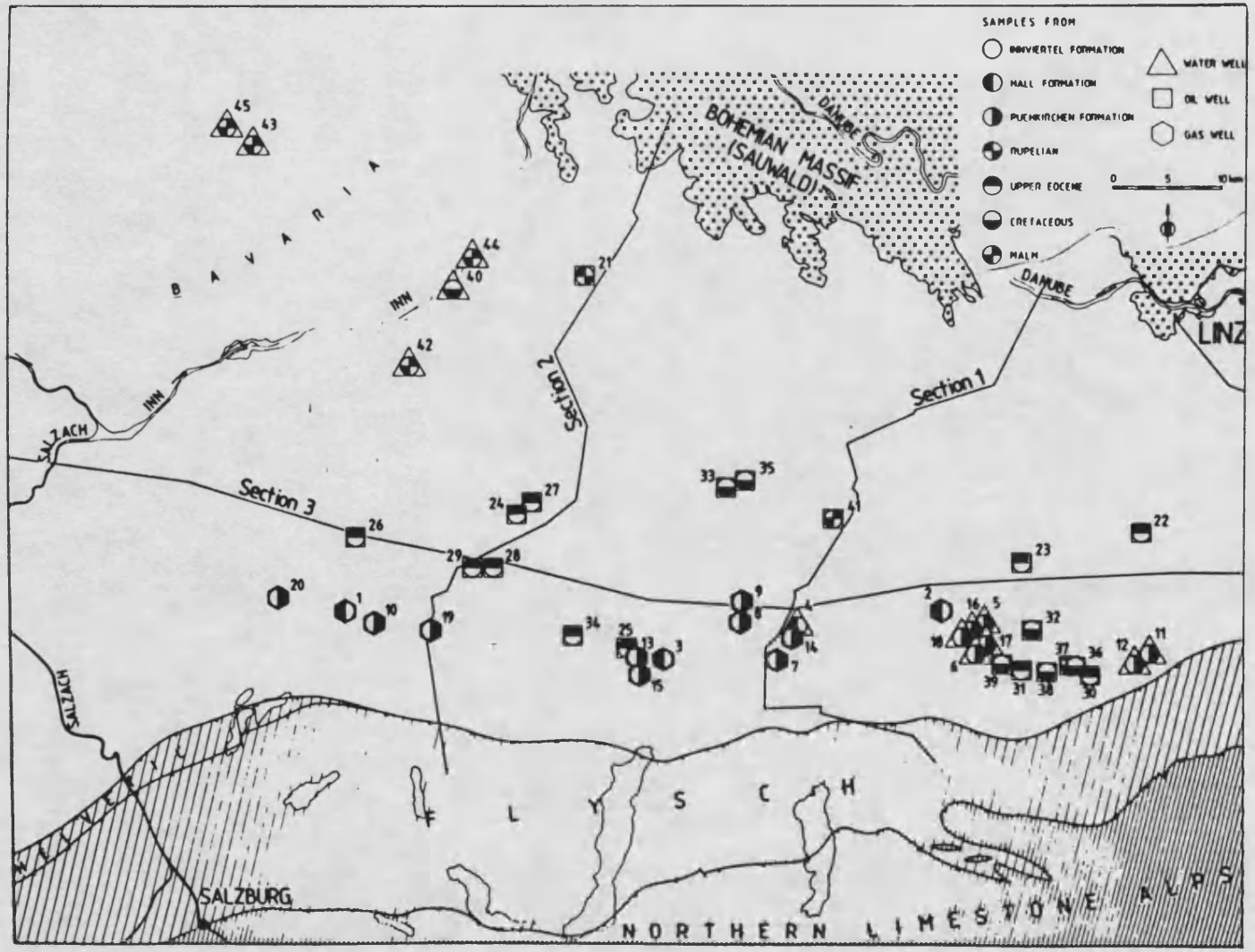

Figure 4.2 Geological sections through the Molasse basin (for locations in fig 4.1)

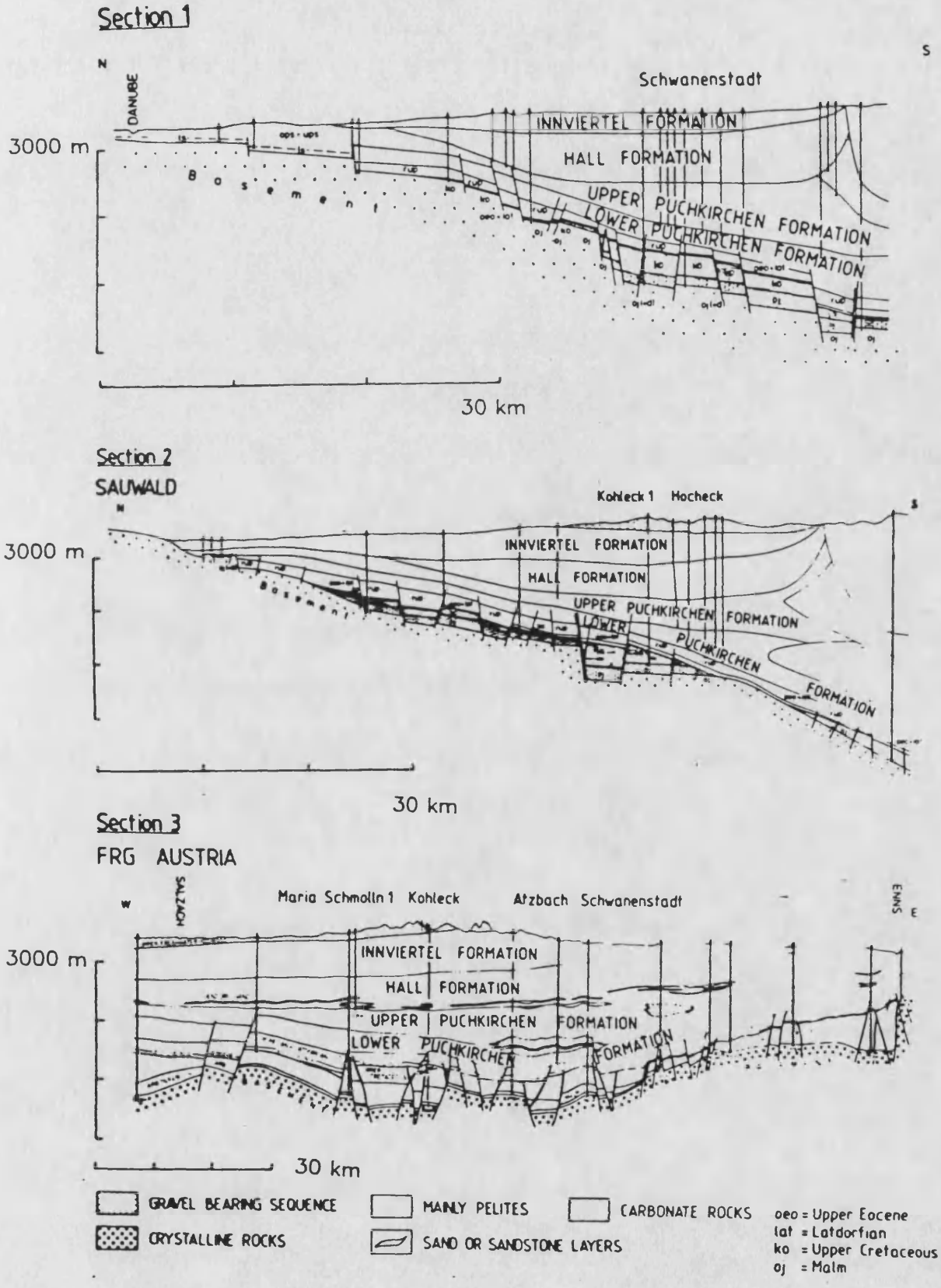

Figure 4.3

Piper diagram for Molasse formation water chemistry
(symbols as for fig. 4.1)

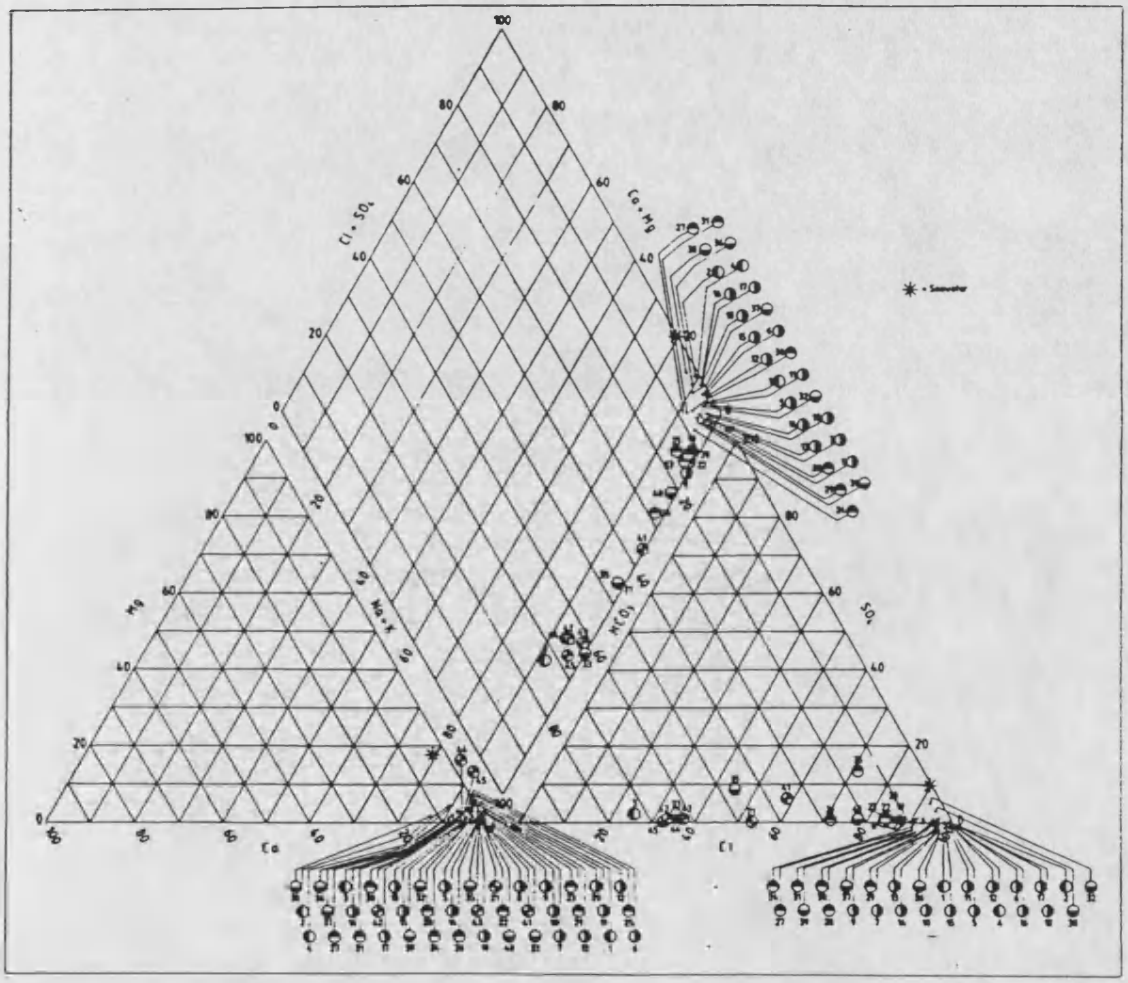

4.3 Stable Isotopes

The hydrogen and oxygen isotopic compositions of the waters are reported in Table 4.3, and $\delta^{18}O$ is plotted against $\delta^{2}H$ in Figure 4.4 Isotopically heavy waters are present in the gas bearing Puchkirchen formation in which waters with $\delta^{18}O$ greater than SMOW occur. Only the shallow Innviertel waters lie on the meteoric water line (Section 1.9), all other waters lie on a mixing line between the Innviertel waters and the Puchkirchen waters.

This suggests that connate waters are being replaced by meteoric water as indicated by the chemical analyses. Figure 4.5 shows the $\delta^{18}O$ content plotted against chloride content, chloride is being used as a conservative parameter. Figure 4.6 shows the $\delta^{2}H$ content plotted against chloride. These graphs also show the mixing line for recent meteoric water and seawater. In the case of $\delta^{2}H$ all waters are heavier than the dilution line except for Malm waters. This suggests the light hydrogen has been utilized in the biogenic process which produced methane. The Malm waters are also the exception in that they do not show an enrichment in $\delta^{18}O$ relative to the dilution line. The enrichment of most waters may be attributed to exchange with carbonate or silicate minerals. Clayton and others have reported similar $\delta^{18}O$ and $\delta^{2}H$ trends for oil field brines in America.

The Malm waters are predominantly of meteoric origin and may be derived by slight mixing with marine waters.

Table 4.3 Stable isotope composition of groundwater and formation waters from Upper Austria

No.	Name	Formation	δ^2H ‰	$\delta^{18}O$ ‰
4021	Engenfeld 1	Upper Eocene	-57	- 6.5
4022	Gundersdorf H1	Upper Puchkirchen	- 9	+ 1.3
4023	Oberaustall 6	Cenoman	-30	+ 2.0
4024	Maierdorf H1	Upper Puchkirchen	-10	+ 1.3
4025	Steinhaus 1	Upper Eocene	-30	- 1.6
4026	Desselbrunn 2	Upper Puchkirchen	- 5	+ 1.7
4027	Atzbach 5	" "	-31	- 1.7
4028	Atzbach 1	" "	- 9	+ 2.0
4029	Friedberg 2	" "	-14	+ 1.2
4030	Munderfing 1	Hall	-17	+ 0.4
4031	Kemating 5	Upper Puchkirchen	-30	- 1.3
4032	Maria Schmolln	Upper Eocene	-57	- 6.1
4033	Puchkirchen 20	Upper Puchkirchen	-38	- 2.0
4034	Ried 18	Innviertler Robulus Schlier	-86	-12.2
4035	Trattnach 4	Cenoman	-68	- 8.3
4036	Haindorf 1	Upper Jurrasic	-58	- 5.8
4037	Aurolzmunster	Innviertler Robulus Schlier	-84	-12.1
4038	Ried 3	Innviertler Robulus Schichter	-72	-10.3
4039	Bad Hall, Tassilo Quelle	Upper Puchkirchen	-24	- 1.6
4040	Bad Hall, Paracelsus Quelle	" "	- 9	+ 1.0
4041	Steinerkirchen	Hall	-13	+ 0.3
4042	Puchkirchen 27	Upper Puchkirchen	- 4	+ 1.9
4043	Hocheck	Lower Puchkirchen	-11	+ 1.9
4044	Pfaffstatt	" "	-14	+ 1.6
4045	Schwanenstadt 17	Upper Puchkirchen	-11	+ 2.3
4046	Puchkirchen 24	" "	-15	+ 0.3
4047	Puchkirchen Ost 1	Hall	-51	- 5.7
4054	Eberstalzell H1	Upper Puchkirchen	-11	+ 0.8
4055	Eberstalzell H2	" "	-12	+ 1.4
4055	Eberstalzell H5	" "	-10	+ 1.4
4057	Schwanenstadt 4	Hall	-20	- 0.8
4058	Voitsdorf 11	Upper Eocene	-42	- 4.4
4059	Voitsdorf 15	Cenoman	-34	- 4.2
4060	Voitsdorf 30	"	-41	- 4.3
4061	Voitsdorf 2	"	-27	- 3.0
4063	Voitsdorf 13	Upper Eocene	-23	- 1.3
4064	Sattledt		-28	- 2.6

Figure 4.4

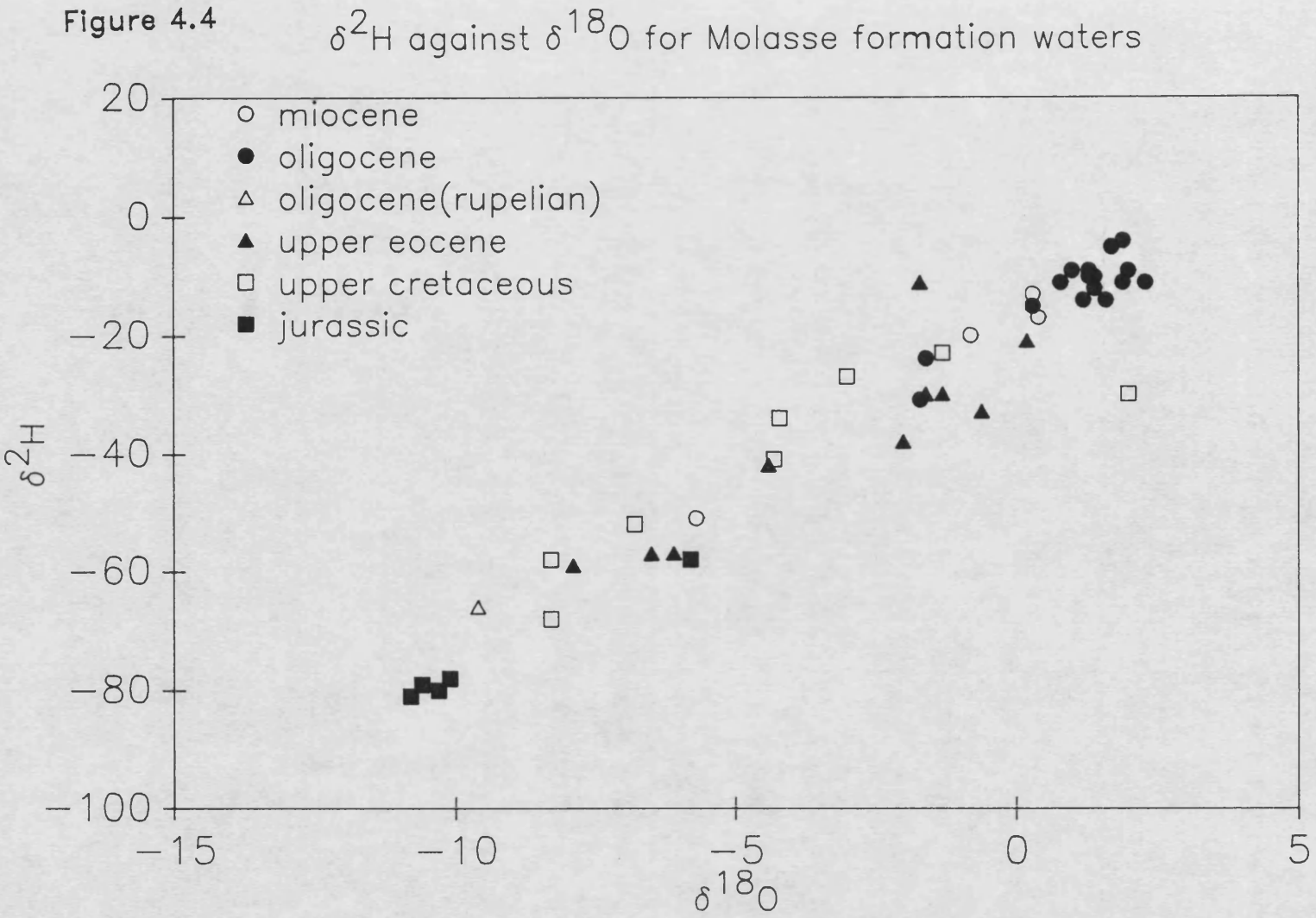
δ2H against δ18O for Molasse formation waters
miocene
oligocene
oligocene(rupelian)
upper eocene
upper cretaceous
jurassic
20
0
−20
−40
−60
−80
−100
δ2H
−15
−10
−5
0
5
δ18O

Figure 4.5 $\delta^{18}O$ variation with chlorinity for Molasse formation waters

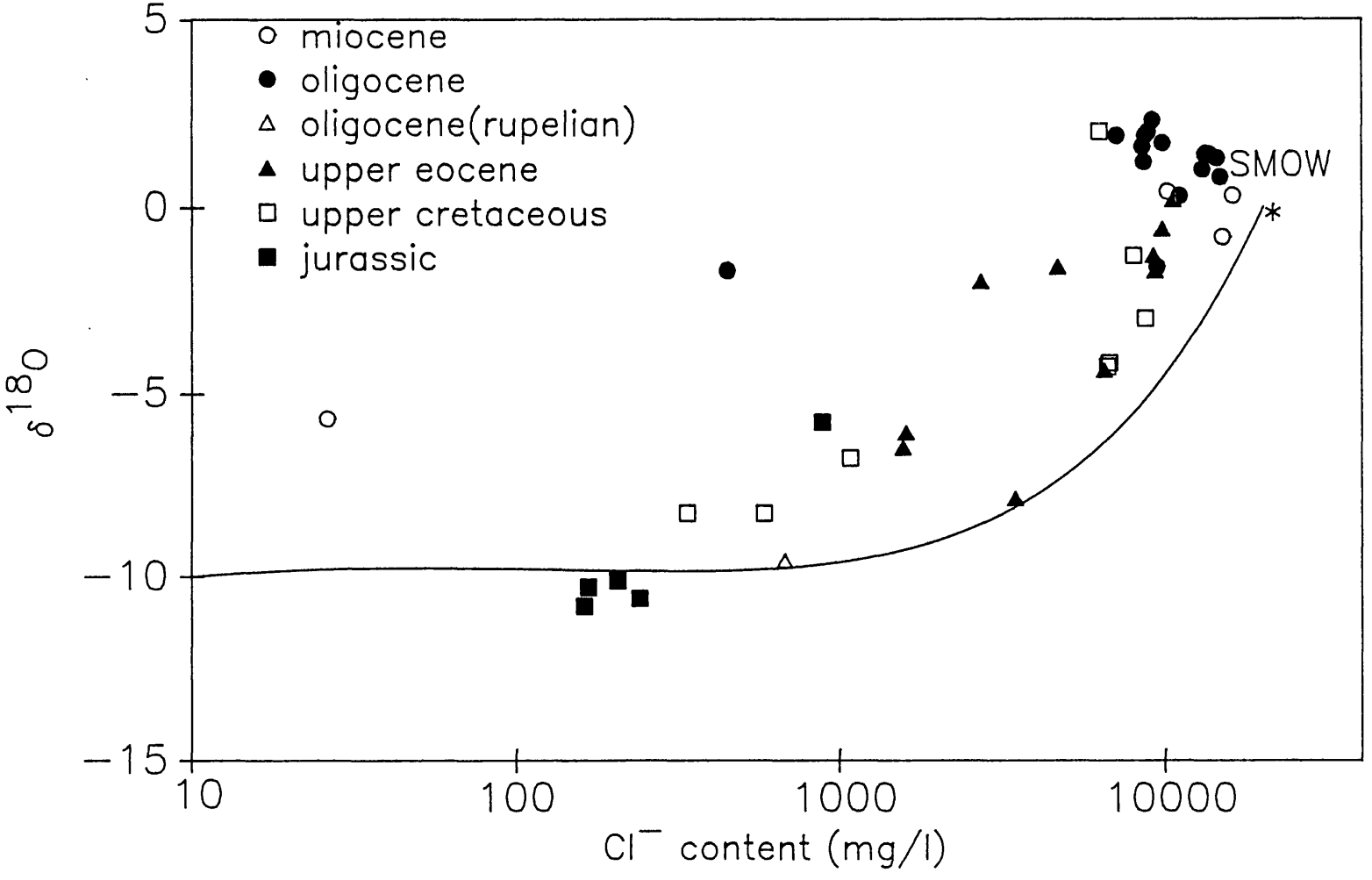

Figure 4.6 δ^2H variation with chlorinity for Molasse formation waters

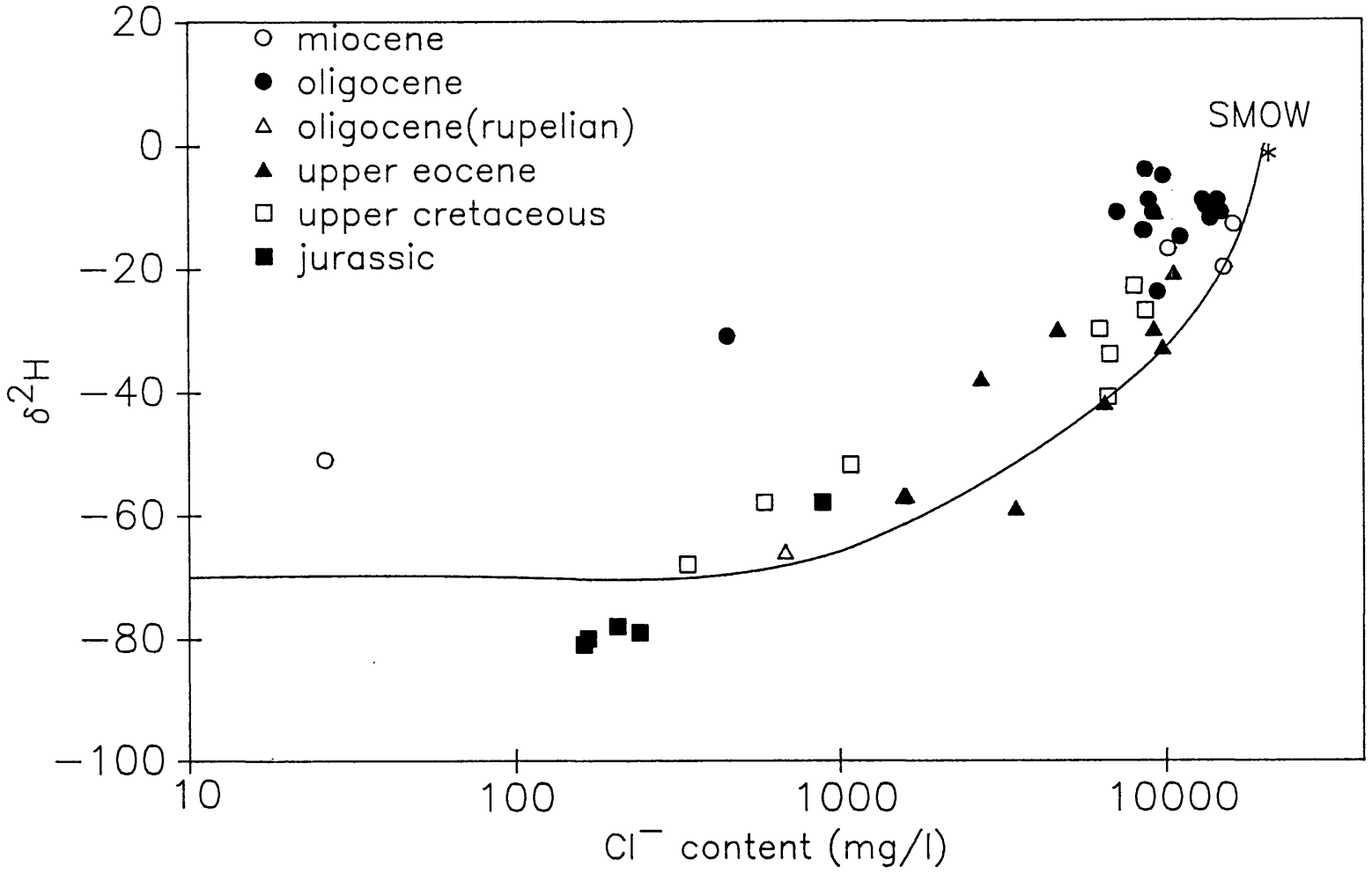

This confirms they are the youngest of the deep groundwaters.

4.4 Gas Ratio

The volumetric ratios of CH_4/Ar, N_2/Ar, He/Ar, Ne/Ar, Ke/Ar, Xe/Ar were determined for gas samples from the Puchkirchen, for oil/brine mixtures from the Eocene and for other groundwaters from the Molasse basin. Argon was chosen as a reference gas against which other gases are expressed. Argon is likely to behave conservatively in groundwater solution (Section 1.15.1), only radiogenic ^{40}Ar is likely to add significantly to Ar.

4.4.1 Argon-40/Argon-36 Ratio

The isotopic ratio for Ar is shown in Table 4.4 For the Puchkirchen gas samples it is close to the atmospheric value of 295.5 It is concluded that these gases have inherited the atmospheric ratio from their parent brines which has been preserved since the brine was removed from contact with the atmosphere. The Eocene $^{40}Ar/^{36}Ar$ ratios are considerably enriched in ^{40}Ar, which corresponds to the addition of a volume of Ar at least as great as that dissolved when the brine was in contact with the atmosphere. This suggests argon has been released from rock matrices in a high temperature environment. Figure 4.7 shows the $^{40}Ar/^{36}Ar$ relationship with chlorinity.

Table 4.4 CH_4/N_2 and N_2/Ar ratios for groundwaters from the Molasse Basin

No.	Name	Formation	Type	N_2/Ar	+/-	CH_4/N_2	+/-	$^{40}Ar/^{36}Ar$
4022A	Gundersdorf H1	Upper Puch.	w	31.5	0.03	12.7	0.7	-
4024C	Maierdorf H1	Upper Puch.	w	29.1	4.2	7.5	1.0	-
4025C	Steinhaus 1	Upper Eocene	o	105.0	2.9	7.1	0.2	298.6
4026B	Desselbrunn 2	Upper Puch.	g	44.9	1.6	22.9	1.4	289.5
4027A	Atzbach 5	Upper Puch.	g	69.1	2.4	7.8	0.2	304.0
4028A	Atzbach 1	Upper Puch.	g	45.0	3.2	22.7	1.6	278.8
4029B	Friedburg 2	Upper Puch.	g	40.0	0.06	20.2	0.2	292.5
4030A	Munderfing 1	Hall	g	36.6	0.2	27.9	1.8	293.8
4031D	Kemating 5	Upper Puch.	o	78.0	3.0	10.1	0.8	304.3
4032C	Maria Schmolln	Upper Eocene	o	42.1	2.6	2.9	0.3	297.1
4033C	Puchkirchen 20	Upper Puch.	o	93.0	1.3	4.1	0.5	-
4034D	Ried 18 (Hohenzell)	Innviertler Roblus Schl.	w	43.8	0.2			-
4035D	Trattnach 4	Cenoman	o	63.9	0.5	2.5	0.4	297.0
4037D	Aurolzmunster 2	Innviertler Roblus Schl.	w	38.5	0.2	0.74	0	-
4041E	Steinerkirchen	Hall	g	39.8	1.6	39.3	1.1	301.0
4042D	Puchkirchen 27	Upper Puch.	g	55.0	1.0	26.7	1.5	293.9
4043D	Hocheck	Lower Puch.	g	69.3	1.0	21.3	1.1	293.5
4044D	Pfaffstatt 3	Lower Puch.	g	82.5	5.4	23.6	0.8	311.2
4045D	Schwanenstadt 17	Upper Puch.	g	56.2	3.7	27.8	2.0	303.2
4046D	Puchkirchen 24	Upper Puch.	g	53.4	2.6	30.8	2.2	289.5
4047D	Puchkirchen DST 1	Hall	g	46.4	0.5	44.5	2.8	-
4048B	Horgersteig 1	Cenoman	o	67.0	6.3	0.067	0.002	-
4049A	Eggerding 1	Rupelian	o	30.9	0.5	19.8	0.2	293.6
4050B	Kemating N1A	Upper Eocene	o	54.0	0.6	40.2	3.8	302.7
4051A	Kohleck 2	Upper Eocene	o	52.2	1.5	9.8	1.1	308.0
4054D	Eberstalzell H1	Upper Puch.	w	31.0	1.6	91.0	6.6	294.3
4056	Eberstalzell H5	Upper Puch.	w	29.5	1.7	16.3	0.3	294.0
4057D	Schwanenstadt 4	Hall	w	17.2	1.3	115.0	17.0	294.0
4058A	Voitsdorf 11	Upper Eocene	o	98.2	0.3	3.1	0.1	575.0
4059A	Voitsdorf 15	Cenoman	o	88.2	3.6	5.2	0.3	506.0
4060A	Voitsdorf 30	Cenoman	o	101.0	9.8	3.0	0.2	516.0
4061	Voitsdorf 2	Cenoman	o	113.0	3.0	7.6	0.3	494.0
4062	Voitsdorf 10	Upper Eocene	o	86.4	4.2	1.9	0.2	627.0
4063	Voitsdorf 13	Cenoman	o	95.7	1.5	3.5	0.4	563.0

Figure 4.7 $^{40}Ar/^{36}Ar$ ratio against chlorinity for Molasse formation waters

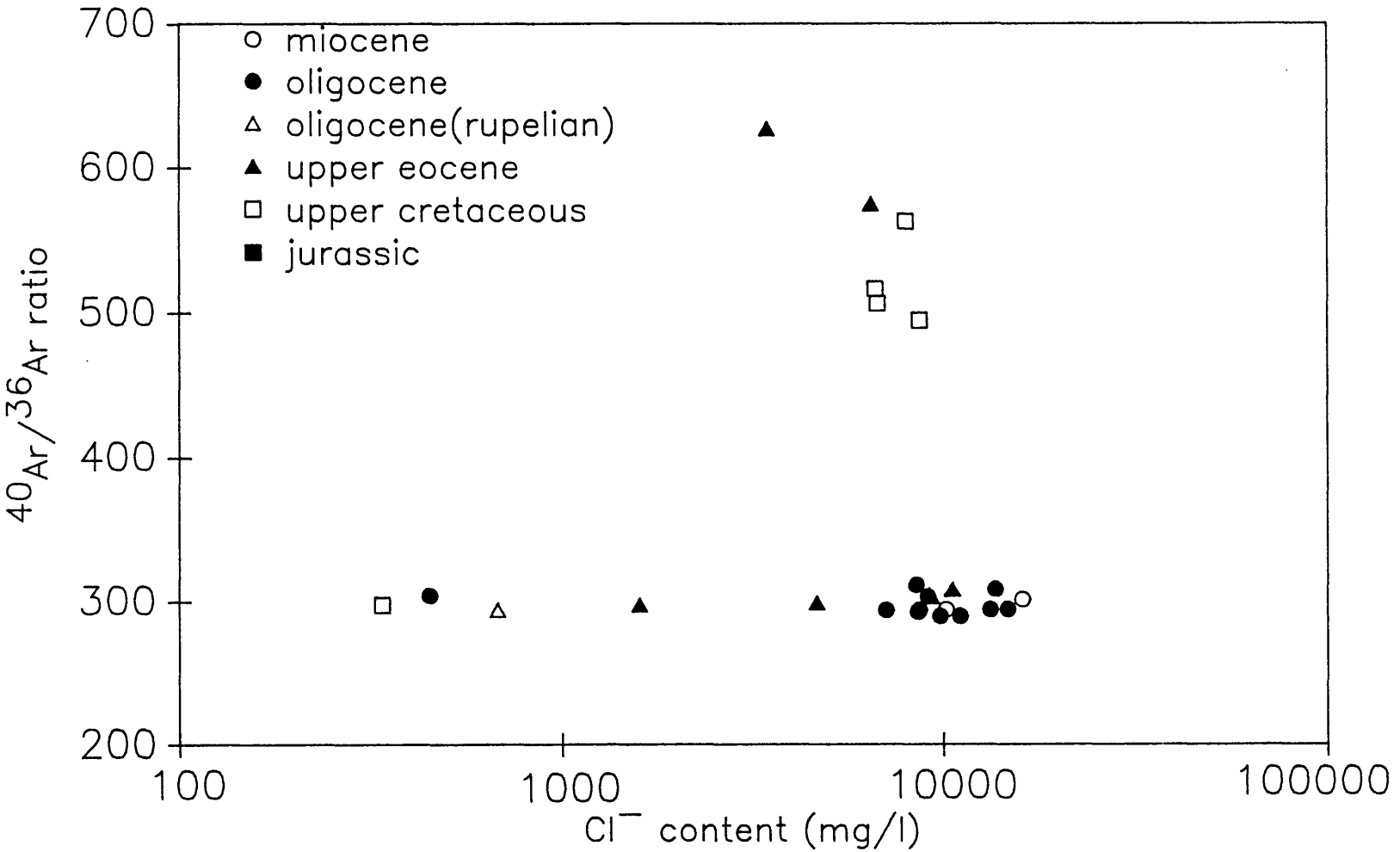

4.4.2 Helium/Argon Ratio

The volumetric He/Ar ratio corrected for presence of radiogenic Ar (using the $^{40}Ar/^{36}Ar$ ratio), is plotted against chlorinity in Figure 4.8. There is little correlation of helium/argon with chlorinity which suggests that both He and chloride increase with groundwater age or the proportion of connate water present. The plot of He/Ar against depth (Figure 4.9) shows the Puchkirchen samples show a good correlation. A correlation of helium content with depth suggests a diffusion controlled helium content of these waters.

In section 3.7 it was shown that on helium isotope evidence that the most likely source of helium is the granitic basement. The waters from the Eocene and Cretaceous formations lie below the helium/depth trend for the Puchkirchen. This is expected if there has been flushing of these formations with meteoric water as discussed earlier.

4.4.3 Methane/Argon and Nitrogen/Argon Ratios

The methane/argon and nitrogen/argon ratios have been plotted against ammonium ion content (Figures 4.10 and 4.11). The ammonium content of oil associated brines is a possible index of thermodegradation in a strongly reducing environment. Both methane and nitrogen would be expected to be produced during thermodegradation of organic materials. Samples from the oil bearing Eocene and

Figure 4.8 He/Ar variation with chlorinity for Molasse formation waters

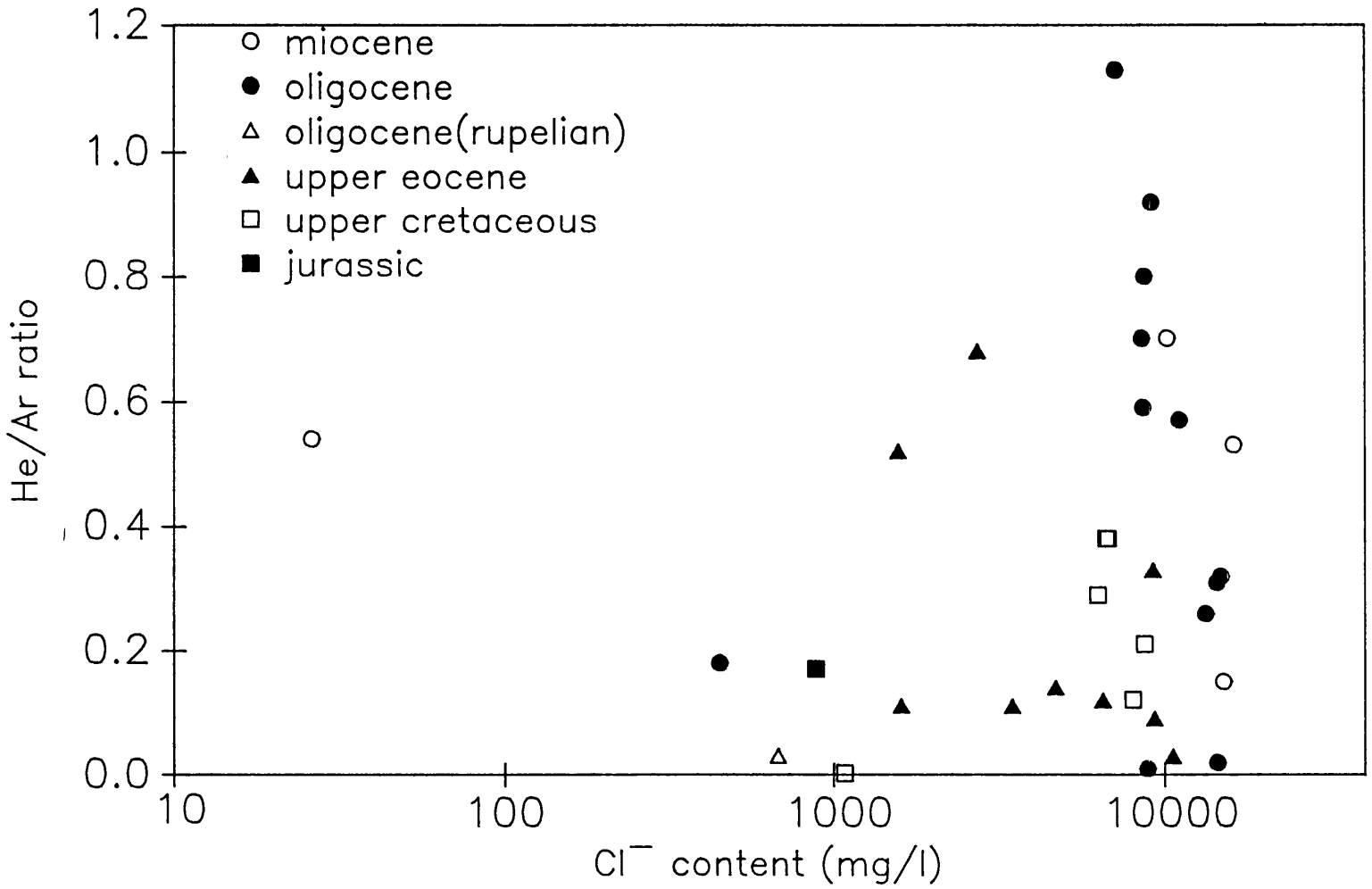

Figure 4.9 He/Ar variation with well depth for Molasse waters

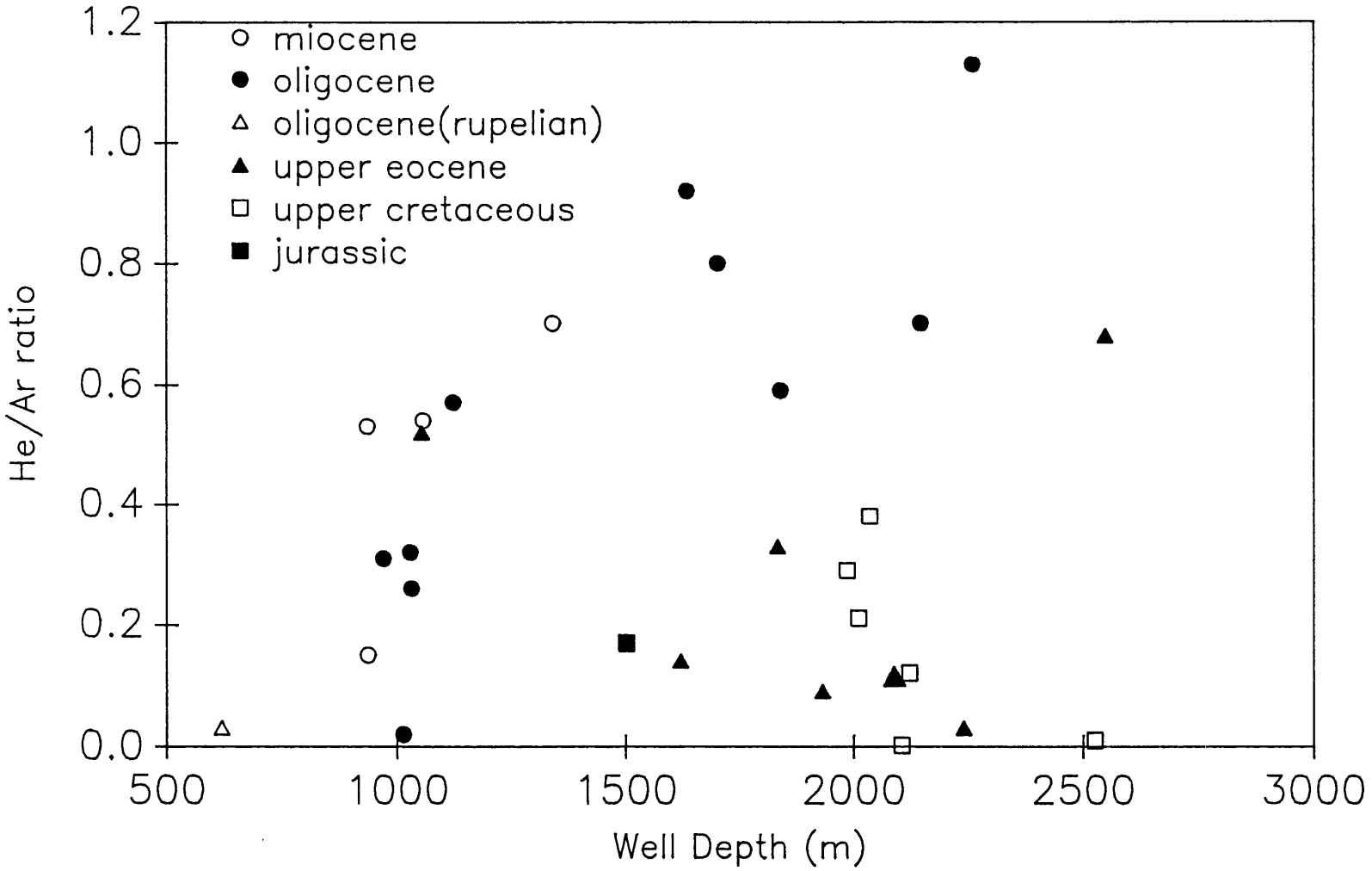

Figure 4.10

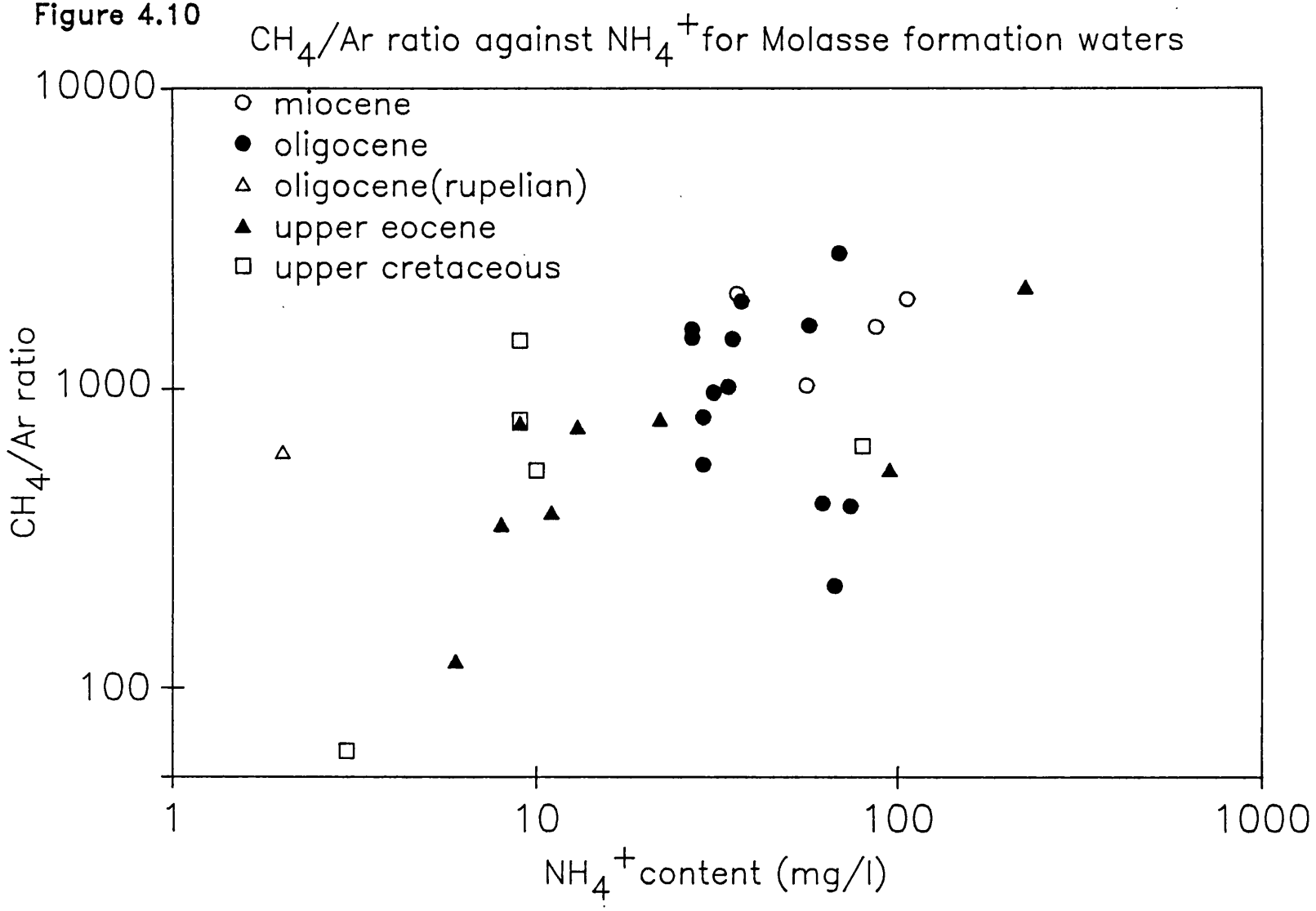
CH4/Ar ratio against NH4+for Molasse formation waters
10000
1000
100
CH4/Ar ratio
miocene
oligocene
oligocene(rupelian)
upper eocene
upper cretaceous
1
10
100
1000
NH4+content (mg/l)

Figure 4.11 N_2/Ar ratio against NH_4^+ for molasse formation waters

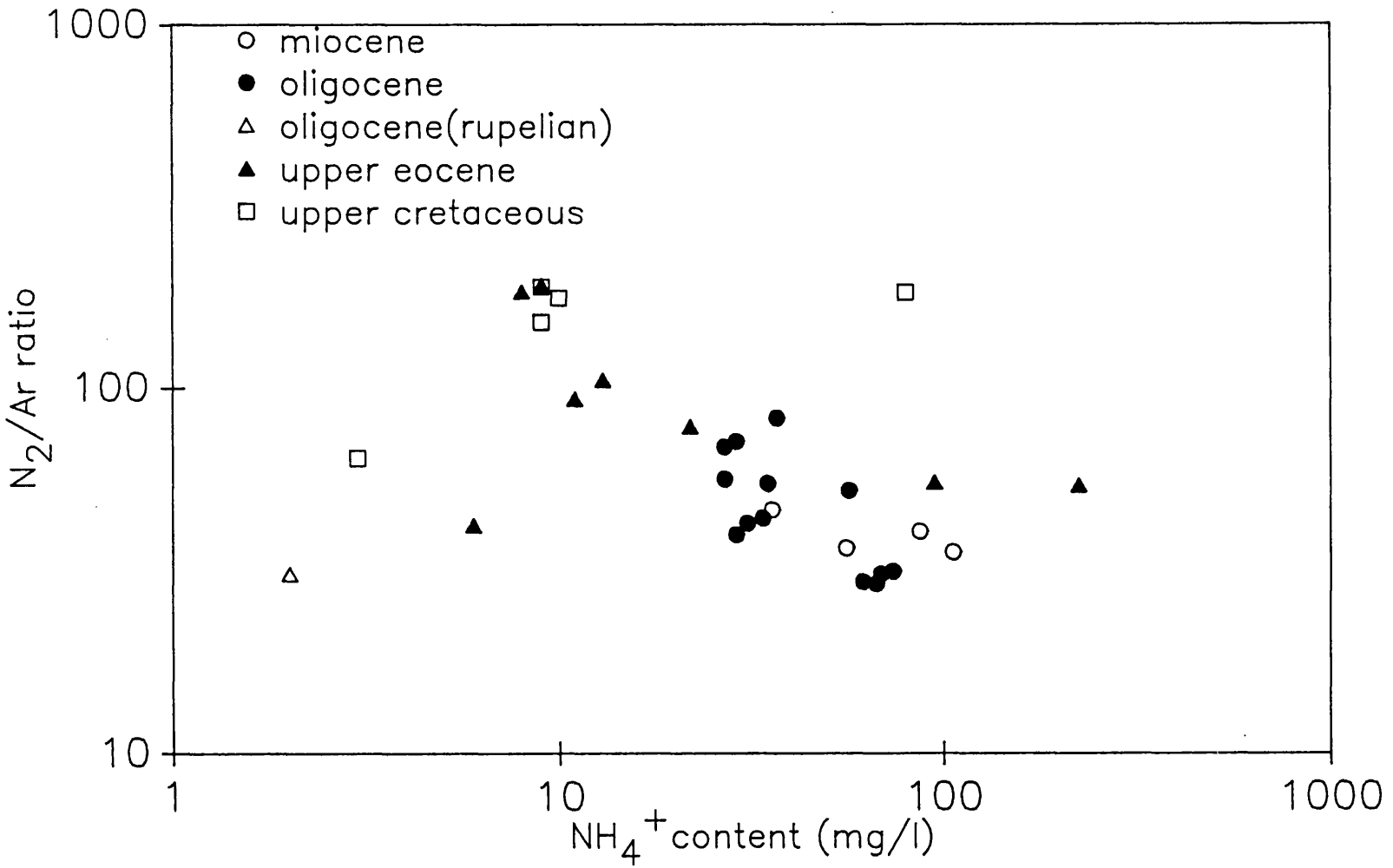

Cretaceous formations show a trend of increasing CH_4 with ammonium, however Oligocene (Puchkirchen) samples show no such correlation. This is as expected as the Oligocene formation contains biogenic methane not produced by thermodegradation. The nitrogen/argon ratio of the Oligocene waters is close to that for air saturated water which suggests these connate waters have preserved their nitrogen since burial. The oil bearing horizons have very high nitrogen contents which could be indicative of thermogenic nitrogen production, however there appears to be no trend with ammonium content. Further work with nitrogen isotopes would be needed to attain the source of this nitrogen.

4.5 Inert Gas Ratios

The ratios of Kr and Xe to Ar in air saturated water are 2.38×10^{-4} and 3.41×10^{-5} respectively. The ratios of the heavy noble gases to argon in the Molasse formation waters greatly exceed these values (Figures 4.12 and 4.13). The xenon concentration is up to 10 times the air saturated water value and krypton is up to 1.5 times the air saturated water value. Therefore the heavy inert gases are concentrated in the oil and gas bearing formations. These concentrations cannot be explained in terms of groundwater outgassing prior to collection. High xenon concentrations have previously been observed in shale formations (Bernatowicz and others 1984). Thus

Table 4.5 Inert Gas ratios for samples from the Molasse Basin

No.	Name	Formation	Type	He/Ar	Ne/Ar x 10^3	Kr/Ar x 10^4	Xe/Ar x 10^4
4041B	Steinerkirchen	Hall	g/w	0.52	12.7	3.7	1.1
4042B	Puchkirchen 27	Upper Puch.	g/w	0.81	13.2	2.3	0.72
E				0.5	55.0	-	-
C				0.4	4.1	-	-
4043E	Hocheck	Lower Puch.	g/w	1.14	244.0	-	-
C				0.58	4.4	-	-
B				1.11	20.0	2.5	0.70
4044E	Pfaffstatt 3	Lower Puch.	g/w	0.13	41.9	-	-
C				0.32	5.0	7.2	1.0
B				0.67	24.2	2.9	1.0
4045E	Schwanenstadt 17	Upper Puch.	g/w	0.18	83.8	-	-
				0.49	4.7	6.6	0.91
B				0.93	18.3	2.9	0.9
4046E	Puchkirchen 24	Upper Puch.	g/w	0.044	74.0	-	-
C				0.25	5.0	-	-
B				0.58	10.4	7.2	1.5
4047E	Puchkirchen DST 1	Hall	g/w	0.14	64.5	-	-
C				0.22	2.45	2.6	1.3
B				0.54	17.4	5.3	1.1
4054C	Eberstalzell H1	Upper Puch.	w	0.32	23.1	2.7	6.7
B				0.30	5.6	5.0	4.9
4056C	Eberstalzell H5	Upper Puch.	w	0.24	12.6	3.0	1.2
B				0.26	4.8	3.7	1.1
4057B	Schwanenstadt 4	Hall	w	0.14	13.7	2.9	1.7
C				0.16	2.1	3.0	1.8

g/w water from a gas well.

Table 4.6 **Inert gas ratios from oil/water mixtures from the Molasse Basin of Upper Austria.**

No.	Name	Formation	Type	He/Ar	Ne/Ar x 10^3	Kr/Ar x 10^4	Xe/Ar x 10^4
4021A	Engenfeld 1	Upper Eocene	o	0.077	1.2	1.5	0.35
B				0.52	0.67	2.3	0.39
4023C	Oberaustall 6	Cenoman	o	0.29	1.07	3.7	1.19
4025A	Steinhaus 1	Upper Eocene	o	0.14	11.7	30.6	2.04
B				0.087	2.02	0.99	0.53
4027B	Atzbach 5	Upper Puch.	g	0.18	32.7	-	-
4028B	Atzbach 1	Upper Puch.	g	0.009	64.9	-	-
4029C	Friedburg 2	Upper Puch.	g	0.60	84.0	-	-
4030B	Munderfing 1	Hall	g	0.70	1.8	-	-
4031B	Kemating 5	Upper Puch.	o	0.32	4.6	18.2	1.03
C				0.29	2.7	4.9	0.64
4032A	Maria Schmolln	Upper Eocene	o	0.043	2.1	5.3	1.5
B				0.11	1.3	24.8	0.41
4033D	Puchkirchen 20	Upper Puch.	o	0.68	0.89	1.86	0.27
B				0.052	0.46	0.59	0.22
4035B	Trattnach 4	Cenoman	o	0.073	0.51	1.79	-
C				0.068	1.43	2.33	0.48
4036B	Haindorf 1	Upper Jurr.	o	0.11	1.21	4.11	1.71
C				0.22	1.18	5.18	0.78
4048D	Horgersteig 1	Cenoman	o	0.01	259.0		
4049B	Eggerding 1	Rupelian	o	0.03	1.2		
4050E	Kemating N1A	Upper Eocene	o	0.09	56.8		
4051E	Kohleck 2	Upper Eocene	o	0.03	169.0		
4058B	Voitsdorf 11	Upper Eocene	o	0.06	18.6		
4059B	Voitsdorf 15	Cenoman	o	0.22	25.8		
4060B	Voitsdorf 30	Cenoman	o	0.12	120.0		
4061B	Voitsdorf 2	Cenoman	o	0.07	300.0		
4062C	Voitsdorf 10	Upper Eocene	o	0.05	62.0		
4063B	Voitsdorf 13	Cenoman	o	0.0012	10.3		

Figure 4.12 Kr/Ar ratio for Molasse basin formation waters

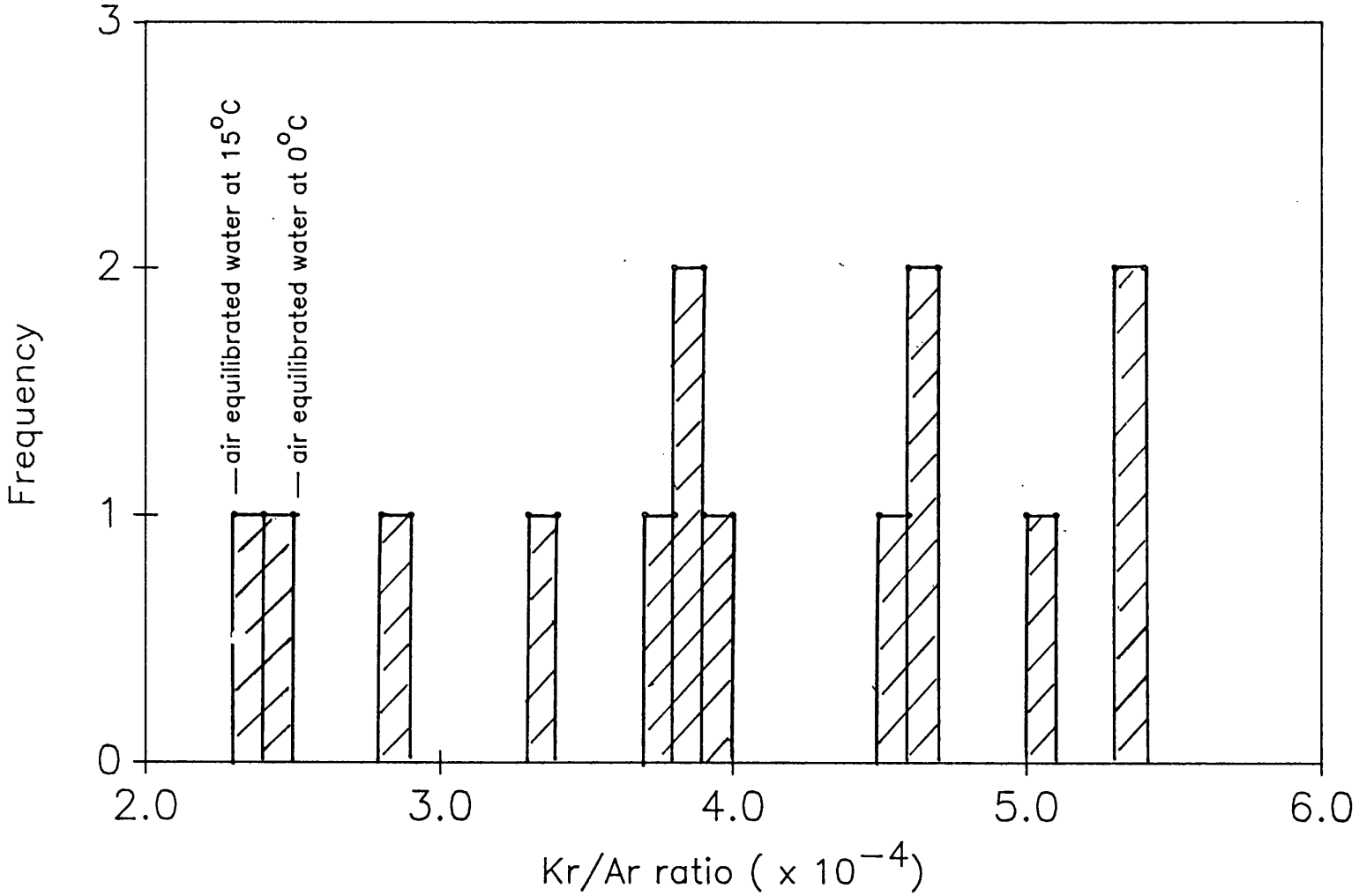

Figure 4.13

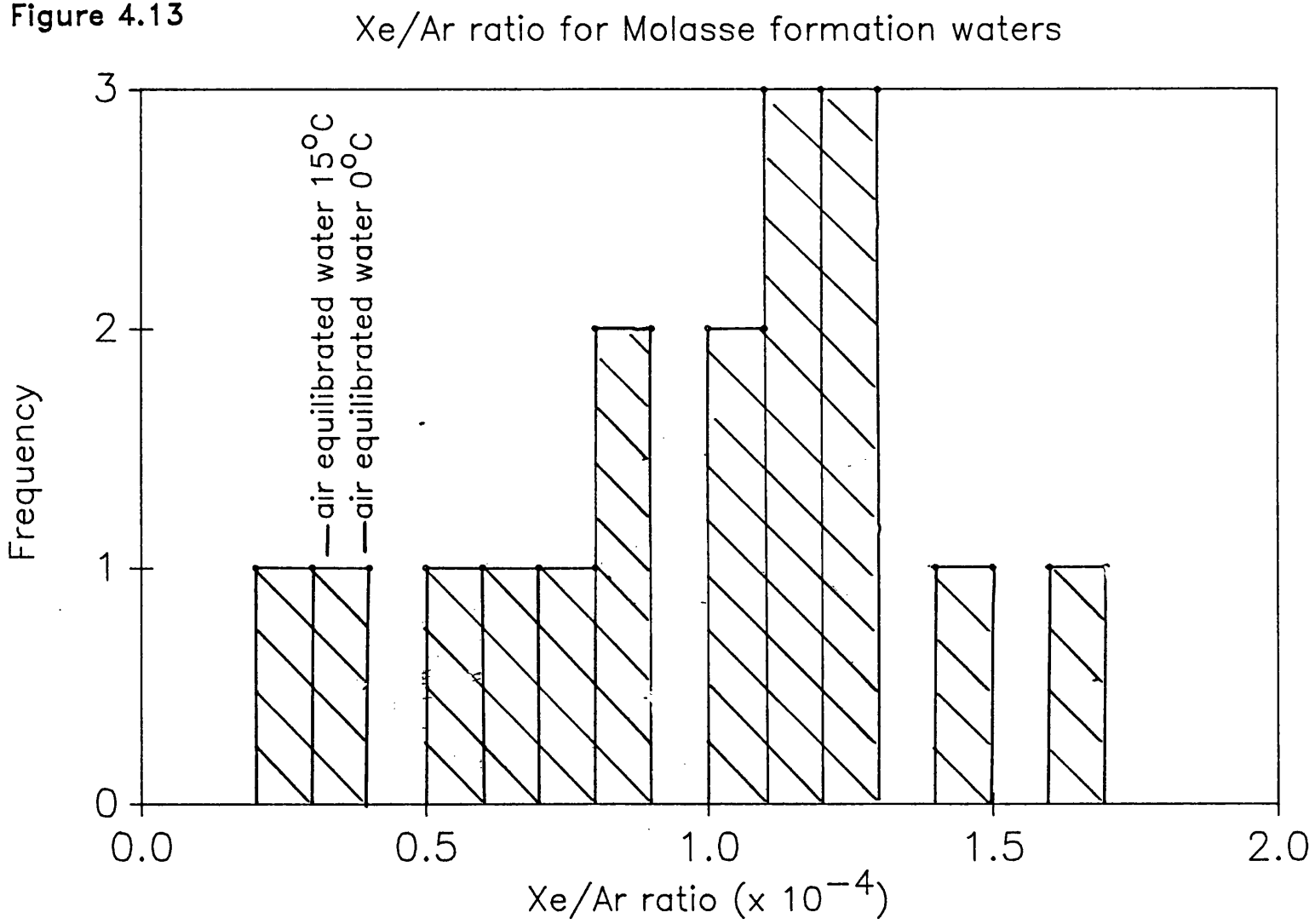
Xe/Ar ratio for Molasse formation waters
Frequency
—air equilibrated water 15°C
—air equilibrated water 0°C
0
1
2
3
0.0
0.5
1.0
1.5
2.0
Xe/Ar ratio (x 10⁻⁴)

Figure 4.14 Ratio of inert gases for the Oligocene waters of the Molasse basin

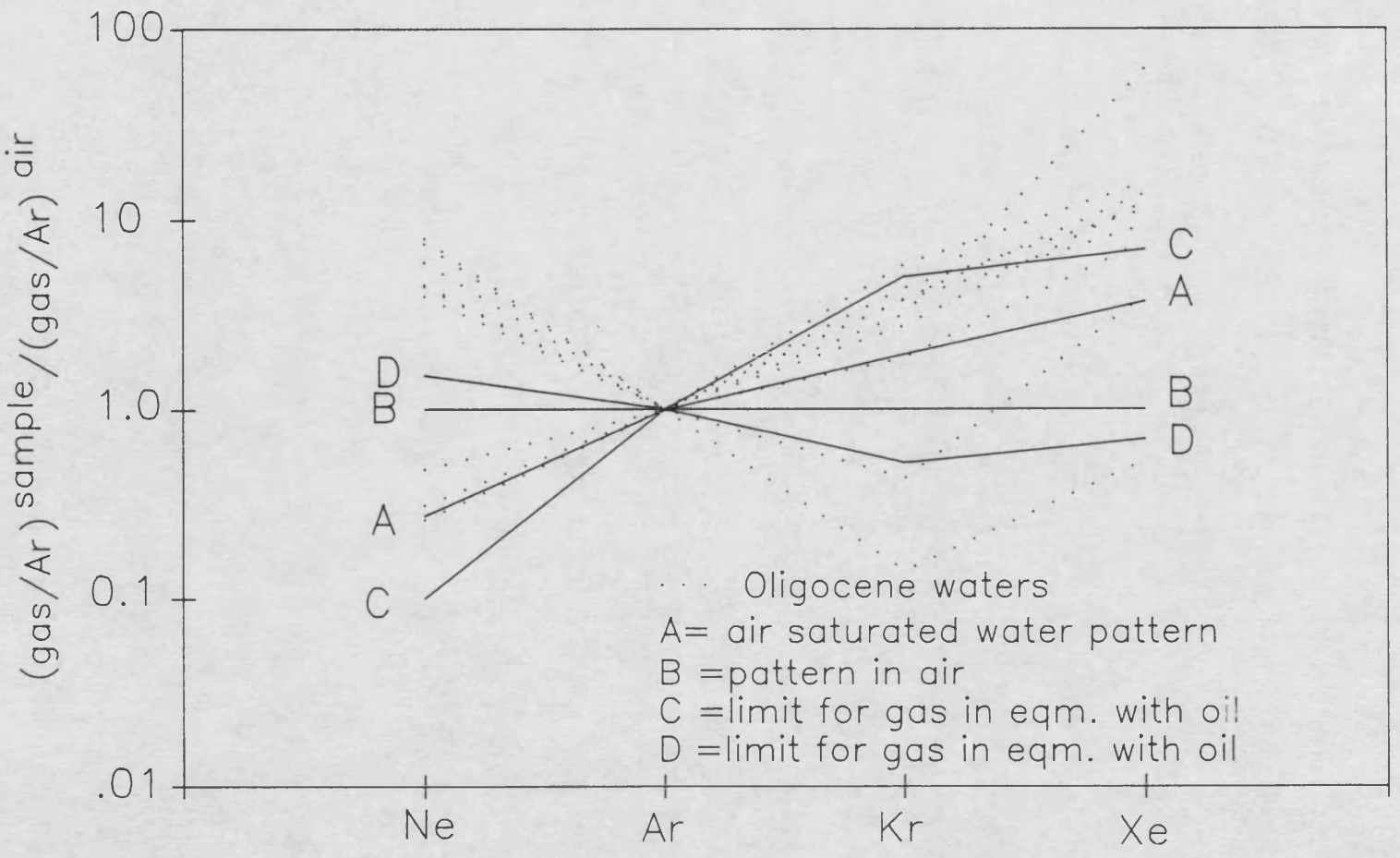

shale formations are a likely source of these enhanced xenon concentrations. Kr/Ar enhancement may also be explained in this way. The smaller concentration of krypton might be expected when considering the physical properties of the heavy inert gases.

Figure 4.14 shows the relationship for inert gases for equilibrium distribution between natural gas and water phases, providing the atmospheric inert gas are introduced into the hydrocarbon system via recharge. Theoretical atmospheric inert gas patterns of natural gas, degassed from oil (previously equilibrated with water) should fall between lines C and D (figure 4.14), (Bosch and Mazor, 1987). Natural gas in equilibrium with water should fall between lines A and B. This diagram does not explain the inert gas contents of the formation waters. This could be due to a multiple stage degassing process, or release of noble gases absorbed on sedimentary rocks.

4.6 Radioelements

Uranium contents of saline waters are very low compared with the sea water concentration from which they are likely to have been derived. The original uranium content is likely to have been deposited during the reducing conditions which prevailed during diagenesis of these formations. The ^{226}Ra contents of the formation waters increase with salinity (Figure 4.15). The sulphate content of these waters is not controlling the radium

Table 4.7 **Dissolved radioelement contents of groundwaters from the Molasse Basin**

No.	Site	^{222}Rn pCi/kg	+/-	^{226}Ra pCi/kg	+/-	$^{228}Ra/^{226}Ra$	+/-	U content ug/kg	+/-	$^{234}U/^{238}U$	+/-
4021A	Engenfeld 1	128	1.7	13.8	0.06@	nd					
B		123	1.3	13.7	0.08@						
4022A	Gundersdorf Hl	229	3.8	34.3	0.66	nd		0.008	0.001	0.38	0.06
B		226	3.6	32.2	0.20					1.06	0.08*
4023A	Oberaustall 6	liquid in scintillation flask.				nd					
				3.8	0.05@						
				3.4	0.04@						
4024A	Maierdorf Hl	99	1.1	50.2	0.26	nd		0.002	0.0003	0.88	0.18
B		227	1.6	53.3	0.27					1.41	0.34*
4025A	Steinhaus 1	2	0.4	10.6	0.05@	nd					
B		1	0.2	8.7	0.05@						
4026A	Desselbrunn 2	448	10.3	18.8	0.16	nd		0.001	0.0002	3.19	0.63
B		411	9.6	17.5	0.07						
4027A	Atzbach 5	27	3.3**	0.7	0.01	nd		Activity below detection limit			
B		9	1.6**	0.7	0.01						
4028A	Atzbach 1	9	0.7**	6.9	0.04	nd					
B		32	1.6**	7.7	0.04						
4029A	Friedburg 2	9	1.7**	13.9	0.05	nd		0.008	0.001	1.42	0.33
B		11	2.1**	12.5	0.13						
4030A	Munderfing	26	1.4**	14.4	0.06	nd		0.168	0.003	1.00	0.03
B		12	0.8**	14.5	0.06						

Table 4.7 (cont)

No.	Site/Date	^{222}Rn pCi/kg	+/-	^{226}Ra pCi/kg	+/-	$^{228}Ra/^{226}Ra$	+/-	U content ug/kg	+/-	$^{234}U/^{238}U$	+/-
4031A	Kemating 5	9	0.7	75.1	0.5@	nd					
B		7	1.2	78.4	0.7@						
4032A	Maria Schmolln	3	0.3	5.4	0.04@	nd					
B		1	0.2	6.2	0.06@						
4033A	Puchkirchen 20	nd		83.0	0.5@	nd					
				75.1	0.4@						
4034A	Ried 18	3	0.2	0.1	0.004	nd		0.069	0.002	2.35	0.10
B		2	0.1	0.1	0.005						
4035A	Trattnach 4	58	1.7	0.8	0.01@	nd					
B		76	2.0	0.6	0.01@						
4036	Haindorf	nd		2.1	0.03@	nd					
				2.1	0.04@						
4037A	Aurolzmunster	319	6.0	0.4	0.01	nd		0.100	0.005	1.08	0.07
B		256	1.3	0.4	0.01						
4038A	Ried 3	244	1.5	0.3	0.01	nd		0.004	0.001	1.27	0.36
B		236	3.1	0.3	0.01						
4039A	Bad Hall	184	3.1	13.9	0.15	nd		0.008	0.001	2.21	0.33
B	Tassilo Quelle	192	2.2	14.8	0.05						
4040A	Bad Hall	179	2.1	27.4	0.21	nd		Activity below detection limit			
	Paracelsus Quelle			22.2	0.17						
B		281	3.4	24.5	0.20						

Table 4.7 (cont)

No.	Site	^{222}Rn pCi/kg	+/-	^{226}Ra pCi/kg	+/-	$^{228}Ra/^{226}Ra$	+/-	U content ug/kg	+/-	$^{234}U/^{238}U$	+/-
4041	Steinerkirchen 1	157	5.0	27.8	0.2	0.5	0.04	0.016	0.002	0.76	0.13
		11	0.4**	29.3	0.08						
		15	0.5**								
4042	Puchkirchen 27	202	5.0	12.5	0.2	0.8	0.04	0.030	0.005	1.18	0.24
		25	0.7**	12.7	0.05						
		27	0.8**								
4043	Hocheck 2	110	2.0	7.6	0.04	0.3	0.06	0.033	0.004	1.59	0.26
		23	0.5**	6.3	0.04						
4044	Pfaffstatt	169	2.0	16.7	0.06	0.7	0.04	0.013	0.001	0.74	0.11
		20	0.7**	14.3	0.06						
		31	0.9**								
4045	Schwanenstadt 17	85	1.0	9.2	0.04	0.4	0.02	0.036	0.002	1.02	0.08
		11	0.2**	10.9	0.06						
4046	Puchkirchen 24	280	3.0	23.8	0.07	0.6	0.07	0.010	0.001	0.87	0.10
		57	0.5**	22.1	0.08						
4047	Puchkirchen DST 1	161	2.0	0.33	0.01			0.010	0.0004	1.03	0.07
		41	0.5**	0.33	0.01						
4048	Horgersteig 1	Oil/water would not seperate									
4049	Eggerding 1			2.4	0.02@						
				1.1	0.03@						
4050	Kemating NIA			52.6	0.3@						
4051	Kohleck 2			56.5	0.5@						
				39.1	0.8@						

Table 4.7 (cont)

		^{222}Rn pCi/kg	+/-	^{226}Ra pCi/kg	+/-	$^{228}Ra/^{226}Ra$	+/-	U content ug/kg	+/-	$^{234}U/^{238}U$	+/-
4052	Kohleck 6			31.9 34.7	0.4@ 0.1@						
4053	Trattnach 11			1.0 1.3	0.01@ 0.03@						
4054	Eberstalzell H1	284	2.0	73.9 62.9	0.4 0.1	0.6	0.08	0.006	0.001	0.26	0.07
4055	Eberstalzell H2	235	2.0	45.9 46.1	0.1 0.1	1.0	0.06	0.011	0.001	0.69	0.10
4056	Eberstalzell H5	337 397	2.0 2.0	50.6 50.1	0.1 0.1	0.6	0.06	0.082	0.003	0.99	0.05
4057	Schwanenstadt 4	183	2.0	32.5 30.0	0.1 0.09			0.009	0.001	0.83	0.07
4058	Voitsdorf 11	1.2	0.2	49.9 42.4	0.5@ 0.1@						
4059	Voitsdorf 15	192	0.1	80.0 78.1	0.3@ 0.2@						
4060	Voitsdorf 30	0.9	0.1	49.2 53.3	0.3@ 0.2@						
4061	Voitsdorf 2	137	1.0	52.0 55.9	0.3@ 0.2@						
4062	Voitsdorf 10	1.3	0.1	92.6	0.4@						
4063	Voitsdorf 13			21.4 23.9	0.3@ 0.4@						
4064	Sattledt			83.4 92.6	0.4 0.4	0.3	0.02				

** ^{222}Rn content per 1000cm^3 of gas.
@ Ra content pCi/l of water seperated from oil/water mixtures.
nd Not determined.

content as might be expected as radium behaves chemically like calcium and strontium (Figure 4.16).

The radium content distribution can be explained as dilution of high radium content brines with meteoric water. The highest observed radium contents for these waters is 93 pCi/kg, using the average uranium content for the aquifer rocks this is about 5% of the equilibrium ^{226}Ra in the rock. This release is very high compared with ^{222}Rn released in similar rock (Andrews and Lee, 1979). The very high radium contents may not be easily explained but once in solution the highly reducing environment and consequent lack of Fe(III) would keep dissolved radium in solution.

Figure 4.15

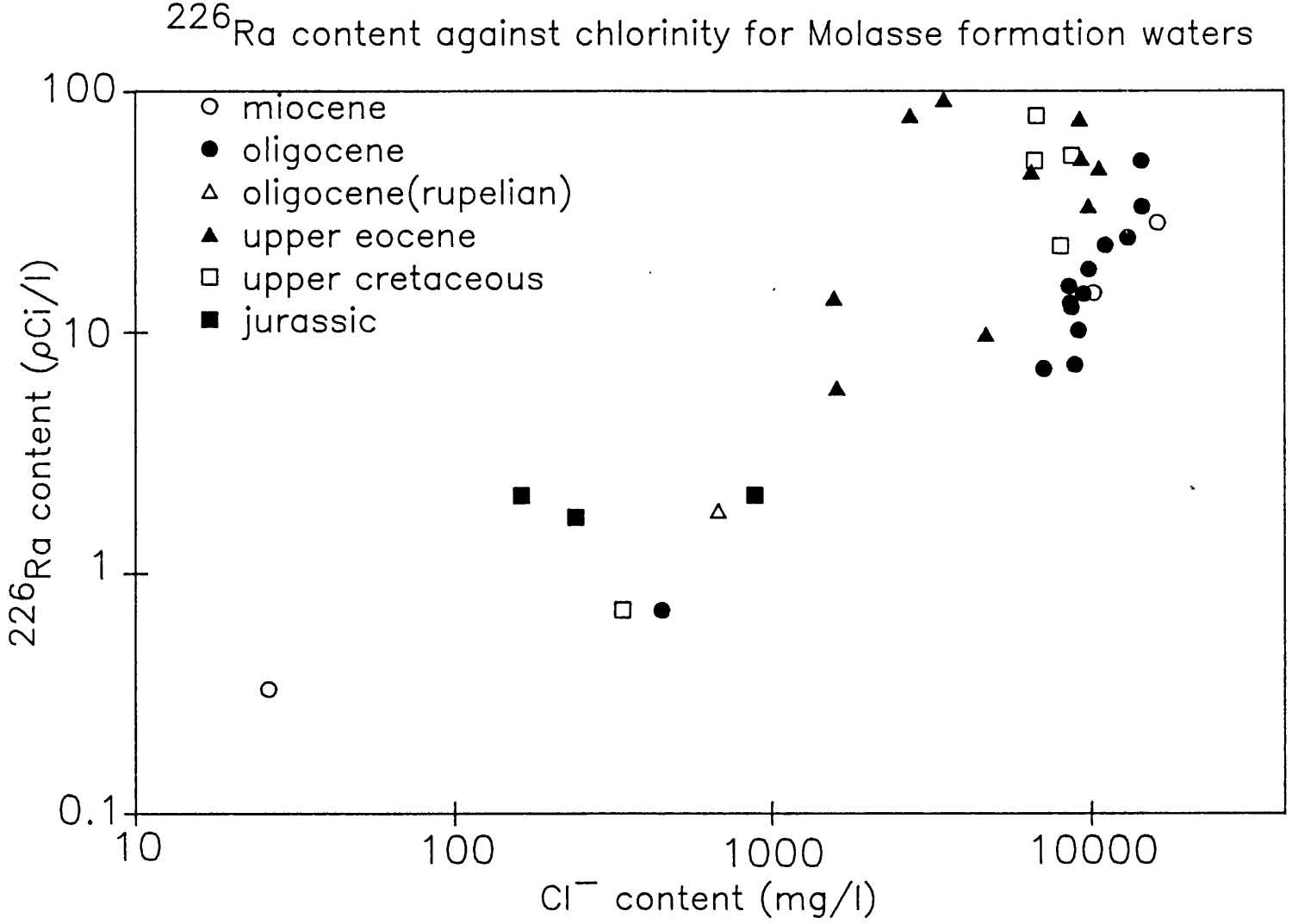
226Ra content against chlorinity for Molasse formation waters
miocene
oligocene
oligocene(rupelian)
upper eocene
upper cretaceous
jurassic
226Ra content (ρCi/l)
100
10
1
0.1
10
100
1000
10000
Cl⁻ content (mg/l)

Figure 4.16 ^{226}Ra content against Sulphate for Molasse formation waters

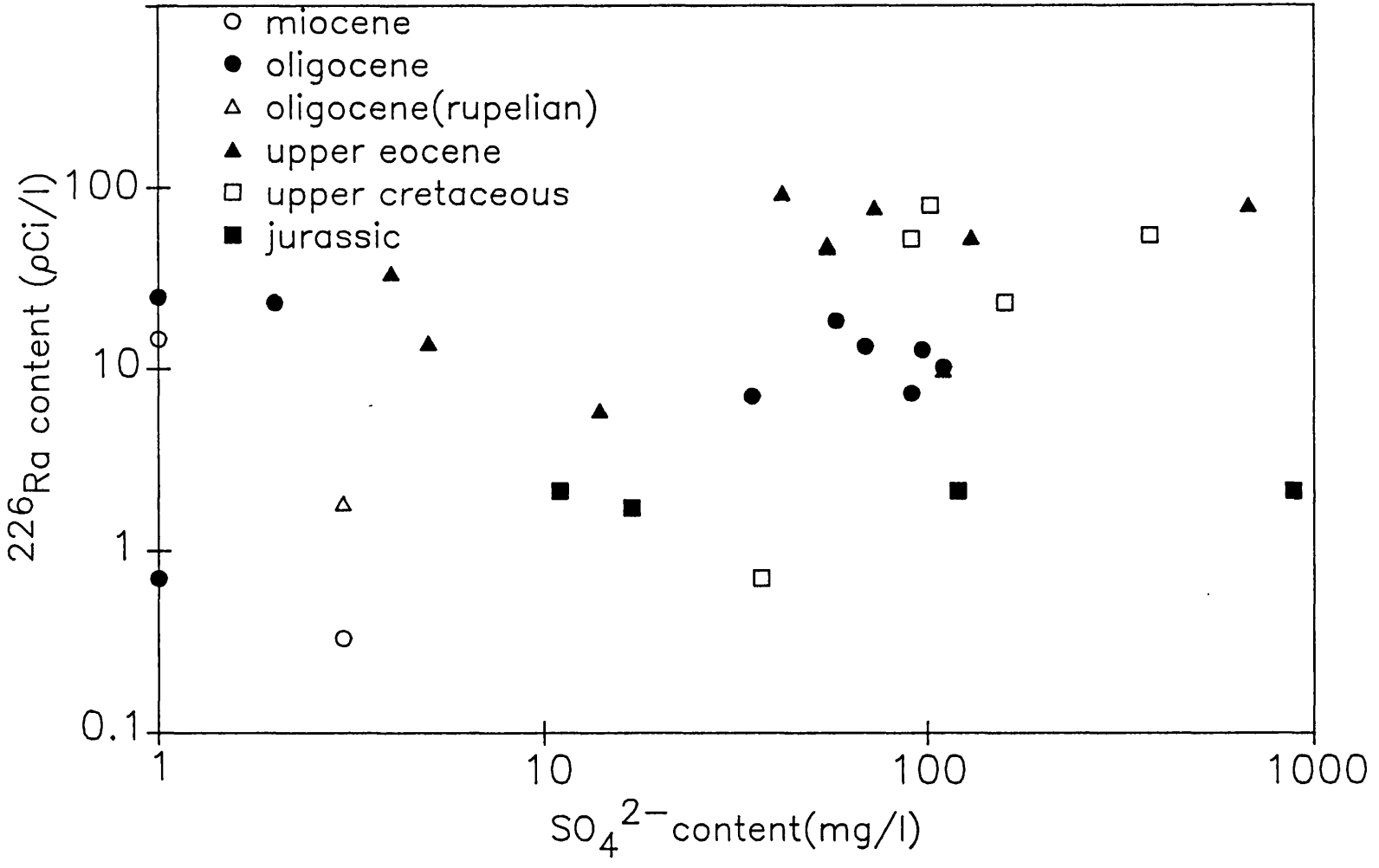

CHAPTER 5

STRIPA GROUNDWATERS

5.1 Geology and Location

The Stripa mine is located in Orebro county south-central Sweden, 250km north-west of Stockholm. The Stripa mine lies within the central Swedish ore province consisting of more than one hundred iron-manganese and copper-zinc-lead mines. Mining at Stripa began around the year 1450 for iron ore. The mining was intermittent until 1976 when it opened as a research site to investigate the origin and evolution of groundwaters in a granitic bed rock.

The bedrock geology of the Stripa region consists of highly folded and deformed Precambrian rocks, primarily metasediments and metavolcanics intruded by several granitic bodies (Nordstrom et al, 1985). The Stripa mine is situated in a small elongated granitic intrusion within a highly metamorphosed sedimentary rock (leptite). The age of the granite is 1691 ± 16 Ma (Wollenberg et al, 1980) and the leptite is somewhat older. A third, less common, metamorphic rock at Stripa is a microschist rich in amphibole. The Stripa granite contains 30-40% quartz, 25-35% plagioclase and 18-34% microcline. An additional 5-10% is muscovite and chlorite.

5.2 Structure and Porosity

The main flow paths in crystalline rocks are joints, fracture zones and shear zones. Joints may be the result of stress relief during crystallisation or tectonic

stresses during crustal movements. They are generally discontinuous but together form continuous flow networks. The transmissivity of joint systems depends upon their aperture which may range from 0.1μm to more than 300μm and their degree of interconnection. Shear zones occur in Stripa granite as a result of post crystallisation stress and tend to be continuous. Fracture zones are regions of closely spaced interconnected fractures which vary in length up to hundreds of metres. Fracture and shear zones may be conductive depending upon the nature of any infilling material.

The total matrix porosity of Stripa granite is 0 to 1.3% and averages 0.5%. However of this only 1% is the flow porosity in which aqueous movement takes place. 5% of total porosity is due to microfractures which are end connected to flow pathways. These have apertures from 0.1μm to 10μm and allow diffusion but no aqueous transport. 94% of porosity is the pore porosity which are not connected to the flow or diffusion porosity.

5.3 Borehole Locations

The deepest mining levels were at 360m and 410m below the ground surface. V2 is a vertical 822m deep borehole from the 410m level. Groundwater flow of 0.1 to 0.5 litres/minute were obtained. At the 360m level three boreholes were drilled, one vertical and two sub-horizontal. V1 is the vertical borehole of 506m depth.

Table 5.1 Physical data for groundwater samples from Stripa for sampling in period October 1983 - March 1984

Borehole	Interval, m	Flow rate, cm^3/min	Temperature °C	pH	Conductivity µs/cm	Eh mV
M3	0 - 14	75	14.5	9.09	235	+100
E1	3 - 300	400	10.3	8.90	165	+109
N1-I	252 - 300	560	10.5	8.89	200	+ 33
N1-II	152 - 251	555	10.3	8.99	215	+ 39
V1	100 - 505	7-18,000	12.3	9.12	1525	+114
V2 I	562 - 822	11	8.2	9.94	1215	+239
V2 II	500 - 561	252	8.6	10.06	1090	+ 43
V2 III	424 - 499	210	9.0	10.04	1210	+ 46
V2 IV	382 - 423	92	8.0	9.51	1140	+ 26

Figure 5.1

Relative borehole disposition:

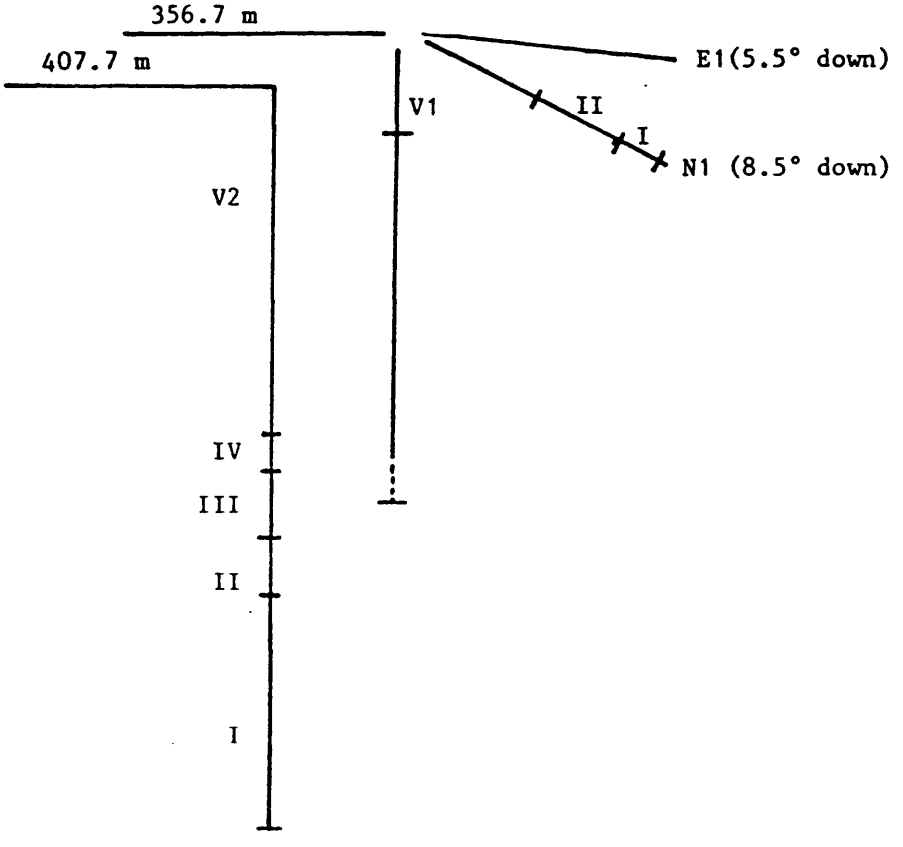

N1 and E1 are subhorizontal boreholes at right angles to one another and both are 300m deep. M3 is situated in a gallery on the 360m level which was constructed to contain heater experiments to simulate decay of stored nuclear waste. Figure 5.1 shows the relative borehole disposition into the Stripa granite. Table 5.1 gives some physical data on these boreholes.

5.4 Radiogenic ^4He

Large amounts of dissolved ^4He up to 3×10^{-3} cm^3 STP/cm^3 H_2O are present in Stripa groundwaters. Table 5.2 shows noble gas contents of flowing boreholes. Since most of radioelements are present in microfractures (Section 5.10) if all helium generated in rocks dissolved in pore fluids the ^4He age can be calculated using

$$[He] = p\ \emptyset^{-1}\ t\ \ 1.19 \times 10^{-13}[U]_r + 2.88 \times 10^{-14}[Th]_r$$

where $[He]$ = ^4He contents of water, cm^3 STP/cm^3 H_2O

$[U]_r$ = Uranium content of rock, ppm

$[Th]_r$ = Thorium content of rock, ppm

$\emptyset$ = fractional porosity

p = rock density, g/cm^3

using value of $\emptyset$ as 0.5 and radioelement contents as in section 5.11 this gives ^4He ages up to 85 M years. This is clearly very much greater than ^{14}C ages of around 25,000 years. The ^4He content are very much greater than which could be generated in the aquifer between recharge and extraction. This indicates as well as a radiogenic

Table 5.2 Noble gas contents (cm^3 STP/cm^3) and recharge temperatures of Stripa groundwaters

Date	Borehole & interval, m	Depth below ground, m	He (1)	Ne (2)	Ar (3)	Kr (4)	Xe (4)	CI	RT °C
790518	PW-1	- 60	.08	2.24	4.60	10.40	1.53	1.0	5.3
790517	PW-4	- 40	.09	2.30	5.00	11.10	1.56	1.1	5.8
790515	PW-5	- 40	.08	2.22	4.58	10.60	1.64	1.0	5.5
831109	M3,	0- 14	336- 350	693	3.84	6.08	12.88	1.83	1.7	2.2
840223	M3,	0- 14	336- 350	389	3.58	6.28	13.04	1.64	1.6	3.3
850219	M3,	0- 14	336- 350	478	4.18	6.09	12.66	1.86	1.9	2.7
820324	E1,	127-130	367- 369	68	2.85	5.35	11.43	1.32	1.3	4.2
840306	E1,	3-300	357- 385	225	6.30	7.10	13.92	1.64	2.9	3.3
850220	E1,	3-300	357- 385	258	4.53	6.94	13.36	1.91	2.0	1.9
840307	N1,	252-300	397- 401	332	4.23	7.22	14.25	1.74	1.9	4.2
840313	N1,	152-251	379- 394	291	3.87	6.85	12.84	1.71	1.8	3.3
831003	V1,	100-505	457- 862	1744	5.40	7.80	13.61	1.87	2.4	2.8
831019	V1,	100-505	457- 862	2860	5.20	7.32	12.43	1.92	2.4	3.9
831105	V1,	100-505	457- 862	3551	3.97	7.56	13.29	1.87	1.8	1.6
840111	V1,	100-505	457- 862	1889	4.63	8.29	14.55	1.85	2.1	2.7
840208	V1,	100-505	457- 862	4369	4.90	8.98	13.99	1.85	2.2	1.9
850219	V1,	103-505	460- 862	1691	4.14	7.99	13.64	2.07	1.8	0.5
820427	V2,	6-822	416-1292	1154	3.46	6.86	13.32	1.37	1.5	0.3
821124	V2,	406-410	816- 820	3010	-	9.14	14.70	1.73	-	-
821213	V2,	413-417	823- 827	1044	-	7.0	12.78	1.75	-	-
830119	V2,	490-494	900- 904	3225	-	7.97	13.41	1.76	-	-
840228	V2,	400-561	910- 971	1877	3.93	7.93	12.91	1.78	1.7	2.6
840228	V2,	382-423	792- 833	1597	4.17	8.48	13.90	1.89	1.9	1.9
850218	V2/1,	559-822	969-1232	1717	3.71	7.71	12.39	1.84	1.7	2.7
850219	V2/2,	550-558	960- 968	3262	6.50	8.77	14.43	2.20	2.9	0.9
850219	V2/3,	490-498	900- 908	1150	3.75	7.44	13.42	1.94	1.7	0.7
850219	V2/4,	402-410	812- 920	1779	4.26	7.10	12.88	1.97	1.9	2.3
850219	V2/5,	389-397	799- 807	328	3.24	7.02	13.46	1.86	1.4	0.7

Notes:
(1) x 10^{-6}; (2) x 10^{-7}; (3) x 10^{-4}; (4) x 10^{-8}
CI = contamination index (see text).
RT = recharge temperature.
PW = shallow well.

component there is a ^4He component due to diffusion from deeper layers, or that there is mixing with ascending deeper groundwaters. Considering the groundwater movement rates in this low conductivity granite, diffusion of helium is generally the more likely of these alternatives. The helium content of the Stripa granite matrix has been determined (Chapter 7). This varies from 1.7 to 2.9 x 10^{-4} cm^3/cm^3 rock. This compares with a total generated helium in the age of the granite of 1691 M years of 3.0 x $10^{-2}cm^3/cm^3$ of rock. Thus only around 1% of helium generated in the rock is currently stored in the rock matrix. This high loss of stored helium can be accounted for as most of helium is generated by uranium which is concentrated on fracture coatings, which allows rapid diffusion of helium.

The diffusion distance from rock matrix to the water phase in the fracture system is so small that the fracture residence times needed to establish concentration equilibrium between the water and rock are short. The ^4He flux from a uniform rock matrix which loses He at one surface is given by

$$F = 2G \left(\frac{Dt}{\pi}\right)^{0.5} \qquad (5.1)$$

where G is the generation rate of He by radioelement decay within the rock, D is the diffusion coefficient for He in the rock matrix and t is the rock age. If the flux of He is dissolved by groundwater within fractures, then the time for the fracture fluid to attain the observed helium

concentrations may be estimated. The diffusion coefficient has been experimentally determined (Chapter 7) for Stripa granite to be in the order of 2×10^{-13} m^2/a at 10°C. However this figure is for helium stored in mineral grains and does not allow for the bulk of helium being generated at fracture coatings. The diffusion coefficient for helium in volcanic glasses has been determined by Jambon and Shelby (1980) to be $3 \times 10^{-6} m^2 a^{-1}$. In a water saturated rock matrix with good fracture interconnection the diffusion coefficient would be close to that for water ($3.16 \times 10^{-2} m^2 a^{-1}$). This would be particularly relevant for the Stripa granite since He is predominantly produced close to the aqueous phase. Since the diffusion coefficient is uncertain an intermediate value is used which is between value for glasses and water, which is $3.2 \times 10^{-4} m^2 a^{-1}$. Assuming helium accumulates in 0.1mm fractures application of this equation (5.1) yields a time to achieve the highest helium concentrations of only 46 years. The helium content of borehole M3 is very low in comparison with the other Stripa groundwaters. The helium content would be released from the granite in only a few years. As there is no reason to assign any different parameters to the granite in this borehole, ^4He is probably being lost by more rapid groundwater movement.

The ^4He groundwater content generally increases with depth in the Stripa granite. The helium concentration/ depth profiles calculated for diffusive loss of helium from the granite can be calculated by solution of the

equation

$$\frac{dc}{dt} = G + D\frac{d^2C}{dZ^2}$$

where C is the concentration of He cm^3 STP$cm^{-3}H_2O$

t is the time helium has been diffusing, years

G is the helium production rate, cm^3 STPcm^{-3} a^{-1}

D is diffusion coefficient of helium, m^2a^{-1}

Z is depth below ground, m

An approximate solution of this equation is given by Andrews (1985) as:

$$c(z,t) = G\,t\left[1 - \exp\left(-\frac{2}{\pi}\cdot\frac{Z}{(Dt)^{0.5}}\right)\right]$$

This equation can be used to calculate helium concentration against depth profiles for the Stripa granite. The profiles shown in Figure 5.2 are for Stripa granite with surface exposure and either a diffusion coefficient for helium appropriate for water or for a granitic system. Figure 5.3 are for Stripa granite with 200m of leptite lying above the granite.

These profiles can only be valid if the rock matrix helium equilibrates with the aqueous phase in a short period of time. This will only occur with aquifers containing small aperture fractures.

Comparison of Figures 5.2 and 5.3 shows that the helium contents of the Stripa waters more closely follows the profile for granite, overlain by 200m of leptite. than that for granite

Figure 5.2 ^{4}He /depth profiles in the Stripa granite

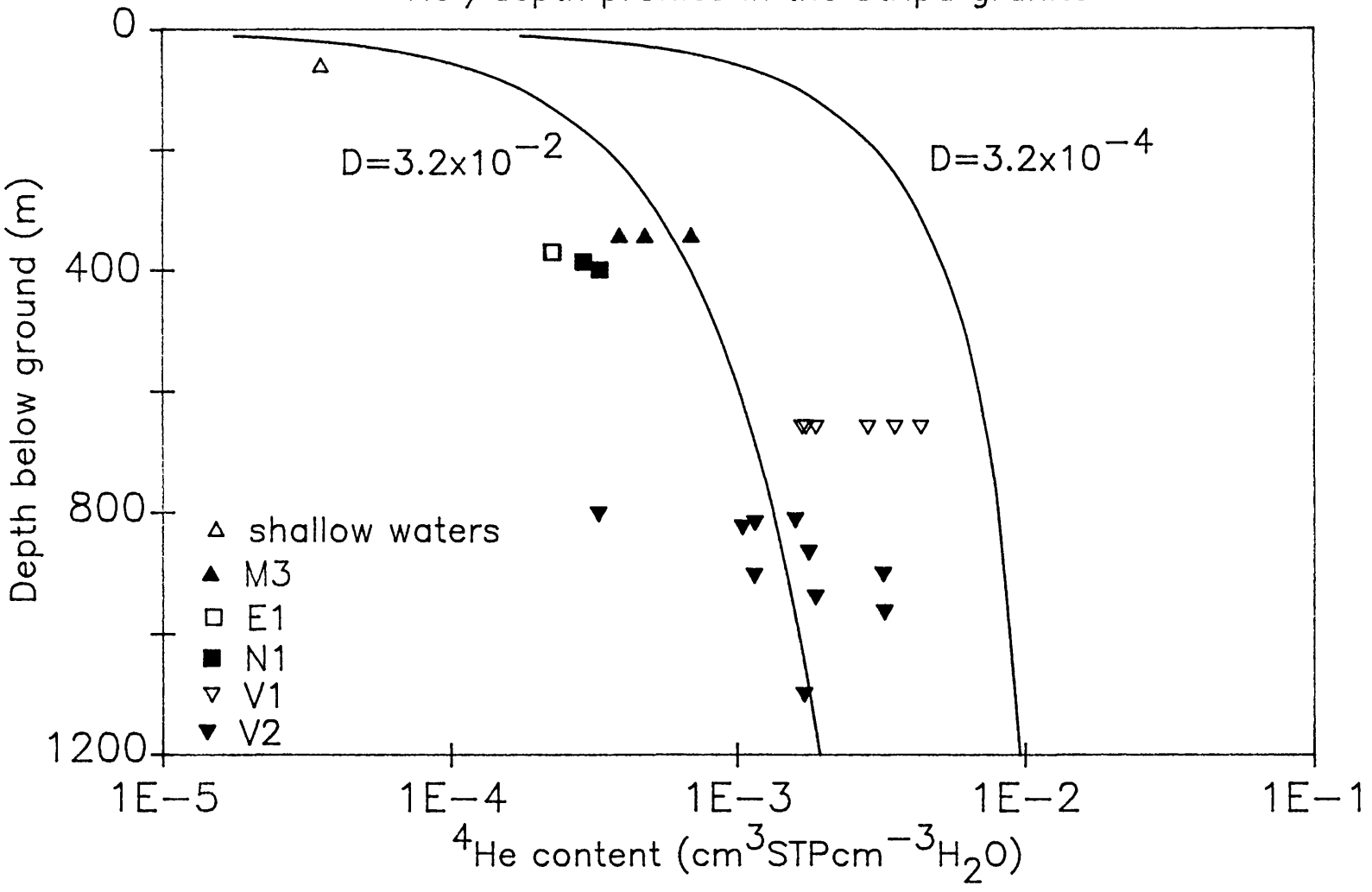

Figure 5.3

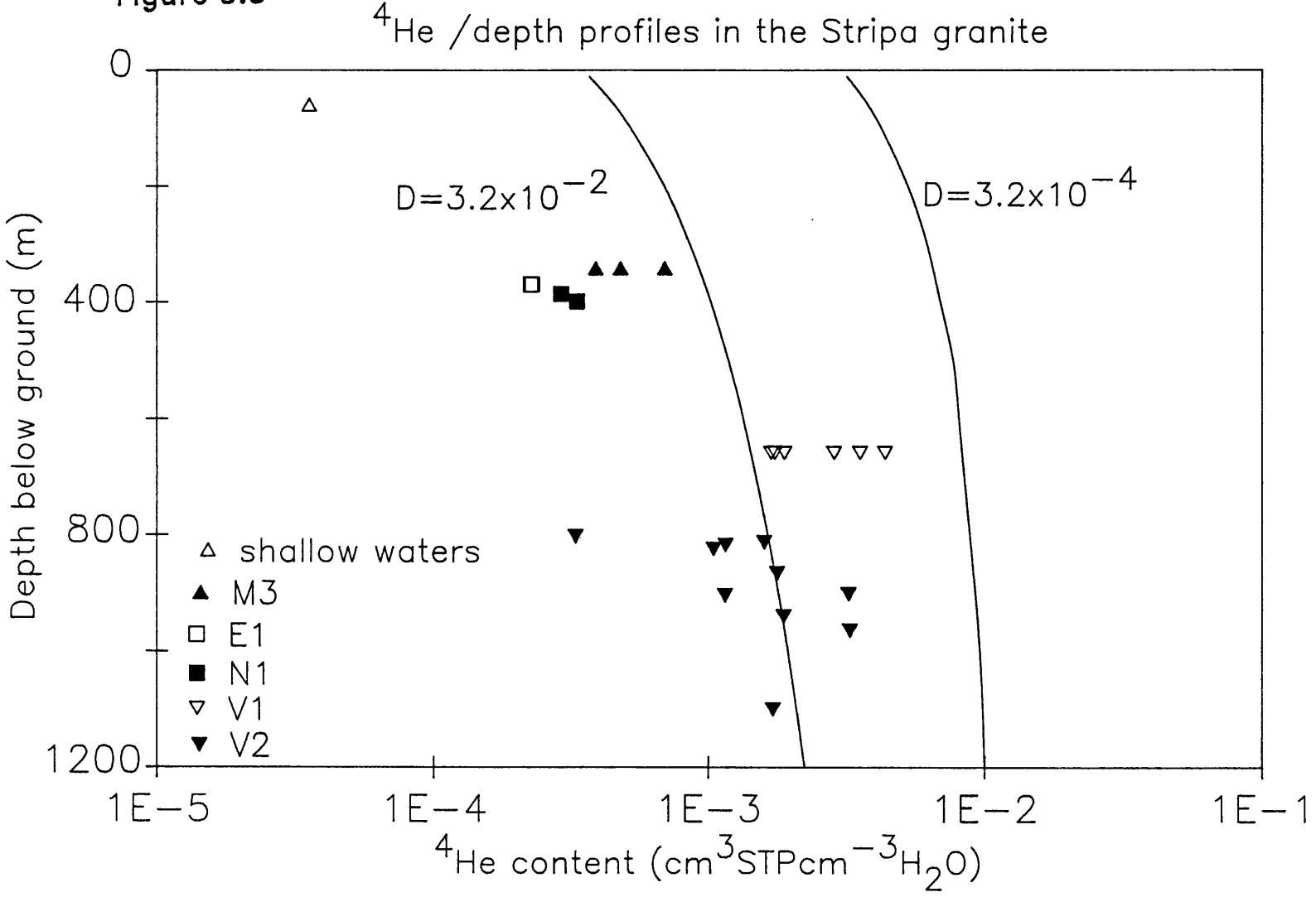
^{4}He /depth profiles in the Stripa granite
0
400
800
1200
Depth below ground (m)
D=3.2x10^{-2}
D=3.2x10^{-4}
shallow waters
M3
E1
N1
V1
V2
1E−5
1E−4
1E−3
1E−2
1E−1
^{4}He content (cm^{3}STPcm^{-3}H$_2$O)

Figure 5.4

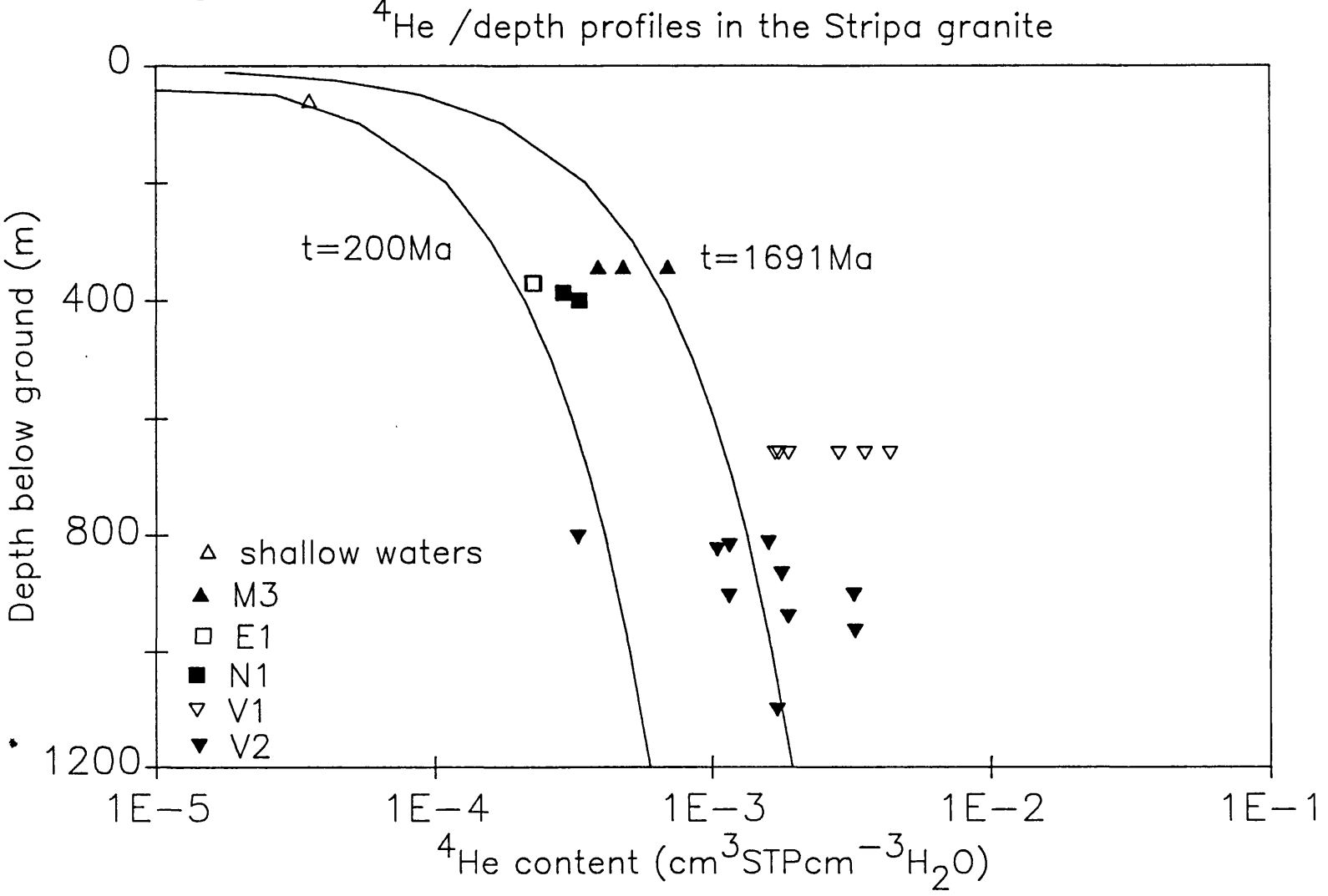
^{4}He /depth profiles in the Stripa granite
0
400
800
1200
Depth below ground (m)
t=200Ma
t=1691Ma
shallow waters
M3
E1
N1
V1
V2
1E−5
1E−4
1E−3
1E−2
1E−1
^{4}He content ($cm^3STPcm^{-3}H_2O$)

Figure 5.3 strongly suggests that a diffusion constant appropriate for water gives the best fit to the measured helium values. This should be the case if the waters are in helium equilibrium with the rock. Since the waters are in equilibrium with the rock it is not possible to use helium contents to estimate their residence times. Figure 5.3 shows there is some departure of the helium contents from the expected profile. Some waters, particularly those above 400 metres have much lower helium contents than expected. This may be due to flushing by air equilibrated water.

The presence of higher flow rates in the shallow boreholes suggests the greater groundwater movement has flushed helium from the granite. This circulation has been particularly active since mining began 400 years ago which suggests the water transit time in the fractures is short. This is consistent with the high ^{3}H contents of these shallower waters (Moser et al, 1987).

Since uranium is concentrated in the microfractures (Belson et al, 1969) it is not unreasonable that helium loss from rock is due to diffusion along the water filled fracture system.

Figure 5.4 shows the effect of helium generation time on the helium-depth profiles in the Stripa granite. This suggests that helium has been accumulating in the granite since it was formed 1690 million years ago. Lower helium generation ages do not fit the data well, particularly the deeper water.

5.5 $^{3}He/^{4}He$ ratio

Measured $^{3}He/^{4}He$ ratios are given in Table 5.3 and are very low at 5.7×10^{-9} for the deeper groundwaters. This suggests there is very little atmospheric derived helium with a ratio of 1.41×10^{-6}. If the $^{3}He/^{4}He$ ratio has been derived purely from production within the granite then this ratio should be found for the calculation in Section 1.14. Using a value for the lithium content of 11 ppm and values for other elements as for an average granite, with the radioelement content of the Stripa granite gives a ratio close to the observed ratio.

5.6 $^{40}Ar/^{36}Ar$ ratios

The measured $^{40}Ar/^{36}Ar$ ratios for the Stripa groundwaters are shown in Table 5.4. The waters from borehole E1 contain atmospheric ratio for argon of 295.5. The other shallow boreholes N1 and M3 contain slightly enhanced ratios equivalent to an added radiogenic argon-40 content of $2 \times 10^{-5} cm^{3} STP cm^{-3} H_2O$. The deeper waters of V1 and V2 contain ratios which indicate an addition of up to 25% radiogenic argon. Diffusive loss from minerals of ^{40}Ar is negligible up to 200°C (Dalrymple and Lanphere, 1969). A mineral containing 5% potassium and 650 Ma old will contain radiogenic argon of $4 \times 10^{-4} cm^{3}/cm^{3}$ rock. This is equal to the air saturated argon content of water at 10°C. The much older Stripa granite will contain argon of around $7.9 \times 10^{-4} cm^{3}/cm^{3}$ but this will not diffuse into

Table 5.3 $^{3}He/^{4}He$ ratios of dissolved helium i Stripa groundwaters.

Date	b/h	Interval, m	Depth below ground, m	$^{3}He/^{4}He$ x 10^{-9}
810715	V1	409-506	819-916	5.58 +/- 0.5
810715	V1	409-506	819-916	5.29 +/- 0.5
810715	V1	409-506	819-916	6.28 +/- 0.6
			average	5.72 +/- 0.4

Table 5.4 $^{40}Ar/^{36}Ar$ ratios for dissolved argon in the Stripa groundwaters.

Date	b/h	Interval, m	Depth below ground, m	$^{40}Ar/^{36}Ar$	+/-
831109	M3	0- 14	336- 350	301.6	4.4
840223	M3	0- 14	336- 350	316.3	0.5
850220	M3	0- 14	336- 350	309.6	1.1
840306	E1	3-300	357- 385	294.3	0.5
850220	E1	3-300	357- 385	307.2	2.6
840307	N1	252-300	397- 401	305.2	3.7
840313	N1	151-251	379- 394	304.1	3.9
831105	V1	100-505	457- 862	342.6	1.7
840111	V1	100-505	457- 862	371.5	3.4
840111	V1	100-505	457- 862	353.1	3.1
840208	V1	100-505	457- 862	368.1	2.8
850220	V1	100-505	457- 862	354.5	2.6
821124	V2	-	-	346.8	1.6
830119	V2	-	-	341.0	1.8
840228	V2	500-561	910- 971	336.2	1.8
850225	V2/1	559-822	969-1232	376.9	3.0
850225	V2/2	550-558	960- 968	350.8	1.0
850219	V2/3	490-498	900- 908	344.0	2.0
850220	V2/4	402-410	812- 820	326.2	0.6
850220	V2/5	384-397	799- 807	325.2	1.9

Figure 5.5 $^{40}Ar/^{36}Ar$ ratio against chloride content for Stripa waters

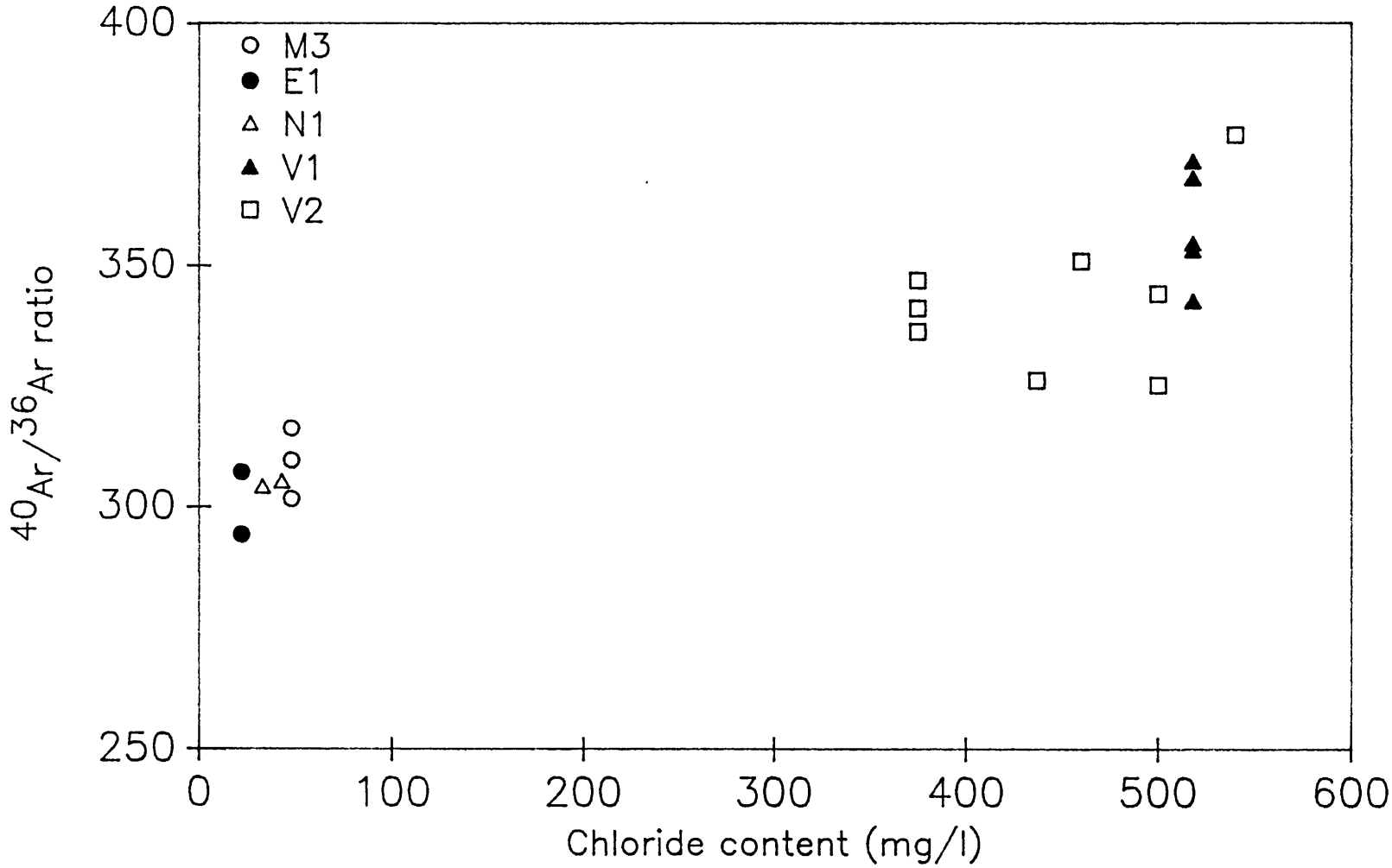

the fracture fluids at the temperatures which exist in the Stripa granite. Mineral alteration would release argon into the groundwater and should be proportional to the water salinity. Figure 5.5 shows argon isotopic ratios against chlorinity for the Stripa groundwaters. This shows a relationship between argon ratio and the chemical alteration of the granite. This suggests V1 and V2 waters have been in contact with the granite for longer than the shallow waters.

5.7 Recharge Temperatures

The inert gas contents of the Stripa groundwater are reported in Table 5.2. Only the most recent samples are included as these represent samples collected under pressure. The small flow rates for the Stripa boreholes mean that a borehole open at the surface will degas prior to sample collection (Chapter 6). Samples must then be collected under pressure, and also the well must have been pressurized and flushed under pressure so any zone of degassed water is removed. The apparatus for collecting samples in this manner is shown in Figure 2.6.

Variations between replicates for inert gases analysis of Stripa groundwaters are much greater than normal. These variations are attributed to the difficulty of obtaining samples for which the boreholes had been adequately pressurised beforehand. All of the samples have Ne contents which indicate the presence of

considerable amounts of excess air. This may be due to entrainment of air with the groundwater during recharge or by degassing in the borehole and consequent incorporation of released gases in the sample. For the estimation of recharge temperatures, the measured Ar contents were first corrected for the presence of radiogenic ^{40}Ar as indicated by the Ar isotopic ratio for the particular borehole. Excess air corrections were made in the usual way by subtracting aliquots of air until the best match was obtained between the recharge temperatures of Ne, Ar, Kr and Xe. The results of excess air corrections are shown in Table 5.2. Normally the match between Ne and Ar temperatures is the best recharge temperature indicator, but in all cases the Ar contents, even after correction for radiogenic ^{40}Ar indicate negative recharge temperatures. This suggests that the excess gases present might be exsolved gas or at least partly exsolved gas. Table 5.5 shows a representative gas analysis for Stripa corrected for excess gas. The proportions of the excess gas vary from purely exsolved gas to air. The exsolved gas partial pressures were calculated using the OUTGAS program as described in Chapter 6. This table shows that when the excess gas is treated as exsolved gas the argon concentration is very much reduced. This produces an average recharge temperature of 1.4° using all four palaeotemperature indicators, assuming the gas is air gives a recharge temperature of -0.1°. However it should be noted that the large errors on each of these tempera-

Table 5.5

Stripa groundwater V1 inert gas contents corrected for excess air or exolved gas

% of excess gas of air composition	Inert gas contents of water cm^3/cm^3 after correction					
	He $x10^6$	Ne $x10^7$	Ar $x10^4$	Kr $x10^8$	Xe $x10^8$	RT
100	1220	2.26	5.67	12.40	1.80	-0.1
88	1208	2.29	5.35	12.41	1.80	0.2
75	1147	2.29	5.33	12.38	1.79	0.3
63	1084	2.28	5.32	12.35	1.78	0.4
50	1008	2.28	5.30	12.32	1.77	0.5
37	918	2.27	5.27	12.27	1.76	0.7
25	825	2.28	5.26	12.25	1.74	0.7
12	698	2.26	5.22	12.17	1.72	1.1
0	554	2.25	5.18	12.11	1.70	1.4

RT is the average recharge temperature indicated by the corrected inert gas contents.

A small amount of exolved gas considerably improves the agreement between temperatures (in particular Ar) Beyond 12 % exolved gas there is no improvement in the agreement between temperatures as indicated by individual inert gases.

tures of 2°C does not favour one estimate over the other. If the extra gas is exsolved gases from the groundwater then the original helium content of the water is very much reduced (Table 5.5).

Another possible explanation for the observed Stripa groundwater inert gases producing a characteristic pattern of inert gas contents, is the sampled waters are partially degassed prior to collection. The computer program OUTGAS has been used to explore the possibility. The parameters needed for input to OUTGAS are salinity, pH, bicarbonate content, argon ratio, helium content, hydrocarbon content, degassing pressure, and the contamination index and recharge temperaure of the original water. Of these all but the last three are measured on the sampled waters. An original recharge temperature of 0°C was chosen on the basis of stable isotope analysis. The contamination index would need to be above the observed range of 1.8-2.0 to produce degassed waters with the same contents as measured. Finally the degassing pressure might vary from 1 atm to a pressure at which degassing will no longer occur under particular conditions. For these waters the pressure at which degassing is prevented will depend on the waters contamination index. A groundwater recharged at 0°C will not degas above 2.0 atm for a contamination index of 3.0, and one with a contamination index of 2.5 will not degas above 1.7 atm.

Various patterns of inert gas contents have been produced for degassed waters, these are represented in

Figures 5.6 to 5.8. Figure 5.6 shows a typical deep inert gas analysis compared with two waters degassed at 1 atm, both with initially high contamination indices. Both degassed samples have inert gas contents very much too low to be Stripa groundwaters.

Figure 5.7 shows a higher contamination index water degassed at pressures up to the maximum possible under the prevailing conditions. None of these waters of moderately high contamination index produces a satisfactory explanation for the Stripa waters. All have a Ne content which is too low compared with the Ar content. Figure 5.8 shows degassing of water with a higher contamination index. Clearly water degassed at 1 atm contains too little inert gas, but degassing at a pressure above this produces a pattern similar to the measured contents. A degassing pressure of around 1.5 atm gives the best fit.

Degassing of a high contamination index water of 3 would appear unlikely as waters with such high air contamination are very unusual and would require unique recharge conditions. It should also be noted that Stripa waters were collected at pressures of 3.7-5.5 bars. These pressures should ensure no degassing occurs except when large quantities of hydrocarbons are present in the waters. Possibly the boreholes were not flushed for sufficient time to exclude water degassed in the borehole prior to collection.

Another cause of lower precision for Stripa waters inert gas analysis is the large ^{4}He contents. These make

Figure 5.6 Inert gas pattern for Stripa groundwaters

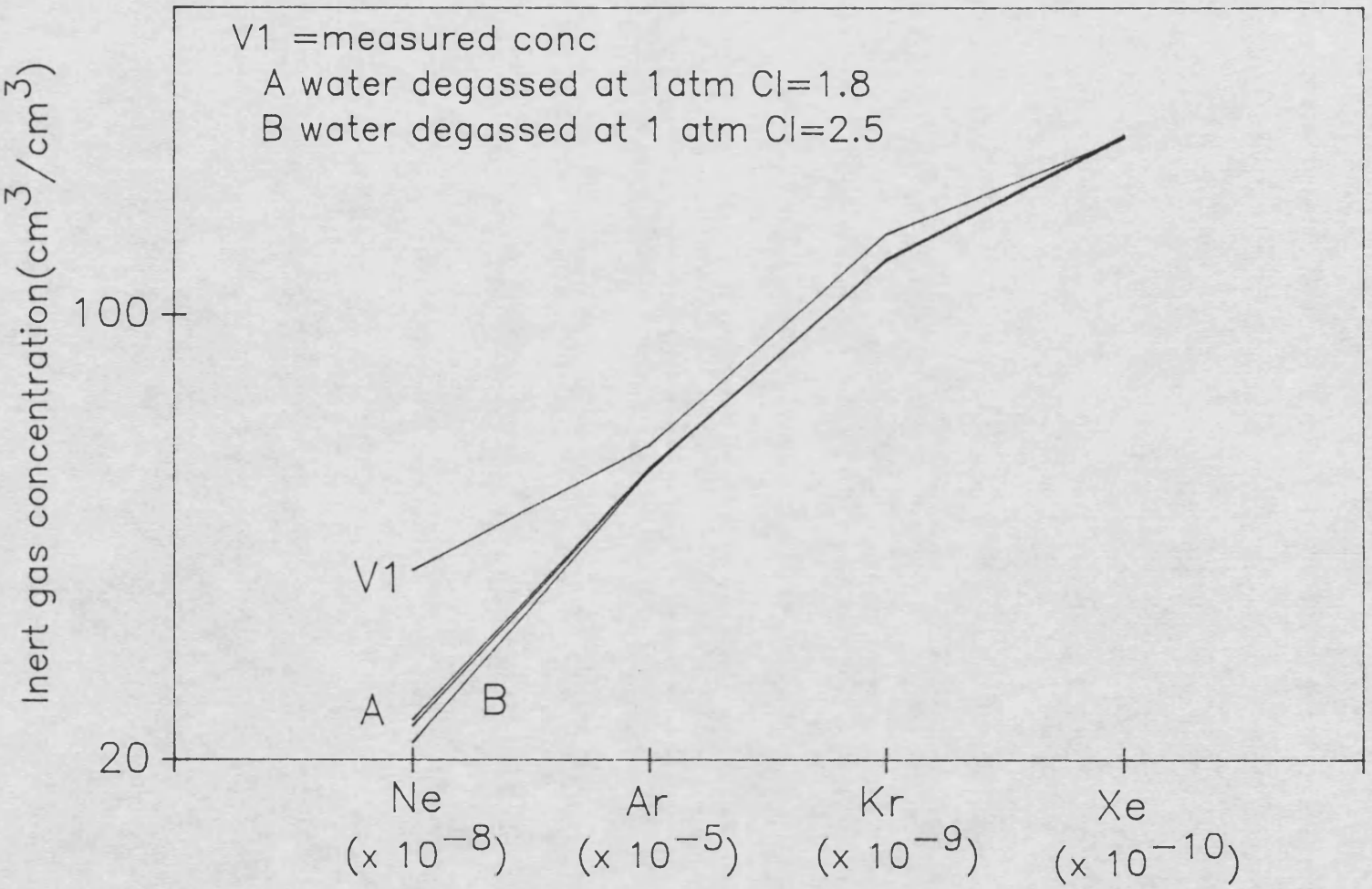

Figure 5.7

Inert gas pattern for Stripa groundwaters

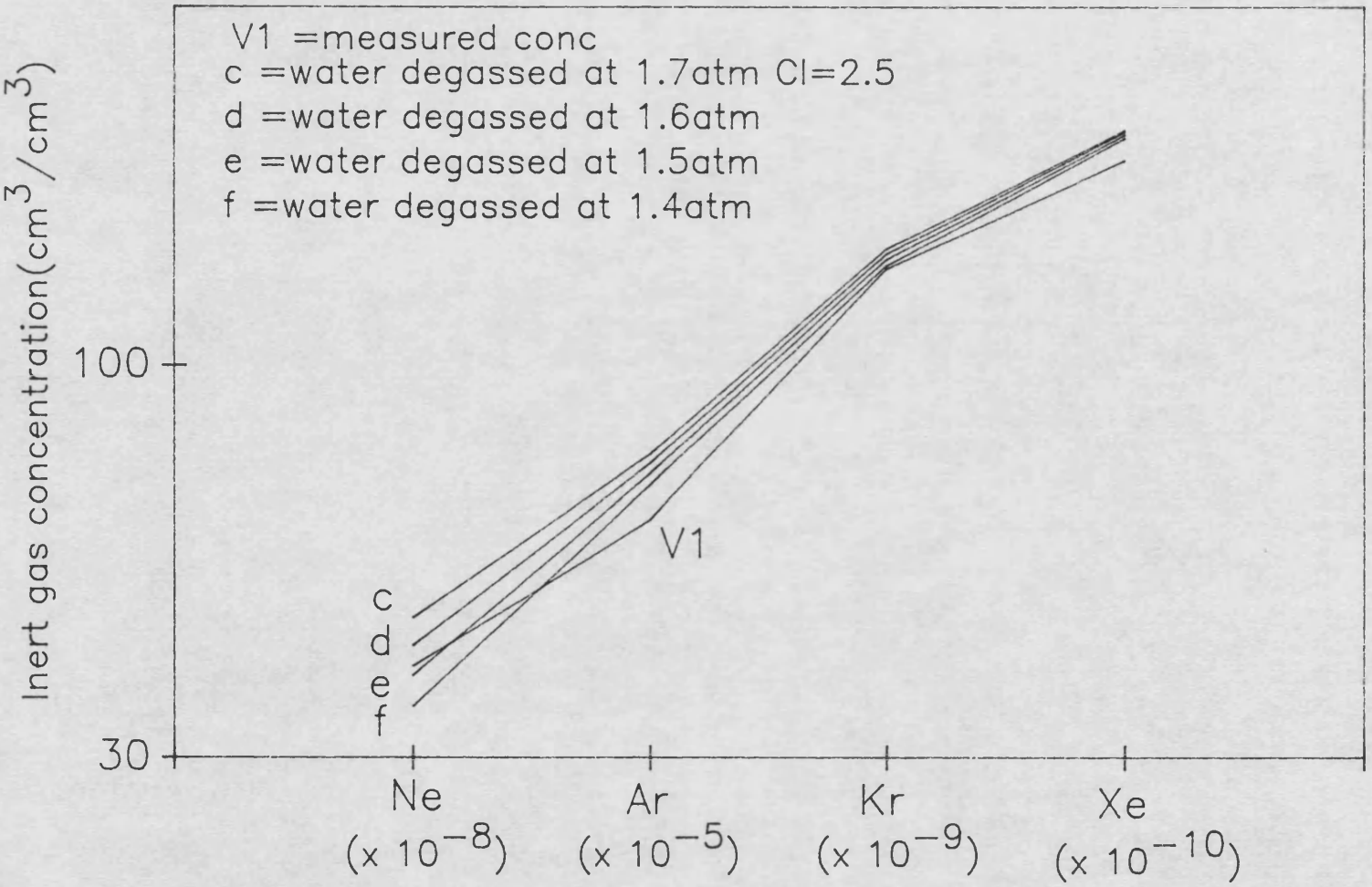

Figure 5.8 Inert gas pattern for Stripa groundwaters

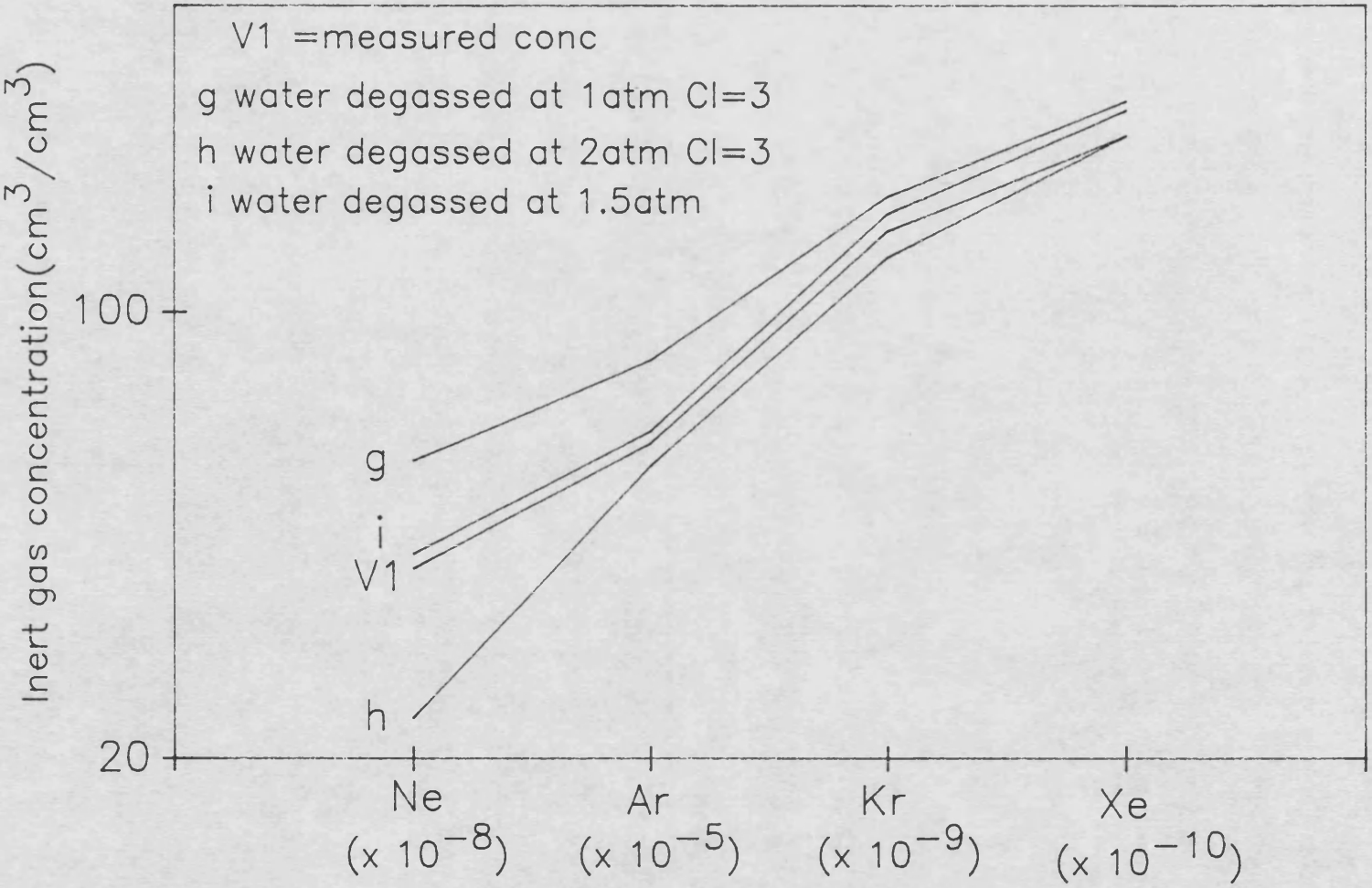

Ne analysis much more difficult with small errors in concentration being very important in the calculation of inert gas recharge temperatures.

Assuming degassing does not affect the recharge temperatures then the boreholes V1, V2 and M3 have indistinguishable recharge temperatures of 2.6 ± 1.5°C. Samples from boreholes N1 and E1 have somewhat higher temperatures of 3.6 ± 1.5 and 4.0 ± 1.1°C respectively.

5.8 Stable Isotope Content

The recharge temperatures collected after 1985 are plotted against the isotopic composition of water $\delta^{18}O$ in Figure 5.9. The $\delta^{2}H$ against $\delta^{18}O$ is plotted in Figure 5.10 for some waters. The shallow waters lie to the right of the global meteoric line, this shift indicates surface evaporation. The deeper groundwaters are depleted in heavy isotopes compared to the shallow groundwaters. The $\delta^{18}O$ and $\delta^{2}H$ contents place them on the world meteoric line so they have maintained their stable isotope composition since recharge. The deeper boreholes have a $\delta^{18}O$ depletion of 2.5°/₀₀ which would indicate this water recharged during post glacial cold periods (> 12ka) or during interstadials (> 25ka). This compares well with the depletion in Molasse sedimentary basin waters stable isotopes. On basis of stable isotope analysis the Stripa minewaters are at least 10ka old.

The relationship between oxygen isotope composition

Figure 5.9

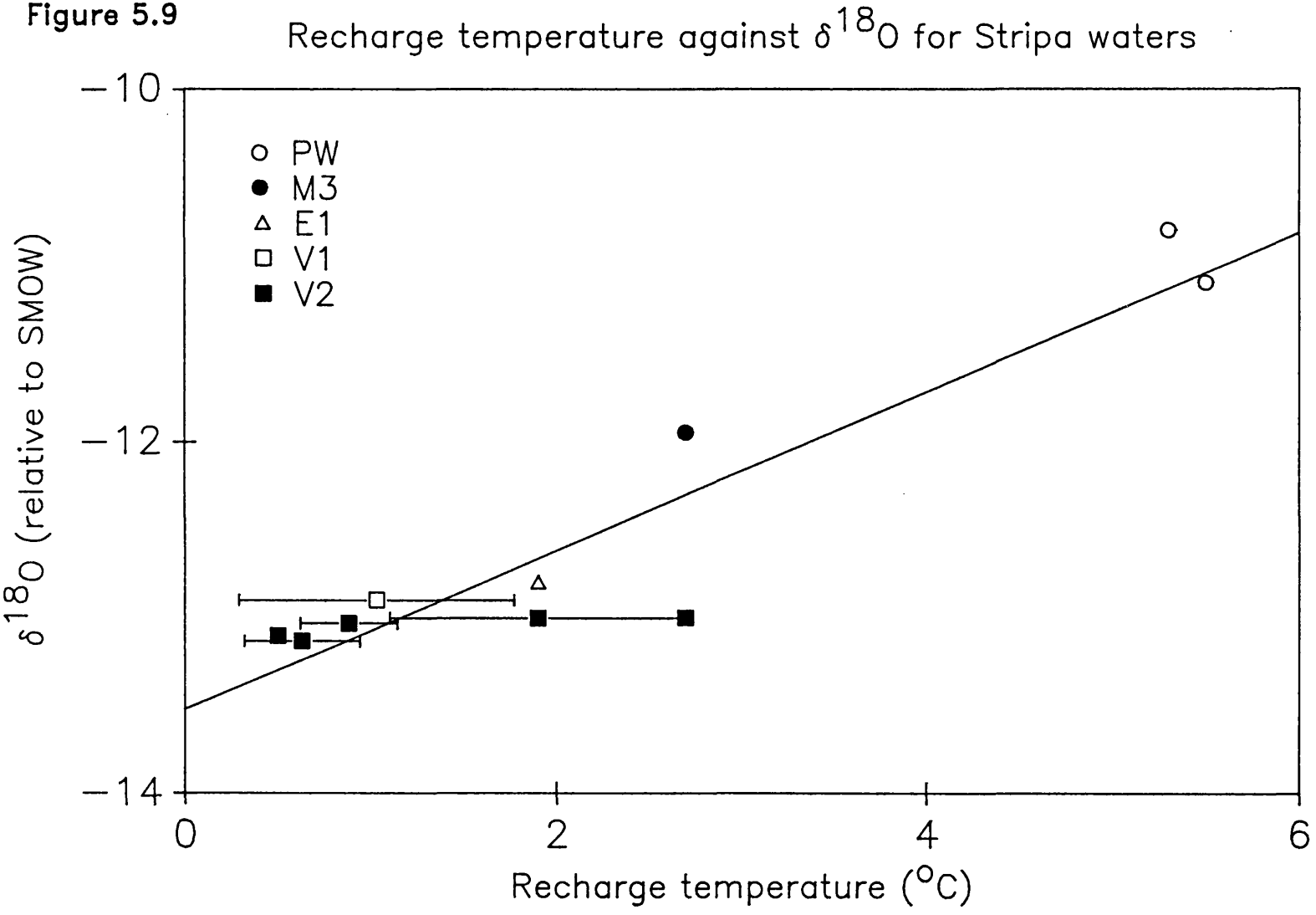
Recharge temperature against $\delta^{18}O$ for Stripa waters
−10
−12
−14
PW
M3
E1
V1
V2
$\delta^{18}O$ (relative to SMOW)
0
2
4
6
Recharge temperature (°C)

Figure 5.10 $\delta^{18}O$ against $\delta^{2}H$ for Stripa waters

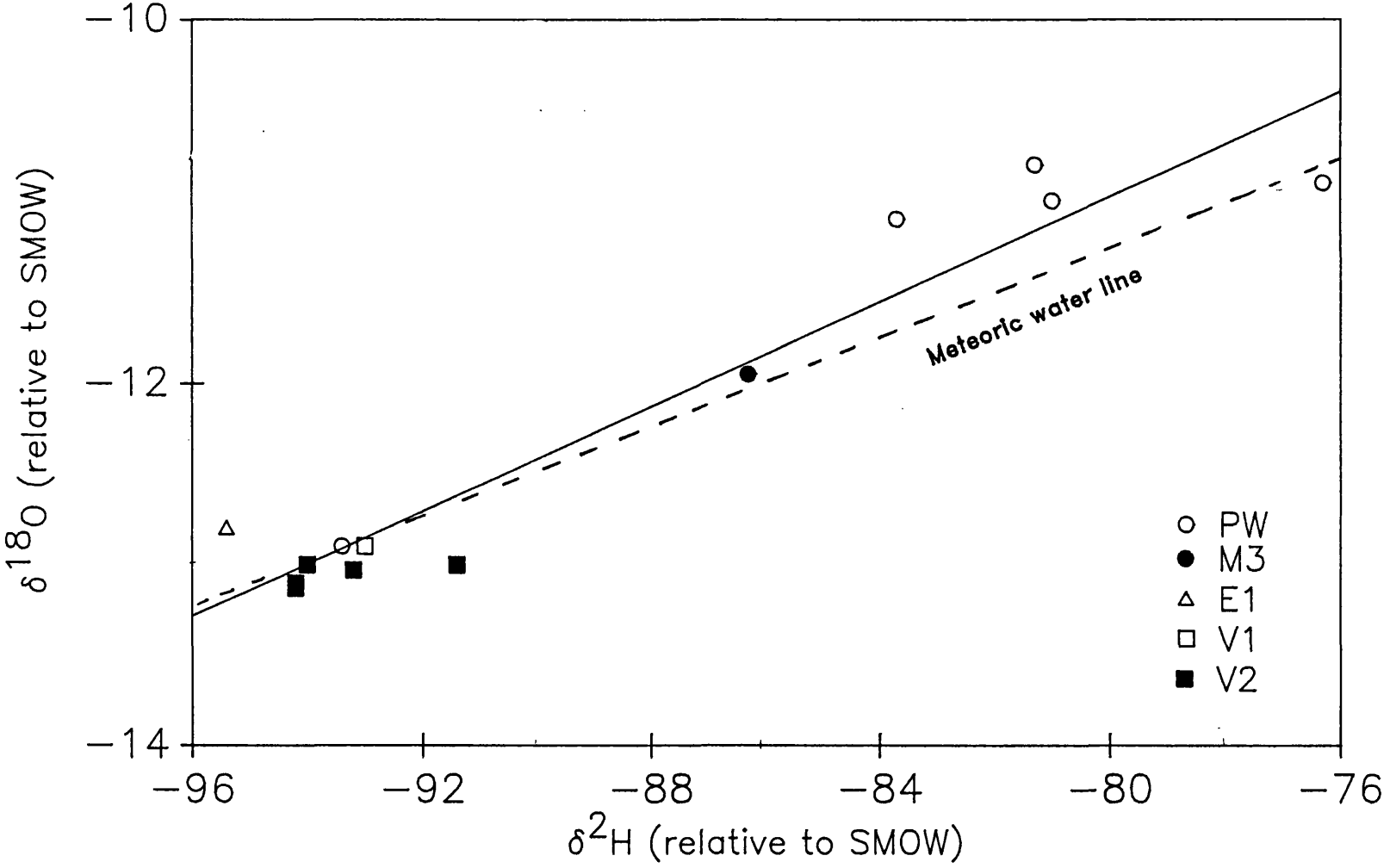

and recharge temperature (°C) may be expressed by the equation (Figure 5.9):

$$\delta^{18}O = 0.33T - 13.2$$

which may be compared with Dansgaards (1964) relationship for mean annual temperature:

$$\delta^{18}O = 0.695T - 13.6$$

where T is the temperature in °C.

5.9 N_2/Ar Ratios

The N_2/Ar ratio for dissolved gases in a groundwater equilibrated with air is 37.7 at 10°C and 37.3 at 5°C. The N_2/Ar ratio for all of the minewaters is greater than expected for air equilibration and indicates the presence of excess air dissolved in them. The ratio of total dissolved Ne to the volume of Ne due to air equilibration has been used as a contamination index. This index was evaluated for samples analysed for inert gas contents. The value of the contamination index required to produce the observed N_2/Ar ratio is compared with the observed values for inert gas analysis in Table 5.2. The high N_2/Ar values suggest samples contain exsolved gas. Degassing of a groundwater results in a gas phase of high N_2/Ar ratio (Chapter 6). There are no very large N_2/Ar ratios greater than 60 such as would suggest the presence of deep crustal nitrogen or large amounts of nitrogen produced by thermodegradation of organic substances.

5.10 Radioelement Content of the Stripa Granite

The uranium, thorium and potassium contents of core samples from boreholes E1, N1, V1 and V2 have been determined by gamma ray spectrometry. The U contents of samples from V1 averaged $44.6^{+}/_{-}$ 10.4 μg/g and from V2 averaged $43.6^{+}/_{-}$ 2.7 μg/g. Uranium in the granite is concentrated as uranite within open microfractures in feldspars (Nelson et al, 1979) and is therefore readily accessible to aqueous leaching. Table 5.6 shows the U content of the granite is uniform throughout the unweathered part of the intrusion and is about 15 times the average for granites.

The thorium content averages 50.4 ± 4.5 μg/g (V1) and 56.6 μg/g (V2) and the Th/U ratio is 1.2-1.29. The thorium content is greater than the world average for granites but the Th/U is less than the world average of 2.8. The high radioelement contents are reflected in the high U and Ra found in the Stripa minewaters.

5.11 Uranium Series Equilibria

The isotopes ^{238}U, ^{234}U and ^{230}Th are related being members of the 4n+2 decay series (Appendix A). Radioactive equilibrium throughout this series would be established within 1.25 Ma as required by the half lives in sequence. The equilibria $^{234}U/^{238}U$, $^{230}Th/^{238}U$ and $^{230}Th/^{234}U$ may therefore be used to determine whether closed system conditions for U and Th have persisted

Table 5.6 Gamma-spectrometric determinations of the U, Th and K contents of the Stripa granite.

B/h	Depth m	U-content ppm (+/- 0.3)	Th-content ppm (+/- 0.5)	Th/U	K-content % (+/- 0.05)
N1	22.53- 22.60	42.2	29.0	0.69	4.1
N1	282.03-282.11	20.2	23.6	1.17	3.0
E1	22.37- 22.43	26.7	28.4	1.06	4.3
E1	286.41-286.47	43.4	29.2	0.67	4.2
V1	25.51- 25.59	37.0	34.3	0.91	3.9
V1	75.45- 75.52	34.2	32.0	0.86	4.2
V1	128.44-128.54	39.1	26.2	0.67	3.8
V1	186.34-186.41	38.8	27.4	0.71	4.1
V1	228.75-228.82	42.9	27.5	0.64	4.0
V1	282.47-282.53	48.8	31.0	0.64	4.1
V1	330.41-330.49	48.0	31.5	0.66	4.2
V1	385.46-385.54	35.4	30.2	0.85	4.2
V1	432.29-432.38	42.8	28.6	0.67	3.9
V1	498.16-498.25	39.7	26.8	0.68	4.3
V1	Excavation	39.2	26.0	0.66	4.1
	Average (V1)	41.3	29.2	0.76	4.1
V2	0.97- 1.06	42.5	31.8	0.75	4.1
V2	55.22- 55.31	44.0	32.4	0.74	4.3
V2	106.03-106.13	36.1	24.1	0.67	3.7
V2	147.08-147.19	38.8	26.2	0.68	3.9
V2	196.04-196.15	40.2	32.2	0.80	4.3
V2	249.68-249.78	42.3	33.0	0.78	4.4
V2	303.10-303.20	42.3	33.2	0.78	4.3
V2	348.52-348.61	42.6	34.4	0.81	4.3
V2	400.54-400.64	43.0	34.7	0.81	4.2
V2	448.79-448.90	43.1	32.8	0.76	4.6
V2	503.84-503.95	45.1	33.2	0.74	4.3
V2	548.78-548.86	41.9	30.7	0.73	4.2
V2	599.21-599.30	42.5	30.3	0.71	4.1
V2	645.11-645.19	44.8	33.1	0.74	3.9
V2	701.54-701.66	46.5	33.7	0.72	4.3
V2	750.93-751.03	47.9	35.3	0.74	4.3
V2	800.14-800.25	47.5	37.4	0.79	4.4
V2	817.44-817.53	53.7	40.8	0.76	4.1
	Average (V2)	43.6	32.8	0.75	4.2

Note: The uncertainties quoted are 2σ errors based on counting statistics.

Table 5.7 U and Th contents of the Stripa granites determined by alpha-spectrometry

Sample		U-content ppm +/-	Th-Content ppm +/-	$^{234}U/^{238}U$ A.R. +/-	$^{230}Th/^{238}U$ A.R. +/-
A	(i)	19.1 0.8	24.4 0.9	0.74 0.05	1.15 0.04
	(ii)	18.5 0.6	27.2 1.9	0.75 0.04	1.27 0.07
B	(i)	24.2 0.7	12.0 0.6	0.98 0.04	0.78 0.03
	(ii)	26.1 0.8	15.0 0.7	1.00 0.04	0.94 0.04
C	(i)	38.6 0.9	25.8 1.1	1.00 0.03	1.00 0.03
	(ii)	38.2 0.9	24.8 1.2	1.02 0.03	0.91 0.03
D	(i)	36.5 0.8	19.2 1.3	0.99 0.03	0.72 0.03
	(ii)	36.0 0.6	16.1 0.9	0.96 0.03	0.61 0.02
E		39.6 0.3	29.9 0.3	1.01 0.01	0.93 0.05
F		51.7 0.2	35.3 0.3	0.98 0.01	0.88 0.04
G		41.8 0.6	25.1 1.1	1.02 0.01	0.98 0.03

Notes:
A.R.: Activity ratio; A: grey granite from outcrop; B: pink granite from outcrop; C: granite from extensometer drift, 350 m; D: granite from V1 excavation, 350 m; E: V1 core from 110.06 - 111.90 m below ground; F: V2 core from 493.35 - 494.35 m below ground; G: V2 core from 701.54 - 701.66 m below ground.

within the rock over the time scale. These activity ratios are reported in Table 5.7. The granite from the extensometer drift (near borehole M3) is in isotopic equilibrium (all ratios = 1) and has therefore been undisturbed for 1.25 Ma. V1 however is depleted in ^{230}Th, since Th is not mobile in groundwaters this can only be explained as a consequence of uranium deposition.

Typically the granites at Stripa at outcrop (grey granite) have a depleted $^{234}Th/^{234}U$ ratio. This behaviour is expected when uranium is mobilized by groundwaters and when ^{234}U is mobilized preferentially to ^{238}U. The other outcrop granite (pink) is in U/Th equilibrium. Its radioelement content is much less than the deeper granites and the main outcrop granite. The grey granite has a Th content similar to that of the deeper granites. If the uranium content was also similar to the deeper granites the $^{230}Th/^{238}U$ ratio would be about 2, considering the observed $^{230}Th/^{238}U$ the loss must have occurred over a period in excess of 150,000 years. Alternatively if the uranium leaching is a recent occurrence the original U content cannot exceed 24 μg/g. The former would seem to be most likely when considering the uniform radioelement distribution in the granite.

5.12 Dissolved Radioelements of Stripa Granite Groundwaters

Samples were taken from all boreholes as described in Table 5.1. Sampling was carried out at particular depths

using packers. Radioelement contents of the fracture fluids may be modified when entering the packed-off volume. The residence times for samples in the packed off volumes and other sampling details are given in Table 5.9. Appropriate decay or ingrowth corrections were made for the elapsed time since collection in the packer volume. Measurements of ^{238}U, ^{234}U, ^{226}Ra, ^{222}Rn are summarised in Table 5.8.

5.13 Uranium in Stripa Groundwaters

5.13.1 Shallow minewaters

The $^{234}U/^{238}U$ activity ratio of dissolved uranium in the shallow groundwaters from depths of 80m or less in the Stripa granite range from 2.18 to 4.8 and their uranium contents 1 to 90µg/kg (Andrews et al, 1982). These are groundwaters close to the unsaturated zone and their high Eh values indicate uranium solution is taking place under oxidizing conditions. Preferential etch of ^{234}U probably causes the dissolution of ^{234}U. These characteristic activity ratios have been observed for oxidizing groundwaters in a sandstone aquifer and attributed to preferential ^{234}U solution (Andrews and Kay, 1983). Hussain and Lal (1986) have explained these characteristic activity ratios by theoretical means. Alpha recoil of ^{234}Th due to decay of the uranium in the microfractures could also be a significant mechanism for generating the observed $^{234}U/^{238}U$ activity ratios in the shallow ground-

waters. Andrews et al (1982) showed that a microfracture opening of 0.5μm with a U-content of 5000 ppm and a dissolved U content of 10μg/kg would produce U activity ratios greater than 4 within 10 years by continuing recoil of ^{234}Th.

Although preferential solution of ^{234}U can adequately explain the observed activity ratios for the shallow groundwaters and their enhanced activity ratios, there may also be some contribution from recoil effects especially within uraniferous microfractures.

5.13.2 Deep Minewaters

Table 5.8 reports measurements of the U-content and $^{234}U/^{238}U$ activity ratio for dissolved uranium in the Stripa groundwaters. Borehole M3 is very constant with regard to these two parameters. The activity ratio is 10.9 with a standard deviation of only 0.2 This is probably attributed to the constant flow which exists in this borehole so that U solution has not been affected by changes in flow pattern.

V1 and V2 have more variation with regard to U content and $^{238}U/^{234}U$ activity ratio. Some of this variation can be attributed to interaction with the borehole walls (Table 5.9) when water remains in the borehole for long periods. During shut-in periods the waters' activity ratio was higher than during continued flow. This suggests the fracture zone at the base of V1

has undergone alpha-recoil enhancement of its activity ratio.

The deeper groundwaters have low U contents of <1 ppb with activity ratios of 3 to 8. Groundwater ages based on recoil ingrowth following chemical leach of U with an activity ratio of 2.5 in a fracture of 100μm range from 1ka to 30ka (Section 1.10). However uranium geochemistry variability makes such ages very uncertain (Andrews and Kay, 1985).

The U content for V2 shows a general decline with depth. The U content is highest in the shallow groundwaters and declines with depth, whilst activity ratio increases to a maximum for groundwaters from about 350m depth and then declines for deeper waters. This pattern could be due to alpha recoil enhancement of the $^{234}U/^{238}U$ activity ratio for the shallow groundwaters.

The high ^{222}Rn contents of waters from around 350m suggests a zone of U deposition to produce the enhanced activity ratio. This pattern of groundwater movement might be produced by mining activities down to 350m.

The decrease in $^{234}U/^{238}U$ activity ratio in V1 and V2 may also be due to incursion of meteoric water from shallower depth. The decrease in activity ratio could also be due to a flow pattern through the neighbouring leptite, so that the U chemistry is partially determined in the leptite. The first explanation seems more likely as recharge is more likely to occur through outcrop. The

Table 5.8 Uranium series radioelements (mBq/kg) in Stripa groundwaters

Borehole/ date/note	^{238}U	^{234}Th	^{234}U	^{226}Ra	^{222}Rn x 10^6	^{210}Pb	^{210}Po
M3/851113/a	114	-	1270	170	-	6280(120)	-
M3/860114/a	131	ns	1470	180	-	18100(1350)	ns
M3/860410/a	-	-	-	110	40.2	-	-
E1/851113/b	154	-	570	260	-	10430(170)	-
E1/860114/b	54	73(20)	450	290	-	4370(470)	278(78)
E1/860411/b	33	7(3)	270	170	0.7	4250(300)*	167(25)
V1/851113/c	0.7	-	3	5680	-	3100(70)	-
V1/860411/c	8.3	23(5)	18	4720	9.3	1950(230)*	ns
V2/851113/d	0.2	-	1	2700	-	1420(50)	-
V2/860115/d	0.8	27(5)	4	2820	-	1620(120)	33(20)
V2/860410/d	0.3	52(7)	1	2420	102.	1200(85)*	320(15)
V2/851113/e	1.2	-	7	3470	-	8150(200)	-
V2/860115/e	1.3	42(7)	5	3230	-	8430(600)	ns
V2/860410/e	1.2	23(3)	8	1730	20.3	4750(330)*	ns
V2/851113/f	2.3	-	20	2950	-	9920(250)	-
V2/860115/f	2.7	52(8)	22	3270	-	9220(670)	ns
V2/860410/f	2.8	28(3)	23	2230	19.2	4430(320)*	ns
V2/851113/g	0.8	-	4	6500	-	7730(100)	-
V2/860116/g	0.7	55(8)	3	4000	-	6880(520)	ns
V2/860411/g	0.8	18(2)	4	3920	18.2	3900(280)*	ns
V2/851113/h	9.2	-	38	630	-	6830(80)	-
V2/860116/h	7.7	7(5)	32	800	-	7680(570)	ns
V2/860411/h	8.0	13(2)	35	430	16.8	5800(430)*	ns

Note	Borehole, interval	Depth, m	Flushing time, hours
a	M3	0- 14	336- 250	20
b	E1	3-300	357- 385	55
c	V1	103-505	460- 862	140
d	V2-1	559-822	969-1232	1350
e	V2-2	550-558	960- 968	2
f	V2-3	490-498	900- 908	2
g	V2-4	401-410	812- 820	7
h	V2-5	389-397	799- 807	16

^{222}Rn values are corrected for decay in borehole.
*Rn was out-gassed from these samples at the time of collection, to prevent subsequent ^{210}Pb ingrowth.
The 95% probable counting errors are given in parentheses.
ns = not significant after correction.

Figure 5.11

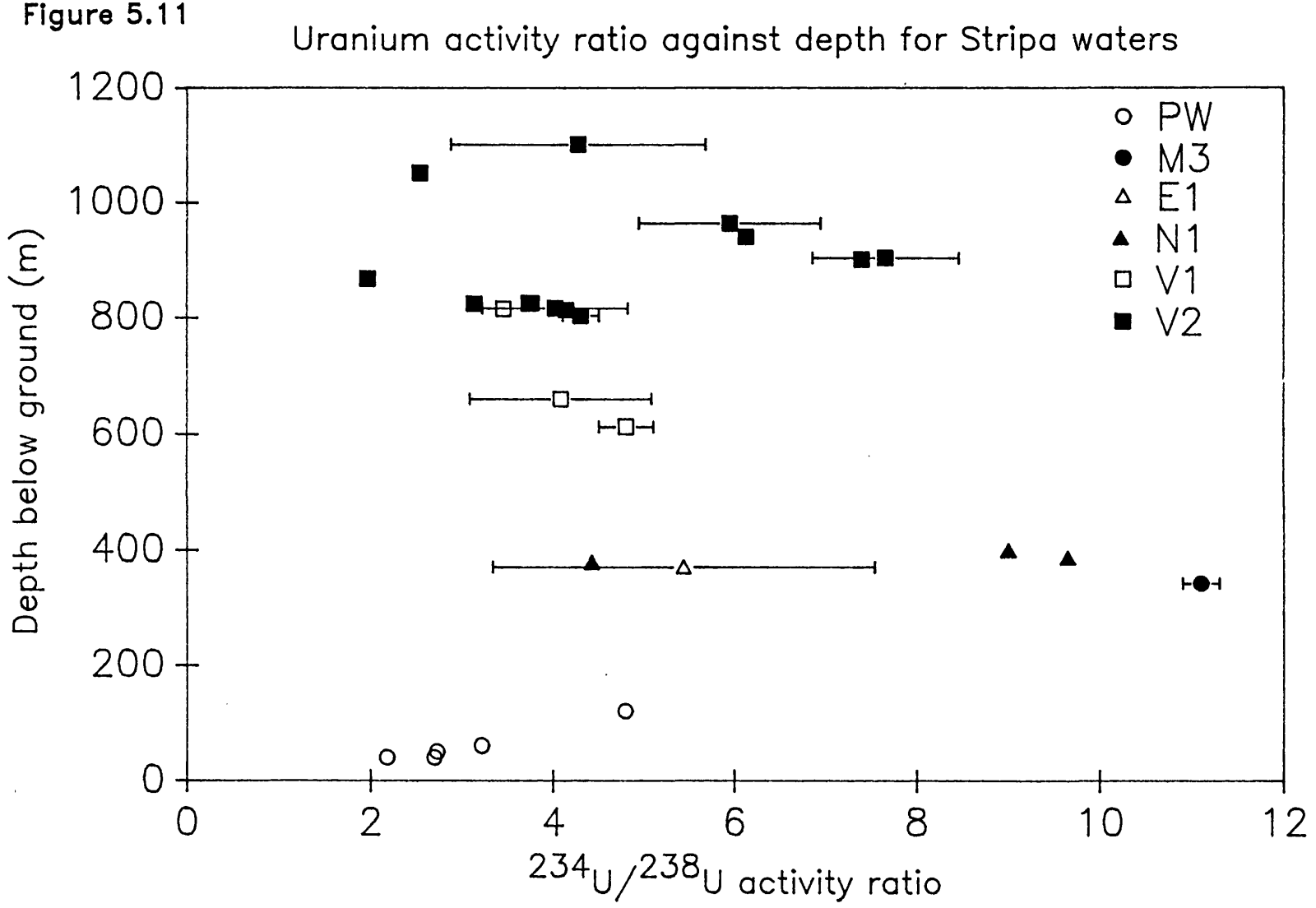
Uranium activity ratio against depth for Stripa waters
Depth below ground (m)
1200
1000
800
600
400
200
0
0
2
4
6
8
10
12
234U/238U activity ratio
PW
M3
E1
N1
V1
V2

change of dissolved uranium activity ratio with depth is displayed in Figure 5.11.

5.14 Thorium in Stripa Groundwaters

The activities of the thorium isotopes ^{232}Th, ^{228}Th and ^{230}Th in all Stripa groundwaters are less than the detection limits of 0.2mBq/kg. The activity of ^{234}Th the immediate decay product of ^{238}U ranges from 7 to 73mBq/kg (Table 5.8). For a recoil production rate of ^{234}Th based on its recoil range and the extent of the water/rock interface, ^{234}Th residence times are less than one day. In the deeper waters from V1 and V2, ^{234}Th is in excess of its parent ^{238}U as recoil solution of ^{234}Th is dominant. Hussain and Krishnaswami (1980) determined residence times of 8 days for ^{234}Th in shallow groundwaters in India.

5.15 ^{222}Rn in Stripa Groundwaters

The ^{222}Rn contents of the Stripa groundwaters are exceptionally high. The waters from shallow boreholes have contents of 5-20 nCi/kg and deeper waters have contents from 200-2,000 nCi/kg. There are marked temporal variations in ^{222}Rn content for some of the deeper waters. For example the determinations between October 1983 and February 1984 for V1 there is a large increase in ^{222}Rn content. This suggests a change in flow regime over this period. The ^{222}Rn content will decrease during shut-in periods because of decay in the borehole. For this reason

Table 5.9 Flow parameters for correction of ^{222}Rn contents (kBq/kg) of fracture fluids in the Stripa granite.

Date	Borehole & interval,m	Isolated volume, litres	section surface area,m^2	Flow rate ml/min	Tube flushing time hours	^{222}Rn Content (a)	(b)
831109	M3 0- 14	64	3.3	75	< 0.1	45.5	50.3
840223	M3 0- 14	64	3.3	75	< 0.1	34.8	38.5
860410	M3 0- 14	64	3.3	52	< 0.1	34.8	40.2
840306	E1 3-300	1347	70.9	400	< 0.1	14.2	20.2
860411	E1 3-300	1347	70.9	408	< 0.1	0.5	0.7
831003	V1 100-505	1837	96.7	> 7000	< 0.1	3.7	3.7
831019	V1 100-505	1837	96.7	> 7000	< 0.1	4.7	4.7
831105	V1 100-505	1837	96.7	> 7000	< 0.1	7.3	7.3
840111	V1 100-505	1837	96.7	> 7000	< 0.1	9.3	9.3
840208	V1 103-505	1824	96.2	> 7000	< 0.1	28.3	28.8
860411	V1 103-505	1824	96.2	215	0.6	4.5	9.3
860410	V2-1 559-822	658	1.4	8	94.6	4.3	102.0
860410	V2-2 550-558	20	1.4	170	4.2	19.3	20.3
860410	V2-3 490-498	20	1.4	190	3.4	18.5	19.2
860410	V2-4 402-410	20	1.4	45	12.2	15.7	18.2
860411	V2-5 389-397	20	1.4	21	25.5	12.3	16.8

Notes:
(a) ^{222}Rn-content on collection (b) Corrected ^{222}Rn-content

samples should be chosen when boreholes have been flowing for long periods.

The ^{222}Rn content of a groundwater is related to the U-content of the rock $[U]_r$ and its porosity by the equation:

$$[Rn] = \frac{F \times 0.7336 \times p \times [U]_r \times 10^3 \ \mu Ci/kg}{\emptyset \times 2.2 \times 10^6}$$

For shallow groundwaters this equation shows less than 1% of the ^{222}Rn generated within the rock matrix is dissolved in the fractures for a porosity of 1%. For deeper water the fraction is much larger and occasionally up to 50%. These high efficiencies of ^{222}Rn release indicate that the U within the rock matrix must be in close contact with the fracture fluids. The highest ^{222}Rn being found in M3 is consistent with the deposition of U in the fracture porosity in the shallower minewaters. As only U is mobilised by groundwater and ^{230}Th decay (half life 80,000 years) requires a long time, the U deposition must have occured long before the mining operations commenced.

5.16 ^{226}Radium in Stripa Groundwaters

The ^{226}Ra contents of the Stripa groundwaters generally increase with depth to 50-100 pCi/kg for V2. The shallow waters have ^{226}Ra contents <1 pCi/kg and the shallow boreholes from 2-12 pCi/kg (Table 5.8).

^{226}Ra solution is strongly influenced by α recoil

following ^{230}Th decay at the rock water interface. The high ^{222}Rn contents show that much ^{226}Ra must also be present at this interface and that it is up to 50% of the equilibrium value with the rock uranium content. ^{226}Ra solution can not proceed to the same extent as ^{222}Rn solution since ^{226}Ra would become depleted in the rock surface and the ^{222}Rn content would become impossible to maintain. The ratio of $^{226}Ra/^{222}Rn$ increases in sequence (Figure 5.12)

$$M3 < N1 < V2 < V1$$

The values range from 3×10^{-6} (M3) to 2×10^{-4} (V1). These low ratios suggest diffusion of radon from the rock is more significant than α recoil solution. In contrast diffusion of radium is a slow process and thus α recoil solution must be more sigificant. Radium solution may also be affected by geochemical factors. The programme WATEQ-II was used to calculate saturation indices for sulphate and carbonate minerals which are important for radium chemistry (Table 5.10). The Stripa waters are undersaturated in terms of sulphate minerals. There is a correlation between ^{226}Ra and Ca^{2+} contents of these waters (figure 5.13) which suggests ^{226}Ra is controlled by Ra/Ca carbonate solid solutions.

If solution of ^{226}Ra is controlled by alpha recoil then the content of the water would approach a limiting factor after 8,000 years when the activity in solution will equal the production rate. The extent of this

Figure 5.12 $^{226}Ra/^{222}Rn$ ratio against depth for Stripa waters

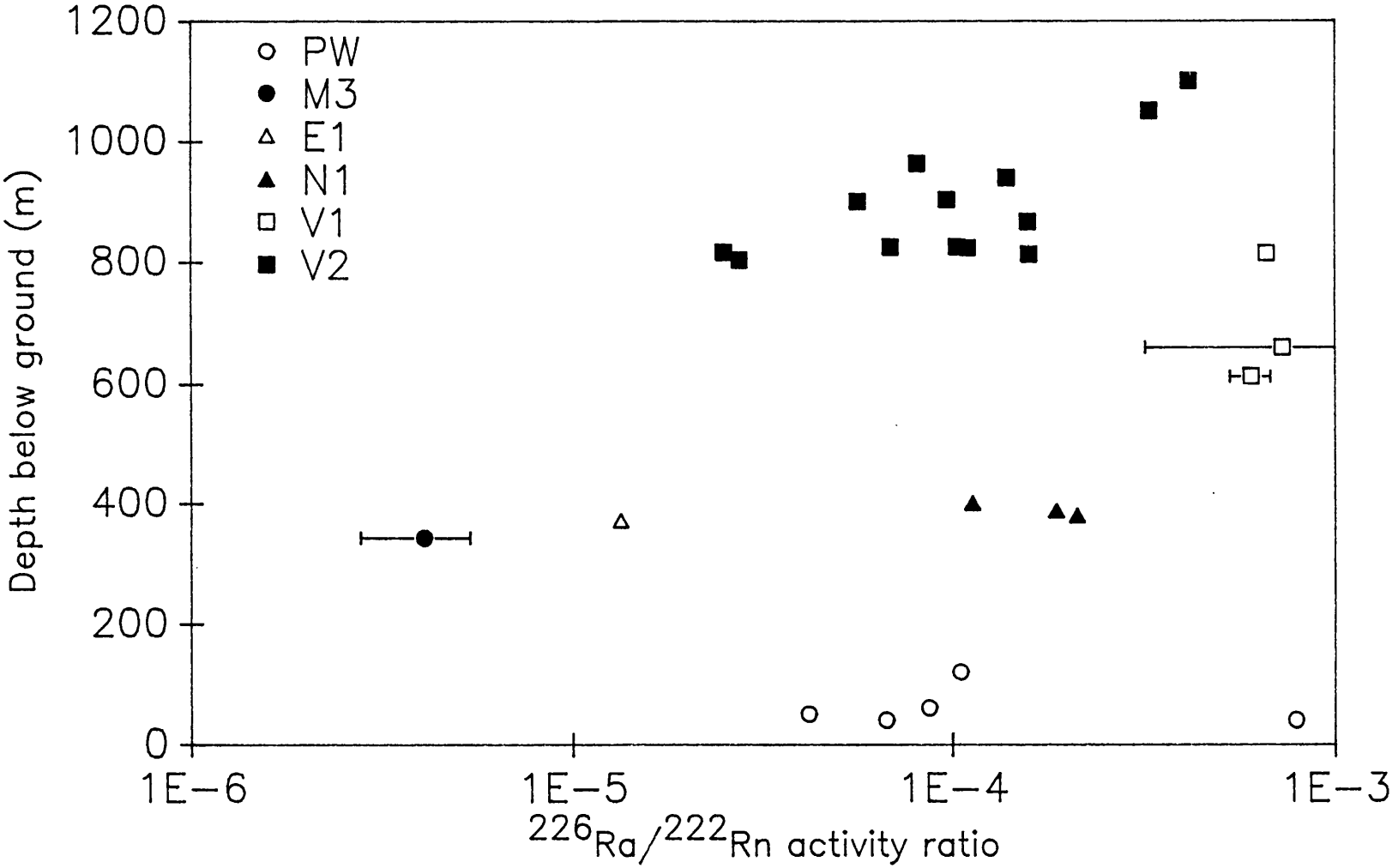

Figure 5.13 ^{226}Ra content against Ca content for Stripa waters

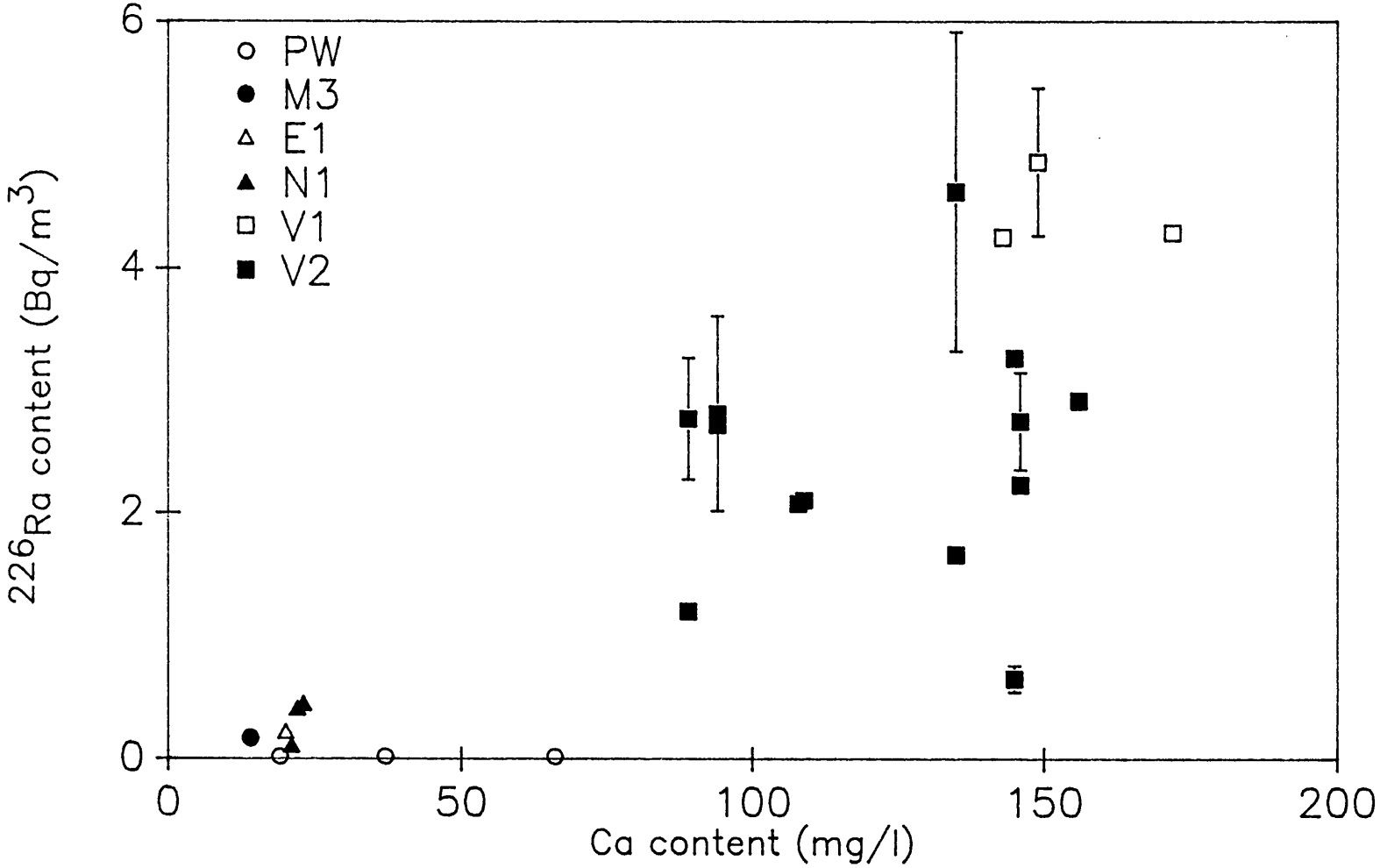

Table 5.10 ^{226}Ra contents and saturation indices for sulphate and carbonate minerals in Stripa groundwaters.

b/h	Depth interval,m	^{226}Ra pCi/kg	^{226}Ra m($.10^{-12}$)	$BaSO_4$ (barite)	$SrSO_4$ (celestite)	$CaSO_4$ (anhydrite)	$CaSO_4.2H_2O$ (gypsum)	$CaCO_3$ (aragonite)	$CaCO_3$ (calcite)
M3	0- 14	1.5	1.1	-	-4.4	-3.48	-3.13	0.0001	0.25
E1	3-300	6.0	2.6	-0.93	-3.99	-3.01	-2.65	0.55	0.79
V1	103-505	138.0	2.0	-0.38	-2.36	-1.51	-1.20	0.008	0.26
V2	412-417	45.0	61.1	-0.38	-2.66	-1.76	-1.38	-0.15	0.09
V2	490-494	32.0	19.9	-0.48	-2.74	-1.92	-1.54	-0.04	0.20
V2	562-822	80.6	14.2	-0.82	-3.0	-1.96	-1.57	0.49	0.74
V2	500-561	87.0	35.7	-0.88	-2.78	-1.89	-1.52	0.88	1.13
V2	424-499	81.0	38.5	-0.95	-2.68	-1.78	-1.40	0.03	0.28
V2	382-423	131.0	35.8	-0.41	-2.71	-1.73	-1.34	0.12	0.36
V2	384-397	18.4	58.0	-	-	-	-	-0.09	0.16

interface is estimated from the ^{222}Rn content and the recoil per unit surface area is given by

$$\text{recoil rate} = 2.87\ p\ [Ur]\ R\ s^{-1}m^{-2}$$

where R is the recoil range (m) of ^{226}Ra. Only for M3 is the groundwater ^{226}Ra content less than the recoil rate. The ^{226}Ra contents are usually up to 80 times the recoil solution rate. This points further to a chemical control on the rate of ^{226}Ra solution. The ^{226}Ra residence time can not be estimated on the basis of recoil solution rate.

5.17 ^{210}Pb in Stripa Waters

^{210}Pb is the longest living daughter of ^{222}Rn. The Stripa groundwaters have very large ^{222}Rn contents which are maintained in equilibrium by ^{222}Rn release from the rock surfaces. The deep waters of Stripa should be old enough to establish $^{222}Rn/^{210}Pb$ equilibrium. However the measured values (Table 5.8) are much less than required for equilibrium suggesting a short residence time for ^{210}Pb residence times. Hussain and Krishnashwami (1982) also have reported short residence times for lead isotopes in groundwaters.

5.18 ^{210}Po in Stripa Waters

^{210}Po levels ranged from 33 to 320mBq/kg (Table 5.8) after correction for ^{210}Pb ingrowth following collection. Usually the ^{210}Pb concentration was not in excess of the contributions from ^{210}Po decay after collection. The

small excess found in borehole E1 corresponds to a residence time of 2 hours for ^{210}Po in the Stripa mine-waters.

CHAPTER 6

GROUNDWATER DEGASSING

6.1 Introduction

Groundwaters dissolve air by air equilibration in the unsaturated zone. In addition excess air is entrained in the groundwater during its downward movement through the unsaturated zone, and enters solution as the hydrostatic pressure increases in the aquifer (Heaton and Vogel, 1981 and Herzberg and Mazor, 1979). Deeply circulating groundwaters may gain additional dissolved gases by geochemical, biogenic and thermogenic processes. Carbonate equilibria leads to a partial pressure of CO_2, nitrate reduction may lead to enhanced N_2 and organic material thermodegradation may lead to N_2 and CH_4 increases. Geothermal heating of the groundwater during its circulation, together with increases in its gas content may cause the groundwater to be oversaturated with gases. Boreholes and wells will permit the exsolution of dissolved gases, as the hydrostatic pressure is reduced.

The composition of exsolved gases and the degassed solution has been modelled so that the initial solution composition can be calculated. The initial solutions can then be used to derive recharge temperatures ^4He ages etc. This technique might be useful when water analyses produce low inert gas contents compared to air equilibration values. This may indicate degassing. Alternatively samples which give poor recharge temperature agreements between various inert gases may contain a proportion of exsolved gas. Both of these possibilities are used to

model the Stripa groundwaters which have been discussed previously.

6.2 Evolution of Dissolved Gases in Groundwaters

The factors which influence the in-situ gas content of a groundwater and hence possible degassing are:

1. The recharge temperature
2. Incorporation of excess air during recharge.
3. Radiogenic He and Ar accumulation
4. Nitrogen production by denitrification and thermo-degradation of organic matter.
5. Methane production by thermodegradation of organic matter.
6. Bicarbonate/carbonate equilibria and production of related partial pressure of carbon dioxide
7. Development of increased salinity during groundwater maturation.
8. Temperature and pressure of groundwater at abstraction.

The important quantity to establish the origin of groundwaters is the gas content while the groundwater is under hydrostatic pressure. It is useful to predict the pressure necessary to maintain gases in solution, and to be able to reconstruct the original contents when degassing has occurred. The computer program OUTGAS has been written for this purpose (Appendix K).

6.3 Calculation of Partial Pressures in Gas Phase

Mass balance of species before and after the degassing requires that:

$$IS\ (I) = VS\ (I) + VG\ (I) \qquad (1)$$

where IS (I) is the initial volume of gas I in solution at the recharge temperature, VS (I) is the volume of I in solution at the degassing pressure and temperature, VG (I) is the volume of gas I in gas phase at degassing temperature and pressure.

The volume of gas I in the gas phase is

$$VG\ (I) = P\ (I) \times GV \times 273 \times DP/(DT \times 760) \qquad (2)$$

where P (I) is the partial pressure of I in gas phase, DP is pressure at which degassing occurs, GV is the total volume of gas phase and DT is the degassing pressure.

The volume of gas I in solution at P (I) and DT is given by:

$$VS\ (I) = P\ (I) \times H\ (I) \qquad (3)$$

where H (I) is the Henrys law constant for temperature DT. Substituting (2) and (3) into (1) we obtain:

$$P\ (I) = IS\ (I) \Big/ \left(\frac{GV \times 273 \times DP}{DT \times 760} + H\ (I) \right)$$

If the volume of gas evolved, GV, can be estimated this equation may be used to calculate the partial pressure of each component. Providing GV has been correctly chosen the sum of the partial pressures will equal the degassing pressure. Any difference between

these two values can then be used to correct GV and the partial pressures recalculated. OUTGAS performs this calculation by iteration until an agreement is reached.

6.4 Estimation of the Initial Gas Volume

The major contributions to the gas phase of a degassed water are nitrogen, water and possibly hydrocarbons. The sum of these partial pressures must approximately equal the outgassing pressure, thus

$$DP = PN + PH_2O + PHC \qquad (1)$$

where PN is partial pressure due to nitrogen, PH_2O is the partial pressure due to water and PHC the partial pressure due to hydrocarbons. If the ratio R, of hydrocarbons to nitrogen is known in the evolved gas then

$$R = PHC/PN \qquad (2)$$

and solving equations (1) and (2) for PN we obtain

$$PN = (P-PH_2O)\ (1+R)$$

If the volume of gas evolved from solution is V_1 then for nitrogen to balance between gas and water phase

$$PN.V_1 = V_i - HN.PN$$

or in terms of V_1

$$V_1 = V_i/PN - HN$$

where V_i is the volume of nitrogen in solution before degassing, HN is the Henrys law constant at the temperature of outgassing.

6.5 Calculation of the True Evolved Gas Volume

If the estimated gas volume and hence its pressure is not equal to the degassing pressure DP, a further correction of the evolved gas volume (GV) is required. The correction used is:

$$GV^1 = GV - (P - PE) \times GV$$

$$= GV (1 - P + PE)$$

This new GV will more closely approach the volume necessary to satisfy the condition

$$DP = \Sigma P (I)$$

If the condition is still not satisfied then the correction formula is reapplied. In practice the out-gassing pressure is equal to the sum of the partial pressures in a few iterations.

6.6 Calculation of Individual Partial Pressures

The partial pressure P(I) for each gas must be calculated to find the total pressure needed in this calculation. The Henrys law constant for each gas can be found using the solubility data of Benson and Krause (1976) and Weiss (1970, 1971). The data of Weiss allows correction for Henrys Law constants for water of high salinity, which will frequently be required for mature groundwaters. However to calculate solubilities the partial pressure of the gas must be known. Fortunately water and carbon dioxide are exceptions to this, because

their partial pressures can be independently calculated. The water pH and bicarbonate content determines the partial pressure of CO_2 using carbonate equilibria. The water vapour partial pressure is calculated using the Theisen equation:

$$\mathrm{Ln}(PH_2O) = 2.303 \times \left[\frac{5.409(t-100)-0.508\times10^{-8}[(365-t)^4-265^4}{t + 273.18} \right]$$

where t is the degassing temperature in °C. This partial pressure of water is one of the major contributions to the gas phase volume (GV). This may then be calculated and another important contribution from nitrogen can also be approximated using:

$$P^1N_2 = \frac{DP - PH_2O}{1 + HN}$$

where P^1N_2 is an approximate value of nitrogen in the gas phase, and HN the ratio of hydrocarbon to nitrogen in the gas phase. A ratio of hydrocarbon to nitrogen of zero will still enable P^1N_2 to be calculated. These three partial pressures PH_2O, PN_2 and PHC can now be added to give an approximate total pressure. This pressure can then be used along with the Henrys law constants for the degassing temperature in question to obtain values for the partial pressures of each of the inert gases and nitrogen, which can be used to calculate the volume in the degassed solution.

Oxygen is not included in this model because it is usually removed from solution, when a groundwater enters

the saturated zone, by oxidation processes. Thus oxygen will not be present when outgassing occurs.

6.7 Using the OUTGAS Programme

A listing of the program OUTGAS is given in Appendix K. A sample OUTGAS output is shown in Figure 6.1. The parameters which are required for input are the recharge temperature and contamination index of the original water, which is used to calculate the initial inert gas and nitrogen contents following recharge. The radiogenic helium and argon contents are also required as these will increase the volume of helium and argon dissolved. The hydrocarbon/nitrogen ratio of the gas phase is input as large hydrocarbon contents introduced by thermodegradation can greatly increase degassing. The bicarbonate and fluid pH are input to calculate a value for the partial pressure of carbon dioxide. Finally the temperature and pressure conditions prevailing during sample collection are necessary.

The effects of varying the input parameters of temperature, salinity, carbonate equilibria, radiogenic He and Ar, biogenic and thermogenic methane and biogenic carbon dioxide were investigated using the OUTGAS programme (Table 6.1).

Figure 6.1 EXSOLUTION OF GASES

Recharge temperature,deg.C	0.0
Degassing temperature, deg.C	10.0
Degassing pressure (atm)	1.0
Excess air cont. index (Ne)	2.0
Radiogenic He (*1E8)	144000.0
Methane / nitrogen ratio	0.0
Bicarbonate content, mg/L	8.5
Fluid pH	9.33
Ar-40/Ar-36 Ratio	354.0
Recharge salinity, g/L	0.00
Groundwater salinity before degassing, g/L	0.97
Groundwater salinity after degassing, g/L	0.97

GAS	GAS PHASE pp (atm)	INITIAL SOLN cm3 STP/cm3	DEGASSED SOLN cm3 STP/cm3	
He	0.06680364907	144011.609	60277.777	* 1E-8
Ne	0.00001926018	4.590	2.176	* 1E-7
Ar	0.01371514797	7.398	5.679	* 1E-4
Kr	0.00000151203	14.096	12.201	* 1E-8
Xe	0.00000012361	2.048	1.893	* 1E-8
N2	0.90680342913	2.830	1.694	* 1E-2
CH4	0.00090680347	0.005	0.004	* 1E-2
CO2	0.00000238141	-0.000	0.000	* 1E-2
Water	0.012			

First gas vol. approximation (cm3)	10.00203
Vol. Gas evolved from 1L water (cm3)	12.99315
Vol. Gas at STP (cm3)	12.53432
Vol. Gas corrected for VP water (STP cm3)	12.38218
Gas conc. prior degassing (STP cm3/L)	30.53264
Gas conc. after degassing (STP cm3/L)	18.15046
Water/gas vol ratio (at degas T and P)	76.96365

Gas Ratios

	N2/AR	HE/NE	KR/XE	CH4/N2
Initial soln.	38.253	%3137.577	6.884	0.002
Degassed soln.	29.819	%2770.415	6.446	0.002
Gas Phase	66.117	%3468.486	12.233	0.001

Recharge salinity, g/L	0
Groundwater salinity before degassing, g/L	.9699999
Groundwater salinity after degassing, g/L	.97

Table 6.1

The effect on dissolved gas content of degassing in the temperature range 0-60°C

Intial solution characteristics

Recharge temperature = 0° C
Degassing pressure = 1 atm
Extra air content = 0
Extra nitrogen content = 0
Methane present = 0
Bicarbonate = 100 mg/l
pH = 8
Radiogenic helium = 0
Radiogenic argon = 0

Neon concentrations in gas and water phase

Degassing temp. °C	Partial pressure in gas phase ($\times 10^{-5}$ atm)	concentration in solution ($\times 10^{-7}$ cc/cc)
10	2.04	2.319
20	1.71	1.802
30	1.52	1.517
40	1.37	1.33
50	1.24	1.18
60	1.09	1.05

Argon concentrations in gas and water phase

Degassing temp. °C	Partial pressure in gas phase ($\times 10^{-2}$ atm)	concentration in solution ($\times 10^{-4}$ cc/cc)
10	1.19	4.98
20	1.32	4.50
30	1.41	4.09
40	1.46	3.72
50	1.46	3.38
60	1.41	3.04

Table 6.1
(cont)

The effect on dissolved gas content of degassing in the temperature range 0-60°C

Krypton concentrations in gas and water phase

Degassing temp. °C	Partial pressure in gas phase ($\times 10^{-6}$ atm)	concentration in solution ($\times 10^{-8}$ cc/cc)
10	1.55	12.62
20	1.60	11.89
30	2.00	11.16
40	2.42	10.43
50	2.57	9.68
60	2.61	8.86

Xenon concentrations in gas and water phase

Degassing temp. °C	Partial pressure in gas phase ($\times 10^{-7}$ atm)	concentration in solution ($\times 10^{-8}$ cc/cc)
10	1.2	1.934
20	1.6	1.868
30	2.0	1.792
40	2.4	1.71
50	2.7	1.61
60	2.9	1.50

Nitrogen concentrations in gas and water phase

Degassing temp. °C	Partial pressure in gas phase (atm)	concentration in solution ($\times 10^{-2}$ cc/cc)
10	0.976	1.835
20	0.963	1.506
30	0.943	1.273
40	0.911	1.090
50	0.862	0.950
60	0.788	0.810

6.8 Factors Affecting Groundwater Outgassing

6.8.1 Temperature and Salinity

Increases in temperature and salinity during groundwater migration can cause supersaturation at atmospheric pressure. As temperature increases the extent of degassing increases. Similarly as salinity increases the extent of degassing will increase. The effect of increasing temperature which increases the extent of degassing is shown for Ne/Ar and Kr/Xe ratios in Figure 6.2 and 6.3. The degassed water had an original inert gas concentration equivalent to air equilibration at 5°C with a small amount of excess air (equivalent to 10% extra neon). The graphs show that the degassed solution changes the Kr/Xe and Ne/Ar ratio with only small amounts of degassing. The loss of inert gas from solution will increase any calculated recharge temperatures. However since the ratio of inert gas changes with degassing in the depleted solution, the presence of degassing is apparent due to a large deviation in the recharge temperatures derived from each inert gas. Recognising the presence of degassed water then allows the gas content of the original groundwater to be reconstructed. Figure 6.4 shows how the N_2/Ar ratio changes in the water phase for increasing degassing. This is important when studying denitrification processes.

Figure 6.2 The Ne/Ar ratio in gas phase and in solution for partial degassing of groundwater at 1 bar

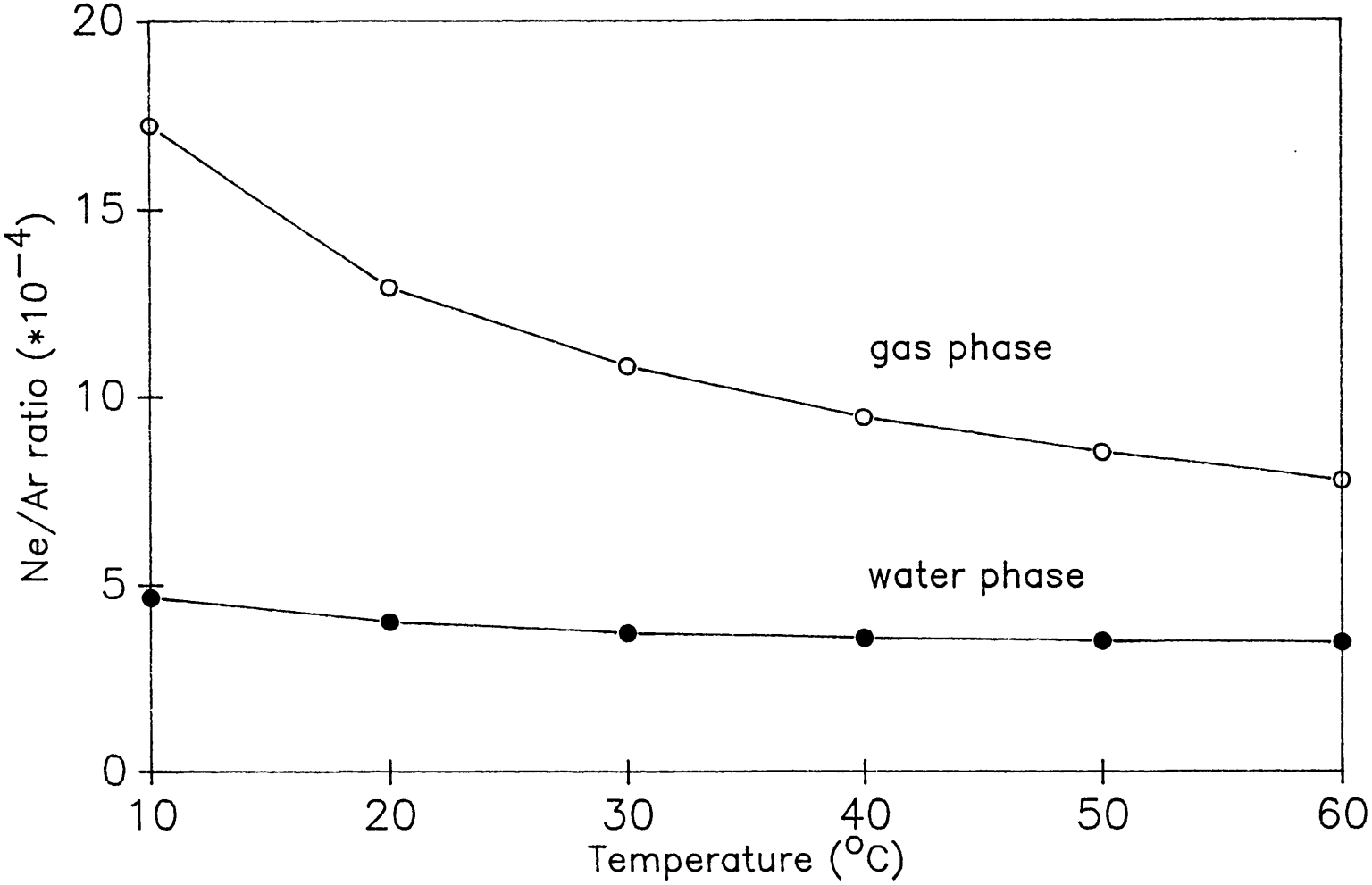

Figure 6.3 The Kr/Xe ratio in gas phase and in solution for partial degassing of groundwater at 1 bar

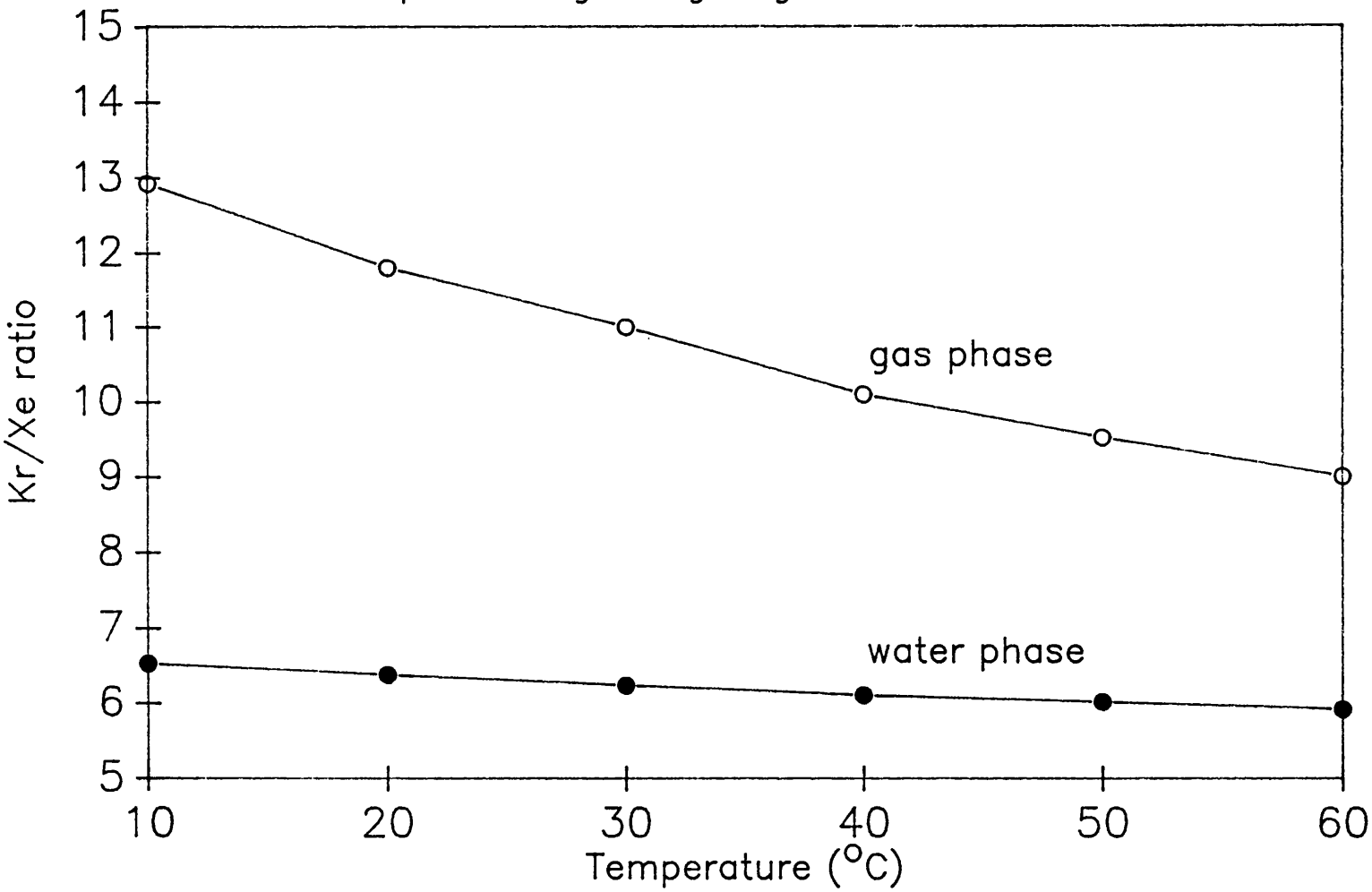

6.8.2 Bicarbonate/Carbonate Equilibria

In solution equilibria exist between carbonate species (Stumm and Morgan, 1970). At low pH CO_2(aq) is the dominant species, so that groundwaters can contain a significant volume of carbon dioxide. This carbon dioxide will increase the pressure necessary to maintain all gases in solution during collection.

6.8.3. Biogenic and Thermogenic Nitrogen

Biogenic nitrogen produced by denitrifying bacterias action on dissolved nitrate can increase the N_2/Ar ratio of a groundwater. The highest ratios caused by anthropogenic input of nitrate can cause N_2/Ar ratios of about 60. Higher ratios can be the result of thermodegradation of organic matter. Figure 6.5 shows the pressure necessary to prevent degassing of waters with enhanced N_2/Ar ratios. The gas contents are for 5°C air equilibration apart from nitrogen.

6.8.4. Thermogenic Methane

Thermodegradation of organic compounds will produce methane as well as nitrogen. Since nitrogen is a minor component relative to carbon in most organic molecules the CH_4/N_2 ratio for thermogenic gas is likely to be large. Figure 6.5 shows the hydrostatic pressure needed to retain gases in solution at 10°C for in-situ N_2/Ar and CH_4/N_2 ratios due to thermogenic production of N_2 and CH_4.

Figure 6.4 N_2/Ar ratio in gas phase and in solution for partial degassing of groundwater at 1 bar

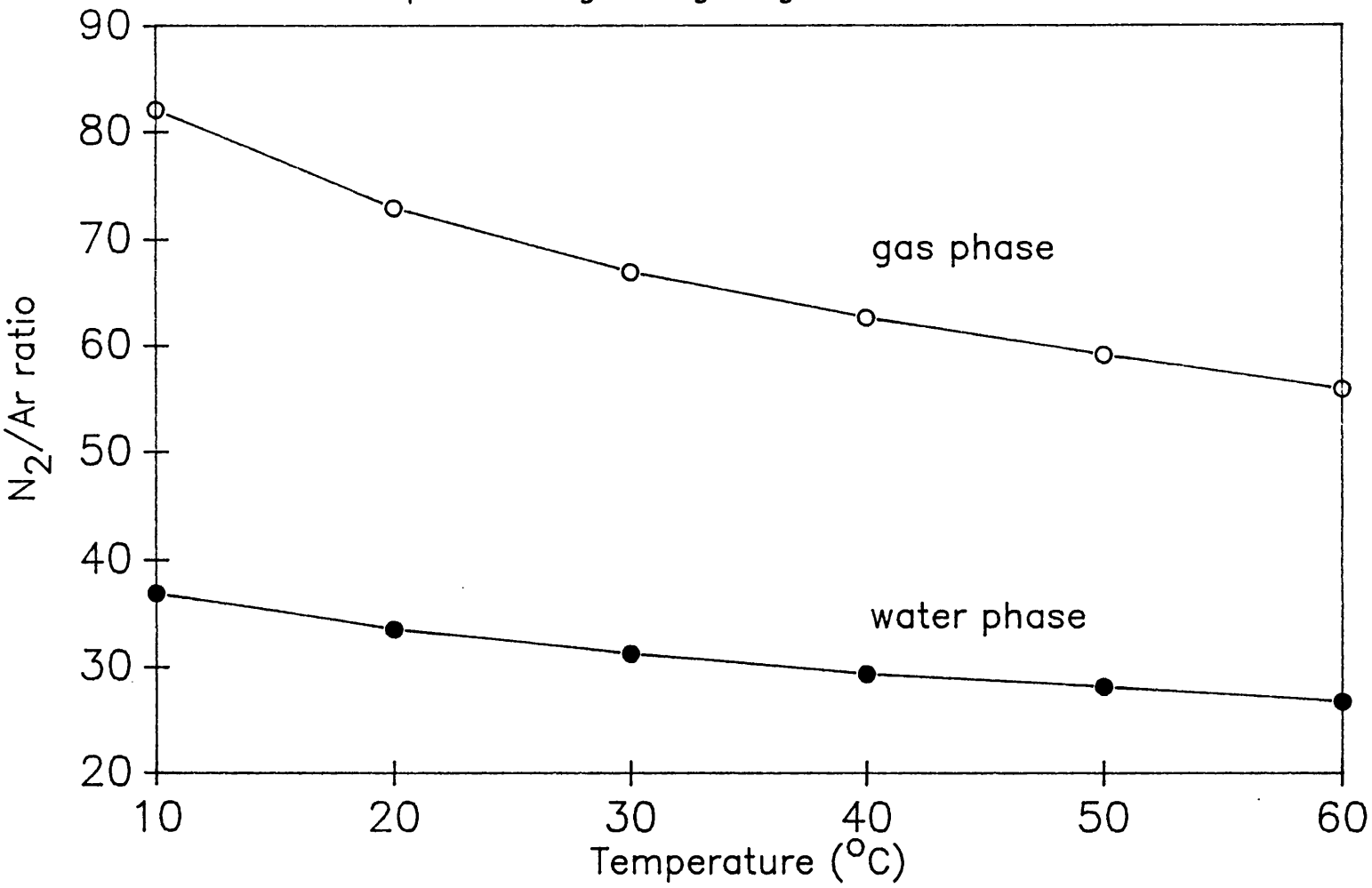

Figure 6.5 Pressure needed to retain gases in solution for in–situ N_2/Ar and CH_4/N_2 ratios

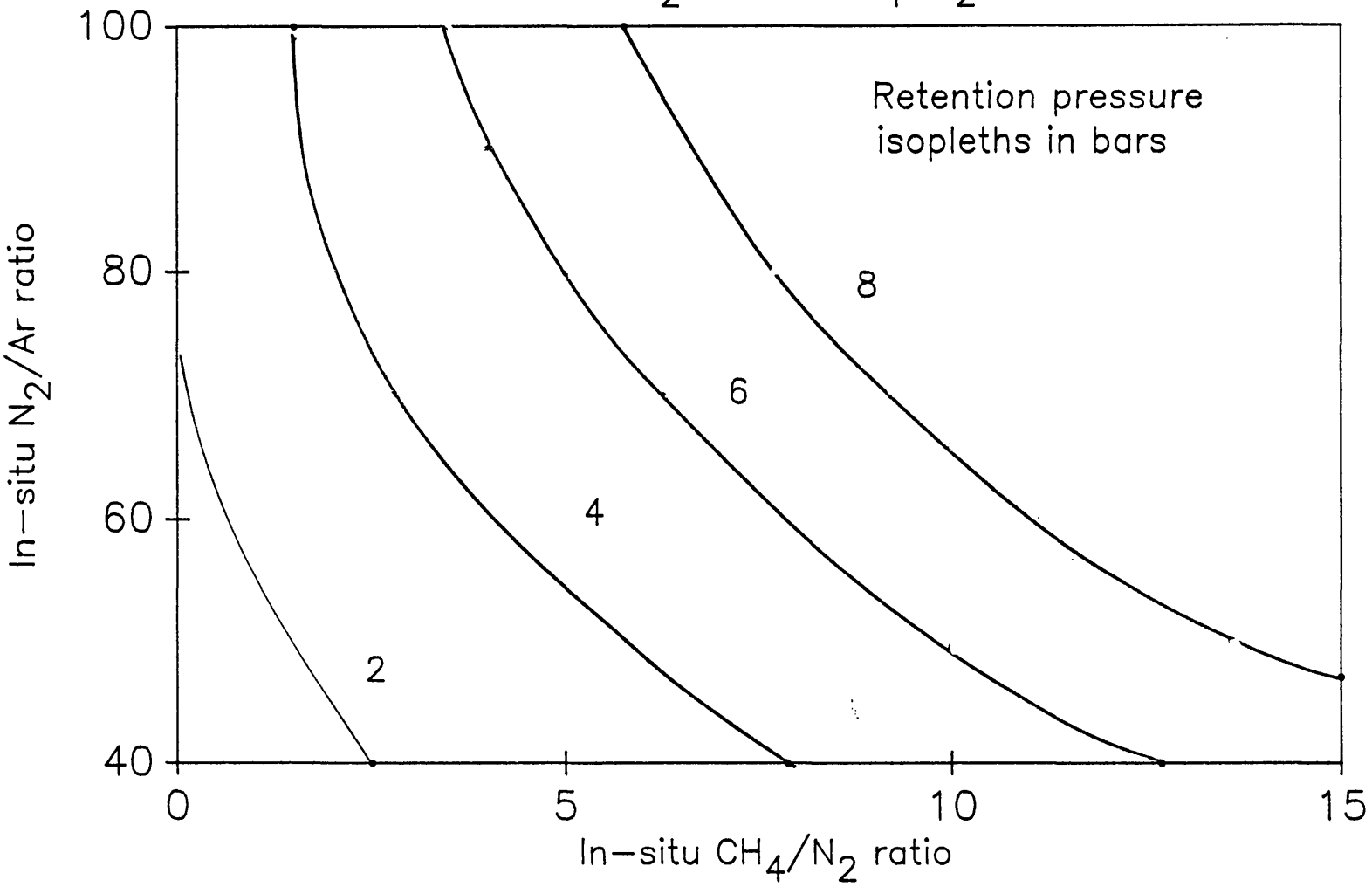

The presence of methane in excess of dissolved nitrogen is likely to cause considerable outgassing of all in-situ gases if a groundwater is depressurised to 1 bar.

6.9 Estimation of In-Situ Gas Contents

If a groundwater has been depressurised to 1 bar, the N_2/Ar and CH_4/N_2 ratios may be determined on samples of the exsolved gas. The in-situ N_2/Ar and CH_4/N_2 ratios may then be estimated using Figures 6.6 and 6.7. Figure 6.6 gives the N_2/Ar ratio of the in-situ gas for various gas phase N_2/Ar ratios and degassing temperature. Figure 6.7 shows the in-situ CH_4/N_2 ratio for gas phase CH_4/N_2 and degassing pressures. This procedure is sufficiently accurate to determine the extent of denitrification or thermodegradation processes.

The estimation of recharge temperatures from dissolved noble gases is most easily achieved by collection under sufficient pressure to avoid outgassing. This is easily achieved with groundwaters containing little N_2 and CH_4. However when significant amounts of CH_4 or N_2 are present then very high collection pressures become necessary. It should be noted that for such waters degassing in a borehole open to the atmosphere will occur down to around 200m. Thus when collecting under pressure this degassed water must be flowed to waste.

If samples cannot be collected under pressure then separate samples of the water and gas phases may be used

Figure 6.6

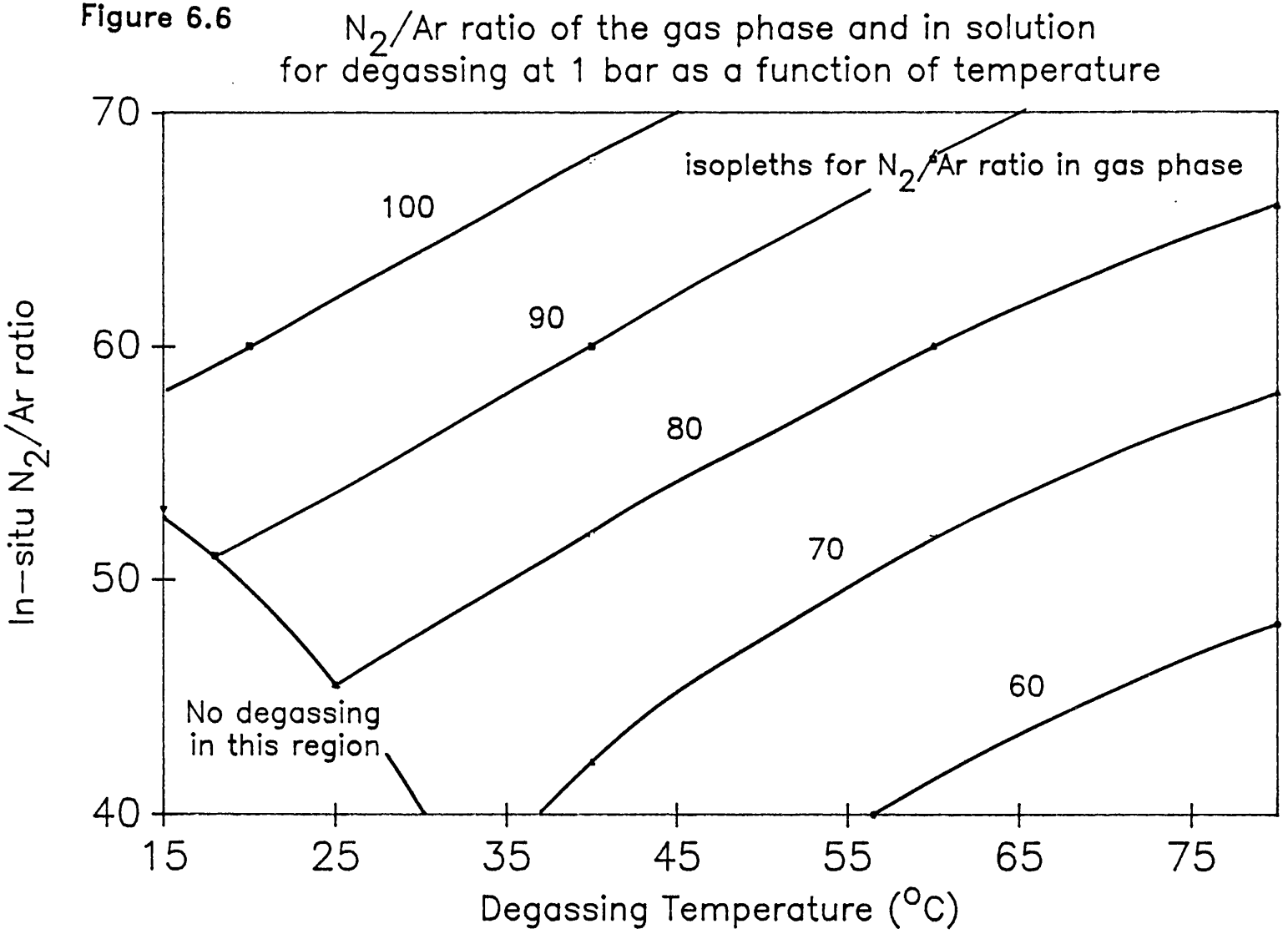
N_2/Ar ratio of the gas phase and in solution
for degassing at 1 bar as a function of temperature
isopleths for N_2/Ar ratio in gas phase
100
90
80
70
60
No degassing
in this region
In-situ N_2/Ar ratio
70
60
50
40
15
25
35
45
55
65
75
Degassing Temperature (°C)

Figure 6.7 CH_4/N_2 in the exolved gas as a function of in-situ CH_4/N_2 and temperature (for N_2/Ar ratio of 38)

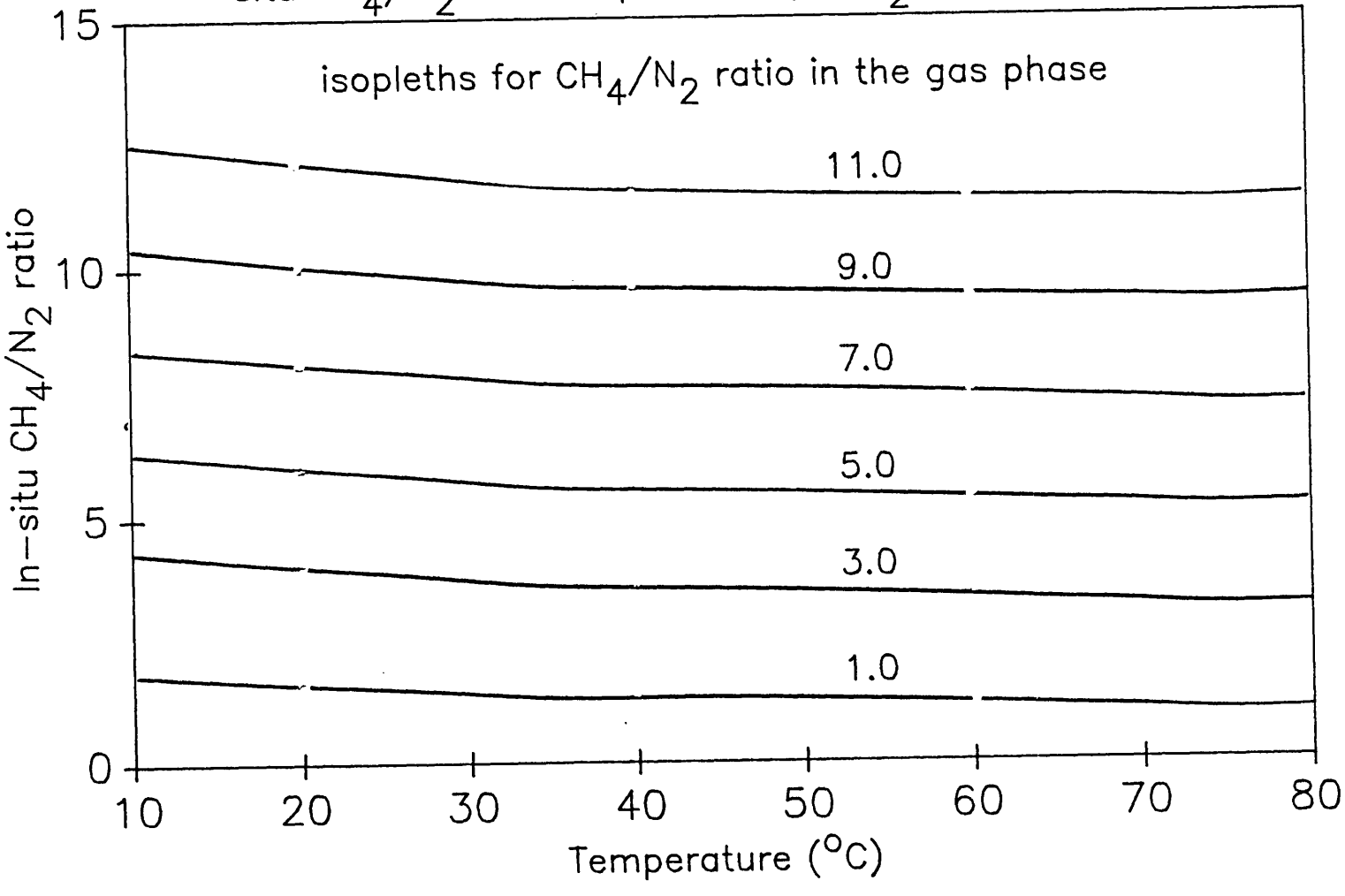

to construct in-situ contents. These must be obtained using a closed system water/gas separator. Accurate determination of flow rates both of gas and water also becomes necessary. The analysis of each phase when used in conjunction with the OUTGAS programme can be used to model the in-situ contents.

CHAPTER 7

THE HELIUM CONTENT OF ROCKS

7.1 The Total Helium Content of Rock Cores

The helium-4 contents of some rock core samples are presented in Table 7.1. The samples represent a wide range of lithologies from granites to a limestone. The measured helium contents range from $3.6 \times 10^{-6} cm^3/cm^3$ of rock for the limestone to $7.6 \times 10^{-4} cm^3/cm^3$ for a sample of Carmanellis granite from Cornwall. Table 7.2 shows the calculated helium concentrations in these same rocks. This calculation uses the radioelement content and age of the rock and assumes that helium has been quantitatively stored after production. Table 7.2 also compares the calculated stored helium values with the measured values from Table 7.1. This comparison shows that the amount of helium generated which is stored in the rock varies from 0.7% for the Stripa granite to 85% for the very fine sandstone from the Triassic formation at Winterbourne.

The proportion of helium generated which is stored in the matrix is likely to be dependent on the diffusion coefficient of helium in the rock matrix, and the depth of the core in the aquifer. The presence or absence of low helium containing groundwater flowing through the aquifer might also disrupt the establishment of a diffusion profile in the aquifer matrix. The two triassic sandstones from Winterbourne and Marchwood appear to have helium contents controlled by diffusion from the matrix. The Marchwood sandstone is much larger grained and therefore more porous than the Winterbourne sample and

Table 7.1

Total measured helium contents of rock cores

Sample	Depth (m)	Helium-4 ($\times 10^{-4}$ cm^3/cm^3 rock)
Stripa granite N1 Sweden	220	1.67
Stripa granite V2	465	1.81
Stripa Leptite	300	3.2
Carmanellis granite Cornwall	1689 10	1.01-1.60 1.89-7.6
Marchwood sandstone	2605	0.32-0.49
Winterbourne sst	2322	2.98-4.28
Ballymacilroy sst Ireland	1542	0.17-0.21
Senones granite France	-	2.44
Andlau granite France	-	1.3
Azel granite Niger	-	1.0
Holyrod granite Newfoundland	-	0.5
Whately limestone Somerset	<10	0.036

Table 7.2

Parameters for calculating total Helium generated in a rock and comparison with measured helium

Rock	Depth (m)	U (ppm)	Th (ppm)	Age (Ma)	He-4 generated ($\times 10^{-4}$ cm^3/cm^3)	% He left
Stripa granite mine level	380	44	33	1640	263.4	0.7
Stripa granite N1	380	44	33	1640	263.4	0.9
Stripa granite V2	465	44	33	1640	263.4	0.7
Stripa Leptite	<300	6.4	16.6	1800	458	5.5
Carmanellis granite	1689	12.8	7.0	290	13	11.3
Marchwood sandstone	2605	1.2	3.0	200	1.19	33
Winterbourne sandstone	2522	4.3	2.8	200	4.29	84.6
Whately Limestone	-	1.2	0.3	315	0.48	7.5

this is reflected in their ability to store helium. The granite samples which are of similar compositions show a wide range of helium storage capabilities, from 0.7 to 11% of the generated helium is stored in the matrix. This difference is unlikely to be due to bulk diffusion coefficient differences.

The stored helium may differ because some rocks are subject to prolonged flow of low helium containing fluids. A further possibility is that helium is more tightly stored in a mineral of one particular granite. In order to study this more closely diffusion coefficients were measured on individual rock cores. In addition experiments were made to find if helium is concentrated in any particular minerals, which control its diffusive loss.

In order to ascertain the likely maximum stored helium content for a rock core from a particular depth it is necessary to model the diffusion of helium through the rock horizon.

7.2 Helium Concentration/Depth Profiles for a Rock Layer

Helium is lost from rock by diffusion of helium through the rock matrix. The effective diffusion coefficient for such diffusion is uncertain but must lie between the values for lattice diffusion ($10^{-11}m^2/a$) and water diffusion ($3.16 \times 10^{-2}m^2/a$) assuming all the pores are water filled. The diffusive loss from a depth z in a medium can be calculated using the equation:

$$\frac{dc}{dt} = G + D\frac{d^2c}{dz^2} \qquad (7.1)$$

where G is the rate of helium generation and D is the diffusion coefficient. If the helium content of the newly formed aquifer matrix is zero and helium is continuously lost from the upper surface to the atmosphere (such that the helium concentration near the surface is zero) then the change of helium with depth and time is approximately given by

$$c(z,t) = G_t \left[1 - \exp \left(\frac{-2}{\sqrt{\pi}} \cdot \frac{z}{(Dt)^{0.5}} \right) \right] \qquad (7.2)$$

The appendix gives a full analytical solution of this equation. This equation also assumes that the aquifer is sufficiently thick such that no helium diffusive loss occurs near the base, so that the helium concentration is equal to the total helium generated. This equation gives the helium concentration/depth profiles shown in Figure 1.13 for radioelement contents appropriate for an average sandstone and an average granite. These profiles show that the concentration gradient $dc/_{dz}$ becomes vanishingly small at depth. At depths greater than $4(Dt)^{0.5}$ the helium concentration is determined only by the rock age and radioelement content. Equation 7.2 has been used to determine the expected helium content of the rock cores assuming helium has been generated over the age of the aquifer. Two diffusion coefficients were used one between the values for diffusion in the matrix and water, and the

other appropriate for aqueous diffusion. The calculated helium contents are given in Table 7.3. Comparison of these values with measured helium contents for the Stripa granite shows the measured values are an order of magnitude lower than that suggested for helium diffusion in water. This suggests that down to 465 metres in the granite water has been removed by flushing with low helium containing groundwater. In contrast the measured values for the Carmanellis granite are close to those for diffusion in water. Thus helium diffusion through water filled pores is controlling the helium/depth profile. The values for the Triassic sandstones at Marchwood and Winterbourne also suggest that helium diffusion through water is the dominant process.

7.3 The Measurement of Helium Diffusion Coefficients in Rock Cores

Helium diffusion coefficients have been determined experimentally on rock cores. These will be compared to the values assumed for producing diffusion profiles in a rock horizon.

The experimental values determined are shown in Table 7.4. Diffusion coefficients were measured using the rock cores stored helium. A large 1.4cm diameter x 1cm long piece of core was heated under vacuum and the volume of helium evolved determined after various time intervals. Relatively low temperatures up to 300°C were used so that the released helium is negligible compared with the stored

Table 7.3

Model helium contents of rocks with differing diffusion coefficents for helium

Sample	Depth (m)	Expected helium content (x 10^{-4} cm^3/cm^3 rock)	
		for D = 3.2 x 10^{-2} m^2/a	for D = 10^{-7} m^2/a
Stripa mine	380	14.1	263.4
Stripa N1	380	15.3	263.4
Stripa V2	465	18.5	263.4
Stripa Leptite	300	2.5	58
Carmanellis granite	1689	6.1	13
Carmanellis granite	10	0.1	16.5
Marchwood sandstone	2606	0.8	1.2
Winterbourne sandstone	2522	2.8	43

helium. For each helium volume evolved - time pair a value of the diffusion coefficient at the particular temperature can be calculated. The helium flux from a core is given by:

$$F = (GT - C) \cdot \left(\frac{D}{\pi . t}\right)^{0.5} \qquad (7.3)$$

where GT is the total stored helium content

C is the volume of helium evolved

t is the time over which the helium is released

D is the diffusion coefficient.

Thus:

$$Ci = \int_{o}^{ti} GT \cdot \left(\frac{D}{\pi . ti}\right)^{0.5} S \cdot dt \qquad (7.4)$$

where Ci is the volume of helium evolved in time ti, and S is the rock core surface area. Integrating of this equation gives:

$$Ci = 2\ GT \left(\frac{D.t}{\pi}\right)^{0.5} \cdot S \qquad (7.5)$$

or in terms of D:

$$D = \frac{1}{4} \left(\frac{Ci}{GT.S}\right)^{2} \cdot \frac{\pi}{ti} \qquad (7.6)$$

The values calculated for D using experimental helium volumes and times are given in Table 7.4. These values were then used to construct Arrhenius type plots to find values for Do and the activation energy of diffusion (Figure 7.5). These calculated values are given in Table 7.5. The experimental values may be compared with

Table 7.4

Diffusion Coefficents of rock matrices in temperature range 90 - 320 °C

Rock Core	T°C	Diffusion coefficent ($\times 10^{-8}$)	% of He extracted
Stripa N1	90	.112	0.1
granite, Sweden	210	242	4.1
	320	16500	30
Carmanellis	100	.05	.06
granite, Cornwall	200	6.30	.9
	260	23.3	1.8
	300	146	3.7
Andlau granite	100	.043	.0003
France	200	1.76	2.2
	300	196	1.5
Senones granite	100	.079	.07
France	200	1.12	0.2
	240	27.7	1.0
	280	2060	9.0
Azel granite	100	0.713	0.25
Niger	200	1.22	0.30
	300	130	2.6
Ballymacilroy	200	4423	16
sandstone	205	6707	18
Ireland	233	6200	16
1542 m	314	9700	30
Winterbourne	100	16	1.9
sanstone	200	3248	17
2322 m	300	22150	25
Marchwood	90	6.2	0.8
sandstone	100	262	6.4
	205	25600	37
	310	56200	43
Whately Quarry	93	3020	12
Carb. Limestone	172	2460	12
	222	3500	15

Table 7.5

Stored helium content, diffusion coefficents and activation energies for diffusion

Sample	Stored helium (cm^3/cm^3 rock) $x10^4$	D_o (m^2/a)	Activation Energy (kJ/mole)
Stripa granite	2.34	22608	92.4
Carmanellis granite	1.41	.472	57.7
Carmanellis granite	2.24	8.77	70.4
Andlau granite	1.3	5.37	73.3
Senones granite	2.44	49.2	78.8
Azel granite	1.0	5.37	73.3
Holyrood granite	0.5	$1.8x10^9$	147
Ballymacilroy sandstone	0.21	.0036	18.2
Marchwood sandstone	0.4	2443	68.4
Winterbourne sandstone	3.6	47.4	59.7
Whately Limestone	0.036	0.0038	0.88

literature values given in Table 1.8. The experimental values fall in the range 59-147 kJ/mole (except for the limestone and very coarse sandstone from Ballymacilroy). This range is very similar to that given in the literature of 39-242 kJ/mole. The values of Do also agree well with the literature values (excluding the two samples with low activation energies). These measured values suggest diffusion coefficients at aquifer temperatures of 20°C of $2 \times 10^{-6} m^2/a$ for the Ballymacilroy sandstone and $10^{-9} m^2/a$ for the other sandstones. Values for diffusion coefficient of less than 10^{-11} are indicated for granite samples. A value of 10^{-11} for granites is similar to that of diffusion in a silicate matrix.

While these values are appropriate for helium diffusion inside a rock matrix, they most probably underestimate the diffusion coefficient of helium diffusing from depth through an aquifer. Aquifer rocks contain water filled fractures and pores which allow a much more rapid diffusion of helium. Measurements of helium contents of water in the Stripa granite indicate a helium diffusion coefficient much closer to that in water is appropriate.

In the Carmanellis granite of Cornwall there is evidence that the experimental determinations of helium diffusion coefficient do not represent the in-situ diffusion coefficient. Minerals such as uranite which may be present in water filled microfractures, are likely to have dried up following rock recovery from the reservoir.

This will allow rapid air diffusion of helium. The absence of this easily lost helium when measuring diffusion coefficients will mean the in-situ coefficient will be very much underestimated.

7.4 The Site of Stored Helium in Rocks

The release of helium from rock cores was studied to determine if there was any temperature where the release of helium is enhanced. This might suggest a concentration of helium in particular minerals. Plots have been made of the release of helium against time at various temperatures. Figure 7.1 shows a sample of Ballymacilroy sandstone. Below 200°C there is a very small helium release, probably indicating very little helium is absorbed on the core. Above 200°C the release rate is fairly constant up to 800°C, suggesting for this rock the release is not very temperature dependent, and helium is stored at sites which are close to interstices in the rock. This would be the case if helium were primarily produced in relatively radioelement rich fracture coatings. Figure 7.3 shows the same experiment for a sample of Stripa granite. In this case helium release is very temperature dependent up to around 550°C. At 550°C there is a large increase in the rate of helium release, this corresponds to the alpha to beta quartz transformation. Above 550°C the release rate slows, this is probably due to over 50% of the stored helium having been released, and thus the helium flux from

Figure 7.1 Release of Helium–4 from Ballymacilroy sandstone core in the temperature range 200–800°C

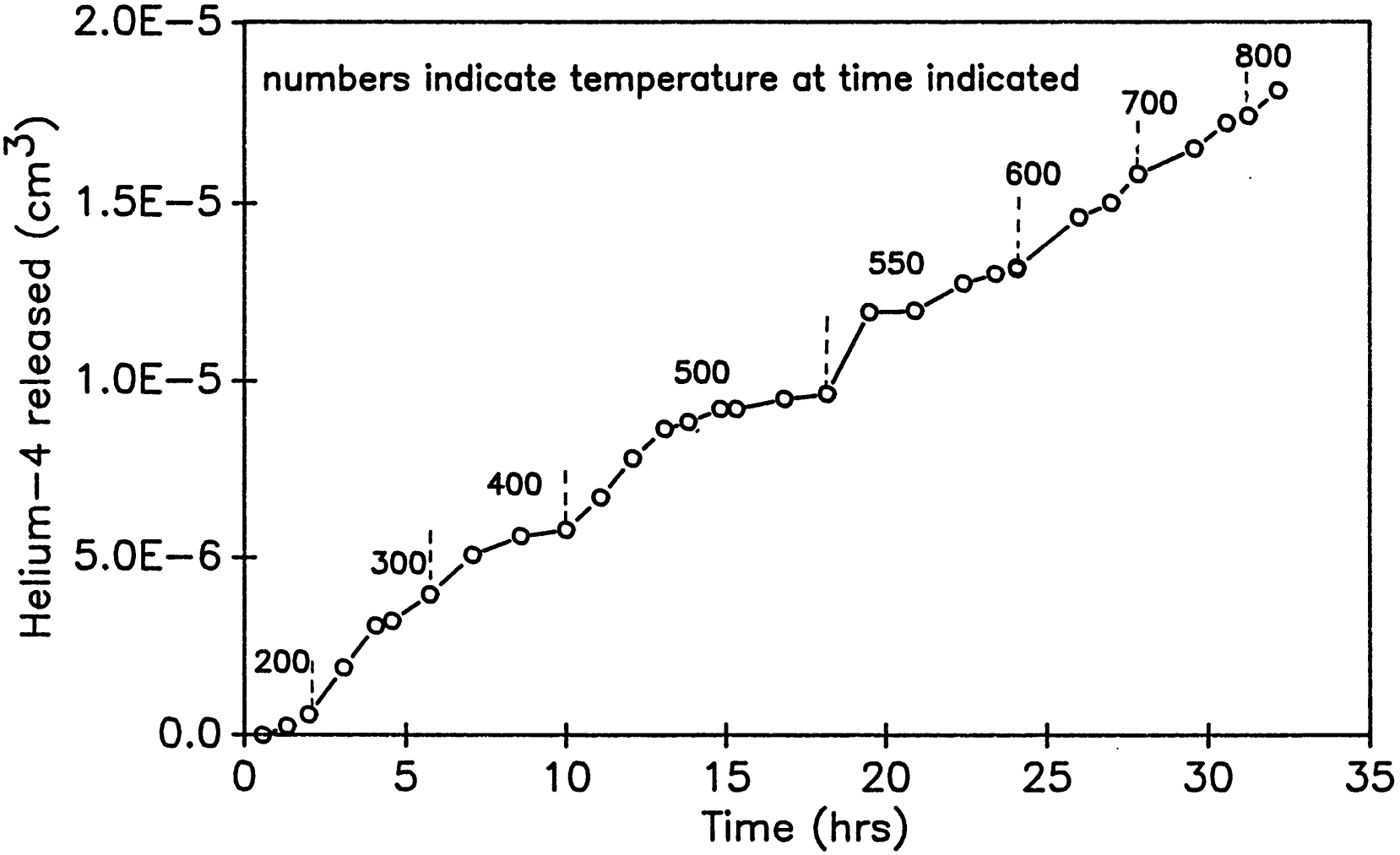

Figure 7.2

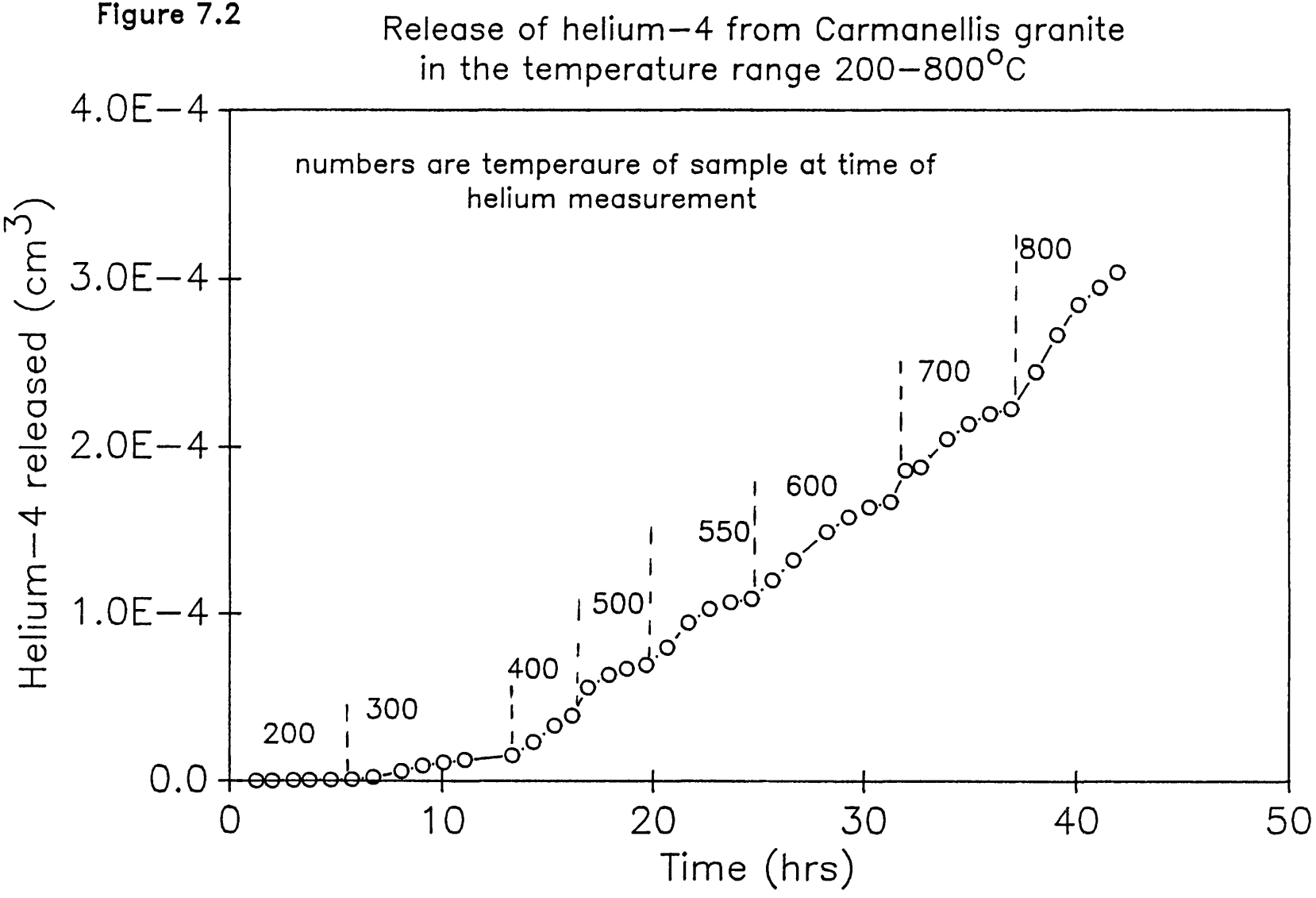
Release of helium−4 from Carmanellis granite
in the temperature range 200−800°C
numbers are temperaure of sample at time of
helium measurement
Helium−4 released (cm3)
4.0E−4
3.0E−4
2.0E−4
1.0E−4
0.0
0
10
20
30
40
50
Time (hrs)
200
300
400
500
550
600
700
800

Figure 7.3

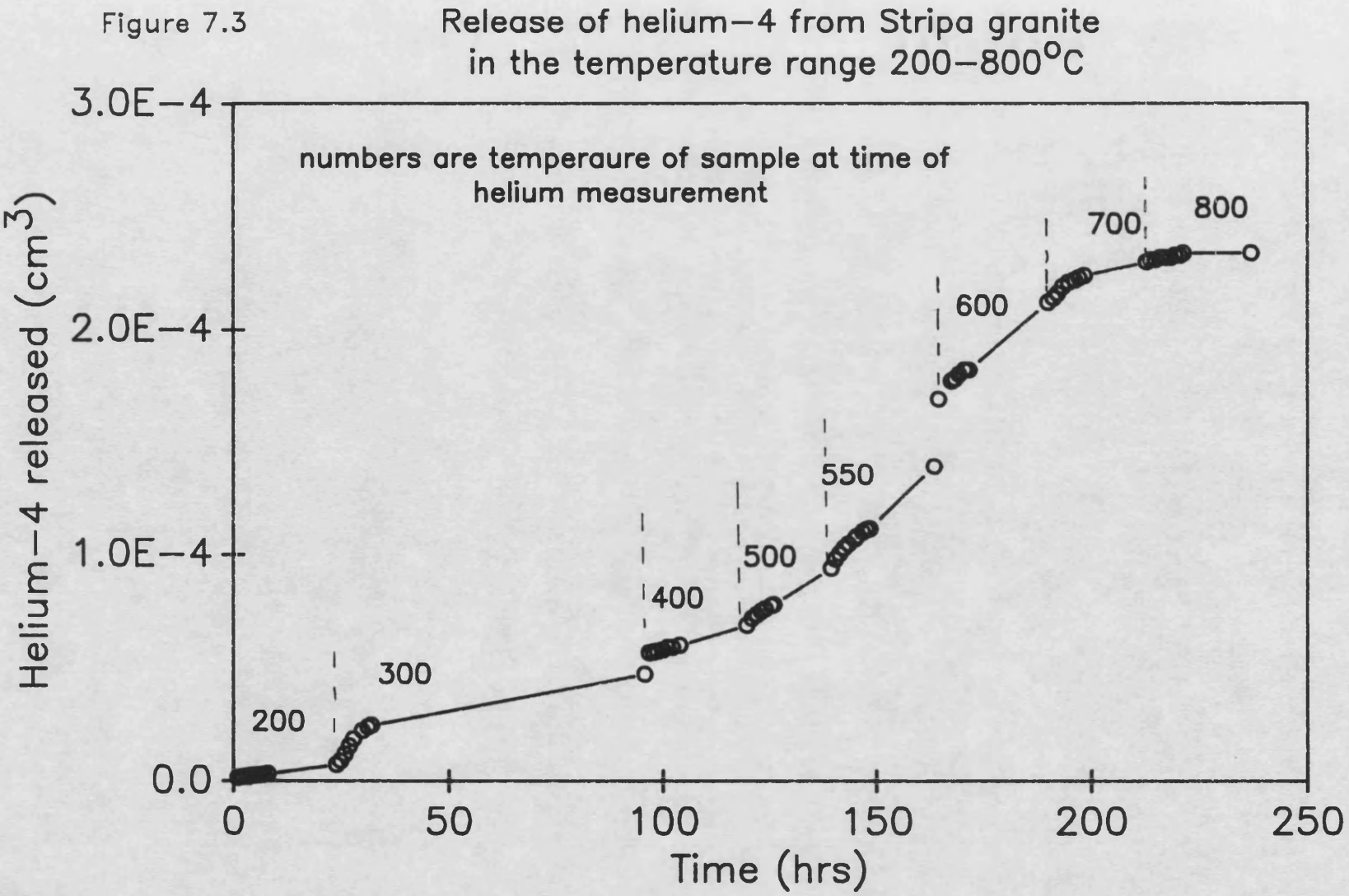
Release of helium−4 from Stripa granite
in the temperature range 200−800°C
numbers are temperaure of sample at time of
helium measurement
Helium−4 released (cm3)
3.0E−4
2.0E−4
1.0E−4
0.0
0
50
100
150
200
250
Time (hrs)
200
300
400
500
550
600
700
800

Figure 7.4

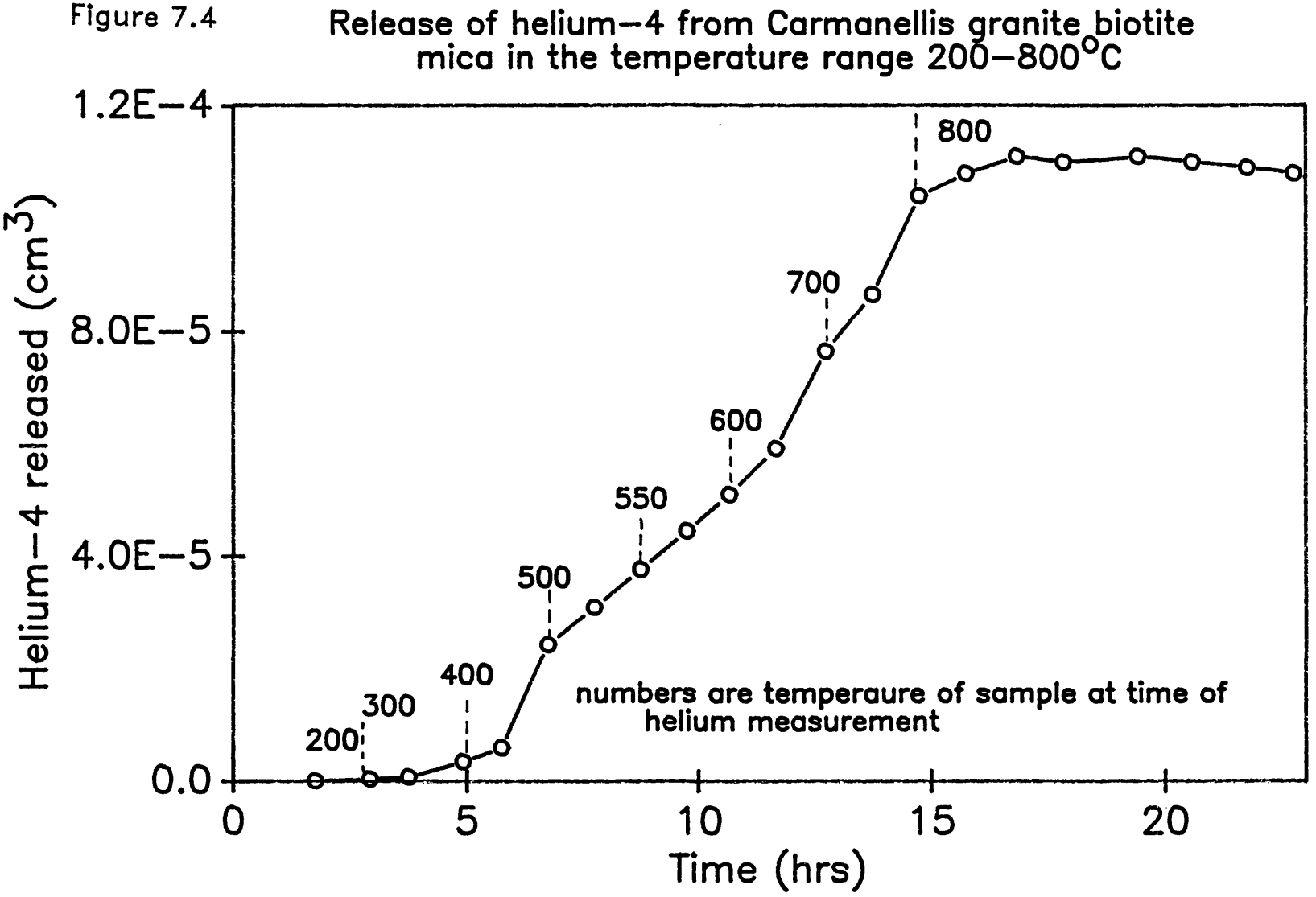
Release of helium–4 from Carmanellis granite biotite mica in the temperature range 200–800°C
1.2E–4
8.0E–5
4.0E–5
0.0
Helium–4 released (cm3)
0
5
10
15
20
Time (hrs)
200
300
400
500
550
600
700
800
numbers are temperaure of sample at time of helium measurement

Figure 7.5 Arrhenius plot for helium diffusion in rock cores

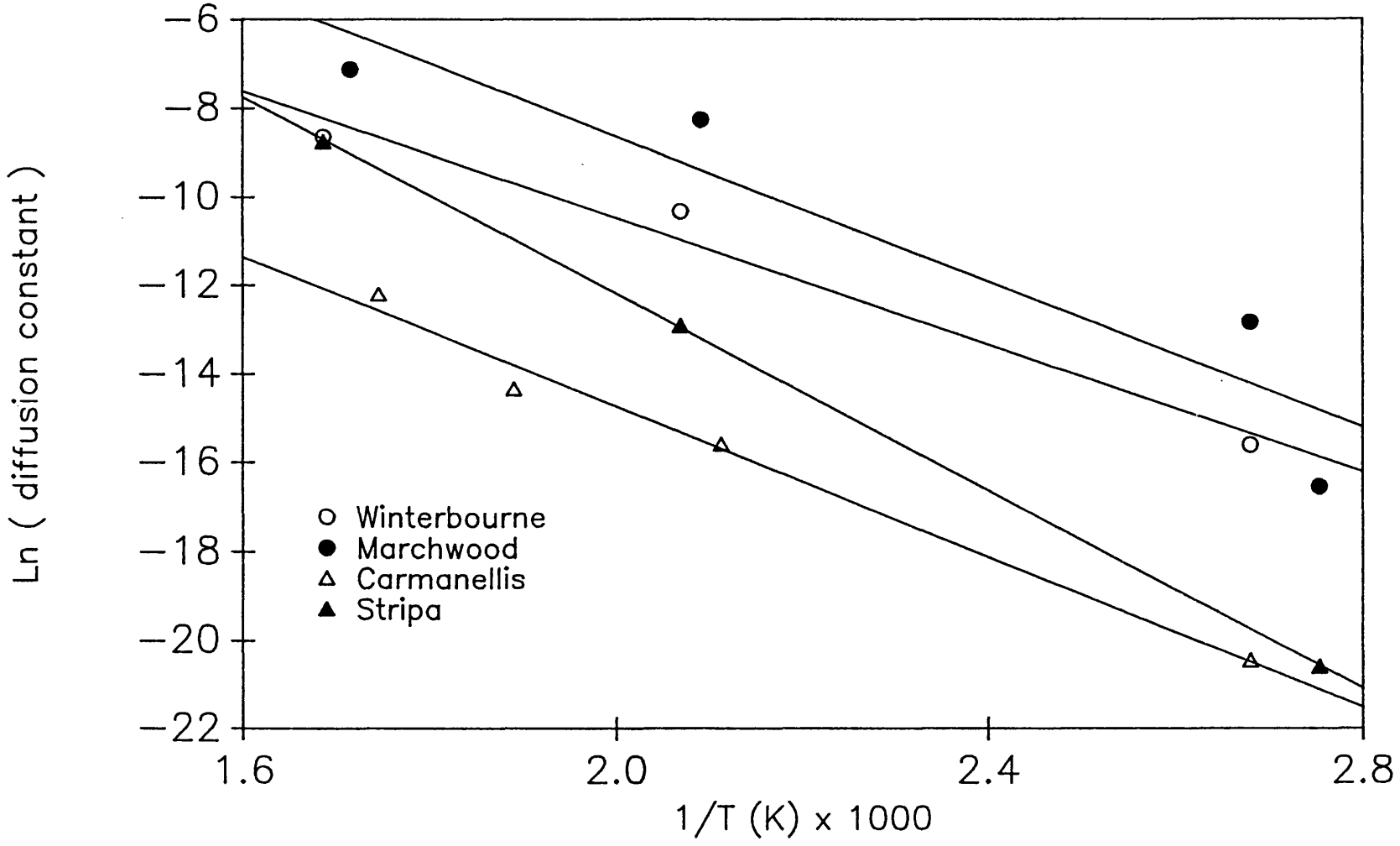

the core will decrease. Figure 7.2 shows the release of helium from Carmanellis granite. This is very similar to the release profile for Stripa granite and indicates helium release is very much temperature dependent. In the case of these granite samples there is no evidence of helium being concentrated close to fracture surfaces.

Figure 7.4 shows the helium release from biotite separated from the Carmanellis granite. This shows a steady increase in helium release rate up to 500°C when the helium depletion limits the flux. There is no evidence of any enhanced release which might accompany mineral alteration. The total helium released is 2.8 x $10^{-4}cm^3/g$ for the biotite, which is slightly less than the bulk rock content release of 4.2 x $10^{-4}cm^3/g$. This suggests that for the granite the radioelements are fairly evenly distributed throughout the rock.

These experiments emphasise the need to carry out diffusion coefficient measurement at low temperatures. Only at low temperatures will the condition be satisfied that the helium released is negligible compared with the total stored helium.

7.5 The Helium Concentration at Fracture Surfaces

The Carmanellis granite has been dated at 290 Ma. It has mean uranium and thorium contents of 14 and 18 ppm respectively. The accumulated helium content of the matrix is 1.6 x $10^{-3}cm^3/cm^3$ of rock. Air equilibrated

water has been pumped into this granite at Rosemanowes quarry in the Hot Dry rock experiment. The fluid returned at the surface has a helium content of $1.6 \times 10^{-3} cm^3/cm^3$ water. Table 7.6 shows how constant this value has been since 1985 since which 1.5 million cubic metres of water have been produced. Assuming an aquifer rock volume of 3000 cubic metres of which 1% is active flow volume, then the total helium lost from the aquifer rock is 0.6% of the stored helium.

Equation 7.1 was solved numerically by Hussain et al (1980) to obtain the concentration gradient at a fracture surface as a function of time following the initiation of flow in the fracture. This assumes that the helium content of the granite is the total helium accumulated over its age, and the fluid helium content is negligible Using a value for the diffusion constant of 1.4×10^{-8} m^2/a values for the percentage helium loss from the fracture surface have been calculated (Table 7.7). These show that to remove 80% of stored helium to a depth of 1 centimetre requires a flow time of 10,000 years.

Equation 7.3 used to determine diffusion coefficients in section 7.3 can also be applied to calculating the flux of helium to a groundwater from a fracture surface providing the initiation of flow is much more recent than the rock age (i.e. there has been no significant reduction in the rock helium content). In this case t represents the flow time. Hence the helium flux is inversely proportional to the square root of the flow time.

Consequently helium flux will decrease rapidly following the onset of groundwater flow. This effect has already been noticed for the Stripa granite, in that the stored helium in the shallow aquifer is much less than that predicted by diffusion of helium from depth.

The fall in helium content of the Carmanellis granite fracture fluids with time is supported by the data in Table 7.6. The overall trend is to lower helium contents in the return fluids, but there is an overlying variability in helium content as a result of the changing helium content of injection waters.

Table 7.6 Inert gas contents for HDR circulation waters (cm^3STP/ cm^3water)

Collection date	^{4}He (10^{-8}) RH12	RH15	RH11	Ne (10^{-7}) RH12	RH15	RH11	Ar (10^{-4}) RH12	RH15	RH11
100187	8.4	86	1079	1.87	1.95	2.26	2.89	3.21	3.85
280187	22.5	217	-	1.85	2.21	-	3.65	4.19	-
100287	95.8	201	-	2.05	2.22	-	3.77	4.43	-
230387	28.9	125	1053	2.03	2.14	2.22	2.92	3.51	3.85
280487	17.1	201	985	1.83	1.93	2.02	2.98	3.16	3.21
220587	70.3	229	980	1.94	2.00	2.03	3.33	3.30	3.34
240587	47.4	243	922	1.94	1.87	2.03	3.05	2.94	3.23
040987	25.7	337	1052	1.87	1.60	2.02	2.94	2.73	3.18
250987	23.8	304	1000	1.98	1.83	2.05	3.07	2.91	3.21
021287	12.7	206	971	1.98	2.00	2.07	3.27	3.38	3.17
031287	5.3	-	-	2.07	-	-	3.76	-	-
041287	-	203	943	-	2.04	2.13	-	3.46	3.39
051287	-	-	1044	-	-	2.27	-	-	3.36
061287	-	-	934	-	-	2.01	-	-	3.18
071287	-	-	947	-	-	2.09	-	-	3.41
081287	-	215	1028	-	2.31	2.24	-	4.18	3.69
091287	5.4	203	933	2.43	2.22	2.06	4.55	3.99	3.45
101287	-	210	929	-	2.29	2.04	-	4.14	3.33
111287	-	177	-	-	2.28	-	-	3.79	-
141287	-	191	-	-	2.08	-	-	3.09	-
151287	-	199	1050	-	2.24	2.35	-	3.97	3.68
161287	-	-	939	-	-	2.34	-	-	3.67
171287	-	-	927	-	-	2.09	-	-	3.38
181287	4.6	207	949	2.03	2.22	2.11	3.78	3.92	3.59
090388	5.4	184	895	2.03	2.13	2.10	3.75	3.95	3.63
130488	4.4	167	-	1.43	2.23	-	3.43	4.03	-
	(2409 m)	339*			2.27*			4.00*	
100588	-	138	-	-	2.05	-	-	3.36	-
	(2464 m)	567*			2.24*			3.85*	
100688	0.8	160	843	0.97	1.84	2.08	2.14	3.10	3.57
290688	4.3	173	874	1.58	2.10	2.21	3.07	3.47	3.61
	(2218 m)	180*			3.62*			4.29*	
080788	(2507 m)	1242			2.13*			3.55*	

Cont'd./...

Table 7.6 (cont) Inert gas contents for HDR circulation waters (cm^3 STP/ cm^3 water)

Collection date	^4He (10^{-8}) RH12	RH15	RH11	Ne (10^{-7}) RH12	RH15	RH11	Ar (10^{-4}) RH12	RH15	RH11
180788	-	137	-	-	2.63	-	-	3.95	-
	(2218 m)	181*			2.39*			3.63*	
	(2409 m)	418*			3.11*			4.30*	
	(2464 m)	530*			2.71*			3.94*	
	(2507 m)	1244*			2.32*			3.57*	
300988	5.6	293	994	2.13	1.99	2.21	3.84	3.36	3.63

* Denotes drill pipe samples

Table 7.7 The cumulative ^4He loss from fracture surfaces in the HDR during water circulation

Depth below surface, cm	% He-loss at cumulative flow times, 10a	100a	1000a	10000a
1	4	13	41	77
2	2	6	21	58
3	1	4	14	43
4	<1	3	10	32
5	<1	2	8	26

$GT_a = 1.65 \times 10^{-3}$ cm^3 STP cm^{-3} rock
$D = 1.4 \times 10^{-8}$ m^2a^{-1}

CHAPTER 8

CONCLUSIONS

8.1 Uranium and Thorium

The natural radioelements potassium, uranium and thorium are widely distributed in crustal rocks. The interaction between fluids and radioelements in rock matrices can be used to study processes in aquifers. The solution of natural radioelements, in a groundwater, is dependent upon its chemical character, that is its pH, Eh salinity and the dissolved species present.

Very frequently the U-234/U-238 activity ratio for uranium dissolved in a groundwater is not in equilibrium, the ratio generally being greater than 1. Such disequilibrium may be considered as a consequence of either preferential solution of U-234 or α recoil induced solution of U-234. The rate of Th-234 recoil solution due to U-238 decay may be estimated from the U content of the matrix and its recoil range; and the extent of the rock/water interface. This recoil solution rate is the most significant control of U-234/U-238 change with time. The estimation of groundwater residence times from activity ratio changes is in principle possible but requires a detailed knowledge of the geochemical processes which occur in different aquifer zones, and on its hydrological character. This is only well known in aquifers where samples can be obtained from various locations.

In contrast with the mobility of uranium in the hydrosphere, thorium is very insoluble and generally not above detection limits in natural waters. This is a

consequence of its ready hydrolysis at pH values typical of groundwaters. The decay product of Th-232 is Ra-228 which may enter solution. This can support Th-228 in solution, but this is readily hydrolysed and absorbed on colloidal particles.

8.2 Radium and Radon

Dissolution of Radon-222 occurs mainly by a recoil process at the rock/water interface. This equilibrium is attained when residence times in an aquifer exceed 25 days. The equilibrium concentration of radon is determined by the uranium activity in the aquifer matrix, the fractional porosity of the aquifer and its bulk density. Measurement of these parameters provides an indicator of the fractional release of radon to waters. Fractional release factors for various aquifer types can be used to measure aquifer porosity in-situ, a parameter very difficult to measure by other means. Radon concentrations also provides useful information on the factors controlling the rate of helium accumulation in groundwaters.

The chemical solution of radium-226 increases in importance as the groundwater salinity increases, provided there are sufficient Ba or Ca ions in solution. The residence time of radium in solution depends upon congruent/incongruent solution of Ba and Ca. Coprecipitation of Ra with Ca prevents its activity ever attaining

its equilibrium value with uranium. However high Ra contents are good indicators of groundwater maturation.

The activity ratios Pb-210/Rn-222 and Po-210/Rn-222 have been used to estimate residence times for Pb and Po in solution. The behaviour of these isotopes may be used to assess that of homologous fission products and actinide constituents of nuclear waste in groundwater.

Measurement of the extent to which equilibrium has been established between Pb-210 or Po-210 with the parent Rn-222, which is maintained in concentration by continuous release from the matrix, enables residence times to be measured. Calculated residence times are generally very short ranging from a few days for Pb and hours for Po. Migration of homologous actinides present in nuclear waste should therefore be considerably retarded. Actual residence times depend greatly on chemistry, Eh and pH of the actual groundwater.

8.3 Atmospheric Gases

The concentration of dissolved inert gases in groundwaters at recharge is controlled by the average temperature of air equilibration. This inert gas pattern is conserved after recharge so that the recharge temperature can be derived by measurement of Ne, Ar, Kr and Xe concentrations of a groundwater. This conservation of recharge temperature can be used for a variety of hydrological uses. The mode of recharge may be deduced

from recharge temperatures. Slow recharge through a porous media produce recharge temperatures reflecting the local ground temperature in the unsaturated zone. Fast conduit type recharge will reflect the average temperature of the rainy season.

Additions of excess air are always observed in inert gas contents of groundwaters. These are air entrained by a groundwater during passage through the unsaturated zone, and consequently dissolved by increasing pressure. Excess air is always recognisable by its inert gas pattern. The neon contents are most enhanced and the heavy inert gases only slightly. The air-equilibrated inert gas contents may be discovered by removing very small aliquots of air from the total inert gas contents. This leads to a unique solution for the temperature of air equilibration.

Recharge temperatures may be used to indicate groundwater ages. Where air equilibration is found to have occurred at different temperatures to those prevailing today indicates ancient recharge. This will not give a unique groundwater age but a useful indicator to be used in conjunction with other age determining methods. The stable isotopic composition of water is a useful parallel technique to be compared with inert gas recharge temperatures. Inert gases have one important advantage as they are not subject to exchanges with isotopes in the aquifer.

Inert gas contents also indicates saline recharge. Brines equilibrated with air during recharge will have low

gas contents. Waters which evolve into brines by dissolution of rock will retain their original fresh water inert gas contents. Inert gas solubilities in saline water may be used to produce recharge temperatures in the same way as for fresh waters.

In addition to gases dissolved by equilibration with the atmosphere groundwaters accumulate other gases. Excess air is entrained by groundwater in the unsaturated zone. Deeply circulating groundwater may gain additional N_2, CH_4 and CO_2 by geochemical, biogenic and thermogenic processes. Geothermal heating of groundwater during its circulation, together with increases in its gas content, may cause the water to become supersaturated with gases. Drill holes will permit the exsolution of dissolved gases unless sufficient pressure is applied at the well head. Groundwaters which evolve gas at atmospheric pressure can be prevented from degassing by pressurisation to 20 bars at temperatures up to 60°C, even when containing 95% of additional methane. If degassing is allowed to occur the in-situ gas contents can be reconstructed from analysis of exsolved gas, the degassed solution and the relative volumes of each.

Outgassing has been studied for groundwater at Stripa where low flow rates require long flushing times to remove outgassed water from the boreholes. The measured inert gas contents have been studied to determine whether they can be produced when partial outgassing of the aqueous phase occurs. The waters of the Molasse basin have all

been collected under pressures well in excess of that necessary to keep dissolved gases in solution. Measurements of radiogenic inert gas contents and of thermogenic and biogenic gases have been used to confirm that degassing can not occur at the temperatures and pressures prevailing at collection.

8.4 Radiogenic Gases

8.4.1 Helium

Helium-4 has been successfully used as an indicator of increasing groundwater age. However, ages produced using in-situ production and accumulation of helium in the aquifer are usually many times older than those suggested by techniques such as C-14 dating and hydrologic ages.

Helium has several important advantages over many radiochemical methods of dating groundwaters. The amount of dissolved helium increases with time, unlike radioisotopes such as tritium and C-14; thus there is no upper limit on ages obtainable. The low levels of He in the atmosphere mean that no assumption of past air composition is needed such as for C-14, Cl-36 and Kr-81 which are produced in the atmosphere by nuclear reactions. Helium dating has the further advantage in that it is non-reactive with groundwater or the rock matrix. Other dating methods are complicated by exchange processes with the aquifer matrix.

The helium-3/helium-4 ratio is vitally important when

considering helium age dating of groundwater. The He ratio may establish if the observed helium has been produced in the aquifer matrix or has diffused from deeper levels. A ratio appropriate for the aquifer matrix will validate He ages calculated using the in-situ He production. Helium ratios can also indicate mixing of atmospherically derived helium with radiogenic helium. This mixing can be used as a dating method for up to 100,000 years at which time the radiogenic He will dominate the atmospheric input. Diffusion of He from crustal basements may occur and if the characteristic helium ratios are different for the two sources, then measurement of helium ratios can yield information on diffusion from crustal basement.

Diffusion of helium along water filled fractures and aqueous transport of helium can be a much more significant process than rock matrix diffusive loss of helium. Helium depth profiles using appropriate diffusion constants have shown that at depth helium is effectively stored. Even if a diffusion constant for water is used He-4 is virtually stored at depths greater than 1 km. In comparison with transport by flowing groundwater, diffusion over long distances is not an effective mechanism for helium loss from crustal rocks.

In the case of groundwaters in a fractured medium where the water phase is less than 1 percent of volume, helium loss occurs by a two stage process; firstly diffusive loss from the matrix and then transport in these

fluids. After prolonged flow the helium content in the fracture surfaces may become much less than the matrix helium content. Age estimates may then only be made if the length of time flow has been occurring in a fracture can be estimated. If the flow time is small then the fluid helium concentration will be close to that of the matrix, so that very quickly air equilibrated water will approach rock matrix helium contents. For this reason only short residence times for groundwaters can be measured.

For intergranular flow aquifers, where regional flows are more important than fracture fluid flow, different considerations are necessary. In an intergranular flow the water-rock interface is much larger so stored helium is much more rapidly flushed from the rock matrix. However intergranular aquifers frequently contain helium in groundwaters greater than that expected to be generated in the matrix during the groundwater residence time. This is possible due to a residual stored helium which has not been flushed from the matrix, which has been observed for many granular rocks. A second explanation appears to be significant for the Molasse groundwaters where a flux from the granitic basement has been used to date the waters.

8.4.2 Argon-40

Radiogenic Ar-40 is produced by decay of K-40 in rock matrices. Ar-40 is a useful indicator of groundwater age.

However since many minerals stored argon almost quantitatively at temperatures up to 200°C it is of limited value for absolute age determination. Radiogenic Ar-40 has been detected by measurements of Ar-40/Ar-36 isotopic ratio. Small inputs of radiogenic argon are indetectable because of the large input of atmospheric Ar-40 at recharge. Enhanced ratios have been detected and are concluded to be due to mineral alteration processes which have released stored argon without diffusion. The Ar-40/Ar-36 ratio is thus much more closely related with groundwater chemistry than absolute age.

8.5 Molasse basin shallow waters

8.5.1 Uranium

The uranium contents of the Molasse waters are low due to the prevailing Eh, pH conditions which place these waters close to the UO_2 deposition boundary. The uranium-234/uranium-238 activity ratio is close to unity for the young groundwaters (group 1) and increases in groups 2 and 3 which is most probably due to preferential solution of U-234 by α recoil solution or an increased solution rate in radiation damaged lattice positions.

8.5.2 Radon and Radium

The efficiency of radon-222 release in the Molasse basin has been calculated to be 0.04, similar to values for the Triassic sandstone of the UK. The flow patterns

for the Molasse sediments and the Triassic sandstone are both interstitial in character. The radon-222 contents suggest that variability in uranium content, porosity and density does not vary by more than +/- 27% in the aquifer.

The radium-226 contents are much less than radon-222 contents and are hydrochemically controlled rather than radiochemically.

8.5.3. Atmospheric Gases

The group 3 groundwaters have lower recharge temperatures than the younger waters and are concluded to have recharged during the interstadial from 20,000-70,000 years ago. The delta-18 oxygen values also indicate recharge under cooler climatic conditions for the group 3 waters.

The measured nitrogen/argon values for the Molasse waters are higher than air equilibrated water in the temperature range 0-15°C.

Removal of quantities of nitrogen and argon in the ratio of air produces dissolved gas concentrations appropriate for air equilibration between 0 and 15°C. The indicated recharge temperatures are broadly similar to those suggested by inert gas measurements. There is no evidence for the process of denitrification having occurred in these waters.

Figure 8.1 Characteristics of the Innviertel waters

Group1	Group 2	Group 3
Oxidising	Reducing groundwater	Reducing groundwater
Eh $>$ + 70 mV	+82 mV $<$ Eh $>$ −15 mV	Eh $<$ + 40 mV
Cl $>$ 1 mg/kg	Cl $>$ 1 mg/ kg	Cl $>$ 1 mg/kg
Congruent solution of calcite	Incongruent solution of dolomite	Cation exchange and carbonate dissolution
p CO_2 $>10^{-2}$atm	$10^{-2.5}<$ p$CO_2>$ $10^{-3.1}$	$10^{-2.6}<$ p$CO_2>10^{-3.5}$ atm
No radiogenic ^{4}He	^{4}He $>$atmospheric equilibration	^{4}He content high
$^{234}U/^{238}U = 1$	$^{234}U/^{238}U$ high	$^{234}U/^{238}U$ high
He age $<$ 1000 years	He age 800−7000 years	He age $>$ 8000 years
Recharge temperarures same as modern recharge	Recharge Temperatures slightly lower than modern	Recharge temperatures lower than modern

8.5.4 Radiogenic gases

The He-3/He-4 ratio of dissolved helium shows it to be a mixture of atmospheric He and radiogenic He. The radiogenic component is concluded to have diffused from the granitic basement on the basis of the basement Li, U and Th contents. Groundwater ages have been estimated on the basis of solution of He diffusing from the basement. The calculated ages range from less than 1000 years for group 1 waters to greater than 8000 for group 3 waters.

8.5.5 Groundwater Age

Piezometric data shows that the direction of groundwater flow in the Innviertel formation is in general north to northeast, and the flow velocity is 1 metre per year. This is supported by the radiogenic He-4 contents and the inert gas derived recharge temperatures, and the oxygen and hydrogen stable isotopic composition. The characteristics of each sample group are summarised in Table 8.1.

8.6 Molasse Formation Waters

8.6.1 Uranium

The uranium contents of the Molasse basin formation waters are very low, suggesting U deposition in the existing reducing environment. Migration of the brines since deposition of U probably means that uranium is not deposited in the interstices of the formation rocks.

8.6.2 Radium

The Ra-226 increases with salinity in the formation waters. This trend is probably best explained by dilution of high Ra containing brines with meteoric water, rather than by a geochemical control such as coprecipitation with Ca. The absence of iron (111) in these highly reducing environments would mean Ra will not be absorbed on hydroxyl sites associated with oxidized iron. This is a likely contributing factor to the high Ra contents.

8.6.3 Stable Isotopes

Only the Innviertel waters of the Molasse basin have delta-2H and delta-180 values which lie on the meteoric water line. The formation water stable isotope contents lie on a line which can be described broadly in terms of mixing of connate seawater and meteoric water. However there is enrichment in both H-2 and O-18. This suggests that isotopically light hydrogen has been used in the biogenic process to produce methane and that oxygen has been exchanged with matrix carbonate or silica.

8.6.4 Dissolved Gas Composition

8.6.4.1 Argon isotopic ratio

The argon isotopic values are very variable ranging from atmospheric values to very high values suggesting release of argon from rocks at high temperature.

8.6.4.2 Helium-4/argon ratio

Helium-4 concentrations do not seem dependent on groundwater age. The presence or absence of radiogenic He is dependent on the degree of flushing by meteoric waters. Only the Puchkirchen formation waters show an increase in helium-4 with depth probably as a result of helium diffusion from the granitic basement.

8.6.4.3 Methane/argon ratio

The methane content increases with the increasing thermodegradation of organic matter, as indicated by the ammonium ion content. The Puchkirchen formation does not show this trend as the methane is of biogenic origin.

8.6.4.4 Nitrogen/argon ratio

The Puchkirchen formation has N_2/Ar ratios which are described by air saturation of brines with some excess air content. The oil bearing formations have very high N_2/Ar ratios which are indicative of thermogenic nitrogen production accompanying oil formation.

8.6.4.5 Xenon/argon and krypton/argon ratios

The ratio of these heavy noble gases to argon shows a very large variation. Ranging from the values expected in air saturated water to much higher values. It is concluded that the heavy noble gases are concentrated in oil and gas bearing formations. The concentration of

xenon and to a lesser extent krypton on shales may be the cause of this phenomena.

8.6.5 Characterization of the Molasse Formation Waters

The methane content of the Puchkirchen waters are a result of biogenic processes. The high helium content suggests these waters are largely connate. The presence of radiogenic argon in large quantities in the Eocene oil reservoirs suggests migration from a high temperature environment. The deepest waters from the Cretaceous and Jurassic have been replaced by meteoric water. In contrast the chemistry of the Miocene and Eocene suggests there has been no significant vertical infiltration of meteoric water within the Molasse basin.

8.7 Stripa waters

8.7.1 Uranium

The Stripa granite has a high content of uranium which is readily leached to the aqueous phase. The shallow groundwaters in the granite have high dissolved U contents and high U-234/U-238 activity ratios produced by preferential solution of U-234. The deeper waters have low dissolved U contents and very high activity ratios. Groundwater ages based on in-growth of U-234 from its parent Th-234 following chemical leach of U are less than 30,000 years, using a fracture width of 100 microns. However the variability of uranium activity ratio and the

uncertainties in the processes occurring make these ages very approximate. The decrease in uranium activity ratio with depth is most likely explained by mixing of meteoric water with stored fluids in deep fractures.

8.7.2 Radon and Radium

The very low Ra-226/Rn-222 ratios suggests diffusion in the matrix is a significant solution mechanism for Rn-222, and diffusion of Ra-226 must be much slower. The Ra content of the groundwater is controlled by Ra-Ca solid solution as the waters are saturated with respect to carbonate minerals.

The Ra-226/Ra-228 ratio has no dependence on Ra-226 content indicating the similar proximity of the aqueous phase to U-238 and Th-232.

The Ra contents exceed the limiting production rate by α-recoil from the matrix, suggesting Ra in solution is controlled geochemically. This geochemical control makes Ra residence times in solution impossible to calculate.

The Rn contents have been used to deduce fracture widths using an experimentally determined Rn flux; the calculated values range from 20-250 microns. Hydraulic considerations using Darcy's law and the calculated fracture widths suggest shallow water can penetrate into the deepest fractures in a few tens of years.

8.7.3 Atmospheric Gases

The noble gas derived recharge temperatures for the Stripa groundwaters decrease with depth and correlate linearly with delta 18-O values. This suggests the deeper waters were recharged at temperatures about 2°C cooler than the present mean annual air temperature. This is possibly due to recharge during the interstadial 15,000-40,000 years ago, or to snow melt recharge of the deep groundwaters.

The groundwaters probably show slight outgassing prior to collection because of insufficient flushing of the boreholes. This is greatest in the deep boreholes, but is not significant enough to destroy the recharge temperature signatures. The local intrusion of young meteoric waters has been shown to occur using chemical data and tritium contents.

The nitrogen/argon ratios can be explained in terms of air equilibration around 0°C, with the addition of excess air. There is no evidence of thermodegradation of organic substances.

8.7.4 Radiogenic Gases

The deeper groundwaters contain significant amounts of excess radiogenic Ar-40, which suggests that some mineral alteration has occurred to release stored argon.

The large concentration of radiogenic He present in the Stripa groundwater are a result of diffusion from

depth and produce a characteristic helium concentration/ depth profile. In the deep waters equilibration with the host has occurred so it is not possible to estimate helium ages. In the shallow waters helium ages can be determined if the cumulative flow times for the fracture fluids can be made. The helium concentration in the fracture fluids may become less than in the bulk rock matrix due to a decrease in the helium flux by prolonged fluid flow. Since the helium flux at fracture surfaces is dependent upon the helium content maintained in the groundwater and the cumulative flow time, ages can only be determined if flow times are known.

The helium-3/helium-4 isotopic ratio of the radiogenic helium is in good agreement with the value calculated for the Stripa granite, suggesting there is no deep crustal input.

8.7.5 Groundwater Age

Recent carbon-14 measurements and the presence of thermonuclear tritium in the deep boreholes indicates recent ages for Stripa groundwaters. This suggests that the deeper waters were recharged during the period of annual snow melt, whilst shallow groundwaters are replenished throughout the year. Calculated fracture widths suggest infiltration by recent groundwater in a few years. There is also little doubt that drilling of boreholes for hydrological investigation will impose their

own flow regime on the granite, and increase downward percolation of groundwater.

Aegerter, S.K., Loosh, H.H. and Oescheger, H., 1967. Variation of the production of cosmogenic radionuclides. In: Radioactive dating and methods of low level counting. IAEA, Vienna.

Aldrich, L.J. and Nier, A.O., 1948. Argon-40 in potassium minerals. Phys. Rev., v74, p876-877.

Allison, G.B., and Hughes, M.W., 1975. The use of environmental H-3 to estimate recharge to a south Australian aquifer. J. Hydrol., v26

Anderson, E.C., and Libby, W.F., 1951. World-wide distribution of natural radiocarbon. Phys. Rev., 81, p64-69.

Andrews, J.N., and Wood, D.F., 1972. Mechanism of radon release in rock-matrices and entry into groundwater. Trans. Inst. Mining. Metallurgy, v81, p198-209.

Andrews, J.N. and Kay, R.L.F. 1978. The evolution of enhanced U-234/U-238 activity ratios for dissolved uranium in groundwater dating. Short papers of the 14th Int. Conf., Geochron. Cosmochron., Isotope Geol., Colorado, USA, Ed: R.E. Zartman.

Andrews, J.N. and Lee D.J., 1979. Inert gases in groundwater from the Bunter sandstone of England as indicators of paleoclimatic trends. J. Hydol., v41 p233-252.

Andrews, J.N. and Kay ,R.L.F., 1982. U-234/U-238 Activity ratios of dissolved uranium from a Jurassic limestone aquifer. E.P.S.L., v57 p139-151.

Andrews, J.N., 1983. The isotopic composition of helium and its use to study groundwater movement. Proc. 4th Intl. Symp. Water-Rock Interaction, Misasa, Japan 17-21.

Andrews, J.N., 1984. The isotopic composition of helium and its use to study groundwater movement in confined aquifers. Chem. Geol. 49, 339-351.

Andrews, J.N., Balderer, W., Bath, A.H., Clausen, H.B., Evans, G.V., Florkowski, J.E., Goldbrunner, J.E., Ivanovich, M., Loosli, H.H., and Zojer, H., 1984. Environmental isotope studies in two aquifer systems: a comparison of groundwater dating methods. In: Isotope Hydrology p535-576, IAEA., Vienna.

Andrews, J.N., Goldbrunner, J.E., Darling, W.G., Hooker, P.J., Wilson, G.B., Youngman, M.J., 1985. A radiochemical, hydrochemical and dissolved gas study of groundwaters in the Molasse basin of Upper Austria. Earth and Planetary Science Letters, v.73 p.317-332.

Andrews, J.N., Youngman, M.J., Goldbrunner, J.E., Darling, W.G., 1987. The Geochemistry of Formation waters in the Molasse Basin of Upper Austria. Environ. Geol. Water Sci. v.10 no.10 p43-57.

Andrews, J.N., Hussain, N., Ford, D.J., Smith, B. and Youngman, M.J., 1988. Geochemistry of radioelements and noble gases in the HDR reservoir. in: Investigation of the geothermal potential of the UK - Granite-water interactions in relation to Hot Dry Rock geothermal development. (ed. W.M. Edmunds et.al.) British Geological Survey, Keyworth. pp. 96.

Andrews, J.N., Hussain, N. and Youngman, M.J., Atmospheric and radiogenic gases in groundwaters from the Stripa granite. Geochim. Cosmochim. Acta. (accepted for June 1989).

Andrews, J.N., Ford, D.J., Hussain, N., Trivedi, D. and Youngman, M.J., Natural radioelements in circulating groundwaters in the Stripa granite. Geochim. Cosmochim. Acta. (accepted for June 1989).

Andrews, J.N., Hussain, N. and Youngman, M.J., Stored helium in some crustal rocks and its solution by groundwaters. "Gas Release, Reaction and Mobility in Crustal Rocks", Geochemistry Group of the Mineralogical Society, 11-12 April, 1988, London.

Atkinson, T.C., 1977. Diffuse flow and conduit flow in limestone terrain in the Mendip Hills, Somerset, Great Britain. J. Hydrol., v35, p93.

Bahhwar, G.D., Deney, C.L. and Kaplan, M.F., 1969. Differential energy spectrum of proton, helium neuclei and electron. J. Geophys. Res. v74(3), p744-754.

Bath A.H., Edmunds W.M., and Andrews J.N., 1978. Palaeoclimatic trends deduced from the hydrochemistry of a Triassic Sandstone aquifer, United Kingdom. Isotope Hydrol. v2 p545-566. I.A.E.A., Vienna.

Bear, J., 1972. Dynamics of fluids in porous media. American Elsevier, New York.

Beers, R.F. and Goodman, C., 1964. Distribution of radioactivity in ancient sediments. Bull. Geol. Soc. Amer., v55, p1229-1253.

Bell, K.G., 1954. Uranium and Thorium in sedimentary rocks. In: Nuclear Geology, H. Faul ed., Wiley, New York.

Benson B.B. and Krause D., 1976. Empirical laws for dilute aqueous solutions of non-plolar gases. J. Chem. Phys., v64 p639-.

Benson B.B. and Parker P.D.M.,1961. N2/Ar and N-isotope ratios in aerobic seawater. Deep Sea Res., v7 p 237-253.

Bernatowicz, T.J., Podosek, F.A., Honda, M., and Kramer, F.E., 1984. The atmospheric inventory of xenon and noble gases in shales: the plastic bag experiment. J. Geophys. Res. 89, 4597-4611.

Berner R.A., 1971. Principles of chemical sedimentology. McGraw Hill, New York.

Bloch, S., and Key, R.M., 1981. Modes of formation of anomalously high radioactivity in oil field brines. Bull. Am. Assoc. Petroleum. Geol., 65, 154-159.

Bogard, D.D., 1971. Noble gases in meteorites. U.S. National Report 1967-1971, Fifteenth General Assembly, IUGG.

Bremner J.M. and Keeney D.R., 1965. Steam distillation methods for determination of ammonium nitrate and nitrite. Anal. Chim. Acta. v 32 p485-495.

Broecker, W.S., 1974. Chemical Oceanography. Harcourt Brace Jovanovitch.

Bronlow, W.S., 1979. Geochemistry. Prentice Hall.

Bulashevich, Yu.P. and Bashorin, V.N., 1971. Correlation of high helium concentrations in subsurface waters with intersections of distinctive fractures. Dokl. Acad. Nauk. SSSR, 69, 829-832.

Carlston, C.W., Thatcher, L.L., Rhodehamel, E.C., 1960. Tritium as a hydrologic tool, the Wharton Tract study. Intern. Assoc. Sci. Hydrol. Publ. No.52, 503-512.

Chebotarev, I.I., 1955. Metamorphism of natural waters in the crust of weathering. Geochim, Cosmochim. Acta., v8, 22-48, 137-170, 198-212.

Chirkov, A.M., 1971. Rn-222 content in the thermal springs of Kamchātka. Dokl. Acad. Sci. Sect., v199, p196-197.

Clarke, W.B., Beg, M.A., and Craig, H., 1969. Excess He-3 in the sea: evidence for terrestial primordial helium. Earth Planet. Sci. Lett., v6, p213.

Clarke, W.B. and Kugler, G., 1973. Dissolved helium in groundwater: a possible method for uranium and thorium prospecting. Econ. Geol., 68, 243-251.

Clayton, R.N., Friedmann, I., Graf, D.L., Mayeda, T.K., Meents, W.F., Shimp, N.F., 1966. The origin of saline formation waters: 1. Isotopic composition: J. Geophys. Res. 71, 3869-3882.

Cook, F.D.,Wellman, R.P., and Krouse, H.R., 1970. Nitrogen isotope fractionation in the nitrogen cycle. Int. Symp. on Hydrogeochemistry and Biochemistry. Tokoyo, Sept. 6-12th, 1970. Paper B1/6.

Cowart, J.B. and Osmond, J.K., 1971. U-234 and U-238 in the Carrizo Sandstone aquifer of South Texas. IAEA-SM-182/35, p131-149.

Craig, H., 1953. The geochemistry of the stable carbon isotopes. Geochim. Cosmochim, Acta. v3, p 53-92.

Craig, H., 1961. Standards for reporting concentrations of deuterium and oxygen-18 in natural waters. Science, v133, p1833.

Craig, H., 1966. Isotopic composition of the Red Sea and Salton sea geothermal brines. Science, v154, p1544-1548.

Craig, H., Clarke, W.B., and Beg, M.A., 1975. Excess He-3 in deep water of the East Pacific Rise. Earth Planet. Sci. Lett., v26, p126.

Craig, H. and Lupton, J,E., 1976. Primordial Neon Helium and Hydrogen in oceanic basalts. Earth Planet Sci. Lett., v31, p369-385.

Clarke, W.B. and Kugler, G., 1973. Dissolved helium in groundwater: a possible method for uranium and thorium prospecting. Econ. Geol., 68, 243-251.

Crovetto, R., Fernandez-Prini, R. and Japas, L.M., 1981. Solubilities of inert gases and methane in H2O and D2O in the temperature range of 300K-600K. J.Chem. Phys., v76 p1077-1086.

Davis, S.N.(ed.) 1978. Workshop on dating old groundwater. Dept. Hydrol. and Water Resources. Univ. of Arizona, report on contract to Union Carbide Corp. in Oak Ride.(Y/OW1/SUB-78/55412)

Davis, S.N. and DeWeist, R.J.M., 1966. Hydrogeology. Wiley and Sons, New York.

Dalrymple, G.B., and Lanphere, M.A., 1969. Potassium-Argon dating. W.H. Freeman and Co. San Fransisco.

Damon, P.E. and Kulp, J.L., 1958. Inert gases and the evolution of the atmosphere. Geochim, Cosmochim. Acta, v13, p280-292.

Damon, P.E. and Green, W.D., 1963. Investigations of the He age method by stable isotope dilution methods. Radioactive Dating, Vienna. IAEA, 55-71.

Dansgaard, W., 1964. Stable isotopes in precipitation. Tellus, v16 p436-468.

Darling, W.G., Bath, A.H. and Brunsdon, A.P., 1982. Revised procedure for the measurement of hydrogen and oxygen stable isotopes in water sample. Stable Isotope Technical Report No.16, I.G.S. Geophysics and Hydrology Division, Wallingford.

Davis, G.H., 1966. In: guidebook on nuclear techniques in hydrology, IAEA, Vienna.

Davis, S.N., Report of workshop on dating old groundwater. Univ. of Arizona, Tucson, Ariz.

Delwiche, C.C., 1970. The Nitrogen Cycle. Sci. Am., v223 p137-146.

Dincer, T., Al-Mugrin, A., and Zimmerman, U., 1974. Study of the infiltration and recharge through the sand dunes in arid zones with special reference to the stable isotopes and thermonuclear tritium. J. Hydrol., v23.

Domenico, P.A., 1972. Concepts and models in groundwater hydrology. Mc-Graw Hill New York.

Douglas, E., 1964. Solubilities of oxygen, argon and nitrogen in distilled water. J. phys. Chem. 68, 169.

Dyke, W., Jonasson, I.R. and Hard, R.F., 1976. Uranium prospecting with Rn-222 in frozen terrain. J. Geochem. Expl., v5, p115-127.

Dymond, J. and Hogan, L. 1973. Noble gas abundance patterns in deep sea basalts - primordial gases from the mantle. Earth Planet. Sci. Lett., v20, p131.

Eberhardt, P., Eugster, O., Marti, K., 1965. A redetermination of the isotope composition of atmospheric Ne. Zeitschrift fur Naturforshing 20a, 623-624.

Edmunds, W.M., Taylor, B.J., and Downing, R.A., 1969. Mineral and thermal waters of the United Kingdom. XXIII Intrnl. geological Congress, vol. 18, 139-158.

Edmunds, W.M., Bath, A.H., Miles, D.L., 1982. Hydrochemical evolution of the East Midlands Triassic sandstone aquifer, England. Geochim. Cosmochim. Acta 46, p2069-2081.

Elmore, D., Fulton, B.R., Clover, M.R., Marsden, J.R., Gove, H.E., Naylor, N., Purser, K.H., Rilius, L.R., Beukens, R.P., and Litherland, A.E., 1979. Analysis of Cl-36 in environmental water samples using an electrostatic accelerator, Nature 277, 22-25.

Esfandiari, B., 1969. Geochemistry and geology of helium. Norman, Okla.; Univ. Oklahoma. Ph.D. thesis.

Evans, G.V., Otlet, R.L., Downing, R.A., and Roe, G., 1978. Some problems in the interpretation of isotope measurements in United Kingdom aquifers. Isotope Hydrol., v2. I.A.E.A., Vienna.

Evans, G.V., Otlet, R.L., Downing, R.A., Monkhouse, R.A. and Rae, G., 1978. Some problems in the interpretation of isotopic measurements in British Aquifers. IAEA (UNESCO) Int. Symp. on Isotope Hydrol. Neutherberg, GDR.

Evans, R.D. and Goodman, C.,1941. Radioactivity of rocks. Bull. Geol. Soc. Am., v52, p459.

Faul, H., 1954. Nuclear Geology. Wiley New York.

Faul, H., Gott, G.B., Manger, G.E., Mytton, J.W. and Sakakura, A.Y., 1954. Radon and Helium in natural gas. Compt. Rend. 19e Congr. Geol. Intern. Alger., Sec 9, p339-348.

Ferguson, C.W., 1968. Bristecone pine: science and esthetics. Science, v159, p839-846.

Fiege, Y., Ottman, B.G., and Kastner, K., 1968. Production ratio of neutrons in soils due to natural radioactivity. J. Geophys. Res., v73, 3135-3142.

Fisher, D.E., 1974. The planetary primordial component of rare gases in the deep earth. Geophys. Lett., v1, p161.

Fleischer, M. and Parker, R,.L., 1967. Data of geochemistry: composition of the earths crust. U.S. Geol. Surv. Prof. Pap. 440-D.

Fleming, W.H. and Thode, H.G., 1953. Neutron and spontanoeus fission in uranium ores. Phys. Rev., v92, p376-382.

Fluss, M.J., Dadley, N.D., Malewicki, R.L., 1972. Tritium and alpha particle yields in fast and thermal neutron fission of U-238. Phys. Rev. C, v6, 2252-2259.

Focht, D.D., 1978. Methods for analysis of denitrification in soils. Nitrogen in the Environment. v2. Neilson, D.R.(ed), Academic Press.

Folland, K.A., 1974. Ar-40 diffusion in homogenous orthoclase and an interpretation of Ar diffusion in K feldspars. Geochim. Cosmochim. Acta., v38, 151-166.

Fontes, J.C. and Garnier M.J. , 1976. Correction des activites apparent on C-14 de cassons dessous-estimation de la vitesse des eaux en nappes captives. C.R. Rennie Annu. Sci. Terre. Soc. Geol. Fr. Paris.

Fritz, P., Barker, J.F., Gale, J.E., Andrews, J.N., Kay, R.L.F., Lee, D.J., Cowart, J.B., Osmond, J.K., Payne, B.R., and Witherspoon, P.K., 1979. Geochemical and hydrochemical investigations at the Stripa test site (Sweden). Int. Symp. on the underground disposal of radioactive wastes, IAEA-SM-243/6.

Fritz, P., Barker, J.F., Gale, J.E., 1979. Geochemistry and isotope hydrology of groundwater in the Stripa Granite. Results and preliminary interpretation. Lawrence Berkley Lab. Report., LBL-8285, Berkley California.

Gale, N.H., 1967. Development of delayed neutron techniques as rapid and precise method for determination of uranium and thorium at trace levels in rocks and minerals, with applications to isotope geochronology. In: Radioactive dating and methods of low level counting. IAEA, Vienna.

Garnish, J.D., 1976. Geothermal Energy: The case for research in the United Kingdom. A report prepared for the Dept. of Energy, Energy Papers Number 9, HMSO. London.

Gasper, E., and Onescu, M., 1972. Radioactive tracers in hydrology. Elsevier Amsterdam.

Gerling, E.K., 1939. Part taken by close packing of crystals in the diffusion of helium. Compt. rend. acad. sci. U.R.S.S., v24, p274-277.

Gerling, E.K., Mamyrin, B.A., Tolstikhin, I.N., and Yakovleva, S.S., 1971. Isotope Composition of helium in rocks. Geokhimiya, v5, 608-617.

Giletti, B.J. and Kulp, J.L., 1955. Radon leakage from radioactive minerals. Am. Mineralogist, 40, 481-496.

Giletti, B.J. and Tullie, J., 1977. Studies on diffusion-IV Pressure dependance of Ar diffusion in phlogopite. Earth and Planet. Sci. Lett.,v 35, 180-183.

Goldbrunner, J.E., 1984. Zur Hydrogeologie des oberos-terreichishchen Molassebeckens: Steir. Beitr. z. Hydrogeologie, 36, 83-100.

Goldschmidt, V.M., 1958. Geochemistry. Ed. A. Muir, Oxford University Press.

Graf, D.L., 1982. Chemical osmosis, reverse chemical osmosis, and the origin of subsurface brines. Geochim. Cosmochim. Acta. 46, 1431-1448.

Hanshaw, B.B., Back, W. and Rubin, M., 1965. Radiocarbon determinations for estimating groundwater flow velocities in central Florida. Science v148, p494-495.

Heaton, T.H.E., and Vogel, J.C., 1981. Excess air in grounwater. J. Hydrol., v50 p200-216.

Heaton, T.H.E., and Vogel, J.C., 1979. Gas composition and ages of groundwaters in Beaufort Group Sediments. South Africa Water, S.A., v5, 160-170.

Heckter, M., 1934. Radiochemische oberflachembestimmung an glas. Glastech. Ber., v12 156-172.

Hill, R.D., 1941. Production of Helium-3. Phys. Rev. v69, p671-672.

Hitchon, B., and Friedman, I., 1969. Geochemistry and origin of formation waters. in the Western Canada sadimentary basin-1. Stable isotopes of hydrogen and oxygen: Geochim. Cosmochim. Acta., 33, 1321-1349.

Hoefs, J., 1980. Stable isotope geochemistry. 2nd ed. Springer Verlag. New York.

Hollander, J.M., Periman, I. and Seaborg, G.T., 1953. The table of the isotopes. Rev. Mod. Phys., v25, p459-651.

Holmes, A., 1931. Radioactivity and geological time. Physics of the Earth, IV, Nat. Research Council (U.S.) Bull., v80, p124-459.

Hooker, P.J., Betrami, R., Lombardi, S., O'Nions, R.K., Oxburgh, E.R., Helium-3 anomalies and crust mantle interaction in Italy. Geochim. Cosmochim. Acta., v49, 2505-2514

Hurley, P.M., 1954. The Helium age method and the distribution of helium in rocks. In: Nuclear Geology, Faul, H. ed. Wiley New York.

Ingerson, E. and Pearson, F.J., 1964. Estimation of age and rate of movement by groundwater by the C-14 method. Recent researches in the field of hydrosphere, atmospheric and nuclear chemistry. Manizen, Tokoyo, p263-283.

Ingrid, U.O. and Karlen, I., 1963. The half life of C-14 and the problems which are encountered in absolute measurements of beta decaying gases. In Radioactive Dating, IAEA, Vienna.

International Critical Tables of numerical physics,. 1928. v3.

Jambon, A., and Shelby, J.E., 1980. Helium diffusion and solubility in obsidians and basaltic glasses in range 200-300 C. Earth Planet. Sci. Lett., v51, 206-214.

Janoschek, R., 1964. Das Tertiar in Osterreich, Mitt. Geol. Ges. Wien 56, 319-360.

Jenkins, W.J., Rona, P.A., Edmond, J.M., 1980, Excess He-3 in the deep water over the mid-Atlantic ridge at 26 deg N. Earth and Planet. Sci. Lett., v49, 39-44.

Joly, J.J., 1910. The amount of Thorium in sedimentary rocks;2: Arenaceous and Argillaceous rocks. Phil. Mag. (6), v20, p353-357.

Jost, W., 1952. Diffusion in solids, liquids and gases Academic press Inc., New York.

Keevil, N.B., 1942. The distribution of Helium and radioactivity in rocks, II: Mineral seperates from Cape Ann Granite. Am. J. Sci., v240, p13-21.

Kenny, A.W., Crooks, R.N., and Kerr, J.R.W., 1966. Radium, radon and daughter products in certain drinking waters in Great Britain. J. Inst. Water Eng., v20, p123-134.

Khlopin, V.G. and Abidov, Sh.A., 1941. Radioactivity and helium content of beryllium, boron and lithium minerals of the USSR. Compt. rend. acad. Sci. URSS, 32, 637-640.

Kigoski, K. 1971. Alpha-recoil thorium-234: dissolution into water and the uranium isotopic variations in nature. Science v 173, p47-48.

Kronfield, J., Gradsjtajn, E., Muller, H.W., Radin, J., Yaniv, A. and Zach, R., 1975. Excess U-234: an aging effect in confined waters Earth planet. Sci. Lett., v27, p342-345.

Kunz, W., and Schintlemeister, I., 1965. Tabellen der Atomekerne Teil II, Kernreaktionen Akademie - Verlag Berlin.

Kurz, M.D., and Jenkins, W.J., 1981, The distribution of helium in oceanic basaltic glasses. Earth Planet. Sci. Lett., v53, 41-54.

Lambert, I.B., and Heier, K.S., 1968. Estimates of the crustal abundance of thorium, uranium, and potassium. Chem. Geol. , v3, 233-238.

Lal, D. and Peters, B., 1962. Cosmic ray produced isotopes and their application to problems in geophysics.In: Progress in Elementary particles and cosmic ray physics. North Holland Publ. Co. Amsterdam. v6, 1-74.

Larson, E.S. and Phair, G., 1954. The distribution of uranium and thorium in sedimentary rocks. In: Nuclear Geology, H. Faul ed. Wiley New York.

Libby, W.F., 1946. Atmospheric helium-3 and radiocarbon from cosmic radiation. Phys. Rev., v74, p1590-1594.

Libby, W.F., 1961. Tritium Geophysics. J. Geophys. Res, v66.

Loosli, H.H., 1983. A dating method with Ar-39. Earth Planet Sci. Lett., 63, 51-62.

Lord Rayleigh, 1939. Nitrogen, argon and neon in the earths crust with applications to cosmology. Proc. Roy. Soc. London, A170 p451.

Lovelock, P.E.R., 1977 . Aquifer properties of the Permo-Triassic sandstones in the U.K. Inst. Geol. Sci. Bull., No 56.

Lowder, W.M. and Solon, L.R., 1956. Background radiation. U.S. ARC Rept. NYO-4712.

Lucas, H.F., 1957. Improved low level alpha scintillation counter for radon. Rev. Sci. Instrum. 28.

Lupton, J.E. and Craig, H., 1975. Excess helium-3 in oceanic basalts: evidence for terrestial primordial helium. Earth Planet Sci. Lett. v26, p133.

Lupton, J.E., Weiss, R.F., and Craig, H., 1977. Mantle helium in the Red Sea brines. Nature, v266, p244-246.

Macdonald, G.J.F., 1963. The escape of helium from the Earths atmosphere. Rev. Geophys., v1, p305-349.

Malzer, O., 1981. Geologische Charakteristik der Wichtigsten, Erdol und Erdgastrager der oberosterrreichen Molasse. Teil II, Die Konglomerate und Sandsteine des Oligozans, Erdol-Erdgas Z, 97, 20-28.

Mamyrin, B.A., Tolstikhin, I.N., Anufriev, G.S., and Lamanskiy, I.L., 1969. Anomalous isotopic composition of helium in volcanic gases. Dokl. Akad. Nauk. SSSR, v184, p1197-1199

Mamyrin, B.A., Anufriev, G.S., Kamenski, I.L.,and Tolsthikin, I.M., 1970. Determination of the isotopic composition of atmospheric helium. Geochem. Int. v7, 498-505.

Mamyrin, B.A., Tolstikhin, I.N., Anufriev, G.S., and Lamanskiy, I.L., 1972. Helium isotopic composition in volcanic gases of Iceland. Geokhimiya. v11, p1396.

Mamyrin, B.A., and Tolstikhin, I.N., 1984. Helium Isotopes in Nature. Elsevier Amsterdam.

Marine, I.W., 1979. The use of naturally occurring helium to estimate groundwater velocities for studies of geologic storage of radioactive waste. Water Resour. Res., v15, 1130.

Mariotti, A., 1984. Natural N-15 abundance measurments and atmospheric nitrogen standard calibration. Nature, v311 p251-252.

Mariotti, A., Germon, J.C., Leclerc, A., Catroux, G and Letolle, R., 1982. Experimental determination of kinectic isotope fractionation of nitrogen isotopes during denitrification. Stable Isotopes. Schmidt, H., Forstel, H., and Heisinger, K., Eds., Elsevier.

Matsuo, S.,Susuki, M and Miizutani, Y., 1978. Nitrogen to Argon ratio in volcanic gases. Terrestial rare gases. Alexander, E.C. Jnr. and Ozima, M. eds., Center for Academic publications, Japan.

Mazor, E. and Wasserburg, G.J., 1965. Helium, neon, argon, krypton and zenon in gas emanations from Yellowstone and Lassen volcanic National Parks. Geochim. Cosmochim. Acta., 29, 443-454.

Mazor, E., 1962. Radon and Radium content of Some Israeli water sources and a hypothesis on underground reservoirs of brines, oils and natural gasesin the Rift valley. Geochim. Cosmochim. Acta., v26, p765-786.

Mazor, E., Heymann, D., and Anders, E., 1970. Noble gases in carbonaceous chondrites. Geochim. Cosmochim. Acta., v34, p781-824.

Mazor, E., 1972. Palaeotemperatures and other hydrogeological parameters deduced from noble gases dissolved in groundwaters; Jordan Rift Valley, Israel. Geochim. Cosmochim. Acta. 36, 1321-1336.

Mazor, E. and Fournier, R.O., 1973. More on noble gases in Yellowstone National Park hot waters. Geochim. Cosmochim. Acta. 37, 515-525.

Mazor, E., Kaufman, A. and Carmi, I., 1973. Hammat Gader (Israel): geochemistry of a mixed thermal spring complex. J. Hydrol., 18 289.

Mazor, E. and Verhagen, B.Th., 1976. Hot springs of Rhodesia: their noble gases isotopic and chemical composition. J. Hydrol., 28, 29-43.

Mazor, E., 1977. Geothermal tracing with atmospheric and radiogenic noble gases. Geothermics, 5, 21-36.

Meinzer, O.E., 1923. Occurence of groundwater in the United States. U.S.G.S. water supply Pap., 489, p1-371.

Mook, W.G., 1972. On the reconstruction of the initial C-14 of groundwater from the chemical and isotopic composition. Proc. 8th Int. Conf. on radiocarbon dating, Wellington, p D32-D41.

Morrison, T.J. and Johnstone, N.B., 1954. Solubilities of the inert gases in water. J. of Chem. Soc., p3441-3446.

Morrison, P. and Pine, J., 1955. Radiogenic origin of helium isotopes in rocks. Ann. N.Y. Acad Sci., v62, p69-92.

Nagao, K., Takaoka, N., Wakita, H., Matsuo, S., Fuji, N., 1980. Isotopic composition of rare gases in Matsushiro earthquake fault region. Geochemical Journal, v14, 63-69.

Nief, G., 1960. Isotopic abundance ratios for reported for reference samples stocked by the National Bureau of Standards. ed. F. Mohler. N.B.S. Technical Note 51.

Nier, A.O., 1950a. A redetermination of the relative abundances of the isotopes of C, N, O, Ar, Kr. Phys. Rev. v77, 789-793.

Nier, A.O., 1950b. A redetermination of the relative abundances of Ne, Kr, Rb, Xe, Hg. Phys. Rev., v79, 450-454.

Nikonov, V.P., 1969. Relation of helium to petroleum hydrocarbons. Dokl. Acad. Sci. USSR, Earth Sci. Sect., 188, 199-201.

Nydal, R., 1967. On the transfer of radiocarbon in nature. In: Radiocarbon dating and methods of low level counting. IAEA, Vienna.

Oeschger, H.,1978. Some cosmic ray produced radionuclides of interest in dating old groundwater. Davis, S.N.(ed.) 1978. Workshop on dating old groundwater. Dept. Hydrol. and Water Resources. Univ. of Arizona, report on contract to Union Carbide Corp. in Oak Ride.(Y/OW1/SUB-78/55412)

O'Neil, J.R., and Kharaka, Y.K., 1976. Hydrogen and oxygen exchange reactions between clay minerals and water: Geochim. Cosmochim. Acta., 40, 241-246.

O'Nions, R.K. and Oxburgh, E.R., 1983. Heat and helium in the earth. Nature 306, 429-431.

Osmond, J.K., Kaufman, M.I. and Cowart, J.B., 1974. Mixing volume calculations, sources and aging trends of Floridan aquifer water by uranium isotope methods. Geochim. Cosmochim. Acta. v38, p 1083-1100.

Osmond, J.K. and Cowart, J.B., 1976. The theory and use of natural uranium isotopic variations in hydrology. Atomic Energy Review. v144, p621-679.

Oxburgh, E.R., O'Nions, R.K., 1986. Helium isotopes in sedimentary basins. Nature 324, 632-635.

Ozima, M. and Podosek, F.A.,1984. Noble gas geochemistry.

Paneth, F.A., 1937. Chemical exploration of the stratosphere. Nature, v139, p139-180.

Parker, R.L, 1967. Data of Geochemistry: composition of the Earths crust. U.S. Geol. Surv., Professional Paper 440-D.

Pauling, L., 1960. The nature of the chemical Bond. 3rd edition, p514, Cornell University press, Ithaca, New York.

Payne, B.R., and Halevy, E., 1968. In: guidebook of nuclear techniques in hydrology, IAEA, Vienna.

Pearson, F.J., and Hanshaw, B.B., 1970. Sources of dissolved carbonate species in groundwater and their effects on C-14 dating. Proc. Symp. Isotop. Hydrol., IAEA, Vienna, p271-286.

Pearson, F.J., and White, D.E., 1967. Carbon-14 age and flow rate in Carrizo sand Atascosa County Texas. Water Resources Research, v3(1), 251-261.

Piper, A.M., 1944. A Graphic procedure in the geochemical interpretation of water analysis. Trans. Am. Geophys. Union, v25, p 914-923.

Plummer, N.L., Jones, B.F. and Truesdell, A.H., 1970. WATEQ-F FORTRAN 4 Version of WATEQ. U.S. Geol. Surv., Water Res., Invest, 76-13.

Podosek, F.A., Honda, A.M., and Ozima, M., 1980. Sedimentary noble gases. Geochim. Cosmochim. Acta., 44, 1875-1884.

Podosek, F.A., Bernatowicz, T.J., Kramer, F.E., 1981. Adsorbtion of Xe and Kr on shales. Geochim. Cosmochim. Acta., v45, 2401-2415

Rankama, K. and Shama, Th.G., 1950. Geochemistry University of Chicago Press, London.

Rankama, K., 1963. Progress in isotope geology. Wiley New york.

Rankama, K., 1954. Isotope Geology. Pergamon, London.

Reardon, E.J. and Fritz, P. 1978. Computer modelling of groundwater C-13 and C-14 isotope compositions. J. Hydrol., v36, p201-254.

Remy, H., 1956. Treatise on inorganic chemistry. Vol 1, p237, Elsevier New York.

Ridgway, K. and Tarbuck, K.J., 1967. The random packing of spheres. Brit. chem. Eng., 12(3), 384-388.

Rightmire, C.T., 1979. Changes in formation gas composition and isotope content as indicators of unsaturated zone chemical reactions related to recharge events. I.A.E.A.-S.M./228/35, p711-732.

Roberts, A.A., Frudman, I., Donovan,T.J. and Denton, E.H., 1975. Helium survey, a possible method for locating geothermal reservoirs. geophys. Res. Letters, 2, 209-210.

Rodgers, A.S., 1956. Applications of Radon concentrations to groundwater studies near Salt Lake city and Ogden, Utah. Bull. Geol. Soc. Am., v67, p1781.

Rozanski, K., and Florkowski, T., 1978. Krypton-85 dating in groundwater: In Isotope Hydrology I.A.E.A. Vienna., v2,

Rudolph, J., Rath, H.K., Sonntag, C., 1984. Noble gases and stable isotopes in C-14 dated palaeowaters from central Europe and the Sahara. In: Isotope Hydrology p467-477, IAEA., Vienna.

Russel, H.N. and Menzel, D.H., 1933. The terrestial abundance of the permanent gases. Proc. Natl. Acad. Sci. U.S., v19, p997.

Rutherford, E., 1906. The mass and velocity of alpha particles expelled from radium and actinium. Phil. mag. (C), 12, 348-371.

Saunderson, R.T., 1960. Chemical Periodicity. p32, Reinhold, New York.

Schaffer, O.A., 1966. Direct dating of fossils by the He-U method. In: Radioactive dating and methods of low level counting. Monaco, France, Contract AT(30-1) 3029 16p.

Shillibeer, H.A. and Russel, R.D., 1955. The argon-40 content of the atmosphere and the age of the earth. Geochim. Cosmochim. Acta., v8, p16-21.

Shoor, S.K., and Gubbins, K.E., 1968. Solubility of nonpolar gases in concentrated electrolyte solutions. J. Phys. Chem., v73, p483-505.

Shotton, F.W., 1977. The Devensian Stage: its development limits and substages. Philos. Trans. R. Soc. London., Ser. B.,280, 229.

Smith, S.P. and Kennedy, B.M., 1982. The solubility of noble gases in water and in NaCl brine. Geochim. Cosmochim. Acta., V47, p503-515.

Steiger, R.H. and Jager, E.,1977. Subcommision on Geocronology convention on the use of decay constants in geo. and cosmochronology. Earth and Planet. Sci. Lett. v36, 359-362.

Stoker, A. and Kruger, P., 1975. Radon measurements in geothermal systems. Stanford University Technical Report, No.SGP-TR-4.

Stoker, A. and Kruger, P., 1975. Radon in geothermal reservoirs. Second United Nations Symposium on the development and use of geothermal resorces. San Fransisco, CA.

Strutt, R.J., 1908. Helium and radioactivity in rare and common minerals. Proc. Roy. Soc. (London), A81, 572-594.

Strutt, R.J., 1908. The accumulation of helium in geological time. Proc. Roy. Soc. (London), A81, 272-277.

Stumm, W. and Morgan, J.J., 1970. Aquatic Chemistry. John Wiley And Sons.

Suess, H.E., 1949. Abundance of rare gases on Earth and in the Universe. J. Geol., v57, p600-607.

Tanner, A.B., 1964. Physical and Chemical controls on the distribution of 226-Ra and 222-Rn in groundwaters near Great Salt Lake, Utah. In: Adams and Lowder eds. , The Natural Radiation Environment, Univ. Chicago Press.

Tanner, A.B., 1964. Radon migration in the ground: a review. In: Adams and Lowder eds., The Natural Radiation Environment, Univ. Chicago Press.

Thilo, L. and Muennich, K.O., 1970. Reliability of carbon-14 dating of groundwater, In: Isotope Hydrology, p259-270. IAEA, Vienna.

Todd, D.K., 1959. Principles of hydrology. Wiley, New York.

Tolman, C.F., 1937. Groundwater. McGraw-Hill, New York.

Tomkeieff, S.I., 1946. The Geochemistry of Uranium. Science progress, v34, p696.

Torgerson, T., Clarke, W.B., and Jenkins, W.J. The tritium/Helium-3 method in hydrology. In: Isotope hydrology II p917-930, IAEA., Vienna.

Torgerson, T., Clarke, W.B., 1985. Helium accumulation in groundwater I: An evaluation of sources and the continental flux of He-4 in Great Artesian Basin, Australia. Geochim. cosmochim. Acta. 49, 1211-1218.

Torgerson, T., Ivey,G.N., 1985. Helium accumulation in groundwater II: A model for the accumulation of the crustal He-4 degassing flux. . Geochim. cosmochim. Acta. 49, 2445-2452.

Torgerson, T., Clarke, W.B., 1985. Helium accumulation in groundwater III: Limits on the transfer across the mantle crust boundary beneath Australia, and the magnitude of Mantle outgassing. Earth and Planet. Sci. Lett. 84, 345-355.

Toth, J., 1970. A conceptual model of the groundwater regieme and the hydrogeological environment. J. Hydrol. v10, p164-176.

Tresdell, A.H., and Jones, B.F., 1974. WATEQ. A computer program for calculating chemical equilibria of natural waters. Journal U.S . Geol. Survey, 2,

Tudge, C., 1984. Whatever happens to nitrogen. New Scientist. 9th Feb., p13-15.

Vogel, J.C., Talma, A.S. anh Heaton T.H.E.,1981. Gaseous nitrogen as evidence for denitrification in groundwater. J. Hydrol., v50, p191-200.

Walker, 1977. Evolution of the atmosphere. Macmillan New York.

Walton, W.C., 1970. Groundwater Resource Evaluation. Mcgraw Hill, New York.

Ward, R.C., 1975. Principles of hydrology. McGraw-Hill New York, p183-237.

Watson, E., 1977. The periglacial environment of Great Britain during the Devensian. Philos. Trans. R. Soc. London., Ser. B., 280, 183.

Weiss, R.F., 1970. The solubility of nitrogen, oxygen and argon in water and seawater. Deep-Sea Res., v17, p721-735.

Weiss, R.F., 1971. The solubility of helium and neon in water and seawater. J. Chem. Eng. Data v16. p235-241.

Verniani, F., 1966. The total mass of the earths atmosphere. J. Geophys. Res.,v71, 385-391

Wetherill, G.W., 1954. Variations in the isotopic abundances of neon and argon extracted from radioactive minerals. Phys. Rev., v96, p679-683.

Wigley, T.M.L. 1976. Effect of mineral precipitation on isotopic copmposition and C-14 dating of groundwater. Nature, v263, p219-221.

Williams, B.P.J., Downing, R.A. and Lovelock, P.E.R., 1972. Aquifer properties of the Bunter sandstone in Nottinghamshire, England. Proc. 24th Intl. Geol. Cong., Montreal, Section II, 169.

Zaikowski, A., Kosanke, B.J., Hubbard, N., 1984. Progress in radiometric dating of Wolfcamp brines using He-4 and Ar-40. Materials Research Soc. Annual Meeting Symposium Proceedings. v 26, 943-949.

Appendix A Uranium–Radium (4n+2) radioactive series

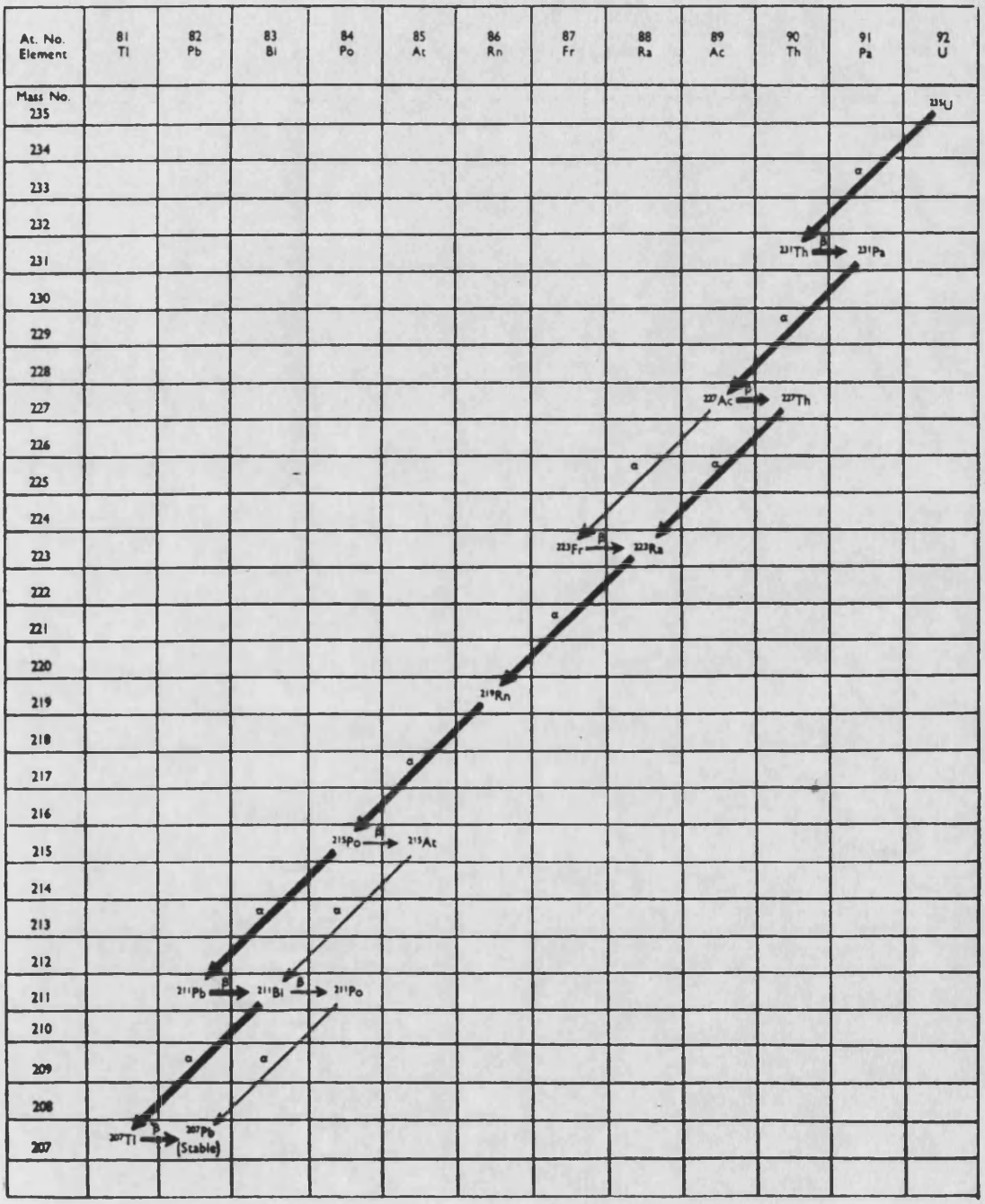

Appendix A Uranium–Radium (4n+2) radioactive series

Isotope	Half-life	α-energies MeV	β-energies MeV	γ-energies MeV	I C
Uranium-238	$4{\cdot}5 \times 10^9$ y	~4·2 — 100%	—	0·048 — 0%	23%
Thorium-234 (UX_1)	24·1 d	—	0·10 — 35% 0·19 — 65%	0·029 0·063 0·091	α — 10 α — 0·2 α — 2·5
Protactinium-234m (UX_2)	1·18 m	—	IT — 1% 0·58 — ~ 1% 1·50 — ~ 9% 2·31 — ~90%	0·75 } most 1·00 } abundant others	—
Protactinium-234 (UZ)	6·66 h	—	1·13 others	0·043 0·80 others	—
Uranium-234 (U II)	$2{\cdot}5 \times 10^5$ y	4·717 — 28% 4·768 — 72%	—	0·051 — 0%	28%
Thorium-230 (Ionium)	$8{\cdot}0 \times 10^4$ y	4·615 — 24% 4·682 — 76%	—	0·068 — 0·6% others —very weak	23·4%
Radium-226	1620 y	4·589 — 5·7% 4·777 — 94·3%	—	0·188 — ~4%	~2%
Radon-222	3·825 d	5·48 — ~100%	—	—	—
Polonium-218 (Radium A)	3·05 m	6·00 — ~100%	? — 0·02%	—	—
Astatine-218	1·3 s	6·70 — ~0·02% 6·65 — ~0·001%	? —very weak	—	—
Radon-218	$1{\cdot}9 \times 10^{-2}$ s	7·13 — very weak	—	0·61 —very weak	—
Lead-214 (Radium B)	26·8 m	—	0·59 — ~56% 0·65 — ~44%	0·24 0·30 0·35 others — weak	—
Bismuth-214 (Radium C)	19·9 m	~5·5 — 0·04%	— 0·4 — 9% 1·0 — 23% 1·51 — 40% 1·88 — 9% 3·26 — 19%	— 0·61 } most 1·12 } abundant 1·76 } 14 others to 2·43 MeV	— —
Polonium-214 (Radium C')	$1{\cdot}6 \times 10^{-4}$ s	7·68 — ~100%	—	—	—
Thallium-210 (Radium C")	1·3 m	—	1·96 — 0·04%	several —very weak	—
Lead-210 (Radium D)	22 y	—	0·017 — 85% 0·063 — 15%	0·047 — ~5%	~80%
Bismuth-210 (Radium E)	5·01 d	5·06 — $1{\cdot}7 \times 10^{-4}$%	— 1·17 — ~100%	— —	— —
Polonium-210 (Radium F)	138·4 d	5·305 — ~100%	—	0·8 — $1{\cdot}2 \times 10^{-3}$%	—
Thallium-206 (Radium E")	4·2 m	—	1·51–1·7×10⁻⁴%	—	—
Lead-206	Stable	—	—	—	—

All percentages refer to disintegrations of U–238

Appendix B Thorium (4n) radioactive series

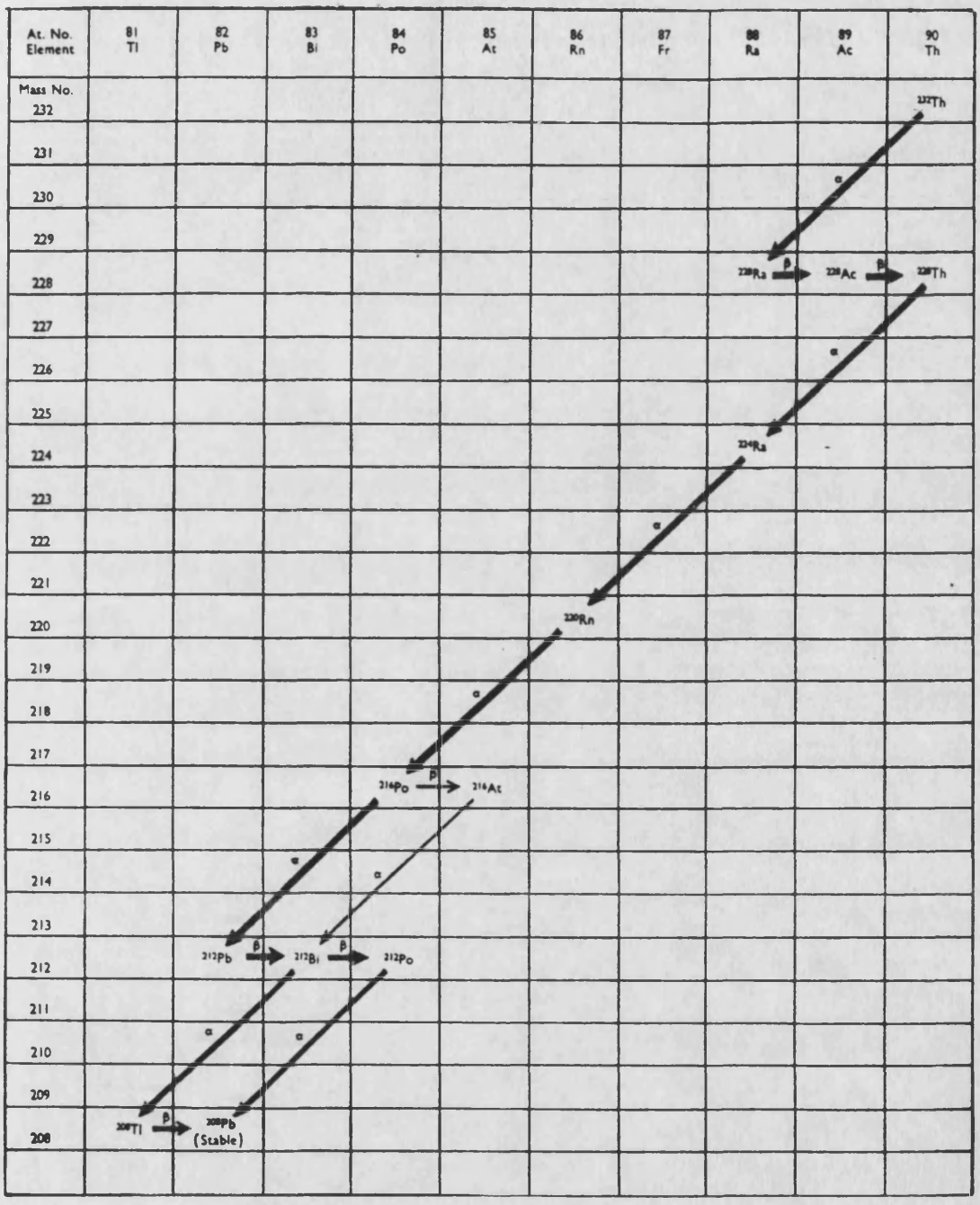

Appendix B Thorium (4n) radioactive series

Isotope	Half-life	α-energies MeV	β-energies MeV	γ-energies MeV	I C
Thorium-232	$1{\cdot}41 \times 10^{10}$ y	3·948 — 24% 4·007 — 76%	—	0·059 — 0%	24%
Radium-228 (Mesothorium-I)	6·7 y	—	~0·04 — 100%	—	—
Actinium-228 (Mesothorium-II)	6·13 h	—	1·18 — ~35% 1·76 — ~12% 2·10 — ~12% others of lower energy — 41%	0·057 to 1·64 (many energies)	—
Thorium-228 (Radiothorium)	1·91 y	~5·2 — 1% 5·338 — 28% 5·421 — 71%	—	0·084 — ~2% others — very weak	26%
Radium-224 (Thorium X)	3·6 d	5·445 — 4·9% 5·681 — 95%	—	0·241 — 3·7% others —very weak	1·3%
Radon-220 (Thoron)	54 s	6·28 —~100%	—	—	—
Polonium-216 (Thorium A)	0·158 s	6·775 —~100%	—	—	—
			? — 0·04%	—	—
Astatine-216	3×10^{-4} s	7·79 — 0·04%	—	—	—
Lead-212 (Thorium B)	10·6 h	—	0·33 — ~80% 0·57 — ~12% others of lower energy — ~8%	0·12 — 0% 0·24 — ~36% 0·30 — ~3%	3% ~36% ~1%
Bismuth-212 (Thorium C)	60·5 m	6·04 — 25% 6·08 — 10% others — 1%	—	0·04 — ~0% others — very weak	~25%
			1·52 — 5% 2·25 — 54% others of lower energy — 5%	0·73 0·79 1·08 1·62 } most abundant ~10%	—
Polonium-212 (Thorium C')	3×10^{-7} s	8·78 —~64% others of higher energy—very weak	—	—	—
Thallium-208 (Thorium C')	3·1 m	—	1·03 — 1% 1·25 — 9% 1·52 — 7% 1·79 — 19%	0·28 — ~3% 0·51 — ~8% 0·58 — 31% 0·86 — 4% 2·62 — 36%	~1% ~1%
Lead-208 (Thorium D)	Stable	—	—	—	—

All percentages refer to disintegrations of Th–232

Appendix C Uranium–Actinium (4n+3) radioactive series

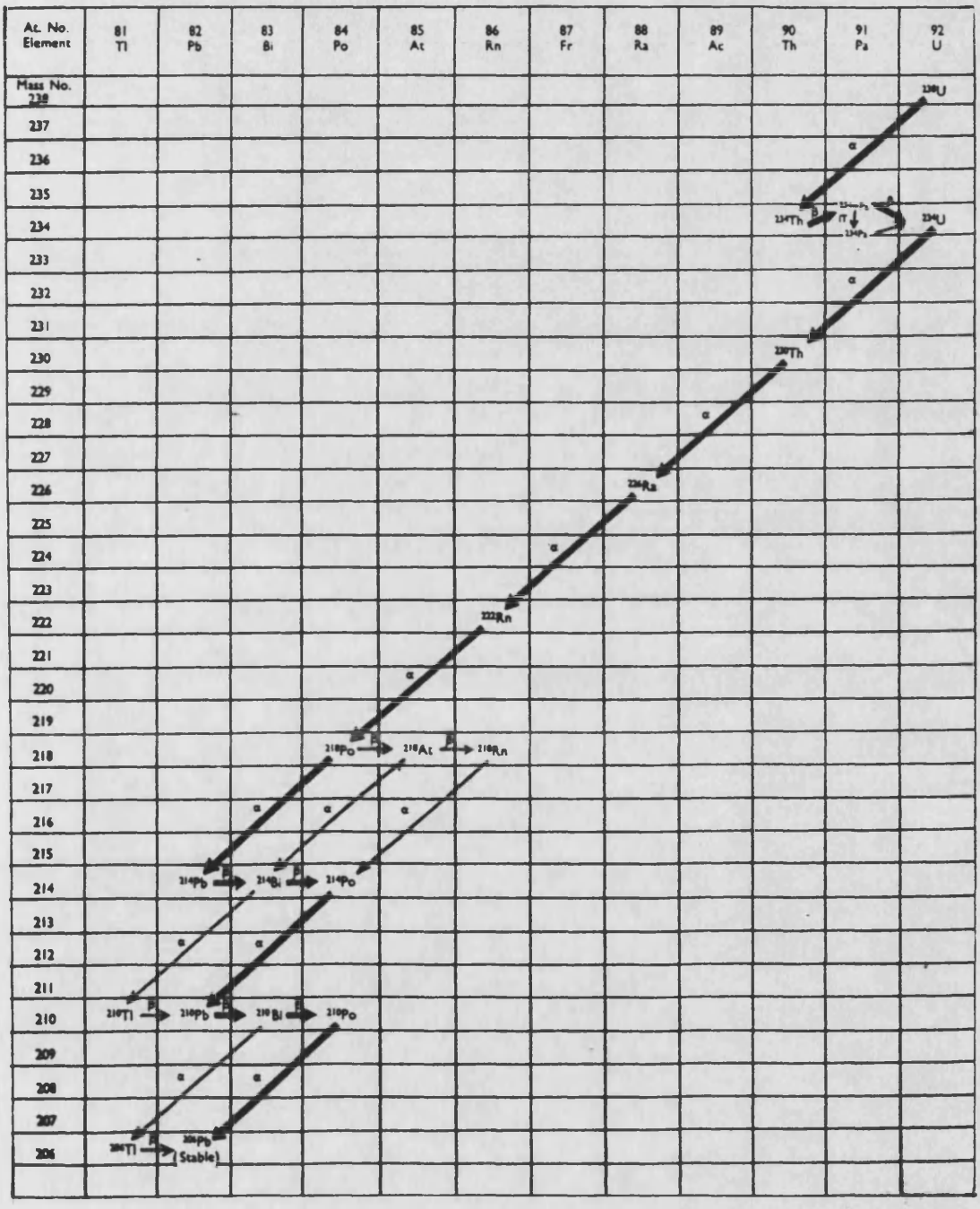

Appendix C Uranium–Actinium (4n+3) radioactive series

Isotope	Half-life	α-energies MeV	β-energies MeV	γ-energies MeV	I C
Uranium-235	7×10^8 y	4·18 to 4·56	—	0·095 — 9% 0·143 — 12% 0·185 — 55% others	—
Thorium-231 (UY)	25·6 h	—	0·30 others	0·084 others	—
Protactinium-231	$3{\cdot}4 \times 10^4$ y	4·666 to 5·046	—	0·02 to 0·39	—
Actinium-227	22 y	4·94 — 1·2%	— 0·04 — ~99%	—	—
Thorium-227 (Radioactinium)	18·2 d	5·699 — 4·0% 5·708 — 8·7% 5·712 — 5·0% 5·755 — 21% 5·865 — 3·0% 5·958 — 3·5% 5·976 — 24% 6·036 — 23% others —~7·8%	—	0·05 — ~7·5% 0·24 — ~10% many others of low energy — weak 0·0885— Ra X-rays (abundant)	
Francium-223 (Actinium K)	22 m	5·34 — very weak	1·15 — ~1%	0·05 — weak 0·08 — weak 0·21 — weak 0·31 — weak	—
Radium-223 (Actinium X)	12 d	5·534 — 10·3% 5·602 — 24% 5·712 — 50% 5·742 — 10·5% 5·830 — 0·05% 5·853 — 0·3% 5·867 — 1·0%	—	0·03 to 0·58	
Radon-219 (Actinon)	3·9 s	6·419 — 5% 6·547 — 13% 6·813 — 82%	—	0·27 — ~9% 0·40 — ~5%	~4%
Polonium-215 (Actinium A)	$1{\cdot}8 \times 10^{-3}$ s	7·360 —~100%	— ? — 0·0005%	—	—
Astatine-215	$\sim 1 \times 10^{-4}$ s	8·00 — very weak	—	—	—
Lead-211 (Actinium B)	36 m	—	~0·5 — ~20% 1·39 — ~80%	0·40 — 6% 0·43 — 6% 0·83 — 13%	—
Bismuth-211 (Actinium C)	2·16 m	6·273 — 17% 6·617 — ~83%	— ? — 0·3%	0·35 — 13%	4%
Polonium-211 (Actinium C')	0·52 s	6·57, 6·90 — weak 7·44 — ~0·3%	—	0·57 — weak 0·89 — weak	—
Thallium-207 (Actinium C")	4·79 m	—	1·44 — ~100%	—	—
Lead-207 (Actinium D)	Stable	—	—	—	—

All percentages refer to disintegrations of U–235

Appendix D Variation of the fresh water solubility of He with Temperature at Atmospheric Partial Pressure (5.2×10^{-6} atm)

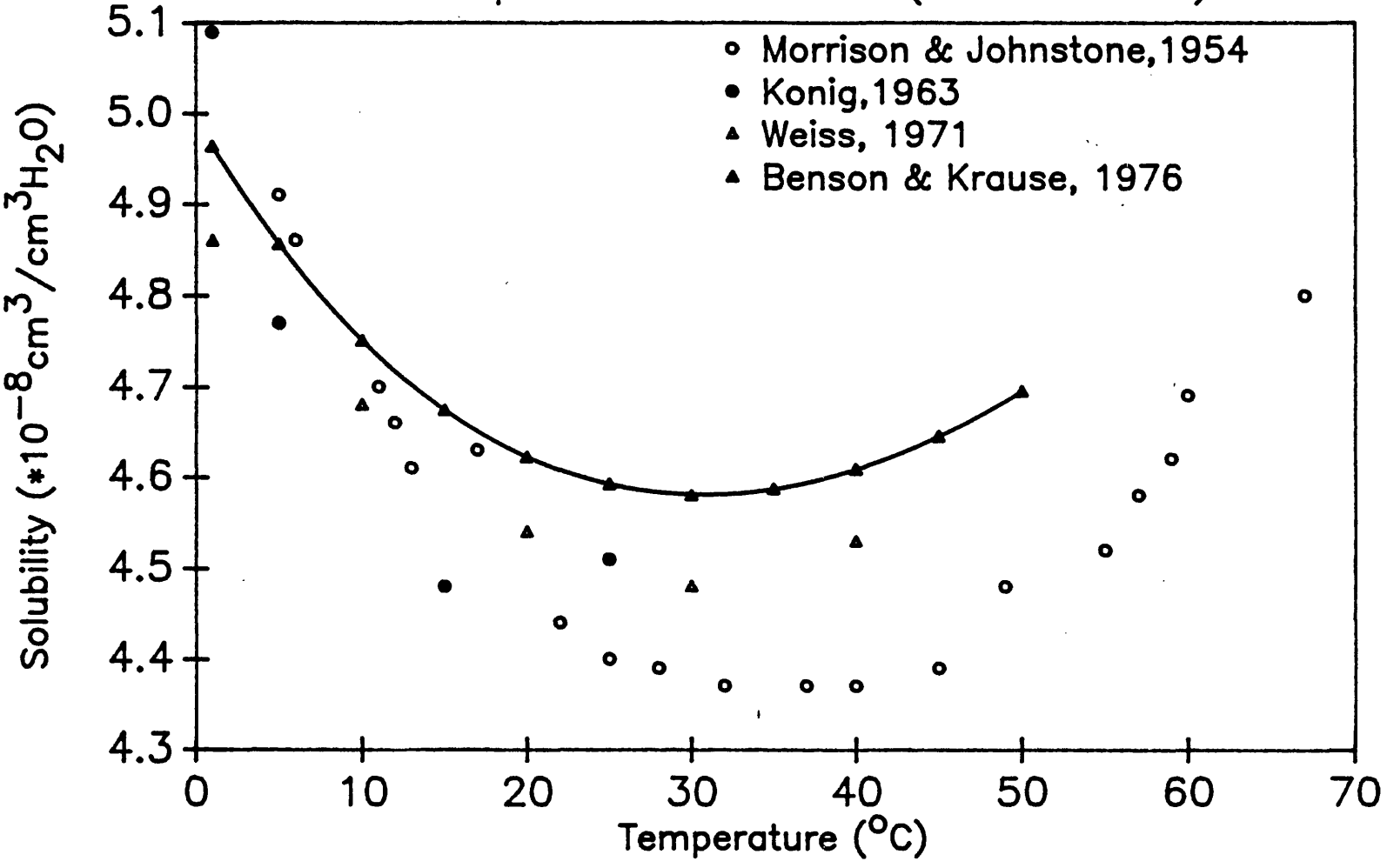

Appendix D Variation of the fresh water solubility of Ne with temperature at atmospheric partial pressure (1.81×10^{-5})

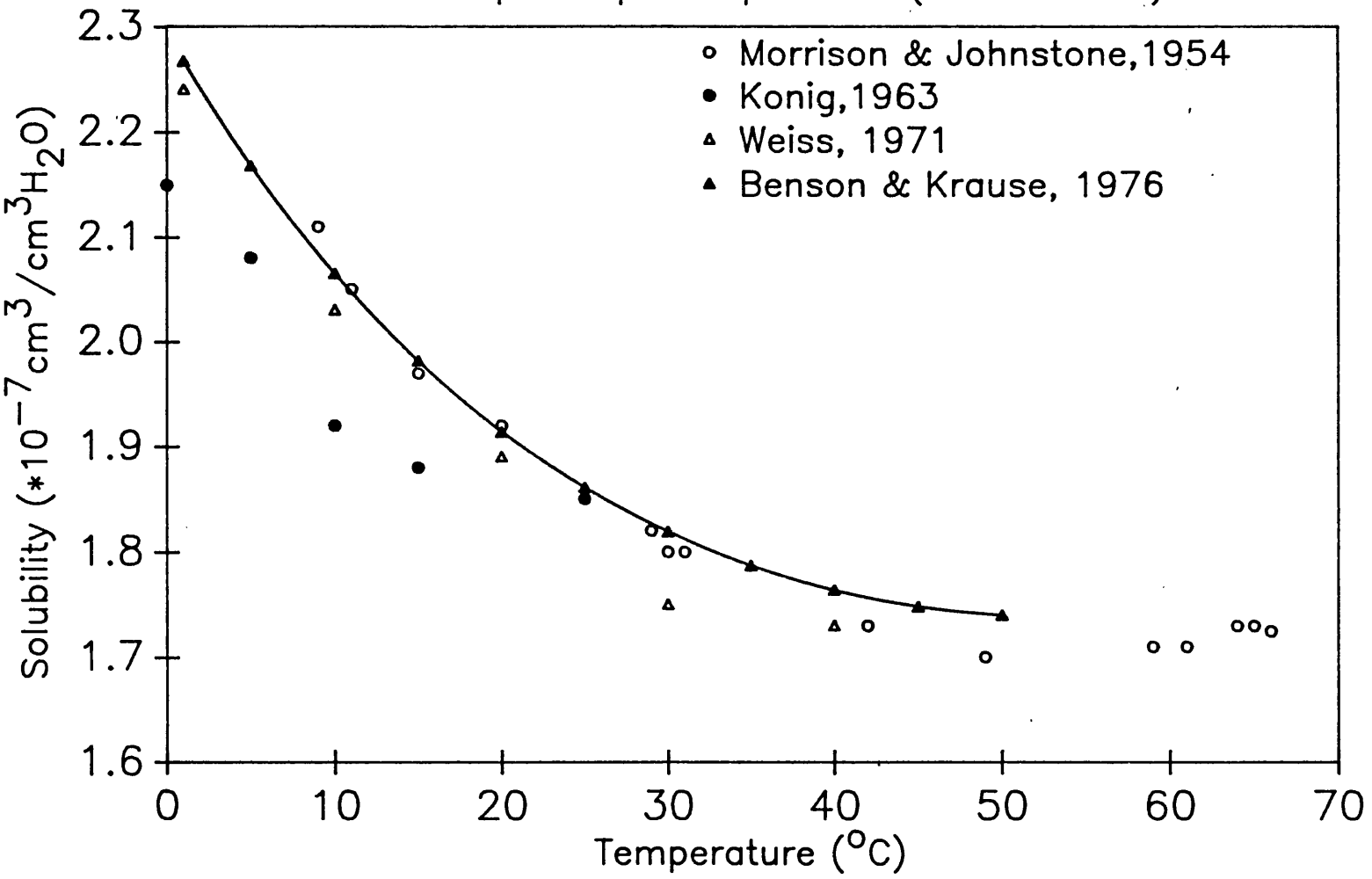

Appendix D Variation of the fresh water solubility of Ar with temperature at atmospheric partial presssure (9.56×10^{-3})

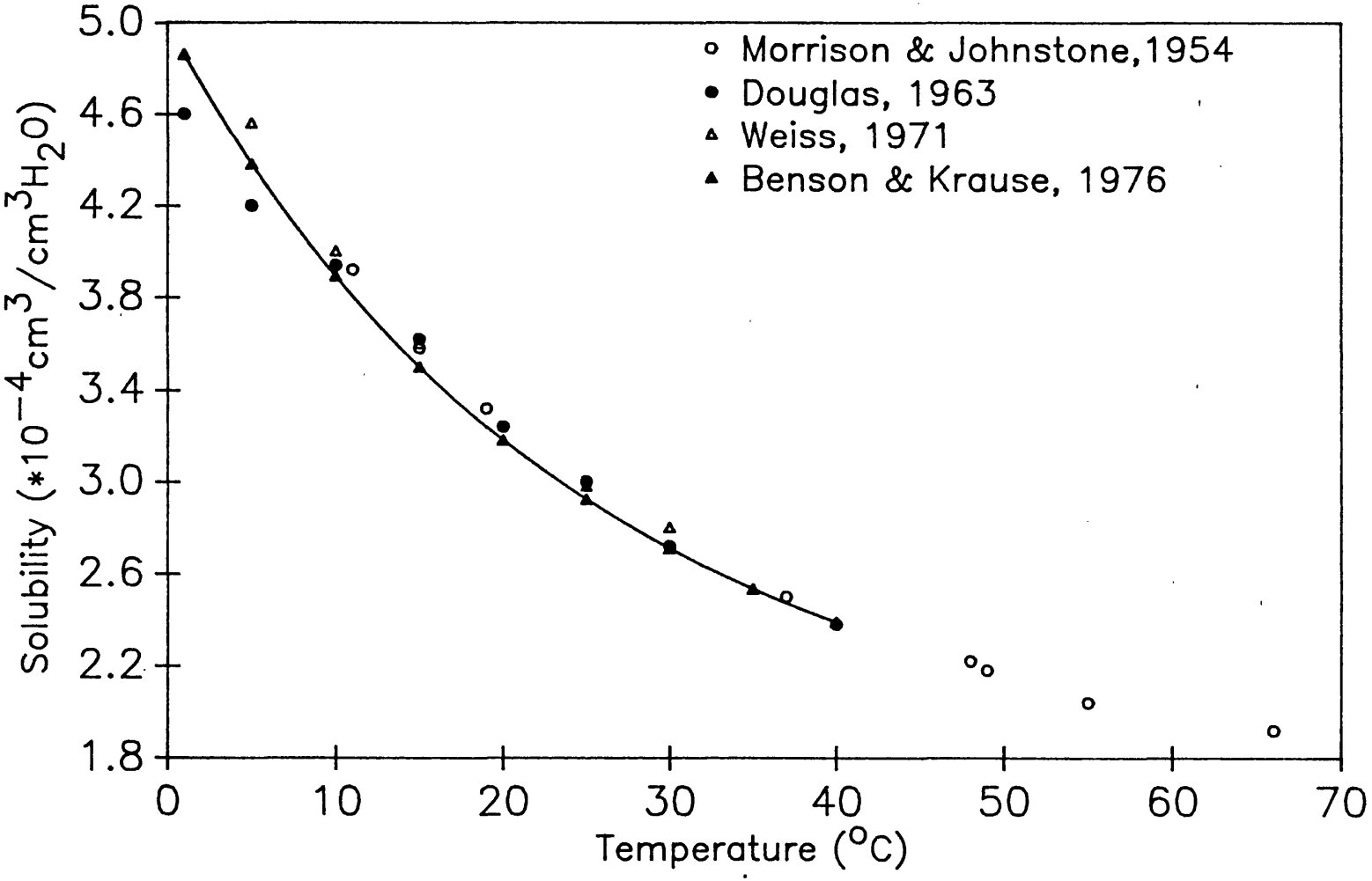

Appendix D Variation of the fresh water solubility of Kr with temperature at atmospheric partial presssure (1.14×10^{-6}atm)

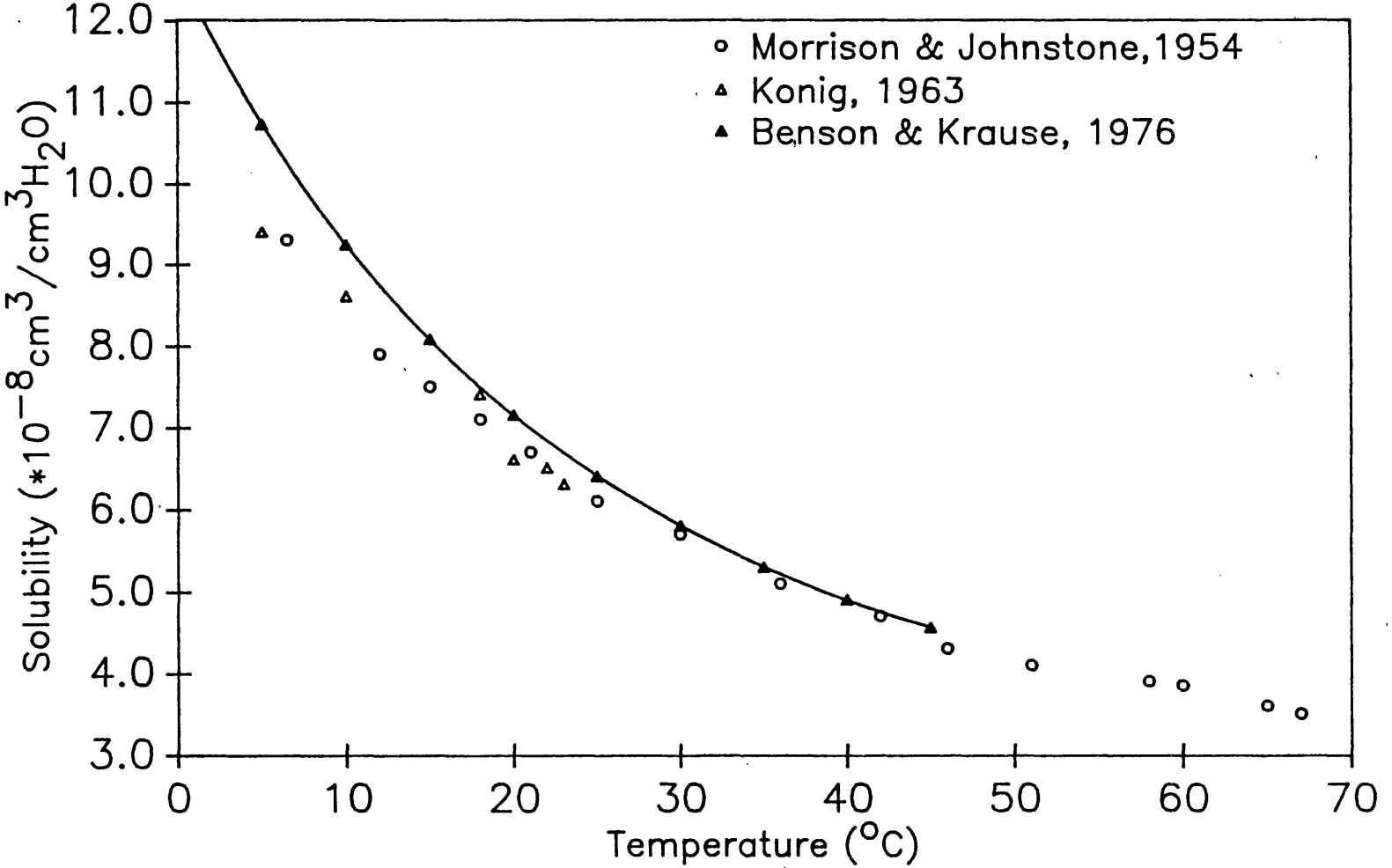

Appendix D Variation of the fresh water solubility of Xe with temperature at atmospheric partial pressure (8.7×10^{-8} atm)

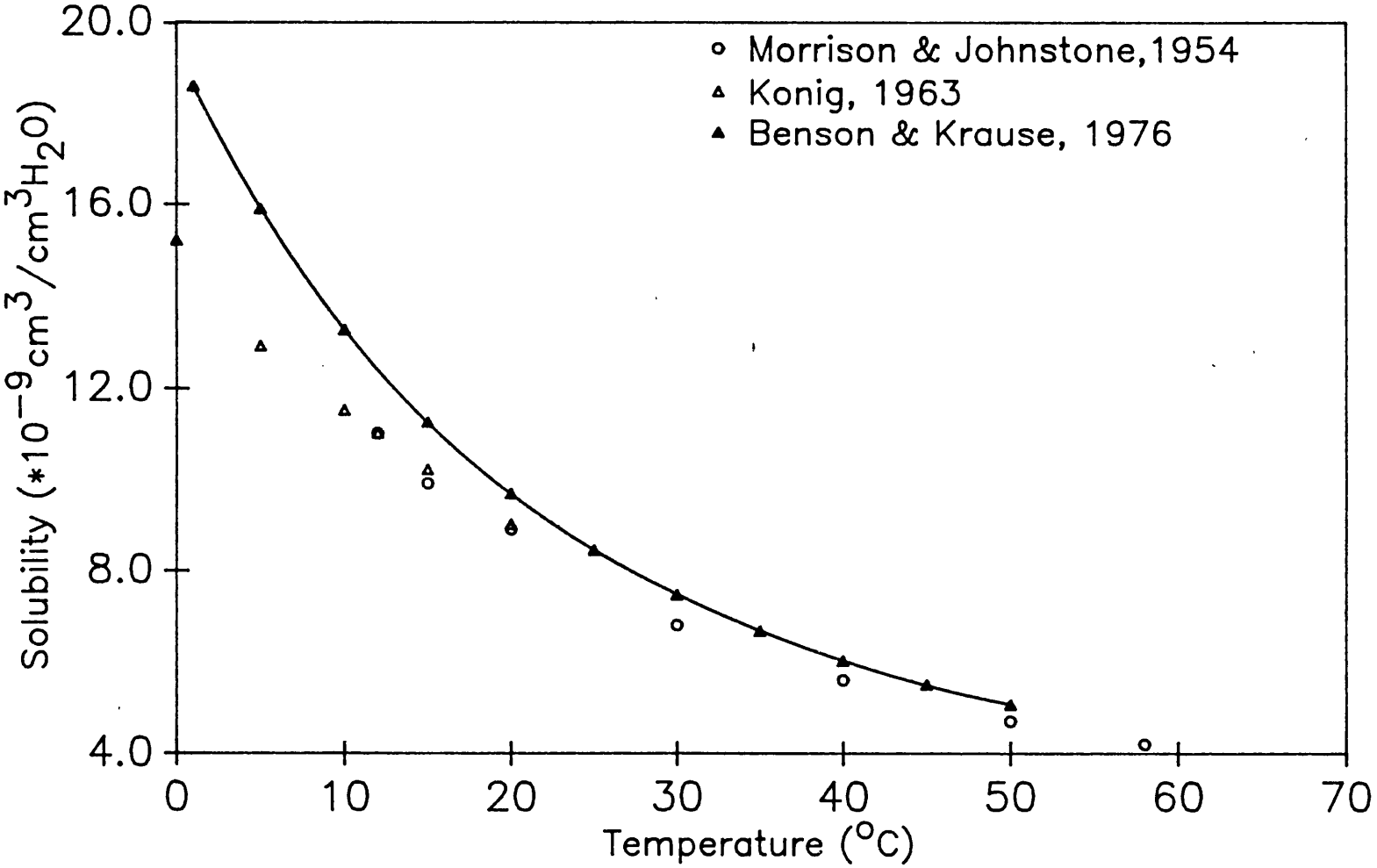

Appendix E

PROCEDURE FOR ANALYSIS OF INERT GASES IN WATER.

1.0 Sample Preparation

Valve numbers refer to figure 2.7

Samples for analysis should be approximately 5.5 cm^3 of water collected in a 3/8" (o/d) soft copper tube. These must be sealed under pressure with 'pinch-off' clamps to make a vacuum tight cold weld. The total weight of the sample tube and clamps must not exceed 500 g. Before analysis, rinse the sample tube ends with distilled water followed by acetone and dry them with warm air. Weigh the samples together with a Swagelok nut and sealing ring (which will be used to attach the sample to the gas extraction line) to +/- 0.001 g using the top pan balance.

2.0 Preparation of Samples And Gas Extraction Line Before Analysis

2.1 Close off the pumping system and then open the sample line to atmosphere. Mount two samples onto the sample inlet systems.

2.2 Using the backing pump, evacuate the line and sample inlet systems to < 0.4 mbar and then using the oil diffusion pump to < 1×10^{-7} mbar (Penning guage).

During sample pump-down the argon bulb, charcoal traps and tracer aliquot volume must also be evacuated. Simultaneously heat the charcoal traps to 350°C (furnace) and the getter to 400°C (with an internal heater current of 2.2A).

Valves open: VTR1, VAS1, VCT1 and VCT2, VAr, VS1, VS2, VMS2, VB, then VP after closing VB
Valves closed: VTR2, VAS2, VG.

Notes about the getter

During analysis the getter is continuously operated at 2.2A (400°C). It is occasionally necessary to regenerate the getter when its action becomes slow (usually after more than 30 analyses). For regeneration, the system is pumped to < 10^{-7} mbar, valves VP and VG are then kept open and the getter operated at 4.4A (750°C) for one hour.

2.3 Open VG when the pressure is < 1×10^{-7} to evacuate the getter. After a few minutes, close VG.

3.0 Analytical Procedure

3.1 Close off one of the sample inlet systems, reserving it for future analysis (VS1 or VS2). Remove the furnaces from the charcoal traps, allow to cool to room temperature and then isolate them from the line (close VCT1 and VCT2). Fill the sample inlet vapour trap with a mixture of dry ice and acetone. Close VAS1. (The air spike is only needed for calibration).

3.2 Admitting a tracer aliquot

Close diffusion pump valve VP. Fill the tracer aliquot volume from the tracer storage bulb (close VTR1, open and then close VTR2, then open VTR1 to line).

Appendix E

3.3 Admitting the sample

Remove the upper clamp from the sample and open out the 'pinched' part of the tube. Warm the copper tube with hot air to accelerate degassing (approximately 10 minutes warming time is necessary). The dry ice level must be maintained in the vapour trap during this time. After a further 5 minutes of mixing, close off the sample inlet (VS1 or VS2 as appropriate).

3.4 Gettering nitrogen from the system.

Open getter valve (VG) and monitor the pressure change on the Pirani guage. Gettering times vary from a few seconds to several minutes depending on the active gases present. Wait for the Pirani to indicate a constant pressure, usually around 10^{-3} to 3 x 10^{-2} mbar. Leave the getter valve open for the remaining steps.

3.5 Adsorbing Kr/Xe on a charcoal trap.

Cool the Kr/Xe charcoal trap in dry ice/absolute alcohol and wait for one minute. Open the valve (VCT1) on the Kr/Xe trap for 10 minutes (to adsorb krypton and xenon). During this period cool the other trap with liquid nitrogen.

3.6 Adsorbing Ar on a charcoal trap.

Close the Kr/Xe trap (VCT1) and Ar storage bulb (VAr). Open the liquid nitrogen cooled Ar-trap (VCT2) for 5 minutes to remove any Ar remaining in the line.

3.7 Separating Ar from the Kr/Xe.

Without closing the Ar trap (VCT2), open the Kr/Xe trap (VCT1) for 5 minutes to remove any Ar adsorbed with Kr/Xe, then close the Kr/Xe trap.

3.8 Measuring He and Ne isotope ratios

Meter the remaining gas in the line into the MS10 mass spectrometer (using VMS1 and VMS2) for He ion current measurements. Between 1 and 10 aliquots are usually sufficient but for high ^{4}He contents, analyses may have to be carried out on the small aliquot of gas retained for Ar analysis.

Measure the tracer and sample peak heights 5 times each for He and other gases in the following procedure. If a scale of <3 is used, then the backgrounds must also be determined after each peak.

After analysis, evacuate the MS10 to 10^{-9} using its ion pump.

3.9 Measuring Ne isotope ratios

If the He pressure is less than 10^{-4} mbar, open the MS10 to the line for Ne analysis and measure the Ne ion currents. If the He pressure is greater than 10^{-4} mbar, only a few aliquots of gas may be metered into the MS10 for analysis. Open the MS10 to the line for Ne analysis and measure the Ne ion currents.

Close the liquid nitrogen cooled Ar-trap (VCT2) and evacuate the MS10 to 10^{-9} mbar using its ion pump, and evacuate the line to 10^{-7} mbar using the diffusion pump.

Appendix E

3.10 Measuring Ar isotope ratios

Expand the contents of Ar bulb into the line (open VAR). Meter 1 or 2 aliquots of gas into the MS10 to obtain ion current for ^{40}Ar on scale.

He analysis may also be carried out at this time.

Evacuate the MS10 to 10^{-9} mbar using its ion pump, and evacuate the line to 10^{-7} mbar using the diffusion pump.

3.11 Further clean-up and desorption of Kr/Xe

a) Open the Kr/Xe trap (VCT1) for exactly 30 seconds while pumping on diffusion pump (VP Open) and then close VP.

b) Change the dry ice/ethanol on the Kr/Xe trap for a furnace at 350°C to desorb Kr and Xe.

3.12 Measuring Kr/Xe isotope ratios

After 5 minutes at 350°C, expand Kr/Xe into the line and open the MS10 (if the pressure exceeds 10^{-4} mbar, Kr/Xe must be metered into the MS10). Measure Kr and Xe isotopic ratios and backgrounds.

4.0 Cleaning the vacuum system between samples

The vacuum line must be evacuated to 1×10^{-7} mbar as in 2.2. Also, heat the two charcoal traps to 400°C whilst pumping for at least one hour.

5.0 Determination of Sample Volume

After gas extraction and analysis, remove the copper tubes complete with their clamps and Swagelock fittings. Dry them overnight in a glass drying cabinet at 80°C prior to reweighing to +/- 0.001 g. The sample volume can then be obtained from the difference in the weights of the full and empty tube.

Appendix F

Mass spectrum in Helium region for air saturated water plus tracer

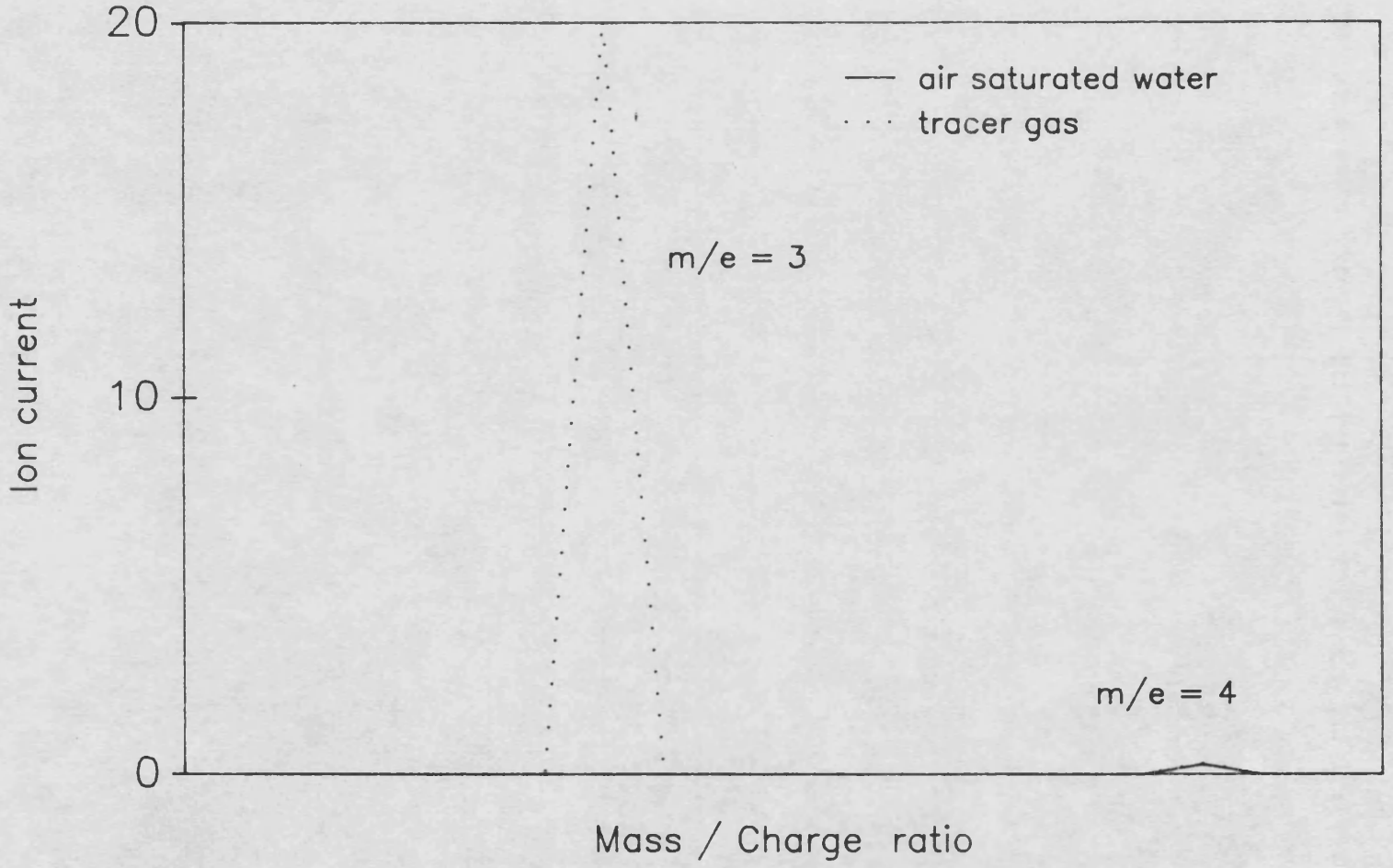

Appendix F

Mass spectrum in Neon region for air saturated water plus tracer

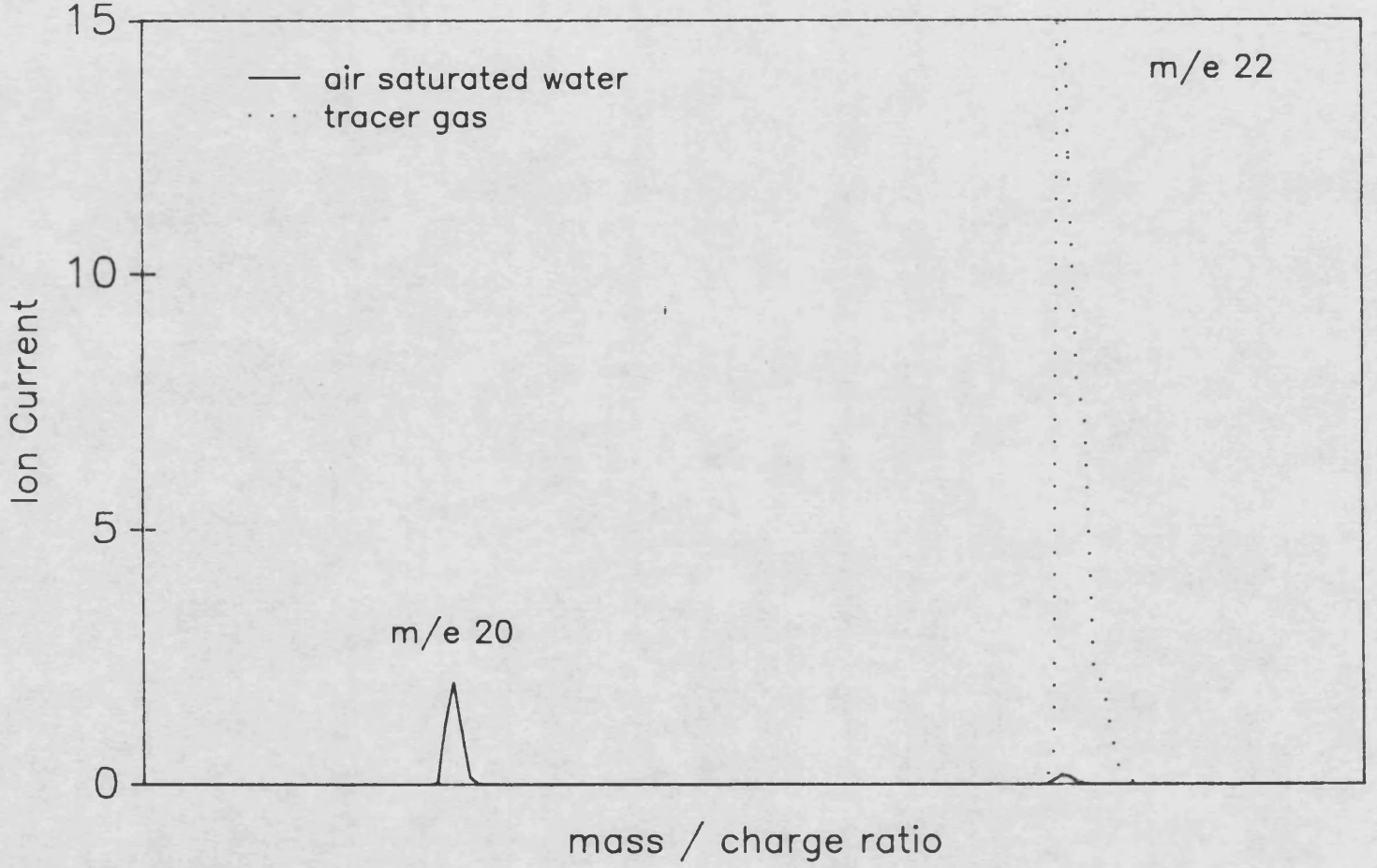

Appendix F

Mass spectrum in Argon region for air saturated water plus tracer

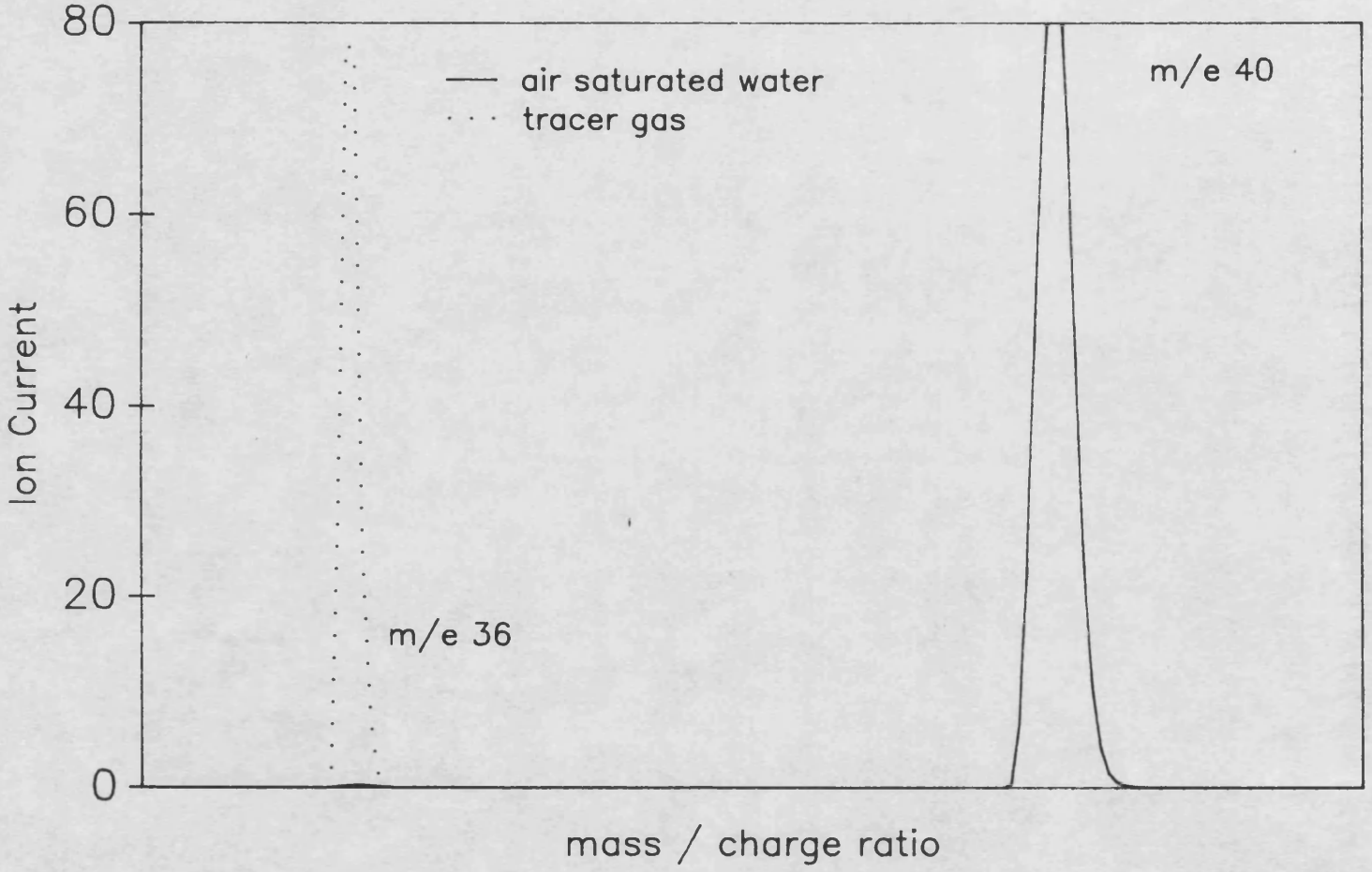

Appendix F

Mass spectrum in Krypton region for air saturated water plus tracer

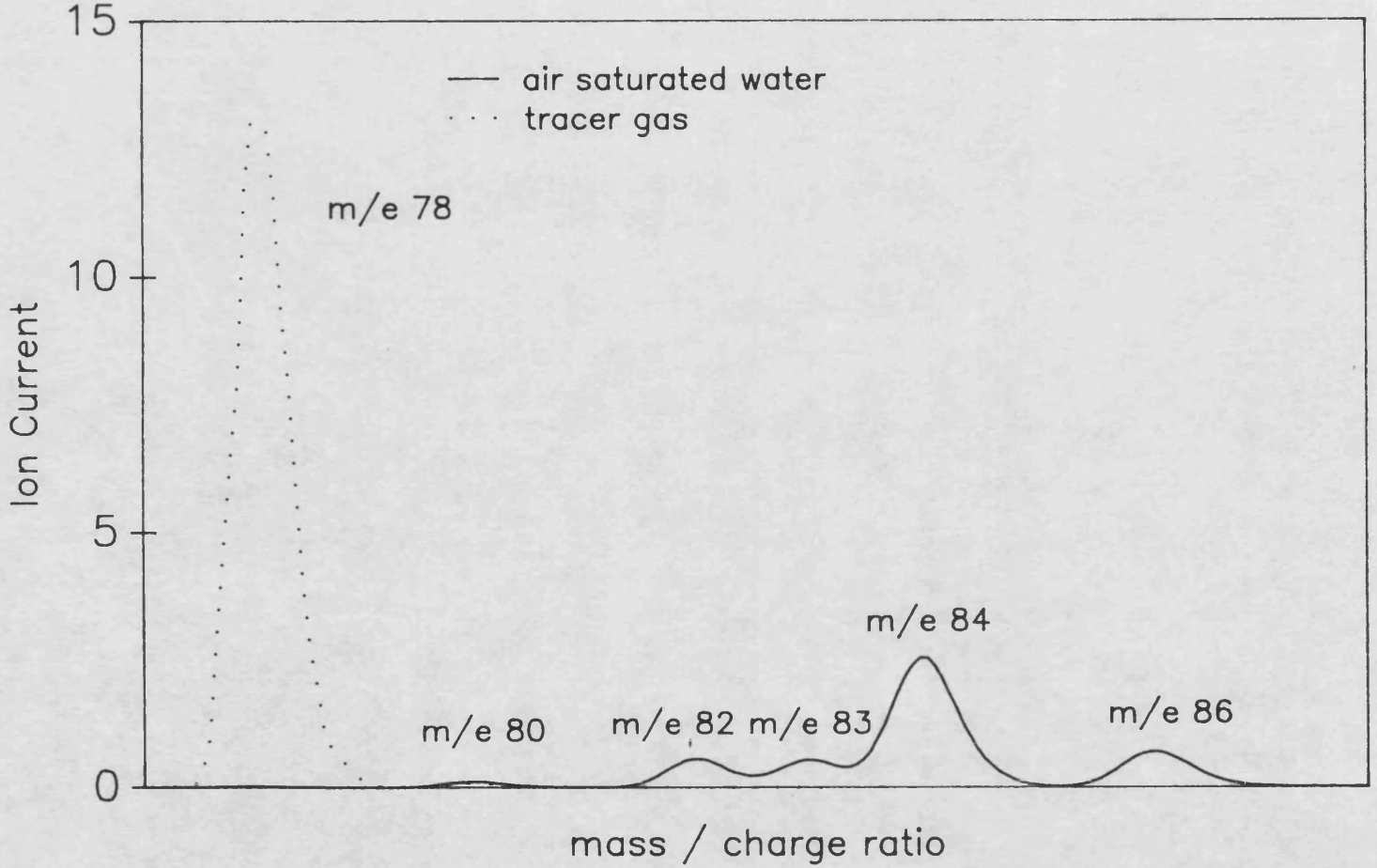

Appendix F

Mass spectrum in Xenon region for air saturated water plus tracer

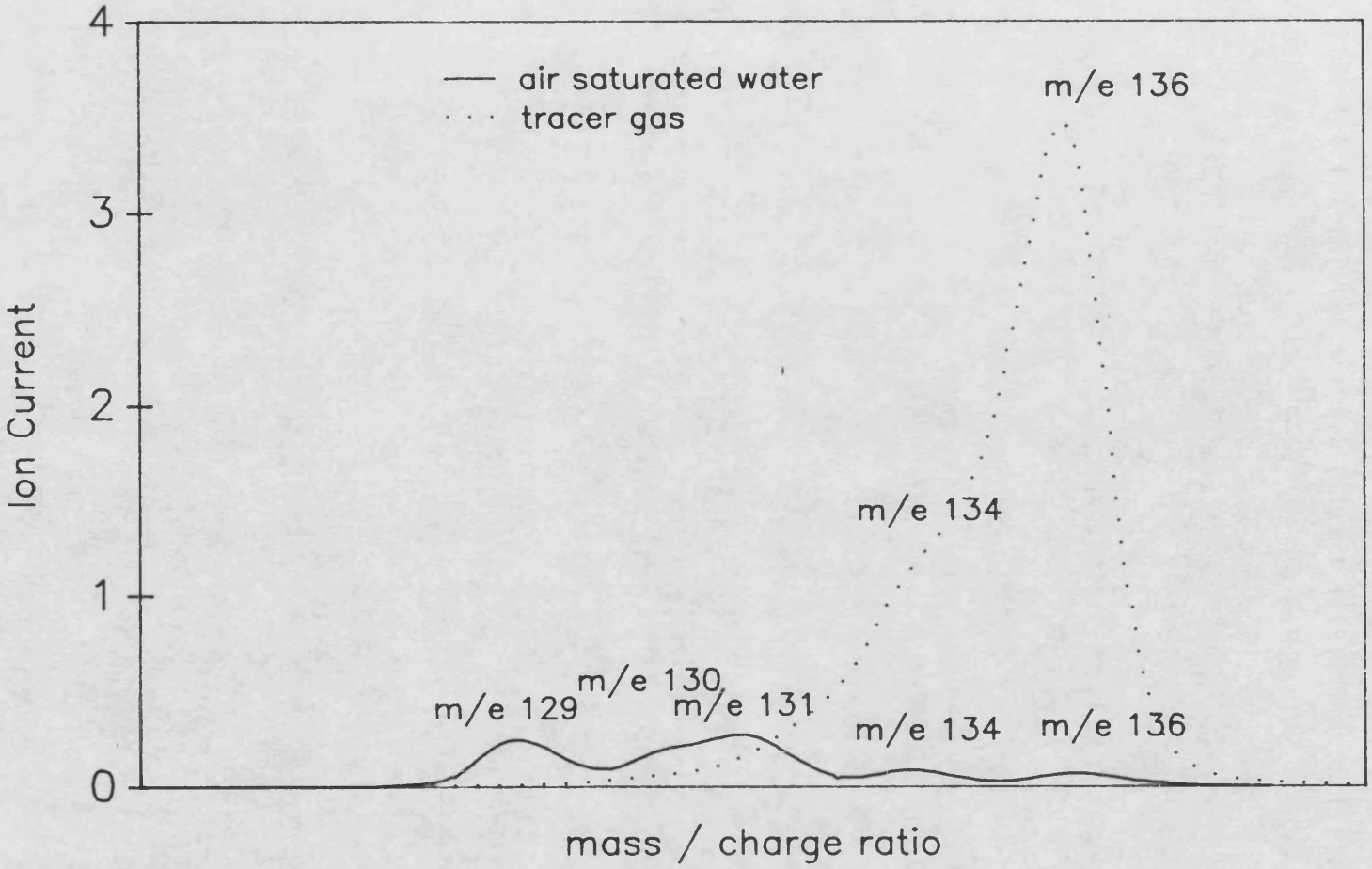

Appendix G Schematic arrangement of the Kratos MS 10 S mass spectrometer

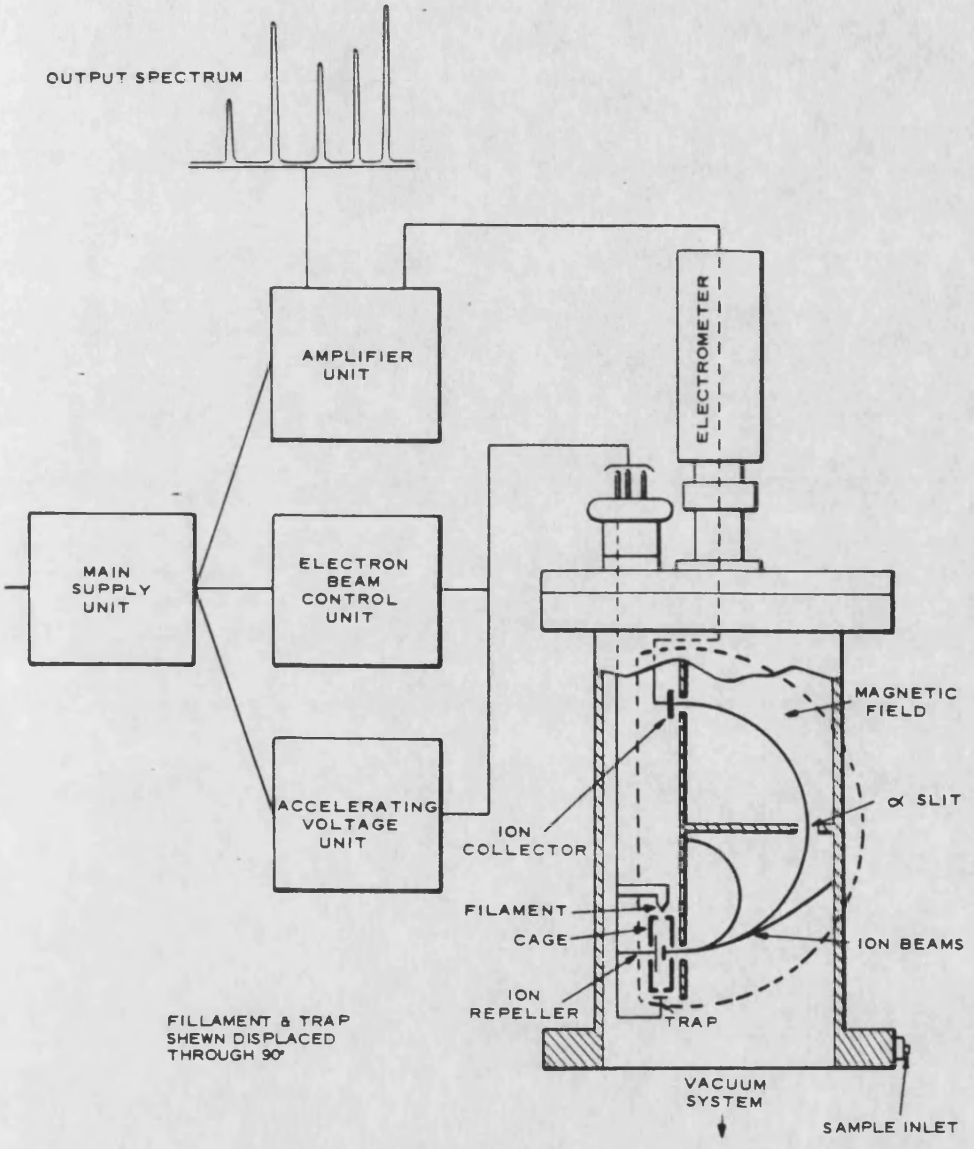

Appendix G

Ion paths in a 180^{o} deflection mass spectrometer

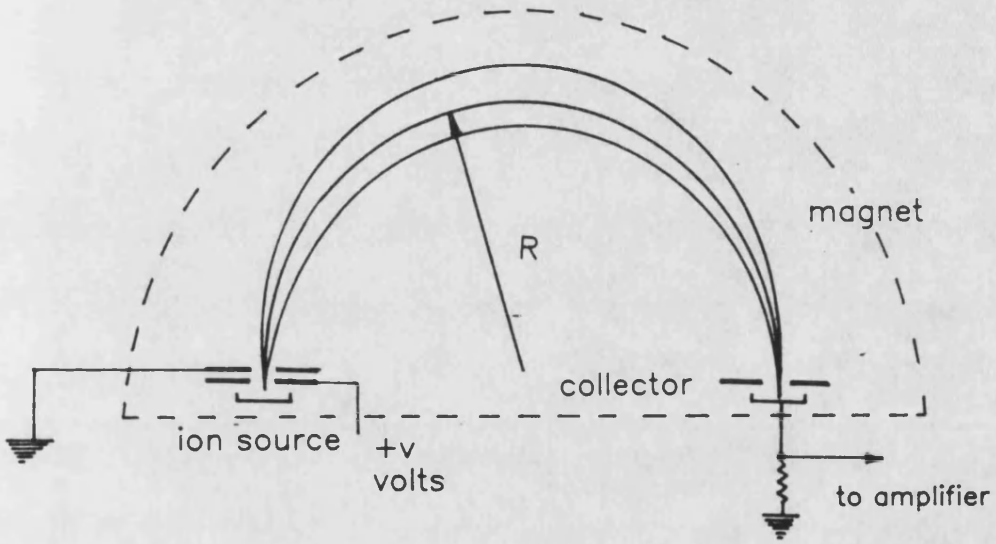

Acceleration in the source $eV = 1/2\ mv^2$

radial acceleration $= mv^2/R = HeV$

$m/e = R^2H^2/2V$

V= accelerating voltage
m = ion mass
e = charge on ion

v = ion velocity
R = radius of path in field
H = magnetic field strength

Appendix H

```
100 REM IG-AN EDITED 6-3-89
110 :REM ORR CALIB OF NOV 88
120 :REM V(1,I)=VOL GAS I IN SAMPLE
130 :REM V(2,I)=VOL GAS I IN TRACER
140 DIM G$(6),E$(8),R(6),M(6),X(4,6),V(3,6),S(3,6)
150 PRINT"ANALYSIS OF DISSOLVED GASES IN WATER"
160 PRINT "ENTER SAMPLE NAME WITH GRID REFERENCE"
170 INPUT N$
180 PRINT"ENTER COLLECTION DATE AND ANALYSIS DATE"
190 INPUT D1$,D2$
200 PRINT "ENTER COLLECTION TEMPERATURE OF SAMPLE"
210 INPUT T
220 PRINT "ENTER TRACER SEQUENTIAL NO."
230 INPUT Y1
240 PRINT "ENTER SAMPLE WEIGHT G"
250 INPUT W
260 FOR I=1 TO5
270 READ E$ (I) :REM ISOTOPE RATIOS DETERMINED
280 DATA "  3HE &  4HE"," 20NE &  22NE","  36AR &  40AR","  78KR &  84KR"
290 DATA "129XE & 136XE"
300 NEXT I
310 FOR I=1 TO 5
320 READ G$(I)
330 NEXT I
340 DATA "HE*1E8","NE*1E7","AR*1E4","KR*1E8","XE*1E8"
350 GOSUB 950  :REM >>>>>>>>>>>>>>>>>
360 FOR I=1 TO 5 :REM CALC OF GAS CONTENTS
370 PRINT"ENTER    ";E$(I);"  ION CURRENTS"
380 INPUT G(I),H(I)
390 IF G(I)=0 GOTO 530
400 IF H(I)=0 GOTO 530
410 R(I)=G(I)/H(I)
420 V(1,I)=V(2,I)*(X(1,I)-X(2,I)*R(I))/(X(4,I)*R(I)-X(3,I))
430 V(1,I)=V(1,I)/W :REM VOL GAS I/CM3 WATER
440 PRINT G$(I)
450 PRINT "I.C. LIGHT ="; G(I)
460 PRINT "I.C. HEAVY ="; H(I)
470 PRINT "CONC       ="; V(1,I)
480 PRINT"IS CONC. WITHIN LIMITS ? YES OR NO?"
490 INPUT Q$:IF Q$="YES" GOTO 530
500 PRINT "ENTER E$(I) ION CURRENTS"
510 INPUT G(I),H(I):R(I)=G(I)/H(I)
520 GOTO 420
530 NEXTI
540 V(1,1)=V(1,1)*1E8:V(1,2)=V(1,2)*1E7:V(1,3)=V(1,3)*1E4:V(1,4)=V(1,4)*1E8
550 V(1,5)=V(1,5)*1E8:V(1,6)=V(1,6)*1E2
560 V(2,1)=V(2,1)*1E8:V(2,2)=V(2,2)*1E7:V(2,3)=V(2,3)*1E4:V(2,4)=V(2,4)*1E8
570 V(2,5)=V(2,5)*1E8:V(2,6)=V(2,6)*1E2
580 Z=Z+1
590 OPEN1,4:CMD1
600 PRINT#1
```

Appendix H

```
610 PRINT#1,CHR$(1)"□A□NALYSIS OF □D□ISSOLVED □G□ASES IN □W□ATER"
620 PRINT#1
630 PRINT#1,"SAMPLE NAME:    ";N$
640 PRINT#1,"SAMPLE COLLECTION TEMP.=  ";T;"   DEG.CENT."
650 PRINT#1,"COLLECTED ON    ";D1$ ;"  ANALYSED ON  ";D2$
660 PRINT#1
670 PRINT#1,"VOLUME OF SAMPLE TUBE  ";  "=";W;"  CM3"
680 PRINT#1,"TRACER  SEQUENTIAL NUMBER  ";Y1
690 PRINT#1
700 PRINT#1, "GAS CONTENTS OF SAMPLE":PRINT#1
710 PRINT#1,"GAS       IC.LIGHT  IC.HEAVY          CONC."
720 OPEN2,4,1:OPEN3,4,2
730 PRINT#3,"AAAAAA  $999.999 $9999.999    $99999999.999"
740 FOR I=1 TO 5
750 IF R(I) =0 GOTO 770
760 PRINT#2,G$(I);CHR$(29);G(I);H(I);V(1,I)
770 NEXT I
780 PRINT#3:CLOSE3:PRINT#2:CLOSE2
790 IF R(6) =0 GOTO 800
800 PRINT#1
810 PRINT#1
820 PRINT#1,"TRACER CALIB. OF  ";T$;"X SEQUENTIAL FACTOR =  ";S9
830 PRINT#1
840 PRINT#1,"GAS             M.F.LIGHT     M.F.HEAVY          VOLUME CM3"
850 OPEN2,4,1:OPEN4,4,2
860 PRINT#4,"AAAAAA           9.999          9.999          9999.999"
870 FOR I=1 TO 5
880 PRINT#2,G$(I);CHR$(29);X(1,I);X(2,I);V(2,I)
890 NEXTI
900 PRINT#4:CLOSE4:PRINT#2:CLOSE2
910 PRINT#1:CLOSE1
920 IFZ<2 GOTO 580
930 STOP
940 REM **********  SUBR ONE *********
950 FOR I=1 TO5 :REM READS MOL FRACTS GAS AND ISOTOPES IN ATM
960 READ M(I),X(3,I),X(4,I)
970 NEXT I
980 DATA5.239E-6,1.3E-6,0.999999
990 DATA1.818E-5,0.9050,0.0923
1000 DATA 9.34E-3,0.00336,0.996
1010 DATA1.139E-6,0.00347,.570
1020 DATA 8.70E-8,0.2644,.0886
1030 FOR I=1 TO5 :REM READS MOL FRACTS ISOTOPES IN TRACER
1040 READ X(1,I),X(2,I)
1050 NEXT I :REM MOL FRACTS LIGHT AND HEAVY GASES IN TRACER
1060 DATA .8861,.1139,.0013,.9987,.9966,.0034,.9926,.0001
1070 DATA .0001,.8052
1080 S9=1-(Y1*.00223)
1090 FOR I=1 TO5
1100 READ V(2,I) :REM READS TRACER CALIB.
1110 V(2,I)=V(2,I)*S9
1120 DATA 1.884E-5,7.466E-6,1.253 E-5,1.488 E-6,1.643 E-7
1130 NEXT I
1140 T$="14 DEC  88":REM DATE OF TRACER CALIB
1150 RETURN
1160 END
```

Appendix I

```
REM ************************************************************************
REM ***************  PROG:  RECHTEMP.BAS  ********************************
REM ************************************************************************
REM Calculates recharge temperature from noble gas contents
   PRINTS = 1
   DIM H(5), L(5), N(5), A(5), B(5), C(5), D(5)
   DIM G(5, 500), T(5, 500), SD(500), M(500), E(5, 500)
   DIM S(5, 700), CI(500), Tabs(700)
REM ************************************************************************
REM ***************  DATA  INPUT  *****************************************
REM ************************************************************************
  CLS : PRINT : PRINT
  INPUT "Sample name                          "; N$
  PRINT : INPUT "Sample reference number          "; R$
  PRINT : INPUT "Upper recharge limit, deg. C     "; upptemplim
  PRINT : CLS
  PRINT : PRINT "Enter He * 1E8"
  INPUT NG(1, 1)
  G(1, 1) = NG(1, 1) * 1E-08
  PRINT : PRINT "Enter Ne * 1E7"
  INPUT NG(2, 1)
  G(2, 1) = NG(2, 1) * .0000001
  PRINT : PRINT "Enter Ar * 1E4"
  INPUT NG(3, 1)
  G(3, 1) = NG(3, 1) * .0001
  PRINT : PRINT "Enter Ar40/Ar36 ratio"
  INPUT arratio
  G(3, 1) = G(3, 1) * 296.5 / (1 + arratio)
  REM Ar_corrected for radiogenic Ar-40
  PRINT : PRINT "Enter Kr * 1E8"
  INPUT NG(4, 1)
  G(4, 1) = NG(4, 1) * 1E-08
  PRINT : PRINT "Enter Xe * 1E8"
  INPUT NG(5, 1)
  G(5, 1) = NG(5, 1) * 1E-08
  CLS : PRINT
  PRINT "INPUT salinity;  for freshwater input zero"
  INPUT "SALINITY in parts per thousand or grams/litre    "; sal
  MOL = sal / 64.113
100 PRINT : INPUT "INPUT ALTITUDE OF RECHARGE ZONE in metres "; ALT
    atmpress = 1
    IF ALT = 0 THEN GOTO 200
    PRINT : PRINT "INPUT   ESTIMATED MEAN ANNUAL AIR TEMPERATURE"
    INPUT "       for  RECHARGE ZONE, in deg. C              "; MAAT
    MAAT = MAAT + 273.15
    atmpress = 1 * EXP(-.031 * ALT / MAAT)
```

Appendix I

```
REM ************************************************************************
REM ***************  MAIN  CALCULATION  ************************************
REM ************************************************************************
200 GOSUB 500: REM solubility table
REM initial Ne correction
    IF G(2, 1) < 2.295E-07 THEN 300
    CC = G(2, 1) - 2.295E-07
    REM removes large air volume from gas contents
    G(2, 1) = G(2, 1) - CC
    G(1, 1) = G(1, 1) - .28817 * CC
    G(3, 1) = G(3, 1) - 513.75 * CC
    G(4, 1) = G(4, 1) - .06265 * CC
    G(5, 1) = G(5, 1) - .0047855 * CC
REM air aliquot subtractions
300 FOR J = 2 TO 500
    G(1, J) = G(1, J - 1) - 1.8011E-10
    G(2, J) = G(2, J - 1) - 6.25E-10
    G(3, J) = G(3, J - 1) - 3.211E-07
    G(4, J) = G(4, J - 1) - 3.9157E-11
    G(5, J) = G(5, J - 1) - 2.9909E-12
    CI(J) = NG(2, 1) *.0000001 / G(2, J): REM contamination index
GOSUB 600: REM compares gas contents with B&K solubilities
GOSUB 700: REM Calculates Mean and S.D. of temps.
    IF T(2, J) >= upptemplim THEN GOTO 350: REM RECHARGE TEMP LIMIT
    MAXJ = J: REM max. number of subtractions
    NEXT J
350  vpwusz = 21.0109 - 5321.01 / (M(bestj) + 273.18)
     vpwusz = EXP(vpwusz): REM vap. press. water in mm at temp
REM ************************************************************************
REM ***************  CONTROL  OF  PRINTOUT  ********************************
REM ************************************************************************
400 GOSUB 1000: REM multiply gas contents for printing
410 GOSUB 2000: REM print input data
    GOSUB 3000: REM print results around min. S.D. for temperature
    INPUT "Is a full printout needed ?   Y or N ?"; Q$
    IF Q$ = "n" OR Q$ = "N" THEN GOTO 450
420 GOSUB 4000: REM full printout
    INPUT "Do you want another copy of output ?  Y or N ?"; Q$
    IF Q$ = "Y" OR Q$ = "y" THEN GOTO 410
    GOTO 450
REM: additional calculation option
450 INPUT "CALCULATE FOR ANOTHER RECHARGE ALTITUDE Y OR N ?"; Q$
    IF Q$ = "Y" OR Q$ = "y" THEN GOTO 100
    GOTO 5000: REM end
```

Appendix I

```
REM ************************************************************************
REM ***************  CALCULATION  SUBROUTINES ******************************
REM ************************************************************************
REM Subroutine calc Ne Ar Kr Xe solubs each 0.1 deg from -10 to 60  deg
500  RESTORE
     FOR K = 2 TO 5
     READ H(K), L(K), pp(K), A(K), B(K), C(K), D(K)
     NEXT K
   DATA 142.50,41.667,1.818E-5,-.3022,3.6278,-13.6641,16.8309
   DATA 168.87,40.404,9.34E-3,-.4050,3.8471,-12.3389,13.6921
   DATA 179.21,39.781,1.139E-6,-.1124 ,1.3282,-5.1423,6.8403
   DATA 188.78,39.273,8.70E-8,-0.1611,1.9007,-7.3019,9.5072
   FOR K = 2 TO 5
     temp = 273.18 - 10.1
     FOR i = 1 TO 700
     temp = temp + .1
     Tabs(i) = temp
     TE = H(K) / temp - 1
     S(K, i) = L(K) + TE + 36.855 * TE * TE
     S(K, i) = EXP(S(K, i))
     S(K, i) = S(K, i) * pp(K) * 1244.142
     IF sal > 10 THEN GOSUB 550: REM salinity corr. not reqd below 10 g/l
     vpw = 21.0109 - 5321.01 / temp
     vpw = EXP(vpw): REM vap. prss. water in mm at temp
     S(K, i) = S(K, i) * (atmpress - vpw / 760)
  NEXT i
  NEXT K
RETURN
REM ************************************************************************
REM subroutine to modify Bunsen coeffiecients for saline water
550  VIN = Tabs(i) / 100
     XY = A(K) + VIN + VIN + VIN + B(K) + VIN + VIN + C(K) + VIN + D(K)
     S(K, i) = S(K, i) / EXP(MOL * XY)
RETURN
REM ************************************************************************
600 REM subroutine to compare g(k,j) with s(k,j) to find t(k,j)
    FOR K = 2 TO 5
    FOR i = 1 TO 700
      T(K, J) = Tabs(i) - 273.18: REM RT match in deg C
      IF G(K, J) < S(K, i) THEN 610
      IF G(K, J) > S(K, i) THEN 620
610 NEXT i
620 NEXT K
RETURN
```

Appendix I

```
REM ************************************************************************
700  REM Subroutine to calc standard deviation
     M(J) = T(2, J) + T(3, J) + T(4, J) + T(5, J)
     M(J) = M(J) / 4: REM M(J) mean temp row J
   FOR i = 1 TO 5
     D(i) = (T(i, J) - M(J)) ^ 2
   NEXT i
     DI = D(2) + D(3) + D(4) + D(5)
     SD(J) = SQR(DI / 3): REM std. dev. RT
     IF J = 2 GOTO 710
     IF SD(J) > LSD THEN GOTO 720
710  LSD = SD(J): REM lowest std. dev.
     bestj = J
720  RETURN
REM ************************************************************************
REM ***************  PRINT OUT SUBROUTINES  ********************************
REM ************************************************************************
1000 REM subroutine to multiply up gas contents for printing
   FOR J = 1 TO MAXJ
     E(1, J) = G(1, J) * 1E+08
     E(2, J) = G(2, J) * 1E+07
     E(3, J) = G(3, J) * 10000
     E(4, J) = G(4, J) * 1E+08
     E(5, J) = G(5, J) * 1E+08
   NEXT J
RETURN
REM ************************************************************************
2000 REM subroutine to print titles and initial gas contents
     LPRINT CHR$(27) + "!" + CHR$(62)
     LPRINT "RECHARGE TEMPERATURE CALCULATION"
     LPRINT CHR$(27) + "!" + CHR$(28)
     LPRINT "SAMPLE name          : "; N$
     LPRINT "       number        : "; R$
     LPRINT "Ar-40/Ar-36 ratio    : "; arratio;
     LPRINT "Upper temperature limit :"; upptemplim
     LPRINT
     LPRINT "Altitude of recharge zone, metres asl          : "; ALT
     LPRINT "Mean annual air temperature at recharge zone   : "; MAAT - 273.18
     LPRINT "Pressure in bars at recharge altitude          : "; atmpress
     LPRINT "Water vap. press., mm, unsat zone              : "; vpwusz
     LPRINT "Salinity parts per thousand (g/litre)          : "; sal
     LPRINT CHR$(10)
     LPRINT "     He       Ne        Ar        Kr        Xe       C       T    S.D."
     LPRINT CHR$(27) + "!" + CHR$(8)
     LPRINT USING "fffff.ff    ff.ff    ff.ff    ff.ff    ff.ff   ";
     NG(1, 1), NG(2, 1), NG(3, 1), NG(4, 1), NG(5, 1)
     LPRINT CHR$(10)
RETURN
```

Appendix I

```
REM ************************************************************************
3000 REM Subroutine print results around min. S.D. for temperature
     FOR J = bestj - 8 TO bestj + 8
     IF J <= 0 THEN GOTO 420
     LPRINT USING "fffff.ff    ff.ff    ff.ff    ff.ff    ff.ff   ";
     E(1, J), E(2, J), E(3, J), E(4, J), E(5, J)
     LPRINT USING "            ff.f     ff.f     ff.f      ff.f      f.ff    ff.
     T(2, J), T(3, J), T(4, J), T(5, J), CI(J), M(J), SD(J)
     LPRINT
     NEXT J
     LPRINT CHR$(27) + "!" + CHR$(0)
RETURN
REM ************************************************************************
4000 REM subroutine prints out full result set
     LPRINT CHR$(27)
     LPRINT
     LPRINT "Full result set"
     LPRINT
     LPRINT CHR$(27) + "!" + CHR$(0)
     FOR J = 2 TO MAXJ
     LPRINT CHR$(27) + "!" + CHR$(8)
     LPRINT USING "fffff.ff    ff.ff    ff.ff    ff.ff    ff.ff  ";
     E(1, J), E(2, J), E(3, J), E(4, J), E(5, J)
     LPRINT USING "            ff.f     ff.f     ff.f      ff.f      f.ff    ff.
     T(2, J), T(3, J), T(4, J), T(5, J), CI(J), M(J), SD(J)
     NEXT J
     LPRINT CHR$(27) + "!" + CHR$(0)
RETURN
5000 END
```

Appendix J

Cracking pattern in MS10S for N_2

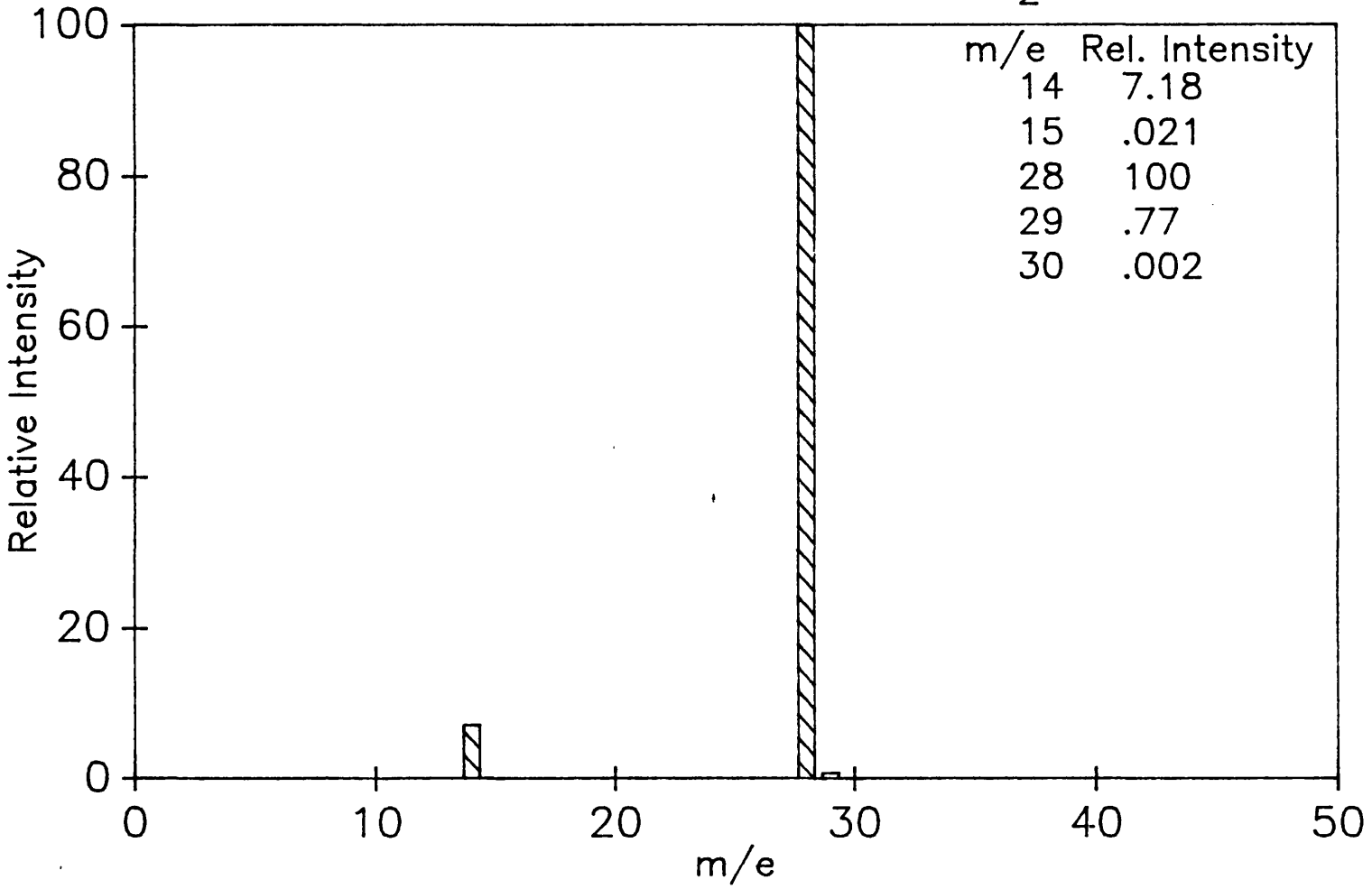

Appendix J

Cracking pattern in MS10S for CH_4

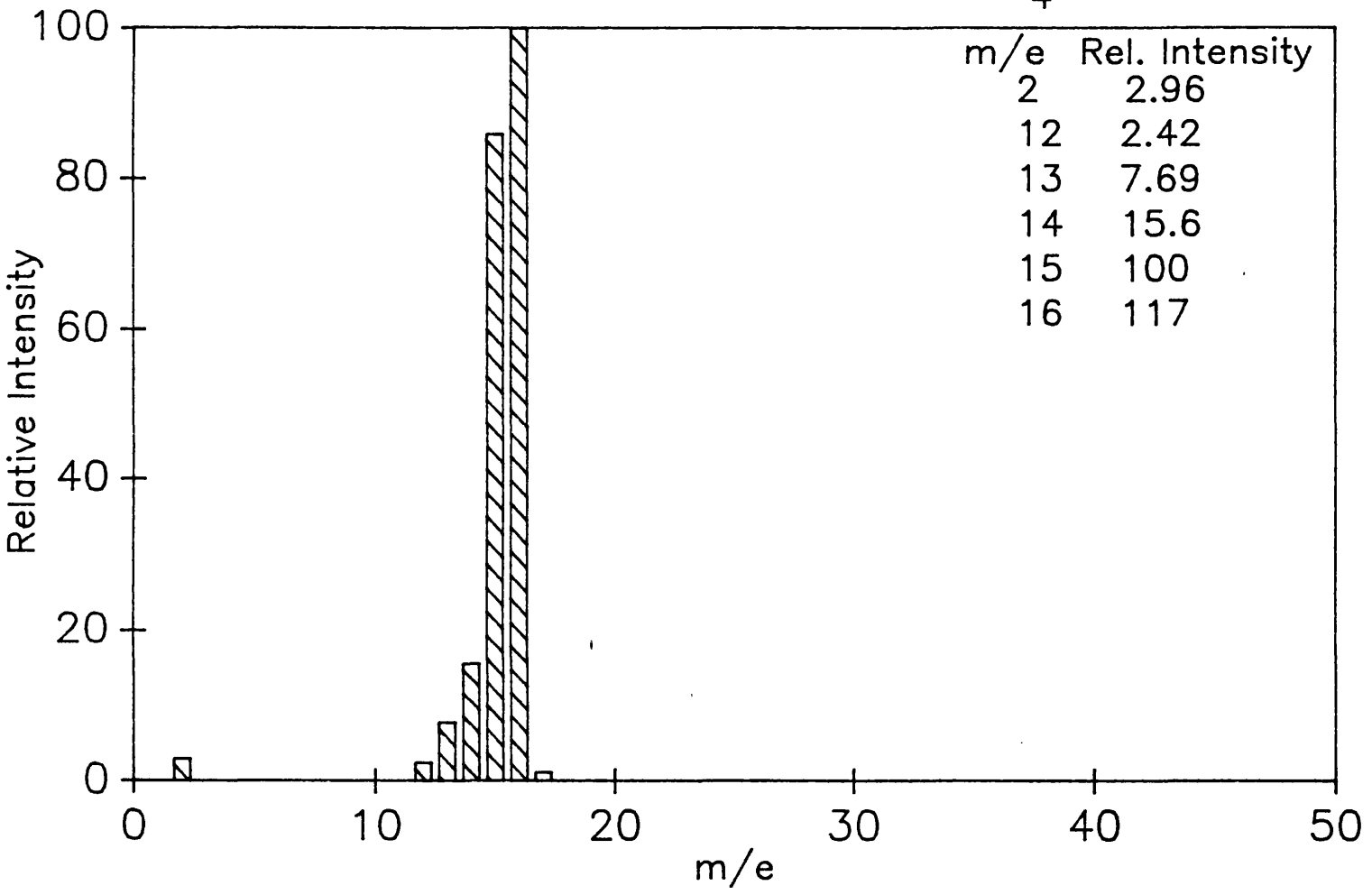

m/e	Rel. Intensity
2	2.96
12	2.42
13	7.69
14	15.6
15	100
16	117

Appendix J

Cracking pattern in MS10S for CO_2

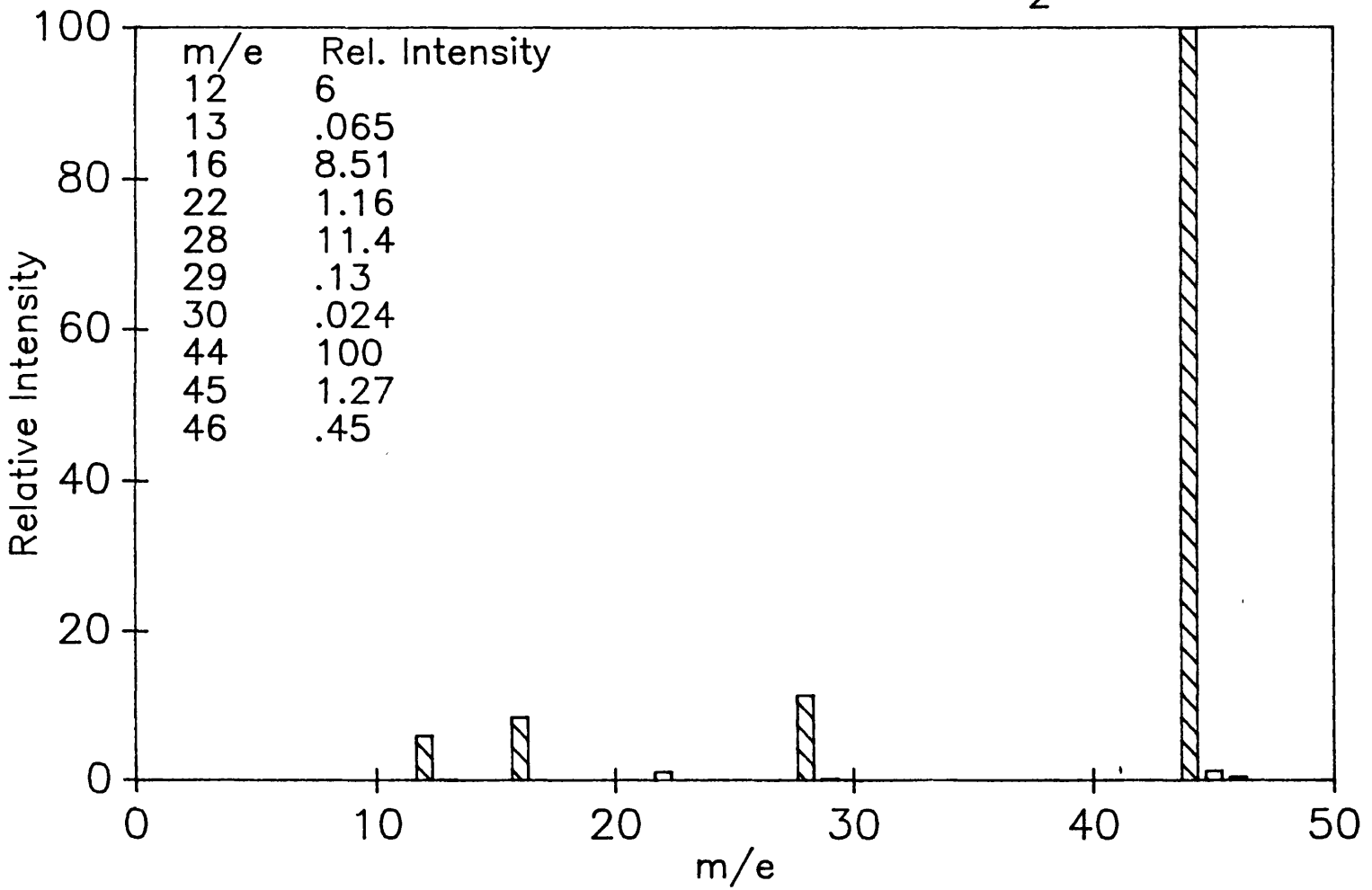

Appendix J

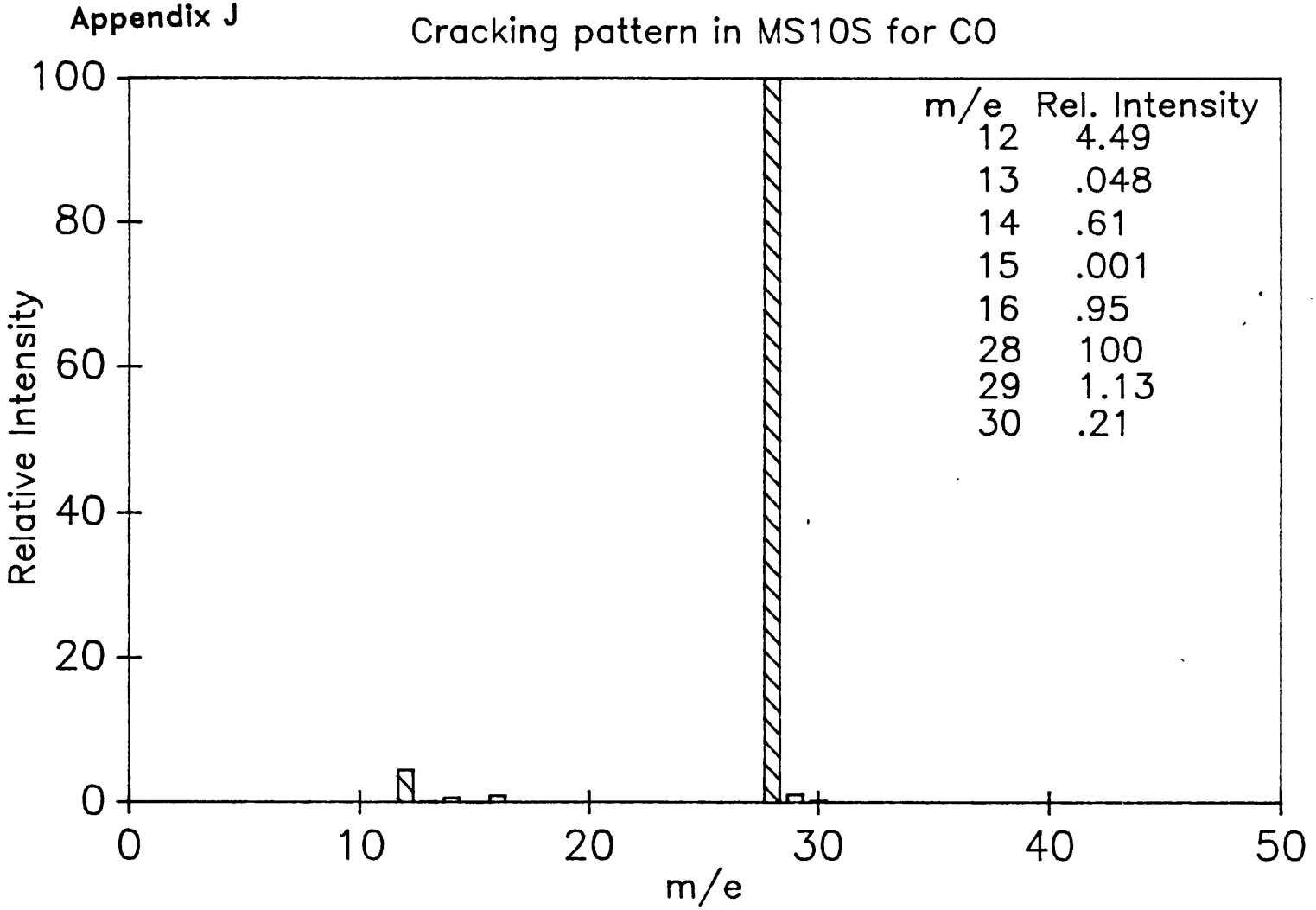
Cracking pattern in MS10S for CO
Relative Intensity
100
80
60
40
20
0
0
10
20
30
40
50
m/e
m/e Rel. Intensity
12 4.49
13 .048
14 .61
15 .001
16 .95
28 100
29 1.13
30 .21

Appendix K

```
    REM Outgas 14-6-89
    REM Cals compostion of gas evolved and gas remaining in solution
    REM for various Recharge Temps. (rechtemp) Degassing Temp. (degastemp)
    REM and pressure (degaspress)

    INPUT "Recharge Temperature :"; rechtemp
    INPUT "Degassing Temperature :"; degastemp
    INPUT "Degassing Pressure (ATM) :"; degaspress
    INPUT "Contamination Index (Ne) :"; CI
    INPUT "HCO3 Content (MG/L) :"; bicarb
    INPUT "Model Radiogenic Ar ? (Y OR N)"; modradar$
    arrat = 295.5
    IF modradar$ = "N" GOTO 200
    INPUT "Ar-40/Ar-36 RATIO :"; arrat
200 INPUT "Model N2/Ar ? (Y OR N)"; modn2arrat$
    IF modn2arrat$ = "N" GOTO 300
    INPUT "N2/Ar Ratio (GAS) :"; n2arrat
300 INPUT "CH4/N2 Ratio (GAS) :"; c4n2rat
    INPUT "Radiogenic He (Cm3/Cm3 H2O *1E8) "; radhe
    INPUT "Fluid PH :"; PH
    INPUT "Recharge Salinity (g/l) "; rechsal
    molrechsal = rechsal / 64.113
    INPUT "Groundwater Salinity (g/l) "; salinity
    molsal = salinity / 64.113

    REM Estimate vapor pressure of water at degastemp
    REM from Thiesen eqn
    PW = ((365 - degastemp) ^ 4 - 265 ^ 4) * 5.08E-09
    PW = 5.409 * (degastemp - 100) - PW
    PW = 2.303 * PW / (degastemp + 273.18)
    vpwat = EXP(PW)

    REM Read Henry's Law data
    FOR C = 1 TO 6
        READ U(C), V(C), atmpp(C), G$(C)
    NEXT C
    DATA 131.42, 41.824, 5.239E-6, He
    DATA 142.5, 41.667, 1.818E-5, Ne
    DATA 168.87, 40.404, 9.34E-3, Ar
    DATA 179.21, 39.781, 1.139E-6, Kr
    DATA 188.78, 39.273, 8.6E-8, Xe
    DATA 162.02, 41.712, 0.7803, N2
```

Appendix K

```
    REM Read salting out coefficients
    FOR I = 1 TO 8
        READ aks(I), bks(I), cks(I), dks(I)
    NEXT I
    DATA -0.2304, 2.2951, -7.7154, 9.006      : REM He
    DATA -0.3022, 3.6278, -13.6641, 16.8309   : REM Ne
    DATA -0.405, 3.8471, -12.3389, 13.6921    : REM Ar
    DATA -0.1124, 1.3282, -5.1423, 6.8403     : REM Kr
    DATA -0.1611, 1.9007, -7.3019, 9.5072     : REM Xe
    DATA -0.2427, 2.1504, -6.61, 7.4294       : REM N2
    DATA -0.021, 0.2089, -0.7894, 1.5653      : REM CH4
    DATA -0.0964, 1.0183, -3.5065, 4.0378     : REM CO2

    REM Calculate initial gas concentrations in cm3/L
    M = molrechsal
    t = 273.18 + rechtemp
    GOSUB 700
    REM Get salting constants, ksalt(x) for gases at rechtemp
    GOSUB 400
    REM Get Bunsen coefficients at rechtemp
    FOR I = 1 TO 6: REM initgasconc(I) = INITIAL GAS CONCS. STP AT RECHARGE
        initgasconc(I) = bunsen(I) * atmpp(I): REM cm3 STP/litre
        NEXT I

    REM EXTRA AIR ADDITION
    exneon = initgasconc(2) * CI - initgasconc(2)
    initgasconc(1) = initgasconc(1) + exneon * .2882 + radhe * .00001
    initgasconc(2) = initgasconc(2) + exneon
    initgasconc(3) = initgasconc(3) + exneon * 513.75
    IF modraar$ = "N" GOTO 110
    initgasconc(3) = initgasconc(3) * arrat / 295.5
110 initgasconc(4) = initgasconc(4) + exneon * .06265
    initgasconc(5) = initgasconc(5) + exneon * .00473
    initgasconc(6) = initgasconc(6) + exneon * 42920.8

    REM ************* Calc. volume gas exsolved ************************

    REM Successive approx exsolv gas vol (exgasvol)
    REM by equalising sum total (pptot) of partial
    REM pressures pp(I) to degassing pressure (degaspress)
    t = 273.18 + degastemp
    M = molsal
    GOSUB 700: REM Get ksalt(x) at degastemp
    GOSUB 400: REM Get bunsen(x) at degastemp
    GOSUB 600: REM GET bunsen(x) CO2 and CH4
    GOSUB 500: REM Get vol CO2 in degassed soln cm3/l
    ppn2 = (degaspress - vpwat) / (c4n2rat + 1)
    REM ppn2 = first estimate ppn2 in gas evolved
    volapprox1 = (initgasconc(6) - ppn2 * bunsen(6)) / ppn2
    REM 1st approx vol gas phase at degastemp
    IF volapprox1 < .001 THEN GOTO 356: REM no outgassing
    exgasvol = volapprox1
```

Appendix K

```
305 pptot = 0
    IF exgasvol < .0005 THEN GOTO 356
310 FOR I = 1 TO 5
        pp(I) = initgasconc(I) / (bunsen(I) + exgasvol * 273.18 / t)
        pptot = pptot + pp(I)
    NEXT I
    IF modn2arrat$ = "N" GOTO 319
    pp(6) = pp(3) * n2arrat
    GOTO 320
319 pp(6) = initgasconc(6) / (bunsen(6) + exgasvol * 273.18 / t)
320 pp(7) = c4n2rat * pp(6): REM pp methane
    pptot = pptot + pp(6) + pp(7) + pp(8) + vpwat
340 IF pptot < degaspress - .0005 GOTO 345
    IF pptot > degaspress + .0005 GOTO 345
    GOTO 350
345 corrfactor = pptot / degaspress
    exgasvol = exgasvol * corrfactor
    GOTO 305

350 stpexgasvol = exgasvol * 273.18 * degaspress / (degastemp + 273.18)
    REM stpexgasvol=VOL GAS AT STP
    corrstpexgasvol = (degaspress - vpwat) * stpexgasvol / degaspress
    REM VOL GAS CORR. FOR VP AT STP
    IF modn2arrat$ = "N" GOTO 355
    initgasconc(6) = exgasvol * 273 / t
    initgasconc(6) = (initgasconc(6) + bunsen(6)) * pp(6)
355 initgasconc(7) = exgasvol * 273 / t
    initgasconc(7) = (initgasconc(7) + bunsen(7)) * pp(7)
    initvoldissgas = 0: REM excl co2
    totvoldissgas = 0: REM  final gas conc
    FOR I = 1 TO 7: REM He to CH4
        finalgasconc(I) = pp(I) * bunsen(I)
        totvoldissgas = totvoldissgas + finalgasconc(I)
        initvoldissgas = initvoldissgas + initgasconc(I)
    NEXT I
    totvoldissgas = totvoldissgas + finalgasconc(8): REM add CO2
    totinitgasconc = corrstpexgasvol + totvoldissgas
    REM Total initial gas conc. cm3/litre
    initgasconc(8) = totinitgasconc - initvoldissgas
    REM Initial CO2 conc. by difference.
    volwatvap = vpwat * exgasvol * 273.18 / t
    REM volume water vapour at STP
    volwat = volwatvap * 18.015 / (22412.7 * 1000)
    REM corresponding vol water in litres
    salbeforedegas = molsal * 64.113 / (1 + volwat)
    REM Salinity mg/l prior degassing
```

Appendix K

```
    R(1) = initgasconc(6) / initgasconc(3)
    R(2) = finalgasconc(6) / finalgasconc(3)
    R(3) = pp(6) / pp(3)
    B(1) = initgasconc(1) / initgasconc(2)
    B(2) = finalgasconc(1) / finalgasconc(2)
    B(3) = pp(1) / pp(2)
    O(1) = initgasconc(4) / initgasconc(5)
    O(2) = finalgasconc(4) / finalgasconc(5)
    O(3) = pp(4) / pp(5)
    H(1) = initgasconc(7) / initgasconc(6)
    H(2) = finalgasconc(7) / finalgasconc(6)
    H(3) = pp(7) / pp(6)

    finalgasconc(1) = finalgasconc(1) * 100000!
    finalgasconc(2) = finalgasconc(2) * 10000!
    finalgasconc(3) = finalgasconc(3) * 10
    finalgasconc(4) = finalgasconc(4) * 100000!
    finalgasconc(5) = finalgasconc(5) * 100000!
    finalgasconc(6) = finalgasconc(6) * .1
    finalgasconc(7) = finalgasconc(7) * .1
    finalgasconc(8) = finalgasconc(8) * .1
    initgasconc(1) = initgasconc(1) * 100000!
    initgasconc(2) = initgasconc(2) * 10000!
    initgasconc(3) = initgasconc(3) * 10
    initgasconc(4) = initgasconc(4) * 100000!
    initgasconc(5) = initgasconc(5) * 100000!
    initgasconc(6) = initgasconc(6) * .1
    initgasconc(7) = initgasconc(7) * .1
    initgasconc(8) = initgasconc(8) * .1

356 REM ***********  Hard copy print out *************************

    LPRINT CHR$(27) + "!" + CHR$(62)
    LPRINT
    LPRINT "         EXSOLUTION OF GASES"
    LPRINT CHR$(27) + "!" + CHR$(28)
    LPRINT
    LPRINT USING "Recharge  temperature,deg.C              ff.f "; rechtemp
    LPRINT USING "Degassing temperature, deg.C             ff.f "; degastemp
    LPRINT USING "Degassing pressure (atm)                 ff.f "; degaspress
    LPRINT USING "Excess air cont. index (Ne)               f.f "; CI
    LPRINT
    LPRINT USING "Radiogenic He (*1E8)                  ffffff.f "; radhe
    LPRINT USING "Methane / nitrogen ratio                 fff.f "; c4n2rat
    LPRINT USING "Bicarbonate content, mg/L               ffff.f "; bicarb
    LPRINT USING "Fluid pH                                  f.ff"; PH
    LPRINT
    IF N$ = "N" GOTO 360
    LPRINT USING "Ar-40/Ar-36 Ratio                        fff.f "; arrat
    GOTO 365
360 LPRINT USING "Ar-40/Ar-36 Ratio                        fff.f "; 295.5
```

Appendix K

```
365 LPRINT USING "Recharge salinity, g/L                    ff.ff "; rechsal
    LPRINT USING "Groundwater salinity before degassing,g/L ff.ff ";
    salbeforedegas
    IF volapprox1 < .001 GOTO 366
    LPRINT USING "Groundwater salinity after degassing, g/L ff.ff "; salinity
366 LPRINT
    IF volapprox1 > .001 GOTO 368
    LPRINT "  Outgassing  CANNOT  OCCUR  at this temperature and pressure"
    GOTO 800
368 LPRINT "GAS         GAS PHASE      INITIAL SOLN      DEGASSED SOLN"
    LPRINT "             pp (atm)       cm3 STP/cm3        cm3 STP/cm3"
    LPRINT
    G$(1) = "He ": G$(2) = "Ne ": G$(3) = "Ar ": G$(4) = "Kr "
    G$(5) = "Xe ": G$(6) = "N2 ": G$(7) = "CH4": G$(8) = "CO2"
    E$(1) = "* 1E-8": E$(2) = "* 1E-7": E$(3) = "* 1E-4": E$(4) = "* 1E-8"
    E$(5) = "* 1E-8": E$(6) = "* 1E-2": E$(7) = "* 1E-2": E$(8) = "* 1E-2"
    FOR I = 1 TO 8
    LPRINT USING " &      f.ffffffff    ffffff.fff     ffffff.fff   &";
    G$(I), pp(I), initgasconc(I), finalgasconc(I), E$(I)
    NEXT I
    LPRINT USING "Water    ff.fff"; vpwat
    LPRINT
    LPRINT "First gas vol. approximation (cm3)              "; volapprox1
    LPRINT
    LPRINT "Vol. Gas evolved from 1L water (cm3)            "; exgasvol
    LPRINT "Vol. Gas at STP (cm3)                           "; stpexgasvol
    LPRINT "Vol. Gas corrected for VP water (STP cm3)       "; corrstpexgasvol
    LPRINT
    LPRINT "Gas conc. prior degassing (STP cm3/L)           "; totinitgasconc
    LPRINT "Gas conc. after degassing (STP cm3/L)           "; totvoldissgas
    LPRINT "Water/gas vol  ratio (at degas T and P)         "; 1000 / exgasvol
    LPRINT : LPRINT
    W$(1) = "Initial soln. ": W$(2) = "Degassed soln.": W$(3) = "Gas Phase
    LPRINT " ------------------------ Gas  Ratios ---------------------------"
    LPRINT "                     N2/AR      HE/NE      KR/XE      CH4/N2"
    LPRINT
    FOR I = 1 TO 3
        LPRINT USING "&     ff.fff     f.fff     ff.fff     f.fff ";
        W$(I), R(I), B(I), O(I), H(I)
    NEXT I
    LPRINT : LPRINT
    LPRINT
    LPRINT "Recharge salinity, g/L                          "; rechsal
    LPRINT "Groundwater salinity before degassing, g/L      "; salbeforedegas
    LPRINT "Groundwater salinity after degassing, g/L       "; salinity
    LPRINT : LPRINT : LPRINT
    REM ************************* End of print out  **********************
    GOTO 800: REM END
```

Appendix K

```
400 REM SUBR Calc bunsen coefficients in cm3 STP/litre
    FOR C = 1 TO 6
        T2 = U(C) / t - 1
        K = V(C) * T2 + 36.855 * T2 * T2
        K = EXP(K)
        B = 124.4142 * 10000! * K
        F = M * ksalt(C)
        F = EXP(F)
        bunsen(C) = B / F
    NEXT C
    RETURN

500 REM SUBR Calc partial pressure CO2 for bicarb equil
    K1 = 5.01E-07: K2 = 5.62E-11
    H = -PH: H = 10 ^ H
    A0 = 1 / (1 + K1 / H + K1 * K2 / H ^ 2)
    A1 = 1 / (H / K1 + 1 + K2 / H)
    A2 = 1 / (H ^ 2 / (K1 * K2) + H / K2 + 1)
    molbicarb = bicarb / (61.006 * 1000)
    pp(8) = molbicarb * A0 / (bunsen(8) * A1)
    CT = pp(8) * bunsen(8) / A0
    CA = A2 * bunsen(8) * pp(8) / A0
    finalgasconc(8) = (CT - molbicarb - CA) * 22.414 * 1000: REM cm3/l
    RETURN

600 REM SUBR bunsen coefficients for CO2(8) and CH4 (7)
    Z = t / 100
    REM for co2
    KH = -6.5455 * Z ^ 3
    KH = KH + 63.6611 * Z ^ 2
    KH = KH - 207.272 * Z + 226.3128
    REM KH IS L/L/ATM
    bunsen(8) = KH / 22.414: REM MOLES/L/ATM
    F = M * ksalt(8)
    F = EXP(F)
    bunsen(8) = bunsen(8) / F: REM Corrected for ksalt mol/L/atm

    REM for CH4
    XL = -.1229 * Z ^ 3
    XL = XL + 1.2416 * Z ^ 2
    XL = XL - 4.1919 * Z + 4.7509
    XL = XL * 1000: REM CM3/L/ATM
    F = M * ksalt(7)
    F = EXP(F)
    bunsen(7) = XL / F: REM Corrected for ksalt
    RETURN

700 REM SUBR SALTING factors ksalt(x)
    Z = t / 100
    FOR I = 1 TO 8
    K7 = aks(I) * Z ^ 3
    K8 = bks(I) * Z ^ 2
    K9 = cks(I) * Z
    ksalt(I) = K7 + K8 + K9 + dks(I)
    NEXT I:
    RETURN
800 END
```

Appendix L

Analytical solution of the diffusion equation for He accumulation during aqueous flow in a fracture

The general equation for He accumulation in and diffusive loss from a He-generating rock is:

$$\frac{\partial C}{\partial T}(z,T) = G + D\frac{\partial^2 C}{\partial z^2}(z,T) \qquad A1$$

where $C_{(z,T)}$ is the concentration of He at depth z after time T, and G is the He generation rate. For a newly opened fracture which is continuously flushed with low He-content water. Appropriate boundary conditions are:

(i) The initial He concentration in a rock of age T_a, is:

$$C_{(z,0)} = GT_a \qquad A2$$

(ii) The He concentration at the fracture surface after low He-content water has started to flow is determined by the He concentration in the water and remains constant at:

$$C_{(0,T)} = C_s \qquad A3$$

where C_s is the constant He concentration in the water.

(iii) The He concentration at great depth below the fracture surface is:

$$C_{(\infty,T)} = G(T_a + T) = GT_a \text{ for } T \ll T_a \qquad A4$$

The corresponding Laplace transform of Eqn. A1 is:

$$GT_a + p\bar{C}(z,p) = G/p + D\frac{\partial^2 \bar{C}}{\partial z^2}(z,p) \qquad A5$$

where $$\bar{C}(z,p) = \int_{-\infty}^{+\infty} C(z,T)\exp(-pT)dT \qquad A6$$

and p is the index of the Laplace transform. The solution of Eqn. A5 after rearrangement is:

$$\bar{C}_{(z,p)} = A\exp(-z\sqrt{p/D}) + B\exp(+z\sqrt{p/D}) + G/p^2 + GT_a/p \qquad A7$$

Appendix L

where A and B are arbitrary constants. The transforms of Eqns. A3 and A4 are, respectively:

$$\bar{C}_{(0,p)} = C_s/p \qquad \text{A8}$$

and

$$\bar{C}_{(\infty,p)} = G/p^2 + GT_a/p \qquad \text{A9}$$

For Eqn. A9 to be satisfied, B must be zero in Eqn. A7 and hence it can be shown that for z = 0:

$$\bar{C}_{(0,p)} = C_s/p = A + G/p^2 + GT_a/p \qquad \text{A10}$$

from which

$$A = -(GT_a - C_s)/p - G/p^2 \qquad \text{A11}$$

and on substituting this value of A into Eqn. A7 :

$$\bar{C}_{(z,p)} = -\frac{GT_a - C_s}{p}\exp(-z\sqrt{p/D}) - \frac{G}{p^2}\exp(-z\sqrt{p/D}) \ldots\ldots + GT_a/p + G/p^2 \qquad \text{A12}$$

The inverse transform of Eqn. A12 is:

$$C_{(z,T)} = -(GT_a - C_s)\,\mathrm{erfc}\{z/(2\sqrt{DT})\} - G\int_0^T \mathrm{erfc}\{z/(2\sqrt{Du})\}du \ldots\ldots + G(T_a + T) \qquad \text{A13}$$

The final solution is obtained on rearrangement of Eqn. A13 :

$$C_{(z,T)} = GT_a\,\mathrm{erf}\{z/(2\sqrt{DT})\} + C_s\,\mathrm{erfc}\{z/(2\sqrt{DT})\} \ldots\ldots + G\int_0^T \mathrm{erf}(z/2\sqrt{Du})du \qquad \text{A14}$$